The development and validation of a bioanalytical hybrid approach to determine active renin and its precursor utilizing high-resolution mass spectrometry

INAUGURAL-DISSERTATION

Zur Erlangung des Doktorgrades
der Mathematisch-Naturwissenschaftlichen Fakultät der
Heinrich-Heine-Universität Düsseldorf

vorgelegt von

Ilja Burdman
aus Tschernigov

Düsseldorf, 28. April 2021

aus dem Institut für Klinische Pharmazie und Pharmakotherapie
der Heinrich-Heine-Universität Düsseldorf

Gedruckt mit der Genehmigung der
Mathematisch-Naturwissenschaftlichen Fakultät der
Heinrich-Heine-Universität Düsseldorf

Berichterstatter:
1. Prof. Dr. Stephanie Läer
2. Prof. Dr. Vlada Urlacher

Tag der mündlichen Prüfung: 22.04.2021

I. Erklärung zur Dissertation

Hiermit versichere ich an Eides statt, dass die folgende Dissertation mit dem Titel “The development and validation of a bioanalytical hybrid approach to determine active renin and its precursor utilizing high-resolution mass spectrometry” selbstständig und ohne fremde Hilfe unter Berücksichtigung der Regeln der guten wissenschaftlichen Praxis an der Heinrich-Heine-Universität angefertigt habe. Diese Dissertation wurde in der vorgelegten oder ähnlichen Form bei keiner anderen Institution eingereicht. Ich habe bisher keinen erfolglosen Promotionsversuch unternommen.

Düsseldorf, den Ilja Burdman

II. Danksagung

An dieser Stelle möchte ich mich für die vielfältige Unterstützung sowohl fachlicher als auch persönlicher Art bedanken, mit deren Hilfe diese Arbeit zustande gekommen ist.

Bei Frau Prof. Dr. Stephanie Läer möchte ich mich bedanken für die Betreuung und Ermöglichung dieser Dissertation. Zudem vermittelte sie mir tiefe Einblicke in die klinische Pharmazie, ich konnte Erfahrungen als Dozent und wissenschaftlicher Mitarbeiter in einer klinischen Studie sammeln.

Für die Übernahme des Koreferats bedanke ich mich bei Frau Prof. Dr. Vlada Urlacher, die mich während meiner Promotion begleitet und durch konstruktive Gespräche unterstützt hat.

Ein ganz besonderer Dank gilt Herrn Dr. Björn Burckhardt, der mir bei den wissenschaftlichen Experimenten durch intellektuellen Austausch zur Seite stand. Für die Übernahme der Ko-Autorenschaft bei verschiedenen Publikationen als auch für die kritische Durchsicht dieser Arbeit gebührt ihm ein ganz besonderer Dank.

Auch meinem Freund und Kollegen Martin Feickert möchte ich ein großes Dankeschön aussprechen, da er mir in meinen Hoch- und Tiefphasen sowohl auf persönlicher als auch auf intellektueller Ebene immer beistand. Durch ihn hatte ich selbst in schwierigen Phasen immer etwas zu lachen.

Für die große Geduld und die häufigen Aufmunterungen bin ich meiner Freundin Ellen sehr zu Dank verpflichtet. Sie half mir nach jedem Misserfolg, wieder neuen Mut zu finden und weiterzumachen.

Nicht zuletzt möchte ich mich bei meinen Eltern, Anna und Alexander, bedanken. Ohne ihren Beitrag und ihre stetige Unterstützung hätte ich mich nie auf diesen Weg begeben, um schlussendlich diese Arbeit anfertigen können. Außerdem bedanke ich mich bei meiner Schwester Sabine und meinem Onkel Yuri für ihren emotionalen Bestand und die zahlreichen Ermutigungen.

III. Zusammenfassung

Das Renin-Angiotensin-Aldosteron System ist von zentraler physiologischer Bedeutung, wobei die Aspartyl-Protease Renin als Geschwindigkeit bestimmender Schritt bei der Aktivierung der Kaskade angesehen wird. Da das Wissen zu Renin und seiner Vorstufe Prorenin bei Kindern limitiert ist, wurde einführend zu dieser Arbeit eine systematische Literaturrecherche entsprechend der PRISMA Methode durchgeführt. Aus den 15 identifizierten und eingeschlossenen pädiatrischen Studie lies eine altersabhängige Abnahme von Renin und Prorenin schlussfolgern. Der Review zeigte außerdem, dass bisher verbreitet eingesetzte Immunoassays sich dadurch charakterisieren, dass sie anfällig für Variationen bei der Durchführung sind. Vor allem aber diskriminieren sie nicht ausreichend zwischen Renin und Prorenin, sodass es durch die vom Hersteller angegebenen Kreuz-Reaktivität von bis zu 50% falsche Renin Werte gemessen werden können. Obwohl die Flüssigchromatographie gekoppelt an einen Massenspektrometer (LC-MS) hier eine vielversprechende Alternative darstellt, sind in der Literatur bisher keine Quantifizierungsansätze zur Bestimmung von Renin und Prorenin beschrieben. Deshalb wurde ein neuer Hybrid-Assay unter Verwendung der Massenspektrometrie mit einer vorgeschalteten Immunoaufreinigung für humanes Renin entwickelt und etabliert. Der hierbei genutzte experimentelle Ansatz des Design of Experiments (DOE), der im Gegensatz zum ‚ein Faktor nach dem anderen Faktor'-Ansatz (engl.: OFAT) in der Bioanalytik noch nicht weit verbreitet ist, erlaubte neben der Reduktion der Versuche vor allem eine systematische Austestung und Kombination der Parameter bei der Proteinquantifizierung. Hierauf aufbauend wurde im Nachgang ebenfalls mit Unterstützung des DOE Ansatzes eine eigenständige Methode für Prorenin entwickelt, die sich durch ein beschleunigtes Verdauverfahren mittels eines organisch-wässrigem Mediums auszeichnete und verglichen mit den konventionell tryptischen ‚Übernacht Verdau' die Analytik dieser Proteine innerhalb eines Labortages ermöglichte. Obwohl durch diesen LC-MS Ansatz nun beide Substanzen verlässlich voneinander unterschieden und bestimmt werden können, bedurfte es einer nachgeschalteten Assayoptimierung, bei der besonders nicht-spezifische Bindung an Verbrauchsmaterialien als Faktor für unzureichende Sensitivität für die Erfassung endogener Konzentrationen ausgemacht werden konnte. Die erfolgreiche Adressierung dieser Punkte haben maßgeblich zur verbesserten Empfindlichkeit des Assays beigetragen. Nach einer erfolgreichen Verifikation der optimierten, schlanken und schnelldurchführbaren Hybridmethode steht nun ein Quantifizierungsansatz zur Verfügung, der nun maßgeblich dazu beitragen krankheitensbedingte Veränderungen der Konzentrationen von Prorenin und aktivem Renin in adulten als auch in vulnerablen Populationsgruppen besser zu erfassen.

IV. Summary

The renin-angiotensin-aldosterone system is of central physiological importance because the aspartyl protease renin is thought to be the rate-determining step of a signaling cascade. Knowledge regarding renin and its precursor prorenin in children is limited; therefore, a systematic literature search, performed according to the PRISMA method, represents the introduction to this work. From 15 identified pediatric studies included in this systematic analysis, an age-related decrease in renin and prorenin levels was identified.

The review also showed that commonly used immunoassays are characterized by high degrees of performance variations. Most importantly, they do not discriminate sufficiently between renin and prorenin, so that up to 50% of the active renin might be detected falsely. Although this value appears to be low, when prorenin concentrations are high, this cross-reactivity can significantly distort the true active renin values. Although liquid chromatography-mass spectrometry (LC-MS) is a promising alternative to immunoassays, no LC-MS approaches for the determination of renin and prorenin have been described in the literature thus far. Therefore, a new hybrid assay using high-resolution MS, combined with the upstream immuno-purification of human renin, has been developed and established in this thesis. The design of experiments (DOE) approach, which was not widely applied in the field of bioanalytical research compared to the 'one-factor at a time' approach (OFAT), was applied to reduce the necessary number of experiments, and a systematic testing approach was used to optimize the combination of parameters to achieve high sensitivity protein quantification. Based on the DOE approach, an independent method for prorenin identification was subsequently developed, which is characterized by an accelerated digestion process using an organic-aqueous medium. Compared to the conventionally used 'over-night' digestion, the duration of the protein's analysis was reduced to a routine laboratory day. Although this MS-based approach allows for the reliable differentiation and determination of both substances, downstream assay optimization was necessary to reduce non-specific binding to consumables and the injection medium, which were determined to represent factors influencing the insufficient sensitivity for endogenous protein detection. By addressing these issues and performing statistical analyses of the injection solvent composition, assay sensitivity was significantly improved. The successful verification of the optimized, lean, and fast hybrid method has resulted in the availability of an MS-based quantification approach for the reliable differentiation and detection of endogenous renin and prorenin levels and which can significantly contribute to the detection of renin-associated diseases in adults and vulnerable populations.

V. Table of contents

VI. Figures

VII. Tables

VIII. Equations

IX. Abbreviations

ABC	Ammonium bicarbonate
ACE	Angiotensin converting enzyme
ACE-I	Angiotensin converting enzyme inhibitor
ACN	Acetonitrile
AEBSF	4-(2-Aminoethyl)benzenesulfonyl fluoride
ANP	Atrial natriuretic peptide
APCI	Atmospheric pressure chemical ionization
APR	Aldosterone-prorenin-ratio
AQUA	Absolute quantification
ARR	Aldosterone-active-renin-ratio
BDG	bidirectional Glenn anastomosis
BEH	Ethylene bridged hybrid
BLAST®	Basic local alignment search tool
CHD	congenital heart disease
CI	Confidence interval
CID	Collision induced dissociation
CPS	Counts per second
CSH	Charged surface hybrid
CV	Coefficient of variation
Da	Dalton
DCM	Dilated cardiomyopathy
DDA	Data-depended acquisition
DNA	Desoxyribonucleic acid
DOE	Design of experiment
DTT	Dithiothreitol
EDTA	Ethylenediaminetetraacetic acid
ELISA	Enzyme-linked immunosorbent assay
EMA	European medicine agency
ER	Endoplasmic reticulum
ESI	Electrospray ionization
eV	Electron volt
FASTA	Fast adaptive shrinkage thresholding algorithm

FDA	Food and drug administration
GCLP	Good clinical and laboratory praxis
HDMB	Hexadimethrine bromide
HEPES	2-(4-(2-Hydroxyethyl)-1-piperazinyl)-ethansulfon acid
HILIC	Hydrophilic interaction liquid chromatography
HPLC	High performance liquid chromatography
IAA	2-Iodoacetamide
ICH	International conference on harmonization
IDA	Information depended acquisition
IDDM	Insulin-depended diabetes melitus
IQR	Interquartile range
IRMA	Immunoradiometric assay
kV	Kilovolt
LBA	Ligand binding assay
LC-HRMS	Liquid chromatography coupled to high resolution mass spectrometer
LC-MS	Liquid chromatography coupled to mass spectrometer
LLOQ	Lower limit of quantification
LOD	Limit of detection
M	Mole per liter
m/z	Mass-to-charge
MALDI	Matrix assisted laser desorption ionization
MAX	Mixed mode strong anion exchanger
MCX	Mixed mode strong cation exchanger
MeOH	Methanol
MLR	Multiple linear regression
mM	Millimole per liter
MRM	Multiple reaction monitoring
mRNA	Messenger ribonucleic acid
MS	Mass spectrometer
NHS	N-Hydroxy succinimide
OFAT	One-factor-at a-time
OMI	O-methylisourea
OVAT	One-variable-at-a-time
P(RR)	Prorenin receptor

PBST	Phosphate buffer saline and tween 20
PC-IDMS	Protein-cleavage isotope dilution mass spectrometry
PLS	Partial least square regression
PP	Polypropylene
PRA	Plasma renin activity
PRC	Plasma renin concentration
QbD	Quality by design
QC	Quality control
QqQ	Triple quadrupole
QTOF	Hybrid quadrupole time-of-flight
RAAS	Renin angiotensin aldosterone system
RE	Relative error
RIA	Radioimmuno assay
RSM	Response surface modeling
SD	Standard deviation
SIL-IS	Stable isotope-labeled internal standard
SISCAPA	Stable isotope standards and capture by anti-peptide antibodies
SWATH	Sequential window acquisition of all theoretical fragment ion spectra mass spectrometry
TCEP	Tris(2-carboxyethyl)phosphine
TCPC	Total cavopulmonary connection
TCPK	L-(tosylamido-2-phenyl) ethyl chloromethyl ketone
THF	Tetrahydrofuran
Tris	Tris(hydroxymethyl)aminomethane
UHPLC	Ultra high-performance liquid chromatography
ULOQ	Upper limit of quantification
V	Volt
WHO	World health organization
XIC	Extracted ion chromatogram

1. Introduction

1.1 The physiology of active renin and prorenin

Renin was first extracted from rabbit renal tissue, discovered by Tigerstedt and Bergman in 1898, who identified the involvement of renin in blood pressure regulation by studying the effects of exogenous renin administration (Tigerstedt and Bergman 1898). Since then, the renin-angiotensin-aldosterone system (RAAS) has been identified, which represents a common drug target for the treatment of several diseases.

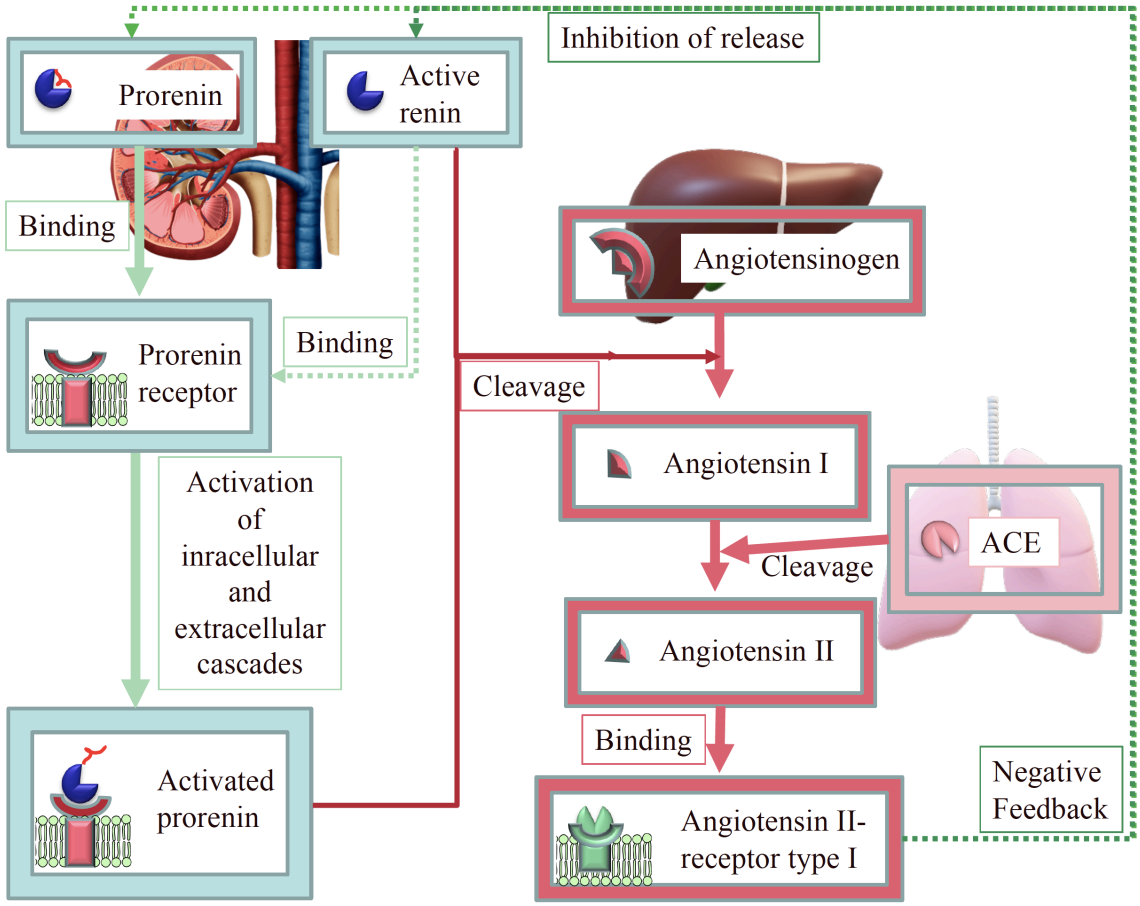

Figure 1-1 Modified RAAS *showing the role played by active renin role in the cascade and the activation of prorenin into a fully active enzyme. The active and bound prorenin can also initiate the classical RAAS, as shown on the left, while also inducing cellular activation, leading to fibrosis and cardiac remodeling like the angiotensin II-receptor type I's intracellular cascade (ACE: angiotensin-converting enzyme).*

The classic RAAS cascade begins with the enhanced release of active renin from juxtaglomerular cells. This enzyme cleaves a decapeptide (angiotensin I) with high specificity from angiotensinogen, which is released by the liver into blood plasma. The further processing

of angiotensin I into angiotensin II by angiotensin-converting enzyme (ACE) occurs in the lungs generates one of the most potent endogenous vasoconstrictors, angiotensin II (Schroten et al. 2012). The activation of this cascade improves blood perfusion in the kidneys and maintains kidney functions. In addition to the classical RAAS, the inactive precursor is also involved in angiotensinogen cleavage, which leads to the same cascade activation as active renin. This activation is triggered by the specific binding of prorenin to the prorenin receptor, which exists in both membrane-bound and soluble forms (Nguyen et al. 2002). Both pathways end with the activation of the angiotensin II-receptor type 1, which induces an intracellular response (Fig. 1-1).

Renin and prorenin are aspartic proteases with unique characteristics compared with other aspartic proteases, such as pepsinogen, which displays optimal activity under acidic conditions, whereas renin and prorenin display optimal catalytic abilities at pH 7.4 due to their residence in human plasma.

The synthesis of renin and prorenin occur primarily in the juxtaglomerular cells of the kidney, where the encoded DNA is transcribed into mRNA and translated by ribosomes into pre-prorenin, which is translocated to the endoplasmic reticulum and Golgi apparatus to undergo further maturation into prorenin through the cleavage of the signal peptide that was essential for translocation (Schweda et al. 2007) (Fig. 1-2).

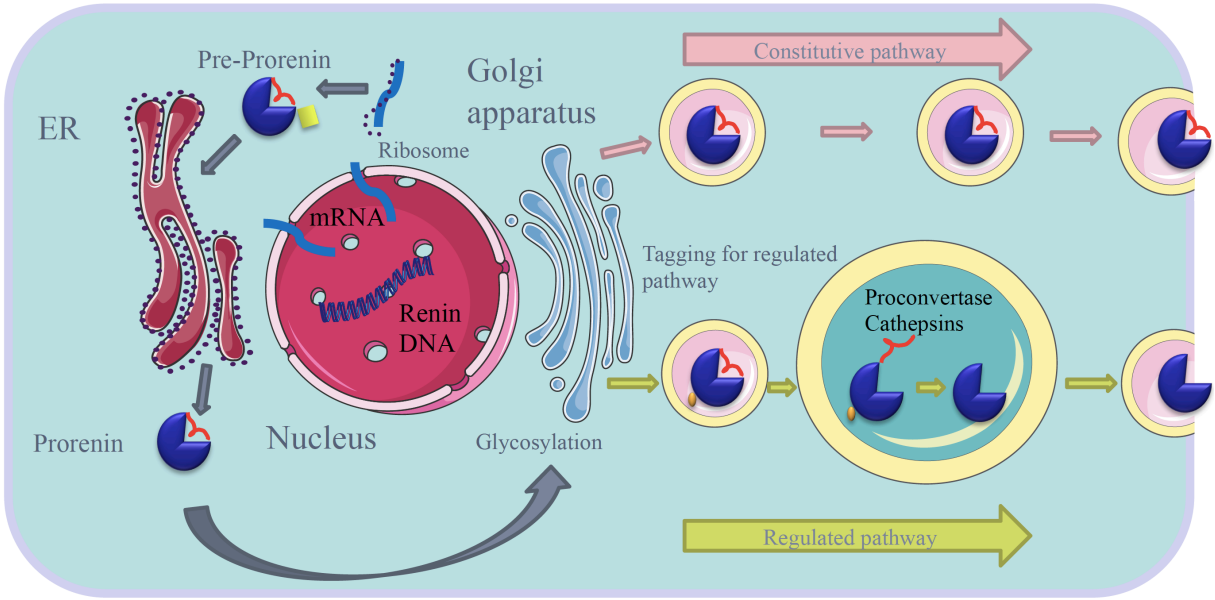

Figure 1-2 Renin and prorenin synthesis and release. *This figure was modified and recreated with permission from Schweda et al. (2007). Renin DNA is transcribed into messenger RNA (mRNA), which is then translated in the endoplasmic reticulum (ER) to form pre-prorenin. The cleavage of the signal peptide occurs after exiting the ER. In the Golgi apparatus, prorenin becomes glycosylated, which is essential for further processing. Although the unglycosylated prorenin is released directly into the bloodstream, the tagged prorenin is cleaved in dense-core vesicles, where a lower pH supports the pro-segment unfolding.*

Two amino acids (both asparagine residues) are found in the glycosylated form that act as a type of marker for the further cellular processing of prorenin to renin (Hsueh and Baxter 1991). The conversion from prorenin to active renin is not completely understood, but the activation can be performed by various enzymes found in lysosomes (Xa et al. 2014). Before cleaving the pro-segment, the 43-amino-acid-long polypeptide must be unfolded from the active site to allow for the steric accessibility of lytic enzymes to the pro-segment. *In vitro* studies have suggested that cathepsin B may represent a favorable candidate for prorenin activation due to its co-localization in lysosomes and their optimal proteolytical activity at pH 5 (Neves et al. 1996). Furthermore, kallikrein might also be able to activate prorenin, but this enzyme does not reside directly next to the juxtaglomerular cells; therefore, activation performed by this enzyme might occur during *ex vivo* reactions (Derkx et al. 1987b). Non-proteolytic activation represents another potential option of the *ex vivo* maturation of prorenin due to exposure to acidic environments or low temperatures (Pitarresi et al. 1992). Cold-induced activation, also known as cryoactivation, has been identified in stored blood plasma and might lead to the proteolytical conversion of prorenin into active renin by plasmin and kallikrein, which may be activated due to the inactivation of their inhibitory counterparts (Campbell et al. 2009).

The mature active renin consists of 340 amino acids, typically form β-sheet tertiary structures, contributing to the tight formation of two homologous lobes, which make mature renin very stable and resistant to proteolytic enzymes. In addition to fully catalytically active renin, prorenin, which still contains the pro-segment on the C-terminus that becomes folded in the mature form of renin, can also be released into the blood plasma (Sielecki et al. 1989) (Fig. 1-3).

After endogenous synthesis and processing, the juxtaglomerular cells secrete both active renin and prorenin, but the amount of active renin secreted by the juxtaglomerular cells represents only approximately 25% of the total renin concentration found in blood plasma (Schroten et al. 2012) (Fig. 1-2). In contrast to active renin, prorenin production is controlled by gene regulation and the chronic stimulation of the RAAS, which can also influence the conversion of prorenin to active renin. Prorenin can be secreted by other tissues, including the eyes, mast cells, ovaries, uterus, placenta, amniotic fluid, testis, and submandibular glands, which contributes to the 5 to 10-fold increased levels of plasma prorenin compared with active renin (Krop and Danser 2008; Sealey et al. 1986).

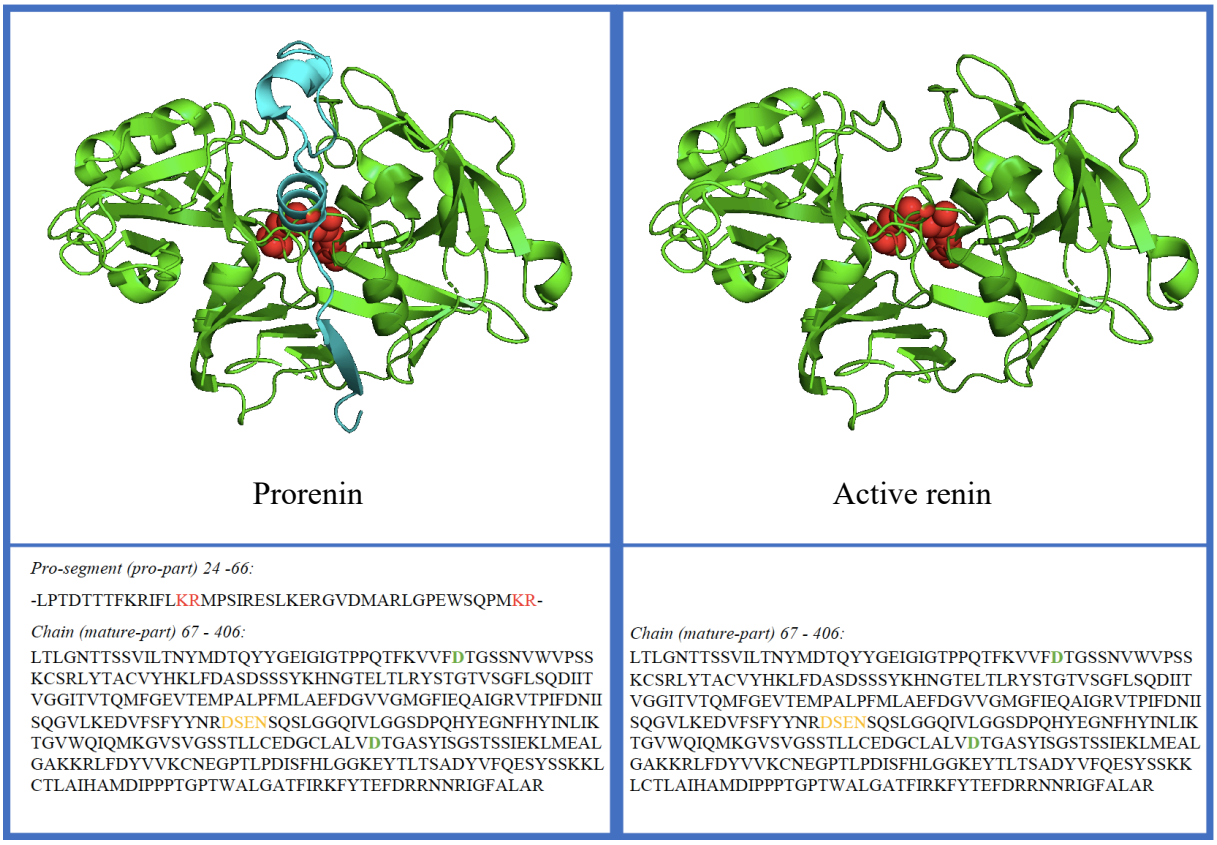

Figure 1-3 Amino acid sequences and 3D structures of prorenin and active renin *obtained from the UniProt database (Entry number P00797 RENI_HUMAN) and PDB databank (modified with PyMOL 2.2.1). The green 3D structure represents the mature part, whereas the light blue structure represents the pro-segment, and the red spheres show the catalytical center. The cleavage site of the pro-segment by prorenin processing enzymes is marked in red (two basic amino acids). Bold and green letters represent the active site (amino acids important for the catalytic conversion of angiotensinogen). Yellow letters represent the missing amino acids in the second isoform of the chain (mature-part).*

The secretion of prorenin and renin from the juxtaglomerular cells occurs through a special mechanism known as the 'calcium paradox.' Typically, vesicles open due to calcium influx, but in the case of prorenin/renin, the mechanism appears to operate in the opposite manner. Because renin is the key rate-limiting enzyme in the RAAS cascade, renin is regulated by a feedback mechanism involving angiotensin II, which is an end product produced by the renin cleavage of angiotensinogen. Angiotensin II can induce a calcium-influx, causing artery vasoconstriction and negatively regulating renin release. Additionally, the stimulation of prorenin and active renin secretion are also influenced by nitric oxide (NO), intrarenal arterial pressure, electrolytes, and β-adrenergic receptor action (Schweda et al. 2007).

Released prorenin and active renin may act as enzymes by cleaving angiotensinogen, resulting in increased blood pressure and water and electrolyte retention, which makes renin an attractive target for pharmacological intervention. However, these enzymes interact with their own receptor, called the prorenin receptor (PRR), which initiates the activation of specific intracellular cascades (Nguyen 2011). Although prorenin, but not active renin, appears to play

a role in pregnancy through interactions with female hormones (Derkx et al. 1987a), recent studies have also reported the ability of renin to interact with the immune system by cleaving the complement factor C3 (Trudu et al. 2013).

As the counterpart to secretion, the degradation of renin and prorenin is regulated by the mannose 6-phosphate receptor, which contributes to renin uptake by Kupffer cells in the liver and directs renin toward lysosomal degradation (Kim et al. 1988).

Many mechanisms that regulate renin release and activation remain unresolved and can affect the precise measurement of prorenin and active renin caused by the pro-segment. In addition to known uncertainties associated with the *ex vivo* processing of prorenin into active renin, the discovery of the prorenin receptor (PRR), which can also activate the catalytic properties of prorenin and can be found in both membrane-bound and plasma soluble forms, could also influence the precise determination of both proteins.

1.2 Plasma renin and prorenin are associated with cardiovascular diseases

The activation of the RAAS is a key element associated with heart failure diseases. Because the failing heart is unable to supply the body with sufficient blood and oxygen, the sympathicus attempts to compensate for the failing heart by releasing catecholamines and activating β-receptors on juxtaglomerular cells, which induces increased active renin synthesis and secretion into blood. In addition to β-receptor-triggered activation, the decreased blood is detected. Various health factors, including obesity and dilated cardiomyopathy, can also trigger the activation of the RAAS cascade (Rossano et al. 2016).
If the RAAS is continuously activated, pathophysiological processes evolve due to increased levels of vasoconstriction, resulting in permanent hypertension. Because the heart is then forced to pump against higher pressure, malignant structural changes, such as arterial stiffness and cardiac fibrosis, can occur (Jia et al. 2018).
Heart failure therapy typically targets various components of the RAAS, such as ACE-inhibitors (ACE-Is), which block the conversion of angiotensin I into the potent vasoconstrictor angiotensin II, and β-blockers are used to inhibit the complete activation of the RAAS. In response to ACE-I therapy, renin release increases in an attempt to compensate for the reduction in angiotensin II. Renin not only acts as an enzyme but also activates the prorenin receptor and initiates a signaling cascade that leads to hypertrophy and myocardial fibrosis (Fig. 1-4).

In the pediatric population, active renin has been identified at high levels in plasma after birth. The pathology of heart failure in children differs from that in adults, characterized by dilated, hypertrophic, and restrictive cardiomyopathies. Dilated cardiomyopathies are caused primarily by genetic disorders or are secondary to inflammatory diseases, such as myocarditis. In addition, malformations, such as left-to-right shunts, have been identified as the sources of cardiac malfunctions (Buchhorn et al. 2003; Lipshultz et al. 2019). During left ventricle dilation and systolic dysfunction, the heart is unable to supply the tissue with sufficient oxygen. The incidence of cardiomyopathies in children is estimated to be 1 case per 100,000 person-years (Lipshultz et al. 2019); however, the true prevalence remains unknown. As in adults, in children, the heart attempts to compensate for its inability to supply organs with oxygen, triggering neurohumoral and RAAS activation.
To counteract these worsening conditions, β-blockers, such as propranolol, have been demonstrated to be promising therapeutic alternatives. Neurohumoral activation becomes blocked, leading to decreased blood pressure due to the inhibition of β-receptors on the kidneys

and the heart (Buchhorn et al. 2001a). Further promising therapeutics include ACE-Is, which downregulate RAAS-associated pathophysiology. These drugs are widely used off-label because of a lack of studies performed in children. The treatment of pediatric heart failure by ACE-Is has been shown to have a beneficial impact, reducing mortality and morbidity (Momma 2006). The key enzymes prorenin and renin can worsen pediatric heart failure caused by continuously activated RAAS. Therefore, better understanding the physiological levels and maturation effects, in addition to disease-induced adaptations that occur in both proteins, may allow for the development of better therapeutic interventions.

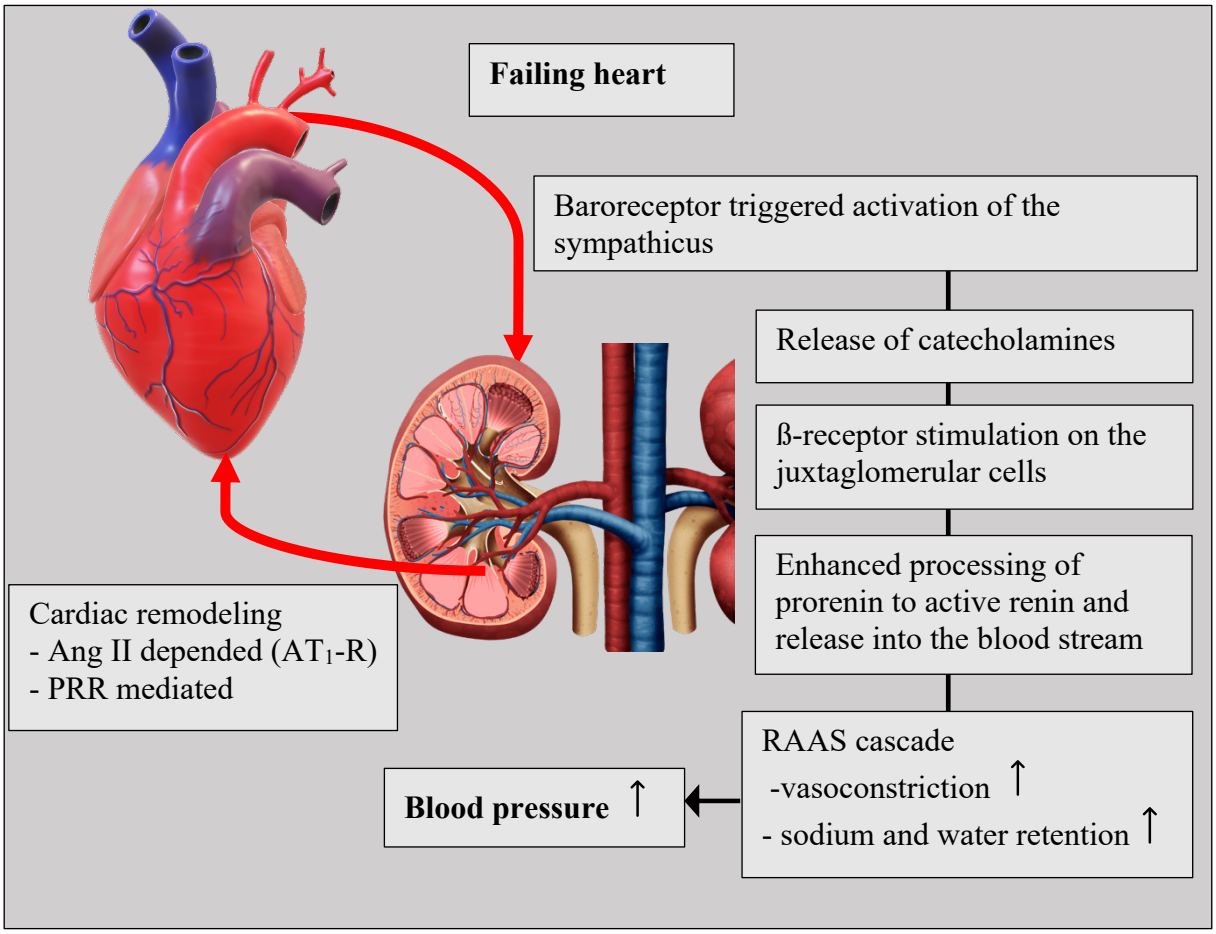

Figure 1-4 Illustration of heart kidney axis. *The failing heart induces several humoral effects, which affect heart hypotrophy and fibrosis (Ang II: angiotensin II; AT_1-R: angiotensin II receptor type I).*

1.3 Challenges in Pediatric research

Several obstacles must be overcome when conducting pediatric research; therefore, only limited studies have been reported investigating the humoral parameters of healthy and diseased children (Chiaruttini et al. 2018). The effects of a disease or its treatment on humoral parameters remain difficult to analyze, typically limited to the personal experience of experts and knowledge gained from animal studies (Tassinari et al. 2011). However, the pediatric population should not be viewed as 'small' adults because pediatric metabolism differs from that in adults. Pediatric ontogeny is marked by multiple stages, and various maturation processes must be considered if therapeutic or diagnostic procedures are necessary. Developmental changes are associated with alterations in the distributions of water and body fat. Higher extracellular water contents and lower body fat are characteristic immediately after birth, which changes with age until they reach similar percentages at approximately six months of life. Furthermore, the enzymatic capacity varies from the first hours and mouths after birth until 10 years of age. The different distributions of metabolizing enzymes affect the elimination of endogenous substances (e.g., bilirubin) and must be considered if drugs are administered. Additionally, renal function is not fully developed during early years, which affects the clearance capabilities of the kidneys. Only after the age of six do the kidneys become nearly completely developed and can be compared to adult organs (Kearns et al. 2003). Renal morphological changes occur during the first 35 weeks of gestation, including the development of additional kidney structures, known as nephrogenesis, which are essential for blood filtration and clearance. These maturation processes are strongly correlated with the glomerular filtration rate, which increases with age and blood pressure (Gomez et al. 1999). Gastrointestinal function shows a different ontogeny through changes in the secretion and production of gastrointestinal fluids and enzymes. Each stage of development is associated with a specific distribution of various factors and activities. For example, hydrochloric acid production remains low until adulthood, whereas bile acid secretion and glutathione conjugation have been measured at higher levels in some pediatric age groups than in adults. Furthermore, body composition also changes with maturation (Kearns et al. 2003).

The regulatory authorities typically subcategorize the developmental stages from neonates to adolescents into separate subgroups. Neonates are subset into pre-term and full-term neonates (0-27 days), whereas the older pediatric populations are subdivided into infants (1–23 months), children (2–11 years), and adolescents (12–18 years) (European Medicines Agency 2009). These subdivisions were defined by the European Medicines Agency (EMA) and regulate the

conductance of pediatric research. Only a few projects (e.g., Labeling enalapril from neonates to adolescents; LENA) have succeeded in collecting high-quality data for diseased pediatric collectives (Bajcetic et al. 2019; Feickert et al. 2020; Makowski et al. 2020).

Due to ethical constraints, the volumes of body liquids that are allowed to be sampled are limited. Because blood is the most important carrier of humoral parameters, and due to the potential, the pharmacokinetic effects of drugs during pharmacological interventions, constraints have been established to ensure patient safety. Limitations on blood volume collection are strongly correlated with patient risk and must be evaluated for each pediatric subgroup individually. To avoid any complications associated with blood withdrawal, illnesses should also be considered. Therefore, the limits for blood sampling have been established as 3% of total blood volume within a single month and at 1% for a single sampling (European Commission Expert group on clinical trials 2017). These constraints significantly narrow the bioanalytical measurements that can be performed, particularly if multiple time points must be analyzed to assess pharmacokinetic and pharmacodynamic parameters of drug treatments.

Small blood volume assays that use less than 50 µL or assays that allow the reuse of obtained plasma are important tools that must be developed to extract all necessary information regarding humoral and pharmacodynamic parameters for the assessment of drug efficacy and safety (Feickert et al. 2020). Because every pediatric subgroup has a limited withdrawable blood volume, and pediatric studies are typically only conducted once (European Commission Expert group on clinical trials 2017), specific and reliable assay procedures Are essential for ensuring the acquisition of meaningful data and better insights into disease, maturation, and physiology.

1.4 Bioanalytic methods for endogenous proteins

1.4.1 Ligand-binding assays in clinical assessments

Karl Landsteiner was the first to demonstrate that antibodies derived from immunized animals could be used to capture endogenous human proteins. Following this discovery, Rosalyn Sussman Yalow and Solomon Berson developed the first radioimmunoassay (RIA) in 1959, which allowed for the detection and quantification of human insulin (Yalow and Berson 1959). These findings were breakthroughs, enabling insights into various biological systems. The use of ligand-binding assays has rapidly gained importance for clinical applications.

This technology has evolved over time, and radioactive iodine was replaced with chemiluminescent chemicals and enzymatic reactions triggered by horseradish peroxidase, alkaline phosphatase, or glucose oxidase. Enzymes coupled with secondary antibodies are able to process a chemiluminescent substance, inducing the release of a photon that can be detected by a photometer (Lequin 2005), allowing for the use of enzyme-linked immunosorbent assays for a broad range of research and clinical purposes (Fig. 1–5).

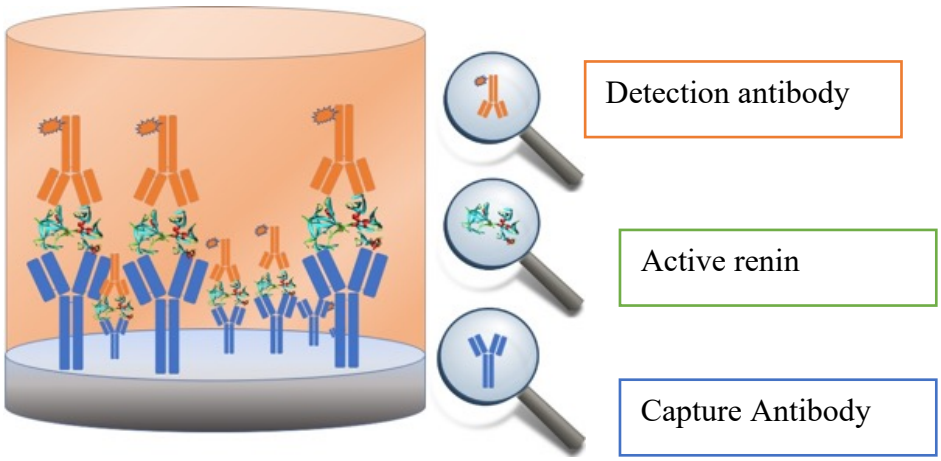

Figure 1-5 Illustration of a sandwich enzyme-linked immunosorbent assay *that can be used to quantify active renin using capturing antibodies for the affinity purification of active renin and the use of detection antibodies conjugated with horseradish peroxidase to catalyze a photometric rection.*

The development of an immunoassay is very costly and time-intensive and can take at least half a year. Because this technology has been applied for several purposes, various limitations have been identified, indicating that endogenous substances with similar structures cannot be differentiated, which can result in inaccurate results, including the false estimation of blood plasma concentrations. A good example of the cross-reactivity problems associated with active

renin immunoassays occurs when prorenin concentrations in plasma are especially high, as measured by Yoshida et al. (1,097 pg/mL), combined with a low level of active renin (12 pg/mL), as measured in patients with coronary artery disease (Yoshida et al. 2015). Because the typical cross-reactivity ranges from 0.4% to 0.7% (Bioassays 2016), in systems with high levels of prorenin, as much as 7.7 pg/mL of measured active renin could represent cross-reacted inactive prorenin, suggesting the potential for large overestimations of active renin in the presence of large concentrations of prorenin.

1.4.2 Liquid chromatography

The high-performance liquid chromatography (HPLC) technique has been used to separate chemical compounds with different physicochemical properties. Small molecules typically show a limited number of interactions due to their small sizes and limited chemical groups. In contrast, biological molecules, including peptides, occur in various sizes (based on the amino acid number) and feature various chemical subgroups, including amines, aromatic, carboxylic, aliphatic, hydroxy, and thiol groups (as amino acid side chains) that may occur in only one peptide, making chromatographic analysis challenging. In addition to various structural properties, many endogenous peptides are low-abundance peptides that can be enriched by HPLC.

A typical reversed-phased HPLC consists of two pumps, in which one pump delivers an aqueous solvent, referred to as mobile phase A, and the second pump delivers an organic solvent, described as mobile phase B. Both solvents pass through a degassing unit that eliminates gaseous bubbles. The pumps can be either isocratic or binary pumps. Isocratic pumps maintain a constant ratio between phase A and B during the measurement, whereas binary pumps allow for the programming of gradients to separate the analytes (Mladek and Kromidas 2014) (Fig.1-6).

Interactions occur between the stationary phase and the mobile phase. The stationary phase is essential to ensure the good retention of the molecule and is part of the column that is placed in an oven to regulate the temperature, which can also have a crucial impact on molecule retention. Commonly used columns include reverse-phase and stationary-phase columns (C18), which are suitable for peptides that contain lipophilic and hydrophilic residues. Various modifications of the reversed-phase and stationary-phase columns can allow for more selective separations, due to either ionic interactions (typically not suitable for MS analysis), van-der-Waals interactions, which occur with the lipophilic side-chains of the peptide, π-π-interactions with aromatic side-

chains, and size-exclusion stationary phases. Strong hydrophilic analytes require HILIC (hydrophilic interaction) column or norm-phase.

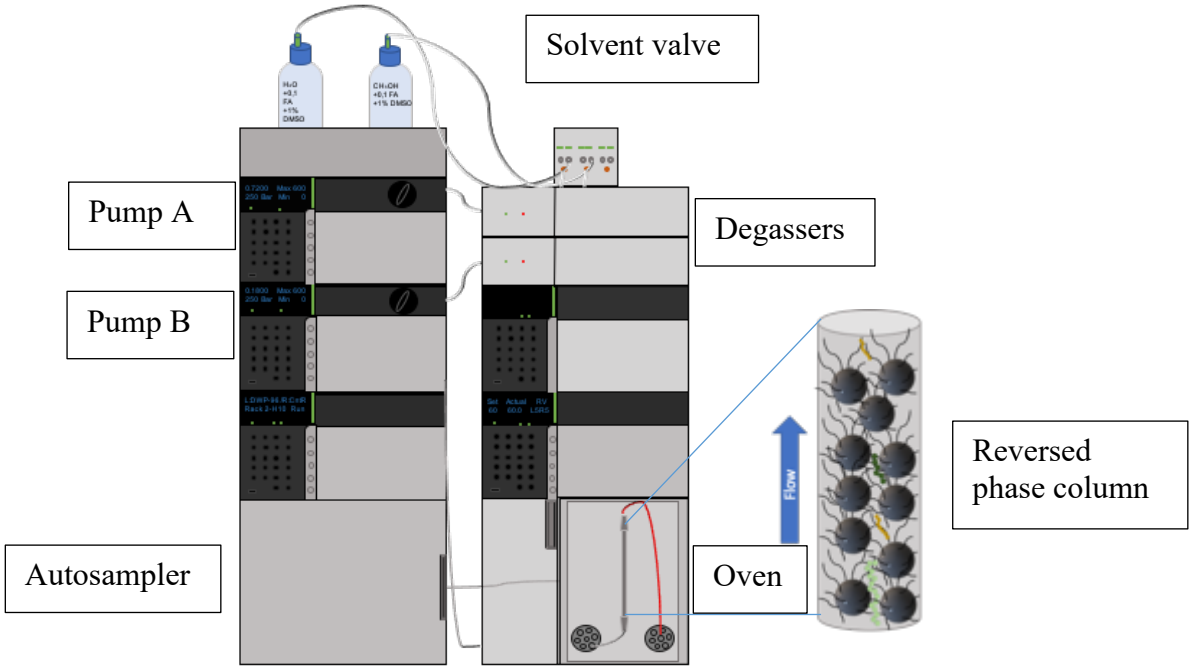

Figure 1-6 Example of an ultra-high-performance liquid chromatography setup. *Shimadzu UHPLC, consisting of two pumps, an autosampler, a solvent valve two degassers, and an oven with a reversed-phase column.*

1.4.3 Mass spectrometry

J.J. Thomas constructed the first mass spectrometer in 1910, laying the foundation of modern analytics, which allowed for the analysis of molecules according to mass and charge. The selectivity of this technique is due to collision-induced dissociation (CID), which produces a unique fingerprint of the parent molecule by fragmenting it into smaller molecules. Different types of mass spectrometers are available. The simplest mass spectrometer consists only of one quadrupole (Q_1), a source, and a detector, which allows for a precursor scan that analyzes the various mass to charge states of the analytes. Matrix-assisted laser desorption, coupled to a time of flight (MALDI-TOF) mass spectrometer, also displays unfragmented molecules. Collision cells are used for fragmentation (Q_2) and the generation of product ions, which specifies the precursor according to 'fingerprint,' based on specific fragmentation patterns.

A primary component of a mass spectrometer is the source, which ionizes molecules prior to entry into the mass spectrometer. Various techniques can be used, including chemical ionization (CI), MALDI, atmospheric pressure chemical ionization (APCI), and electrospray ionization (ESI) (Bhardwaj and Hanley 2014).

ESI represents a mild ionization procedure, which allows for the measurement of peptides and proteins. Before the development of ESI, most ionization techniques were too 'destructive' for biomolecule ionization. ESI is capable of ionizing even large molecules, allowing for intact proteins to be analyzed. The ESI source connects HPLC with the mass spectrometer. Ionization occurs under atmospheric pressure and is supported by the capillary voltage, temperature, and gases (Douglass 2014).

Tandem mass spectrometers have become important tools for routine analytics, especially the triple quadrupole (QqQ), which is applied to various approved regulatory methods.

In addition to typical QqQ mass spectrometers that are used during routine analyses, hybrid mass spectrometer, such as QTOFs, which utilize TOF instead of the Q_3, allows for the performance of proteomics experiments designed to identify new biomarkers with high mass accuracy (<5 ppm mass error). Especially in tryptic digestion experiments, these instruments facilitate the precise peptide mapping of the digested protein (Switzar et al. 2011).

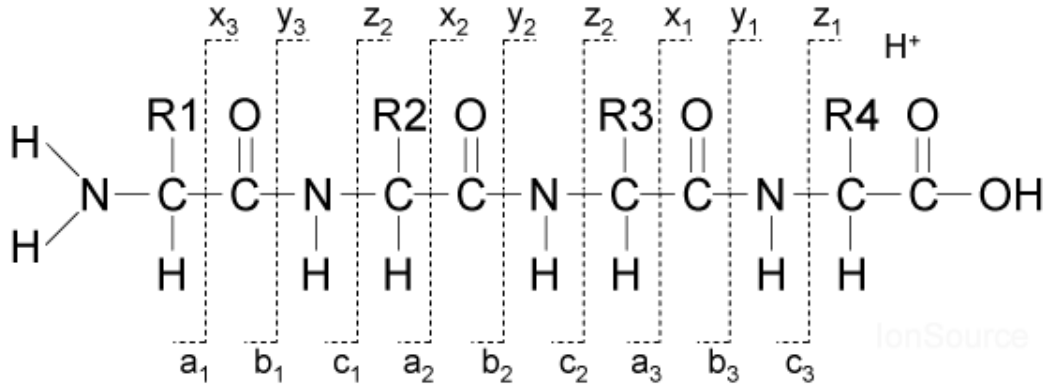

Figure 1-7 Illustration of a possible peptide fragmentation scheme following collision-induced dissociation *(CID) by Fohlman et al. The a, b, c fragments are derived from the amino terminus, and the x, y, z fragments appear from the carboxyl terminus. R_1, R_2, R_3, and R_4 represent different amino acid side chains.*

Peptides show specific fragmentation schemes under low-collision-energy conditions, which were described by Fohlman et al. (Roepstorff and Fohlman 1984) (Fig. 1-7). For peptides that are generated by tryptic digestion, the principal occurring fragments are y-ions, caused by positively charged amino acids at the carboxy-terminal end (Tang et al. 1992).

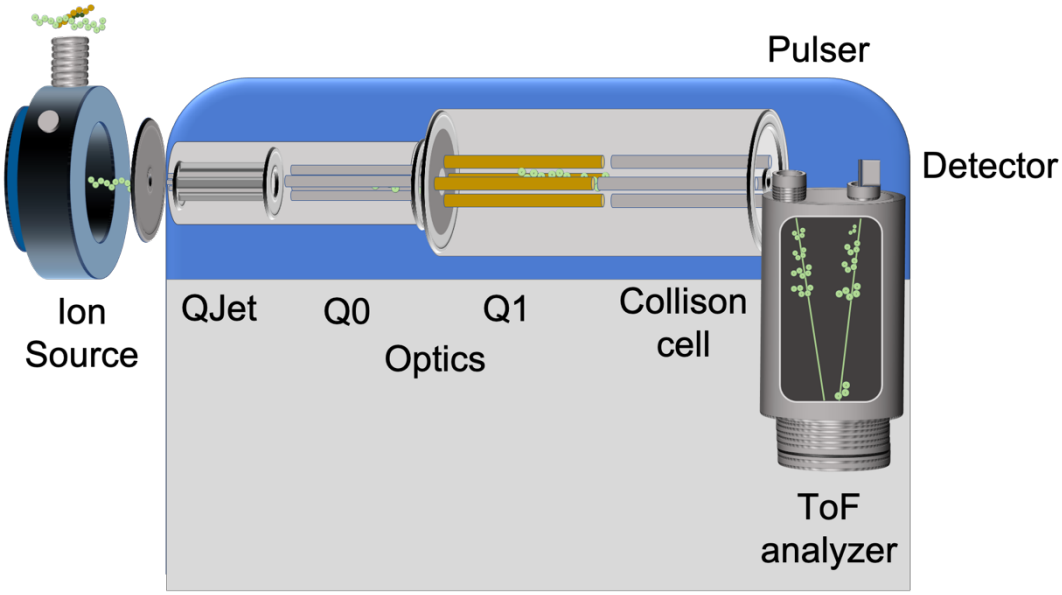

Figure 1-8 Graphical illustration of a high-resolution mass spectrometer. *Sciex TripleTOF 6600® with SWATH acquisitions and very high mass precision. This mass spectrometer consists of an ESI source for analyte ionization, a QJet, a Q_0 quadrupole for ion focusing, the Q_1 for mass filtering, the Q_2 as the collision cell for fragmentation, a time-of-flight mass analyzer, and a detector (ToF: time-of-flight).*

Collisions can be used for the de novo analysis of the amino acid peptide compositions. Additionally, the product ion mode consists of a narrow Q_1 window for a specific mass to charge units, which are then fragmented by the collision cell (Q_2), resulting in the production of ions that serve as fingerprints for a specific precursor.

Proteomic experiments performed to analyze the structures and sequences of multiple simultaneous proteins can be conducted using either data-dependent acquisition (DDA) techniques or data-independent acquisition (DIA) techniques. To perform DIA analysis, the tripleTOF (Fig. 1-8) can also be applied to SWATH (sequential window of all theoretical mass spectra) experiments, which can use the Q_1 mass filter to identify a window of mass ranges, which can be adjusted for each experiment. Fast scanning QTOF instruments allow for the rapid scanning of each sequential window, which fragments all precursors that enter the collision cell, followed by a time of flight mass analyzer, which processes the signal at a high resolution. These data can then be interpreted with the help of advanced software and libraries for the discovery of new proteins or peptide biomarkers (Ludwig et al. 2018).

This SWATH acquisition technique also allows for the modification analysis of one or two proteins by focusing on peptide mapping that involves modification to amino acid integrity or missed cleavages by the protease.

1.4.4 Protein analysis by hybrid ligand binding liquid chromatography coupled to mass spectrometry assays

Immunoassays show a good purification ability in complex matrix, they face the problem cross-reactivity caused by the detection part.

Another quantitative and qualitative method is offered by mass spectrometry. This technique which is usually coupled to high performance liquid chromatography allows a precise and specific measurement of analytes. To make proteins measurable by mass spectrometry requires a reliable sample preparation. Typical bottom-up determination of protein is described by a surrogate peptide approach which represents a part of a unique structure within the protein.

Protein analysis by liquid chromatography coupled to mass spectrometry is becoming an important tool for discovery and quantification. The current focus is not only set on developing analytical methods for therapeutic proteins (Peng et al. 2015; Iwamoto et al. 2016), but is also emerging in biomarker research (Torsetnes et al. 2013; Zhang et al. 2017).

Recent developments in the field of liquid chromatography coupled with mass spectrometry (LC-MS) empowers this technique for the detection and discovery of endogenous substances (Bringans et al. 2017). However, due to their high molecular weight, most endogenous proteins can only be identified by mass spectrometry following proteolytic digestion (Fig 1-9). While there have been successes in the quantification of high-abundance proteins by using e.g. protein-cleavage isotope dilution mass spectrometry (PC-IDMS) (Keith Williams and Muddiman 2009; Pan et al. 2010; Loziuk et al. 2013; Andrews Kingon et al. 2013), the direct determination of low-abundance proteins by LC-MS remains challenging (Pan et al. 2010). The complexity of the digested sample results in substantial matrix effects, causing ion suppression that subsequently impedes the reliable determination of physiological concentration levels of low-abundance proteins (Picotti et al. 2007). Combining the advantages of immunoassays and LC-MS appears to be a promising tool in overcoming this obstacle (Ackermann and Berna 2007). Using immunocapture before LC-MS detection is known as a hybrid approach which is interposed with proteolytic digestion when it comes to the measurement of proteins instead of peptides.

Two approaches are feasible at this stage. The first approach is known as SISCAPA characterized by initial digestion followed by the addition of stable isotope-labeled peptide of the unique surrogate before immunocapture (Anderson et al. 2004), while in the second procedure the complete protein antigen is captured before digestion. While the first approach requires the availability of expensive, individually developed and high-affinity antibodies against cleaved surrogates and their isotope-labeled standards, the second approach is less

expensive and can be established by applying commonly available antibodies against full-length proteins (Nelson et al. 2004; Nicol et al. 2008; Kilpatrick and Bunk 2009). This is advantageous, as the downstream protease cleaves only the captured protein into smaller peptide surrogates, and not the entire matrix. However, the process becomes more challenging if the protein of interest is resistant to cleavage by proteases.

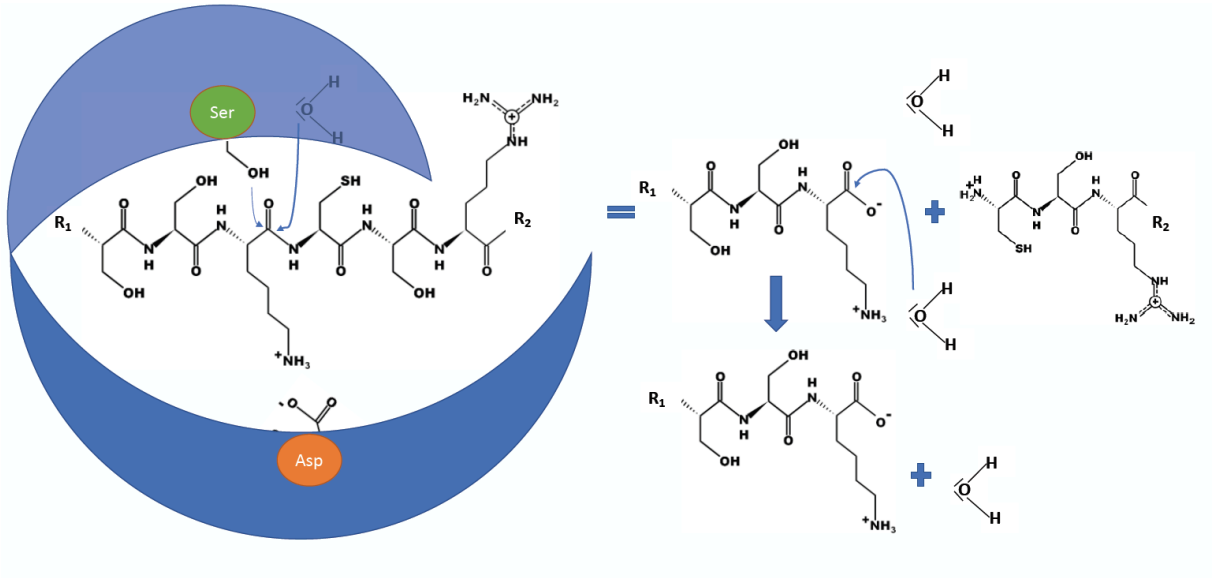

Figure 1-9 Proteolytical digestion of a renin by the serine protease trypsin *which cleaves after lysine and arginine residues by incorporating water via nucleophilic addition followed by a breaking peptidyl bond. The aspartic acid residue is essential to bind the lysine via ionic interaction while the serine residue is important to catalyze the carbonyl group and allow a nucleophilic addition of water (blue: trypsin; R_1: protein chain 67-113; R_2: protein chain 120-406; Ser: serine; Asp: aspartic acid).*

1.4.5 Internal Standard

Every analytical procedure is associated with variations caused by differences in sample pretreatment and sample storage, including LC and MS. To avoid assay imprecision, a standard must be applied throughout the analysis.

An internal standard is an important analyte which can be used to normalize variations introduced by differences in assay procedures or environmental factors. Internal standards are typically either stable isotope-labeled internal standards (SIL-ISs), which are recommended by FDA guidelines, or structural analogs. The optimal internal standard is a SIL-IS, which displays the same physicochemical properties as the analyte being quantified. In the case of small molecules, a deuterated internal standard is widely applied and has been shown to be useful in a variety of quantitative assays. Deuterated internal standards for larger molecules, such as proteins and peptides, are not suitable due to possible proton exchanges, and in the case of multi-deuterated peptides, can impact LC by shifting the retention time. Multiple approaches have been considered feasible for synthesizing or generating internal standards for use during peptide and protein analyses.

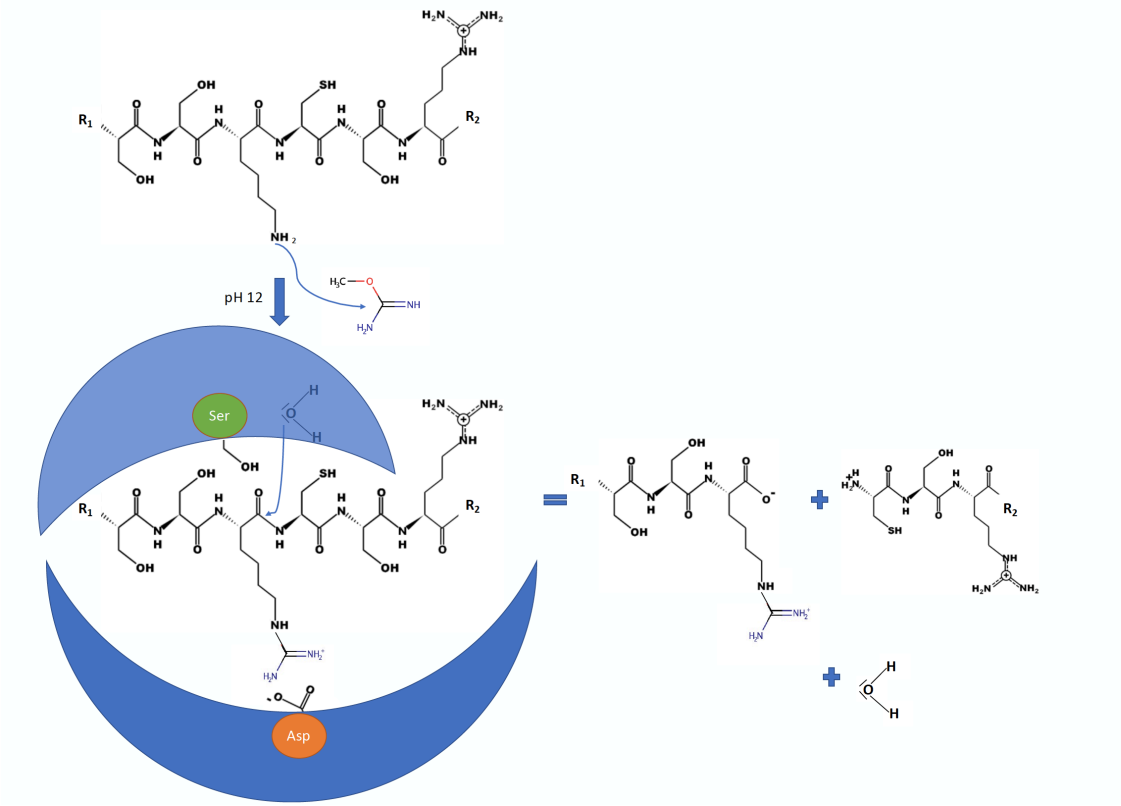

Figure 1-10 Guanidation of renin's lysine residues, utilizing O-methylisourea and alkaline media. *The lysine residues react with O-methylisourea to a structure called homoarginine, which induces a mass increase of 42 Da. Proteolytical cleavage is also performed with trypsin. The aspartic acid residue binds to homoarginine via ionic interactions (blue: trypsin; R_1: protein chain 67-113; R_2: protein chain 120-406; Ser: serine; Asp: aspartic acid).*

However, when a hybrid assay is performed that relies on immunoaffinity as the first purification step, the optimal internal standard is a heavy-labeled protein with incorporated nitrogen (^{15}N) or carbon (^{13}C) isotopes. However, despite the benefits of such an internal standard, the production of labeled full-length proteins is currently limited and costly. Another option, described by Yang et al., utilized O-methylisourea for the guanidation of a protein's lysine residues into homoarginine (Yang et al. 2014). However, long reaction periods and the need for harsh chemicals, such as NaOH, might destroy the protein structure. In addition to causing potential stability issues, the complete guanidation of all lysine residues may not be possible due to accessibility problems (Fig. 1-10).

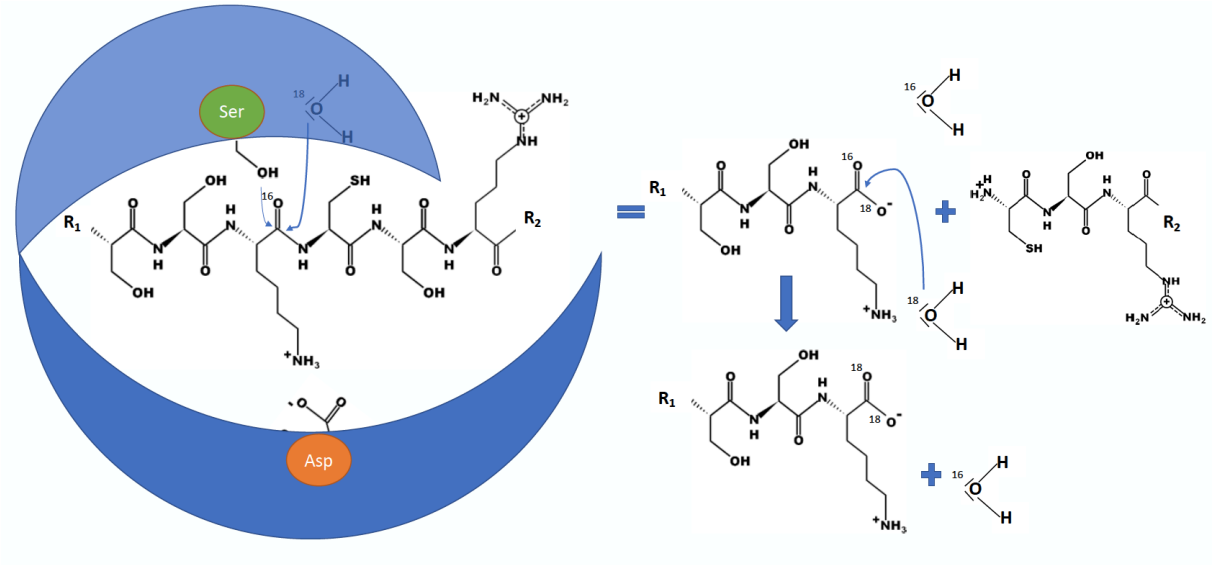

Figure 1-11 Proteolytical cleavage of renin and the labeling of the C-terminal ^{18}O carboxy group *with the help of trypsin during proteolytical cleavage. The aspartic acid residue is essential for binding the lysine via ionic interaction (blue: trypsin; R_1: protein chain 67-113; R_2: protein chain 120-406; Ser: serine; Asp: aspartic acid).*

As a more 'affordable' labeling procedure, the use of ^{18}O-water can be used to incorporate one or two ^{18}O molecules into the c-terminal carboxyl group of lysine, using trypsin, resulting in a mass shift of 2 Da, if one ^{18}O is bound to the carboxy structure, or 4 Da if two ^{18}O are integrated (Havliš and Shevchenko 2004). In addition to the enzymatic integration of the ^{18}O-isotope, acidic conditions obtained through the use of hydrochloric acid can also be used to promote the incorporation of ^{18}O into carboxy groups under cool conditions (15°C) (Havliš and Shevchenko 2004) (Fig. 1-11).

1.5 Design of experiments in LC-MS applications

LC and MS are dependent on several settings that can impact instrument performance and contribute to signal intensity. The effects of specific settings are even more pronounced when these techniques are applied to the quantification of low-abundance proteins. Investigating only one factor at a time (OFAT) or one variable at a time (OVAT) might not lead to the identification of an optimal outcome because both individual effects and also interactive effects must be considered, which are unlikely to be discovered by adjusting single factors while leaving the others unchanged (Hecht et al. 2016; Ganorkar and Shirkhedkar 2017) (Fig. 1-12). Statistical experimental design allows information to be obtained while performing fewer experiments, which is referred to as the 'Design of Experiments' (DOE) approach. The 'Design of experiment' term was first described by Fisher in 1937, based on his primary work examining statistical methods in 1925. However, the idea originates from the agricultural field, introduced by John Lawes when he analyzed artificial fertilizer in 1843. After gaining the industry's attention, DOE approaches have been integrated into industrial and manufacturing production development, leading to new methods, including response surface modeling and design optimality (Niedz and Evens 2016). The further development of DOE models has made this statistical approach accessible to research through the use of powerful computers.

The DOE approach is implemented into the Quality by Quality (QbD) approach, which is also part of 'Good Manufacturing Practice' (GMP). Recent drafts for DOE implementation have been included in Bioanalytics by USP and ICH.

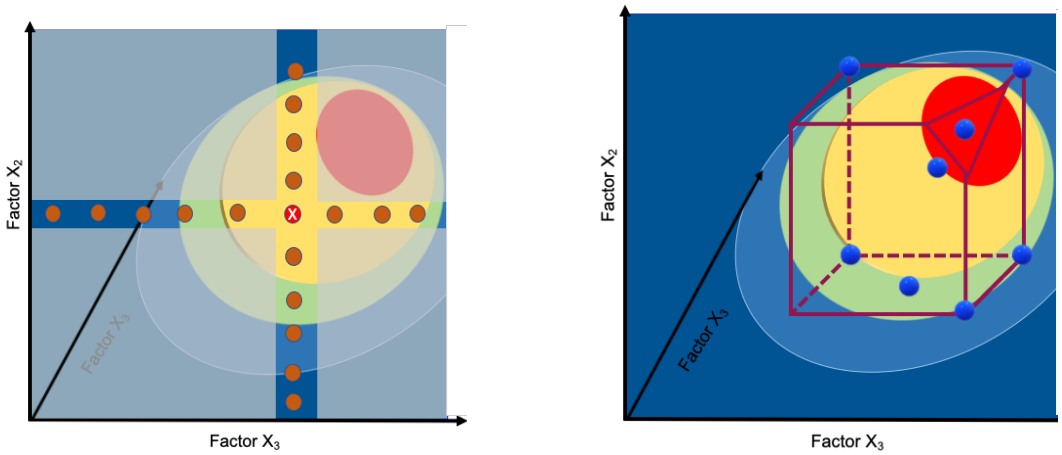

Figure 1-12 Comparison of One factor at time approach vs. exemplary DOE D-optimal model. *The OFAT approach does not yield the 'best' optimum approaches, whereas the DOE experiments show the best outcome (the figure was recreated with the permission of catalysisconsulting.co.uk).*

1.5.1 Full factorial model

Depending on the number of factors and their distributions, the choice of suitable DOE models is essential for a reliable outcome. If the knowledge of a factor's impact is limited, a standard screening model may be performed. The estimated number of experiments is equivalent to 2^k runs, where k represents the number of enclosed factors, which represents a full factorial design (Fig. 1-13). This orthogonal model uses lower and upper levels in the design matrix to investigate crucial parameters.

	FACTOR 1 (X_1)	FACTOR 2 (X_2)	FACTOR 3 (X_3)
1	-1	-1	-1
2	+1	-1	-1
3	-1	+1	-1
4	+1	+1	-1
5	+1	-1	+1
6	+1	-1	+1
7	-1	+1	+1
8	+1	+1	+1

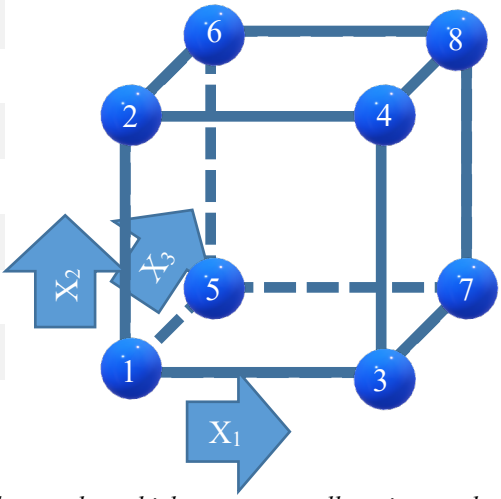

Figure 1-13 Example of a full factorial design matrix *shown by a cube, which represents all settings to be analyzed, which may influence the response (k=3; simple illustration without replicates).*

This model is used to investigate potential factors that affect the chosen responses. Additionally, a center point, which is typically a known condition, is added, and all experiments should be performed in replicate to ensure good reproducibility (Triefenbach 2008).
The resulting yield (Y) that is affected by the coefficient β can be illustrated using the following formula:

$$Y = \beta_0 + \beta_1 X_1 + \beta_1 X_1 + \beta_2 X_2 + \beta_3 X_3 + \beta_{12} X_1 X_2 + \beta_{23} X_2 X_3 + \beta_{123} X_1 X_2 X_3 + \epsilon$$

Equation 1-1 Calculation for full factorial yield *calculated by the addition of the product of coefficient β multiplied by the factor X.*

1.5.2 D-optimal model

After investigating possible interactions, response surface modeling can then be used to perform method optimization. For example, if a process consists of 5 factors, a full factorial design would result in 2^5 = 64 + 3 center points = 67*3 (if each condition is measured in triplicate) = 201 total experiments. Computer-based design, such as the D-optimal design, allows for the generation of model experiments that may be difficult to investigate using standard models. Depending on the experimental educts, this approach could result in a costly investigation. Therefore, a D-optimal model represents a superior alternative for the analysis of an optimal setpoint. The same process can be analyzed by 90 experiments and save material. This model also generates investigative points between the limits and center points given by the processes (Fig.1-14). Another benefit to the use of D-optimal design is that both quantitative and qualitative factors influence the response(s), which may result in certain enzyme activity being difficult to investigate using linear models because their activity optima might have a very narrow parameter setting; therefore, a D-optimal model is a good choice.

	FACTOR 1 (X_1)	**FACTOR 2** (X_2)	**FACTOR 3** (X_3)
1	-1	-1	-1
2	+1	-0.5	-1
3	-1	+1	-1
4	+1	+0.5	-0.5
5	+1	-1	+0.5
6	+1	-1	+1

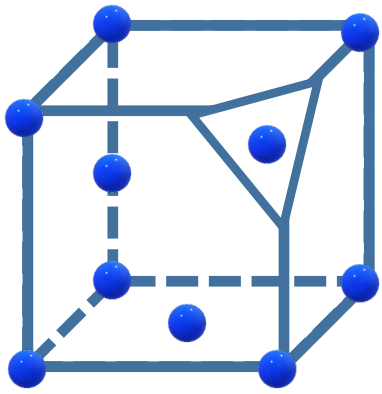

Figure 1-14 Example of a D-optimal design matrix *generated by a computer algorithm with a reduced number of experiments (simple illustration without replicates).*

The D-optimal analysis uses a quadratic variable, which is shown in the formula below:

$$Y = \beta_0 + \beta_1 X_1 + \beta_1 X_1 + \beta_2 X_2 + \beta_3 X_3 + \beta_{11} X_1^2 + \epsilon$$

Equation 1-2 Calculation for D-optimal response surface yield *calculated by the addition of the product of coefficient β multiplied by factor X and the quadratic term X^2.*

To estimate the model quality before performing the experiments, G-Efficiency is used, which compares the calculated D-optimal model to a full factorial design. Values above 0.6 indicate a high-quality model (Equation 1-3).
Another parameter is the condition number, which evaluates a model's sphericity and symmetry (Triefenbach 2008; Ganorkar and Shirkhedkar 2017).

$$G_{eff} = 100\% \times \left(\frac{p}{n \times d_{\max}(X)}\right)$$

Equation 1-3 Calculation of the G-Efficiency*; p is the number of coefficients; n is the number of runs, d_(max)is the largest variance prediction, and X is the model matrix (Eriksson et al. 2008).*

The regression fit is performed by using multiple linear regression (MLR) or partial least squares regression (PLS), depending on the model and the responses. The results are fitted into the applicable model, and an estimation of model validity, referred to as the goodness of fit analysis, is determined by calculating an R^2 value to estimate the model fit and a Q^2 value to appraise the predictive power of the model. Overall, the difference between R^2 and Q^2 indicates whether a design is appropriate.

In summary, the chemometric approach may be used to improve assay procedure steps, such as sample pretreatment (denaturation, alkylation, and tryptic digestion), accelerating proteolytical cleavage, the evaluation of the peptide suitability for quantification purposes, and instrumental setting optimization to achieve the most robust method and high sensitivity. The benefit to protein analytics is a manageable number of experiments and increased knowledge regarding protein characteristics and behaviors under various conditions.

1.6 Objectives

The overall aim of this thesis was to develop a reliable assay to determine the plasma concentration of prorenin and active renin using a hybrid approach to overcome the limitations of immunoassays, which represent the current state-of-the-art for routine analyses here.

First, current knowledge regarding plasma prorenin and active renin concentrations associated with cardiovascular and diabetes-related diseases had to be compiled through a systematic literature review. The main focus was to examine existing knowledge regarding the plasma levels of these proteins in children, who are characterized by large variations dependent on many factors, including age. The applied bioanalytical procedures should also be summarized and analyzed to identify the advantages and disadvantages of all currently utilized approaches (chapter 2; pp.25-43).

Second, the development of a hybrid immunocapture LC-HRMS assay for human renin should overcome the limitation associated with known cross-reactivity in immunoassays. Therefore, a sub aim was the development of an assay that could be applied to routine laboratory testing strategies to allow the implementation of a lean and an easy-to-apply procedure (chapter 3; pp.43-67). Further development included the selective quantification method for prorenin determination by LC-HRMS, which needed to be able to differentiate between active renin and prorenin. Optimizations had to be performed to confirm that endogenous levels of both proteins were measurable (chapter 4; pp.68-98). The applicability of the established assay should be verified to affirm the accuracy and precision of the hybrid approach (Fig.1-15; chapter 5; pp.99-113).

By addressing the above-mentioned objectives, the determination and differentiation of prorenin and active renin by the aimed assay will facilitate the role and effect of ‘true’ active renin in diseased and healthy populations. Additionally, the role of prorenin and active renin’s ratio can be investigated by this assay for evaluating its diagnostic value.

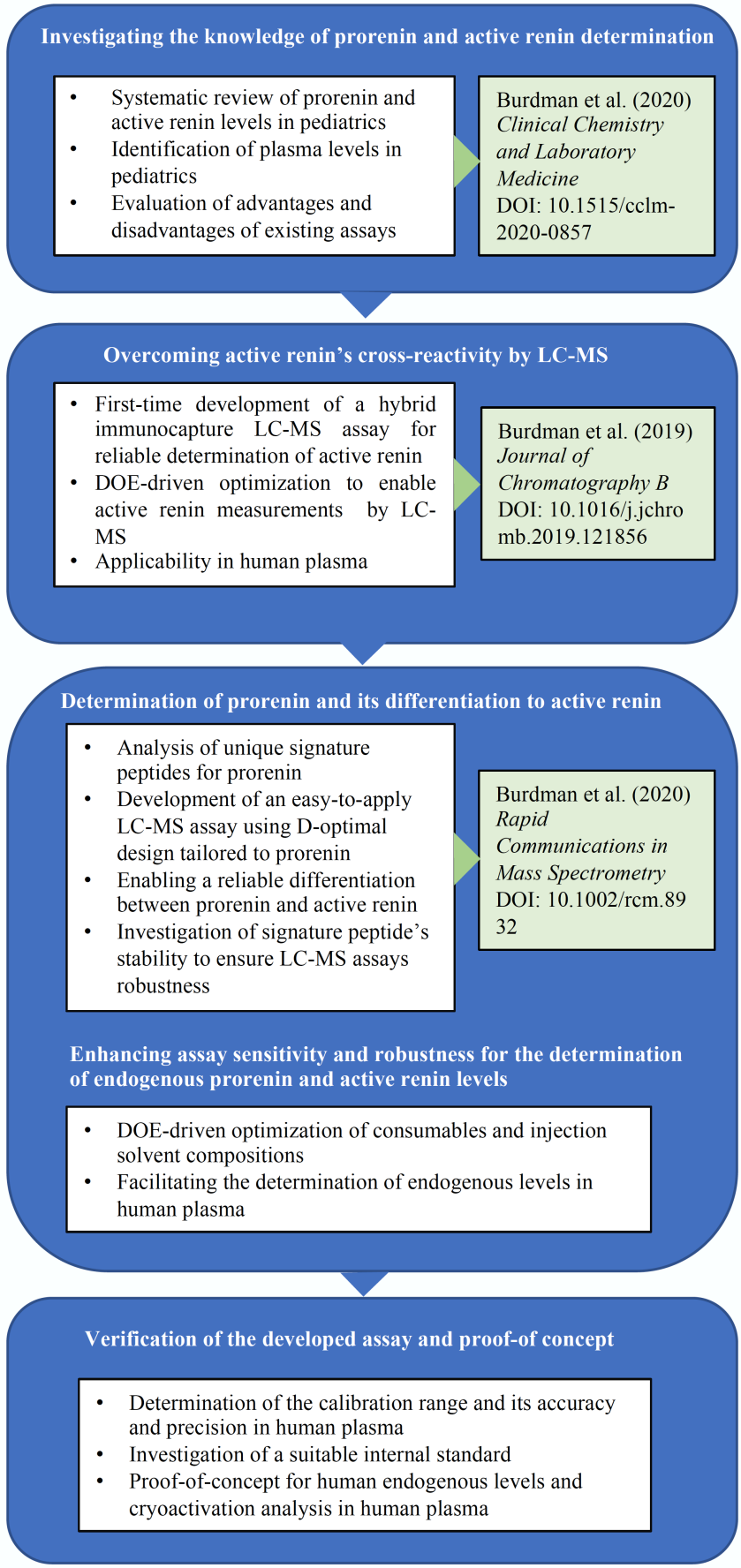

Figure 1-15 Overview of the objectives *(LC-MS: liquid chromatography coupled to mass spectrometry; DOE: design of experiments; DOI: digital object identifier).*

2. Prorenin and renin levels in pediatrics: a bioanalytical review

This chapter had been published in the peer-reviewed journal: 'Clinical Chemistry and Laboratory Medicine' with the title 'Prorenin and active renin levels in paediatrics: a bioanalytical review.' (doi: 10.1515/cclm-2020-0857).

2.1 Background and aim

Renin is a key enzyme in the renin-angiotensin-aldosterone system (RAAS) cascade. It initiates the system by cleaving the liver-produced angiotensinogen to angiotensin I, which itself is converted to angiotensin II by angiotensin-converting-enzyme. The octapeptide angiotensin II is a strong vasoconstrictor that, for example, elevates blood pressure by activating the AT1-receptor. However, the RAAS not only influences blood pressure and electrolyte homeostasis but also promotes maturation of the kidney as well as cardiac remodeling (Schroten et al. 2012). Apart from its proteolytic activity, renin has recently been the focus of research as receptor substrate that activates intra-cellular cascades via the (pro)renin receptor (Nguyen 2011).

Owing to its central functionality, altered renin levels are associated with a broad range of diseases. Low plasma renin levels are associated with primary hyperaldosteronism (Berge et al. 2015), whereas renin levels were found to be elevated in patients with cardiovascular diseases (Tomaschitz et al. 2011) and liver cirrhosis (Paternostro et al. 2017) or extremely elevated in renal cancer diseases including Grawitz tumor, Wilms tumor and pheochromocytoma (Maas et al. 2007; Stoicescu et al. 2011). Correlation of renin levels with disease has been primarily shown in adults and data in children is limited. The limited understanding of renin levels in children also indirectly highlights the limited knowledge about the RAAS in children.

Compared to the catalytically-active renin, prorenin (the precursor of active renin) circulates in plasma at a five- to ten-fold higher concentration (Ichihara et al. 2009). Prorenin is differentiated from renin by a 43 amino acid pro-segment, which covers the catalytic site. Prorenin has been reported to have opposing characteristics, with either direct vasodilative properties, or contrary functions (such as cardiac remodeling) due to its binding to the prorenin receptor (Schroten et al. 2012). In adults, an increased prorenin level is assumed to correlate with microvascular diseases caused by diabetes mellitus (Nguyen et al. 2014). Prorenin's function in the RAAS remains incompletely understood, and has been barely investigated in the pediatric population.

Moreover, the available data for both proteins in the pediatric population is rare and inconsistent, which highlights the need for a comprehensive evaluation of the maturing RAAS to facilitate future progress in pediatric care in all age groups. This review aims to illustrate the current knowledge of prorenin and renin levels in healthy and diseased children.

2.2 Methods: Literature search conducted

A literature search was performed in accordance with the PRISMA statement (Fig. 2-1) and focused on bioanalytical measurements in plasma, excluding tissue level estimation. The search was conducted in the MEDLINE database via PubMed and Google Scholar between December 2019 and April 2020. Overall, 213 findings were screened of which 15 publications were finally classified as relevant for this review. The population of interest were children from the neonatal stage up to adolescence. Studies that reported plasma prorenin, measured directly or indirectly, and plasma active renin concentration were included. Studies presenting solely plasma renin activity was excluded from this review. Further publications, which reported plasma renin values but used unselective immunoassays unable to distinguish between prorenin and renin, were also excluded.

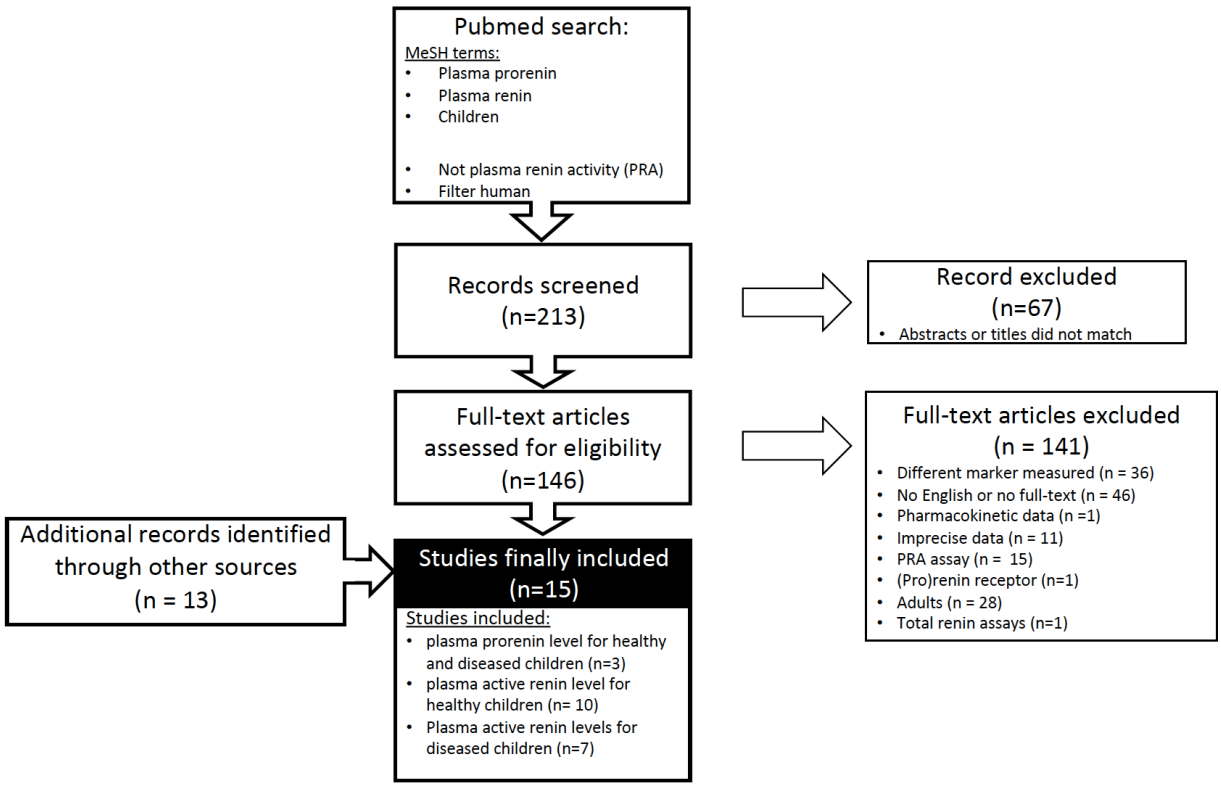

Figure 2-1 PRISMA scheme of the conducted literature search for active renin and prorenin levels in pediatrics.

2.3 Results and Discussion

2.3.1 Bioanalytical determination of renin and prorenin

Bioanalytical investigations of active renin and prorenin levels have historically been performed by immunoassay. Current immunoassays quantify active renin directly using antibodies targeting the catalytic active site (Campbell et al. 2009). However, differentiation between renin and prorenin is still challenging due to their similarity. Inappropriate sample handling procedures have been reported to result in catalytic or non-catalytic activation of prorenin, making a spurious detection by renin-specific antibodies possible (Campbell et al. 2009).

Nevertheless, the direct renin assay is frequently used intentionally for prorenin quantification by unfolding the pro-segment and allowing the renin antibody to bind at the active site (Tu et al. 2012). Therefore, the concentration of prorenin can be determined by three different techniques:

1. Indirect determination with an immunoassay targeted against active renin, with an initial measurement of plasma active renin level followed by the catalytic activation of prorenin by incubation with immobilized trypsin at 4 °C for 72 h. A second assay then determines the level of prorenin in its captured activated form (Campbell et al. 2009).
2. Indirect determination by renin inhibitor (aliskiren or remikiren) treatment for 24 or 42 h at 4 °C, which leads to the unfolding of the pro-segment. After the first and second pre-treatment, open prorenin is determined as ‘active renin’ and calculated back to determine prorenin concentration.
3. Direct prorenin estimation, using a selective antibody against the pro-segment (Krop et al. 2011). This allows direct measurement of prorenin by antibodies that capture the unique regions of prorenin without prior catalytic conversion.

In studies estimating pediatric prorenin level, immunoradiometric assays from the Nichols Institute were widely used (Tables 2-2, 2-3, 2-4). These assays used antibodies against either the catalytic site of active renin or the open form of prorenin. As described above, the measurement of inactive prorenin was achieved by a prior activation to active renin with trypsin (Campbell et al. 2009) which allowed prorenin levels to be calculated by subtraction of active renin from total renin. This method is very time consuming (incubation at 4 °C overnight), and can lead to stresses on the samples and inaccurate measurement due to possible degradation of the active renin form.

Aliskiren induced prorenin activation is more beneficial because the pre-treatment procedure is shorter (48h) compared to trypsin activation (72h) (Krop et al. 2011). Additionally, a potential degradation which is also described in the literature of the mature part of renin can be avoided by using aliskiren instead of trypsin (Blazy et al. 1989). In contrast, the benefit of trypsin activation, compared to aliskiren, is that it does not affect the immunoreactivity of active renin (Krop et al. 2011). Typical assay duration was from 1h (direct prorenin ELISA) to 5h (Diagnostic Pasteur) and 24 h for the Nichols Institute assay (Table 2-1).

High procedure periods were shown to promote prorenin unfolding and subsequently the risk of false detection of prorenin as active renin. The Nichols assay had a duration of 24 hours which shows also the highest cross-reactivity to open form prorenin issued by the unspecific capturing antibody. By using specific antibodies for capturing and detection the prorenin unfolding might be avoided leading to more precise measurements.

The direct active renin assays report a very low cross-reactivity if exogenous prorenin is spiked to the sample. Nevertheless, even if the detection of the prorenin form by the assay is low, it can still lead to inaccuracies due to the higher abundance of prorenin compared to renin (five- to ten-fold in healthy adults). Abundance of prorenin is especially elevated in the diseased population. For example, a study conducted by Yoshida et al. measured a high level of prorenin in plasma (1097 pg/mL) and a low level of active renin (12 pg/mL) for patients with coronary artery disease (Yoshida et al. 2015). A typical cross-reactivity ranges from 0.4% to 0.7% (Bioassays 2016) which would mean that 7.7 pg/mL of the measured active renin is the inactive prorenin. Compared to the estimated renin levels, more than half of the active renin could be measured inaccurately by overestimating the correct value.

The comparability of these three possible methods to determine prorenin level is debatable, as they have different assay procedures and different reactants within the assay kits including calibration standards. The applied standards being used to calibrate the assays differ substantially as a WHO standard for human prorenin is currently lacking. The lack of standardization leads to quantification differences with a magnitude up to 10-fold (Krop et al. 2011).

Table 2-1 Immunoassay applied for the determination of active renin and prorenin within the identified pediatric studies. *Immunoassay applied for the determination of active renin and prorenin within the identified pediatric studies (IRMA: immunoradiometric assay; ELISA: enzyme-linked immunosorbent assay).*

Immunoassay	Assay type	Capture antibody	Detection antibody	Detection	Range, pg/mL	Cross-reactivity (prorenin)	Duration, h	Sample volume, µL
Active renin (Diagnostic Pasteur)	IRMA	Renin and prorenin	Catalytic site of active renin	Radioisotopic	0–640	n.a.	5	250
Active renin (Nichols Institute)	IRMA	Renin and prorenin (biotin labelled)	Catalytical site of active renin	Radioisotopic	0–900	0.3–2%	24	200
Active renin (DSL 25100)	IRMA	n.a.	n.a.	Radioisotopic	5–500	n.a.	3	200
Active renin (Renin III generation kit, Cisbo)	IRMA	Renin and prorenin	Catalytic site of active renin	Radioisotopic	1–320	0.4%	3	300
Active renin (Sanofi diagnostic Pasteur)	IRMA	Not specified	Not specified	Radioisotopic	5–300	n.a.	5	300
Prorenin (Molecular Innovation)	ELISA	Specific for prorenin	Specific for prorenin	Photometric	20–10,000	n.a.	1	100

IRMA, immunoradiometric assay; ELISA, enzyme-linked immunosorbent assay; n.a., not available.

In the past, sample handling had also been described as a crucial aspect for reliable quantification of active renin and prorenin. For example, Campbell et al. recommended fast sample processing at room temperature and immediate freezing to avoid prorenin unfolding and capture by the anti-renin antibody (Lamarre-Cliche et al. 2005; Campbell et al. 2009). In contrast, Glinicki et al. could not prove an impact of the temperature during sampling on the plasma active renin levels (Glinicki et al. 2015). However, there is still a risk of cryoactivation by slow freezing and long storage at 4 °C or by long storage at ambient temperature (Campbell et al. 2009). Moreover, the sampling condition at the bedside, the patient's condition at the blood collection time (circadian rhythm or posture) and the medication can impact the measured levels (Lamarre-Cliche et al. 2005).

2.3.2 Correlation of disease with prorenin or renin levels

Typical mean active renin levels in plasma are 16.3 pg/mL [95% CI: 13.7–19.4] in healthy adults (Tu et al. 2012). These levels have been shown to alter substantially under diverse pathological conditions. An increased median concentration of 46.8 pg/mL [interquartile range, IQR: 31.8–91.8 pg/mL] was observed in patients with myocardial infarction (Tomaschitz et al. 2011). Additionally, high active renin levels are associated with heart failure due to RAAS activation by the sympathicus (Buchhorn et al. 2001a). In contrast, a decrease in active renin has been observed in individuals with primary hyperaldosteronism (mean 3.8 pg/mL) (Nguyen et al. 2014). The use of the aldosterone-active renin ratio (ARR) which is used to diagnose primary hyperaldosteronism and was implement into an international guideline (Funder et al. 2016), was also found to be beneficial in hypertension, which showed a correlation between elevated ARR and high blood pressure that might evolve to cardiac remodeling if it is untreated (Abdel Ghafar 2019). Besides the cardiovascular risk of a high level of active plasma renin, it is also associated with liver cirrhosis and higher mortality in patients with an elevated median plasma renin concentration of 123.8 pg/mL [95% CI: 28.8–2348.4] (Paternostro et al. 2017). There is also a variation in reported concentrations (median [IQR]) based on ethnicity (white men: 18 pg/mL [12.8–25.3]; black men: 10.9 pg/mL [6.6–17.9]) and gender (white men: 12.5 pg/mL [10.6–14.6]; white women: 9.7 pg/mL [8.2–11.5]) (Nguyen et al. 2014). As described previously by Tarek et al. (Abdel Ghafar 2019), the genetic variability through the ethnical groups within the CYP11B2 (-344C/T) allele and the polymorphism on the angiotensinogen coding gene are correlated with the different levels of RAAS components. This mutation affects therefore also the difference in renin and prorenin levels in different ethnic groups. Elevated

plasma levels of active renin's precursor prorenin above 1,100 pg/mL have been significantly correlated with cardiovascular diseases like coronary artery disease (CAD) (Yoshida et al. 2015). Prorenin levels were more accurate than the previously-used plasma renin activity measurements (Yoshida et al. 2015). Up to ten-fold lower plasma prorenin levels were also associated with ovarian failure (plasma prorenin concentration of 93.6 pg/mL vs 263.4–624 pg/mL for healthy pregnant women) (Derkx et al. 1987a). The aldosterone-active-renin-ratio (ARR) has been proposed to be replaced by the aldosterone-prorenin-ratio (APR), which showed a better diagnostic performance and reproducibility in a study by Berge et al. in 2015 (Berge et al. 2015). Prorenin measurement may have a better performance due to its reduced variability and continuous release. The aldosterone-to-prorenin ratio could also differentiate between two aldosterone-induced suppressions, aldosterone-producing adenoma (APR median of 24 pmol/L per pg/mL [IQR: 11.5–50.9]) and idiopathic hyperaldosteronism (APR median of 11.8 pmol/L per pg/mL [IQR: 7.7–17.6]) (Berge et al. 2015). Another monitoring and predictive use for prorenin levels has been shown in diabetes mellitus type I with microvascular complications such as microalbuminuria (386.4 pg/mL [262.2–570] for patients with diabetes and microvascular complications vs a median of 141 pg/mL [IQR: 82.2–241.8] for patients with diabetes without microvascular complications) (Nguyen et al. 2014) or proliferative retinopathy (median of 249.6 pg/mL [95% CI: 60.6–1,026]) (Franken et al. 1990). There is also evidence in the pediatric population that shows a correlation between albumin excretion and elevated plasma prorenin levels (Chiarelli et al. 2001). Elevated prorenin levels were described as the consequence of renal lesions and abnormal enzyme processing (Franken et al. 1990; Allen et al. 1996).

Both increased renin and prorenin levels indicate an activated RAAS, which is shown, for example, by increased blood pressure. This hemodynamic change, due to the two proteins, is commonly associated with accelerated vascular complications including macrovascular disease, retinopathy, and nephropathy. Although hypertension is often considered a manifestation of cardiovascular or diabetic renal disease, it is relevant also in exacerbating or promoting diabetic vascular complications. Overall, the measurement of active renin is implicated in clinical studies which affect the RAAS directly (renin inhibitors, ACE inhibitors) or indirectly (ß-Blockers) (Buchhorn et al. 1998). While active renin is used as a RAAS activity marker in research, its precursor prorenin may gain attention regarding the differentiation of primary hyperaldosteronism (Berge et al. 2015) and diabetes mellitus related complications (Daneman et al. 1994). Similar to the natriuretic peptide ANP, prorenin and active renin has shown their potential in research and clinical investigations (Gangnus and Burckhardt 2019).

However, since the available data on renin and prorenin levels in children is especially limited, the usefulness as a routine biomarker cannot be assessed yet and require careful consideration. In the past, researchers showed for other markers (e.g. troponin (Harris and Gossett 2016)) that the potential use as a biomarker cannot be or only limited derived from adults to specific pediatric age groups. A meaningful statement requires data collection in larger cohorts and over longer periods as it was proved for NT-proBNP, which is nowadays embedded into a pediatric guideline (Rickers et al.; Cantinotti et al. 2014).

2.3.3 The link between age and bioanalytical plasma renin levels in healthy children

In this review, active renin levels in plasma were compared between nine different pediatric studies dating from 1989 to 2014. The bioanalytical measurements were made mainly using immunoradiometric assays (IRMA) from three suppliers (Nichols Institute, Cisbo and Diagnostic Systems). These assays used antibodies targeting the catalytic site of active renin. One study used an in-house assay with limited details provided. The immunoassay used and further details are shown in Table 2-2.
The pediatric population requires critical investigation of the published data, which is not only influenced by gender and body weight but also by different age-dependent stages of development, as kidney maturation and gonadal development influence the RAAS (Schütz et al. 1996). For the presentation of data within this review, the age classification as defined by the European Medicines Agency was used, if applicable.

Newborns

Two investigations specifically enrolled the youngest age group. The study by Kruger et al. showed high variability in renin levels in 82 newborns (birth until 7 days) with a range of 5.6–351.8 pg/mL (Fig. 2-2; Table 2-1) (Kruger et al. 1996). Vaginally-delivered children had higher renin concentrations and higher variability than newborns from caesarean section deliveries (mean [range]: 102.4 pg/mL [22.4–350.8] vs 59.5 pg/mL [42.7–86.9], respectively). This study also indicated that the active renin levels were very high at birth and declined rapidly in the first few hours and days. Additionally, Blazy et al. identified a mean ± SD concentration of 226 ± 58 pg/mL in their population (16 h to 1 month of age) (Blazy et al. 1989).

Infants and toddlers

The first study with healthy children was conducted by Ohyama et al. who reported active renin concentrations (mean ± SD) of 71.6 ± 10.4 pg/mL for boys and 72 ± 15.4 pg/mL for girls between 1 month to 1 year of age (Ohyama et al. 1989). Blazy et al. measured concentrations (mean ± SD) of 133 ± 28 pg/mL to 226 ± 58 pg/mL active renin in children from 16 hours to one month old (Blazy et al. 1989) within the same age range and by applying the same assay as Ohyama et al. A study conducted by Martinerie et al. with children 39 weeks of age showed similar levels (mean ± SD: 78.8 ± 9.6 pg/mL) as Ohyama et al., albeit using another assay (Table 2-1; Fig. 2-2) (Martinerie et al. 2009). In contrast, Krueger et al. reported lower levels using the Nichols Institute IRMA, with mean renin concentration of 24.5 pg/mL (infants 2 weeks to 3 months) and 32.7 pg/mL (infants 4 months to 1 year) (Table 2-2). These values were confirmed in 2006 by Sigirci et al., who also reported levels that were very low compared to the older studies (23.4 ± 21.3 pg/mL) that used different assays (Table 2-1) (Sigirci et al. 2006). These variations in published studies make it challenging to describe accurate pathological active renin concentrations in the young pediatric age groups.

A direct comparison and therefore estimation of developmental changes and maturation can be derived from data from the study by Blazy et al. Within this study the mean renin concentration halved between the youngest age group (16 h to 1 month; 226 pg/mL, n =17) and infants with an age of 1 month to 1 year (133 pg/mL, n = 11). However, this study still reported much higher concentrations compared to Ohyama (Ohyama et al. 1989). As both studies used the same assay, the altered values might be caused by differences in genetic background, which was also reported as a reason for the lower active renin levels in Black Americans compared to White Americans (Tu et al. 2012).

Children

After the first year, there was a rapid decline in renin concentration across all studies (Table 2-1, Fig. 2-2). However, the age-range of the subsets were often broader and consequently, the age-related changes are difficult to estimate because the authors did not subdivide their study population by age group (Fig. 2-2). This decreasing renin level was reported by Hjortdal et al., who found a median renin concentration of 20.4 pg/mL [IQR: 16.2–24.6] for children from 6 to 16 years of age (Hjortdal et al. 2000). While most other authors published comparable concentration levels, higher values for children at the age of 10 ± 1 years were observed by

Mahler et al. in 2012, with renin concentrations of (mean ± SD) 136 ± 37 pg/mL for girls and 117 ± 37 pg/mL for boys (Mahler et al. 2012). The lowest measured concentrations were reported by Shamsuzzaman et al. (median 12.3 pg/mL [IQR: 10.8–13.9], age 5-14 years) (Table 2-1; Fig. 2-2) (Shamsuzzaman et al. 2015).

Adolescents

Data specifically in adolescents was presented in three studies. Ohyama et al. reported (mean ± SD) 27.5 ± 2.5 pg/mL renin in 32 adolescents, Kruger et al. reported (mean) 19.1 pg/mL and Sigirci et al. reported (mean ± SD) 11.8 ± 7.6 pg/mL in their subsets. These values are comparable to reported mean plasma renin concentrations in healthy adults of 16.3 pg/mL [95% CI: 13.7–19.4] (Tu et al. 2012). In summary, an age-related decline in renin concentration across all pediatric age groups and in comparison to healthy adults is observed.

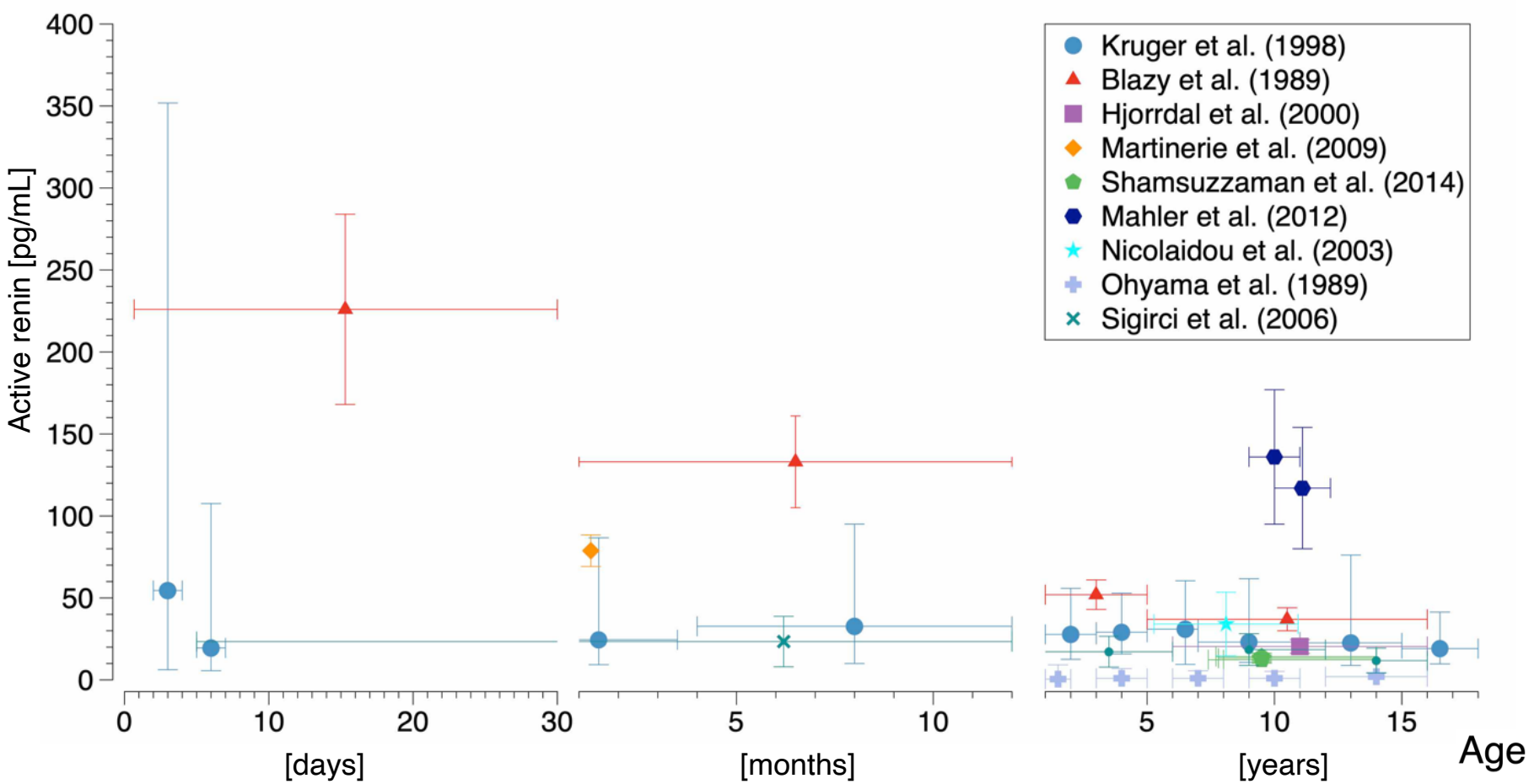

Figure 2-2 Graphical illustration of plasma active renin concentrations from seven studies in healthy children.

Table 2-2 Overview of active renin levels in healthy children *(mean ± SD or mean (range) and median [IQR]; all µU or mU values were converted to pg/mL by a factor of 0.6).*

Authors	Assay	Population	Active Renin, pg/mL
Blazy et al.	IRMA (Diagnostics Pasteur)	16 h–1 month (n=17)	226 ± 58
		1 month–1 year (n=11)	133 ± 28
		1–5 years (n=10)	52 ± 9
		5–16 years (n=19)	37 ± 7
Ohyama et al.	IRMA (Diagnostics Pasteur)	0–1 year (n=22 female)	71.6 ± 10.4 (♀);
		0–1 year (n=20 male)	72 ± 15.4 (♂)
		1–2 years (n=16)	51.4 ± 8.7
		3–5 years (n=17)	42.4 ± 5.9
		6–8 years (=25)	35.6 ± 4.6
		9–11 years (n=17)	38.2 ± 4.2
		12–16 years (n=32)	27.5 ± 2.5
Kruger et al.	IRMA active renin;	38–42 weeks	
	(Nichols Institute diagnostics)	Vaginal delivery (n=33)	102.42 (22.38–350.76)
		Caesarean section (n=7)	59.46 (42.72–86.94)
		2–4 days (n=28)	54.54 (6.24–351.84)
		5–7 days (n=14)	19.5 (5.64–107.52)
		2 weeks–3 months (n=11)	24.48 (9.3–62.34)
		4 months–1 year (n=19)	32.7 (9.96–86.7)
		1–3 years (n=15)	27.78 (12.66–55.86)
		2–5 years (n=11)	29.1 (15.84–52.92)
		5–7 years (n=25)	30.96 (9.48–60.48)
		7–11 years (n=33)	23.1 (10.68–61.74)
		11–15 years (n=65)	22.62 (8.82–76.14)
		15–18 years (n=20)	19.14 (9.78–41.34)
Hjortdal et al.	IRMA active renin (Nichols Institute diagnostics)	6–16 years (n=33)	20.4 (16.2–24.6)
Nlcolaldou et al.	IRMA active renin (Nichols Institute diagnostics)	8.10 ± 2.83 years (12 boys/2 girls, n=14)	34.1 ± 19.42
Sigircl et al.	IRMA active renin DSL-25100 (Beckman Coulter)	5 days–1 year (n=35)	23.4 ± 21.3
		1–6 years (n=48)	17.2 ± 9.4
		6–12 years (n=50)	18.5 ± 9.7
		12–16 years (n=37)	11.8 ± 7.6
Martinerie et al.	RIA renin III generation kit (Cisblo)	39 weeks 5 ± 1 d	78.8 ± 9.6
Mahler et al.	IRMA active renin DSL-25100 (Beckman Coulter)	11.1 ± 1.1 years (boys n=10)	117 ± 37
		10.0 ± 1.0 years (girls n=10)	136 ± 41
Shamsuzzaman et al.	RIA (selfmade)	5–14 years (normal weight control, n=52)	12.3 (10.8–13.9)
		5–14 years (normal-osa, n=47)	13.3 (11.6–15.3)
		5–14 years (overweight control, n=27)	12.3 (10.2–14.7)
		5–14 years (overweight-osa, n=47)	14.3 (12.5–16.4)

All µU or mU values were converted to pg/mL by a factor of 0.6. IRMA, immunoradiometric assay; RIA, radioimmuno assay

2.3.4 Active renin levels in the cardiovascular diseased pediatric population

In the cardiovascular diseased pediatric population, the neurohumoral activation results in the RAAS response, which is associated with malignant structural remodeling. High levels of active renin seem to be the cause of the activity of the juxtaglomerular mediated renin secretion (Buchhorn et al. 2001c). Since RAAS blockers are also used for pediatric illnesses, monitoring of the pharmacodynamic parameters is useful to estimate the effect of the medication on RAAS proteins, (e.g. aliskiren therapy) (Campbell et al. 2009). Only limited data was found in five studies from 1995 to 2003 in children with cardiovascular diseases such as congestive heart

failure (Table 2-3). Four studies from Buchhorn et al. have reported active renin concentrations (mean ± SD) of 170.4 ± 191.4 pg/mL; 202 ± 141.6 pg/mL and 202 ± 138 pg/mL with propranolol treatment and 636.6 ± 461.4 pg/mL; 422 ± 294 pg/mL and 405.6 ± 235.8 pg/mL with digoxin and diuretic treatment for children 4–6 months old in the first study; 3–13 weeks old in the second study and about 7 months to 8 years old in the third study, respectively (Schütz et al. 1996; Buchhorn et al. 2001c; Buchhorn et al. 2001b; Buchhorn et al. 2001a; Buchhorn et al. 2003). Compared to the study by Krueger et al. in healthy subjects, these values are increased five-fold even under beta-blocker treatment (mean of 170.4 pg/mL for the propranolol group vs 32.7 pg/mL for healthy children of the same age), which should reduce the renin releasing effect via beta-receptors on the juxtaglomerular cells (Blumenfeld et al. 1999). Both studies used the same radioimmunoassay from the Nichols Institute which limits the variability due to different assay procedures; therefore, the correlation might be primarily due to a pathophysiological induced increase in renin concentration.

Another study also demonstrated high levels of active renin in children with congenital cardiac malformations. These plasma levels were adjusted to the respiratory rate, which showed a major influence on the active renin (mean ± SD: 106.2 ± 136.2 pg/mL for 4–6 months of age with a respiratory rate below 50 min^{-1} vs 544.2 ± 392.4 pg/mL for 1–5 months of age with a respiratory rate below 60 min^{-1}) (Fig. 2-2) (Buchhorn et al. 2001a). If compared to the study with healthy children of the same age and performed by the same assay, the plasma renin levels are substantially higher (Table 2-1 and 2-2).

In diseases such as glomerulonephritis and insulin-dependent diabetes mellitus, the reported active renin concentrations did not show any increase if compared to values obtained in a healthy population (Daneman et al. 1994; Hjortdal et al. 2000).

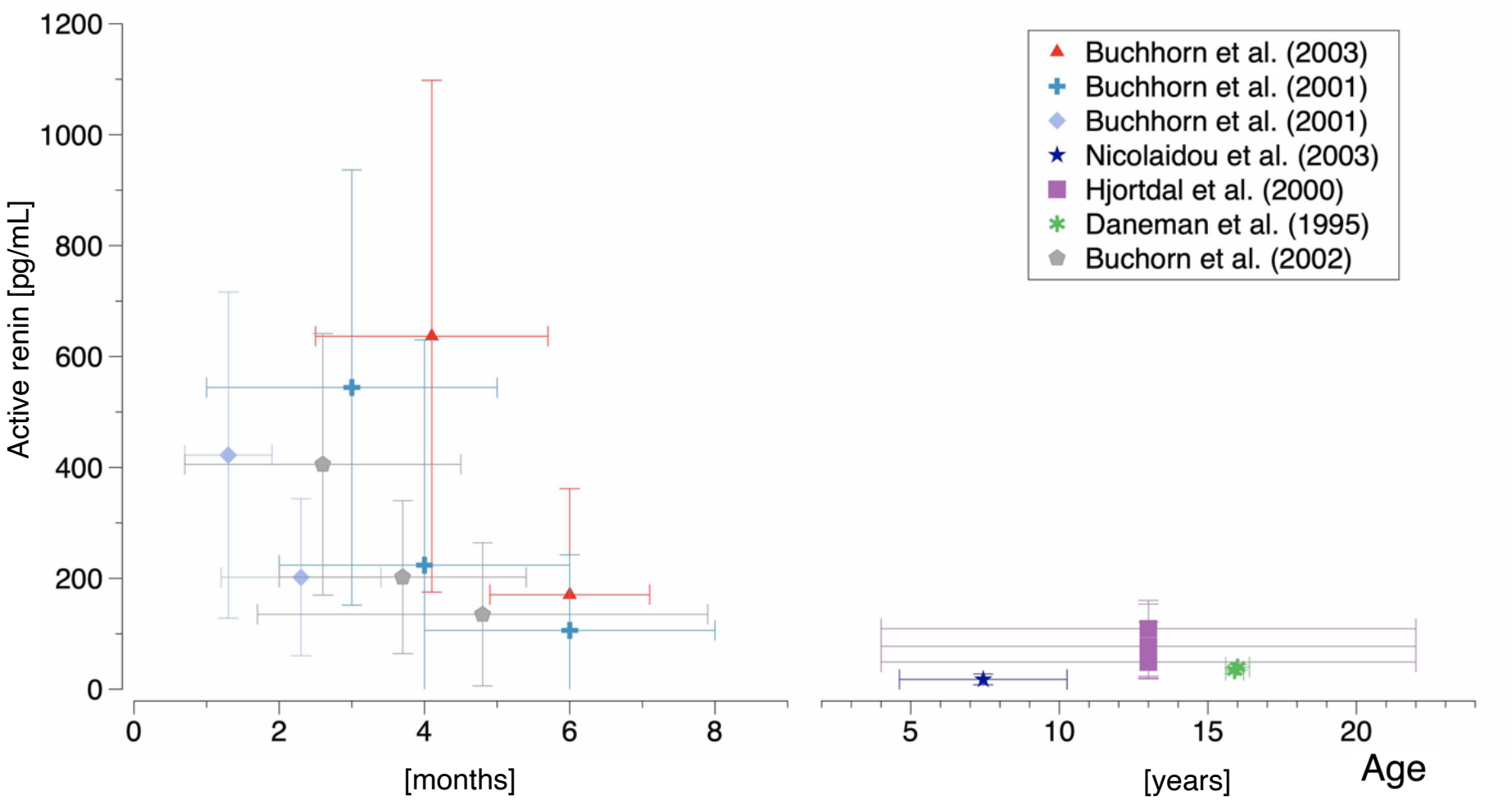

Figure 2-3 Graphical illustration of plasma active renin concentrations from children with cardiovascular and diabetes disease.

Table 2-3 Overview of studies involving diseased children which measured active renin plasma levels *(mean ± SD and median [IQR]; all µU or mU values were converted to pg/mL by a factor of 0.6).*

Authors	Assay	Population	Active renin, pg/mL	Disease
Hjortdal et al.	IRMA active renin (Nichols Institute diagnostics)	4–22 years (TCPC, n=12)	109.2 (18.6–160.2)	Heart failure
		4–22 years (BDG, n=8)	49.2 (23.4–121.2)	
		4–22 years (TCPC + BDG, n=20)	77.4 (20.4–153.6)	
Buchhorn et al.	IRMA active renin (Nichols Institute diagnostics)	6.0 ± 1.1 months (n=9 propranolol)	170.4 ± 191.4	Congestive cardiac failure
		4.1 ± 1.6 months (n=8, digoxin/dluretics)	636.6 ± 461.4	
Buchhorn et al.	IRMA active renin (Nichols Institute diagnostics)	Respiratory rate (min ^1): 6 ± 2 months (n=16, <50)	106.2 ± 136.2	Congenital cardiac malformations
		4 ± 2 months (n=9, 50–60)	223.8 ± 406.2	
		3 ± 2 months (n=9, <60)	544.2 ± 392.4	
Buchhorn et al.	IRMA active renin (Nichols Institute diagnostics)	4.8 ± 3.1 months, (n=12 CHD control)	135 ± 129	Congenital heart disease
		2.6 ± 1.9 months (n = 14 digoxin/ dluretics)	405.6 ± 235.8	
		3.7 ± 1.7 months (n=9 propanolol)	202.2 ± 138	
Buchhorn et al.	IRMA active renin (Nichols Institute diagnostics)	9.2 ± 4.5 weeks (n=10 propranolol)	202 ± 141.6	Congestive cardiac failure
		5.3 ± 2.4 weeks (n=10, digoxin/ diuretlcs)	422.4 ± 294	
Nlcolaldou et al.	IRMA active renin (Nichols Institute diagnostics)	7.44 ± 2.82 years (14 boys/ 4 girls, n=18)	17.72 ± 9.8	Poststreptococcal glomerulonephritis
Daneman et al.	IRMA (Sanofi Pasteur)	16 ± 0.4 years (n=5; with microalbuminuria)	40 ± 4.6	Insulin-depended diabetes mellitus
		15.9 ± 0.3 (n=25; without microalbuminuria)	33.6 ± 4.7	

All µU or mU values were converted to pg/mL by a factor of 0.6. IRMA, immunoradiometric assay; TCPC, total cavopulmonary connection; BDG, bidirectional Glenn anastomosis; CHD, congenital heart disease.

2.3.5 Insights into plasma prorenin levels in children

Prorenin concentration is not frequently determined in children. The limited data available consist of two studies in healthy children, (Table 2-4, Fig. 2-3). A study from 1989 reported calculated prorenin concentrations of (mean ± SD) 765 ± 106 pg/mL for healthy children from 16 hours to 1 month of age and 284 ± 4 pg/mL for neonates from 1 month to 1 year of age. Here a decline in prorenin is indicated which halved the plasma concentration and indicates the maturation of tissues in the newborn (Blazy et al. 1989). However, a recent 2017 study (Terada et al. 2017) measured more than 10-fold higher levels in plasma than Blazy et al. reported in 1989. Prorenin levels were determined by the direct prorenin assay (antibody against the pro-segment) (Fig. 2-3). This limited and highly variable plasma prorenin data make a reliable conclusion on concentration levels in children currently impossible. Further studies reporting reliable data sets are necessary. A possible explanation for the differences in values reported in

the current literature could be the degradation of activated renin or incomplete activation of all prorenin in plasma.

The 2017 study also differentiated prorenin levels between pre-term (less than 37 weeks of gestational age) and full-term (more than 39 weeks of gestational age) newborns, and showed a significant 3-fold difference in prorenin concentration (mean ± SD: 6000 ± 840 pg/mL for pre-term neonates and 2130 ± 250 pg/mL for full-term neonates) (Table 2-4) (Terada et al. 2017).

Similar to reported levels in adult patients, Daneman et al. showed that prorenin levels in adolescents with insulin-depended diabetes and microalbuminuria have significantly elevated compared to adolescents without microalbuminuria (mean ± SD: 226.4 ± 13.6 pg/mL vs 168.5 ± 10.1 pg/mL) (Fig. 2-3) (Daneman et al. 1994).

Interestingly, the reported ratio between active renin and prorenin also changed with age: it was 3.4 in the youngest group (16h – 1 month), then it decreased to 2.1 (1 month to 1 year) caused by different changes in renin and prorenin (renin is decreased twofold; prorenin threefold); after a year it increased to 5.6 and held at this ratio until adolescence (Table 2-4).

The pediatric population shows high variability in plasma levels among the different age groups. Compared to studies in adults, the release of prorenin and renin is differently triggered and caused by kidney development, which is also affected by birth delivery (Kruger et al. 1998; Terada et al. 2017). Animals models showed that renin and prorenin are not only restricted to the juxtaglomerular cells but are also released by intrarenal arteries resulting in high prorenin and renin levels in newborns. These cells lose their ability to release renin and prorenin in older rodents that might explain partially the observed age-depended differences (Gomez et al. 1989).

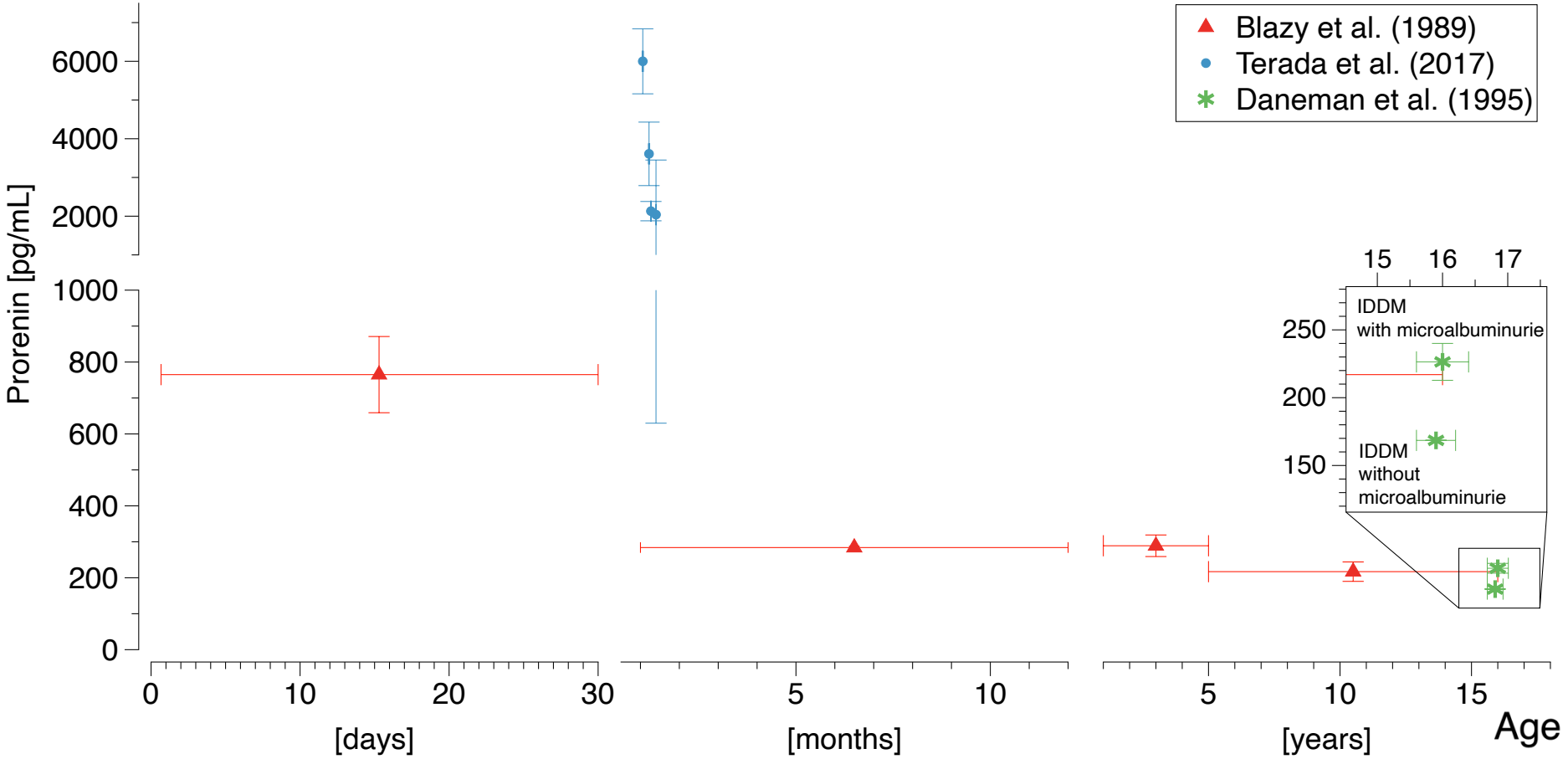

Figure 2-4 Plasma prorenin concentrations of healthy and diabetic children *(IDDM: insulin-depended diabetes mellitus) collected from three studies.*

Table 2-4 Prorenin and active renin plasma levels in healthy and diabetic children, measured by three studies *(mean ± SD)*

Authors	Assay	Population	Active Renin, pg/mL	Prorenin, pg/mL	Conversion
Blazy et al.	IRMA (Diagnostics Pasteur)	16 h–1 month (n=17)	226 ± 58	765 ± 106	Trypsin
		1 month–1 year (n=11)	133 ± 28	284 ± 4	
		1–5 years (n=10)	52 ± 9	289 ± 30	
		5–16 years (n=19)	37 ± 7	217 ± 27	
Terada et al.	ELISA (Molecular Innovation)	32.58 ± 0.52 weeks (preterm, n=57)	na	6,000 ± 840	No conversion
		36.58 ± 0.52 weeks (preterm 28 days, n=57)		3,610 ± 820	
		37.99 ± 0.10 weeks (full-term, n=67)		2,130 ± 250	
		41 99 ± 0.10 weeks (full-term 28 days, n=67)		2,040 ± 1,410	
Daneman et al.	IRMA (Sanofi Pasteur)	16 ± 0.4 years (n=5; insulin-depended diabetes mellitus with microalbuminuria)	40 ± 4.6	226.4 ± 13.6	Trypsin
		15.9 ± 0.3 (n=25; insulin-dependtdend diabetes mellitus without microalbuminuria)	33.6 ± 4.7	168.5 ± 10.1	

IRMA, immunoradiometric assay; ELISA, enzyme-linked immunosorbent assay.

Limitations

This review may include language bias as only publications available in English were included. Additionally, inclusion criteria that were not specifically mentioned in the title or abstract could lead to the exclusion of potential publications. Incomplete reported data (e.g. unspecific age, concentration units, assays, health status of participants) was excluded, resulting in a more precise dataset.

2.4 Conclusion

The available data on plasma renin and prorenin concentrations in healthy and diseased children are limited. Sample handling is still a crucial step, which might particularly affect measured active renin concentrations due to conformational changes of its precursor prorenin. In the extant studies in the literature, an age-dependent decline of renin plasma concentration was observed in newborns compared to adolescents. A fast decline, especially during the first year of life, was reported. A reliable assessment for prorenin levels in the maturating population is yet not possible due to the low number of available publications. However, prorenin might be a specific marker of microalbuminuria within a diabetes pediatric group. More studies are necessary to determine the value of prorenin and renin ratios, which might play a predictive role not only in diabetic patients.

3. Innovative mass spectrometry based determination of human active renin

This chapter had been published in the peer-reviewed journal: 'Journal of chromatography B' with the title 'A concept to make low-abundance endogenous renin accessible to mass spectrometry: A multistep experimental design approach' (doi: 10.1016/j.jchromb.2019.121856).

3.1 Background and aim

One of these low-abundance and proteolytical-resistant proteins is human renin, which is present in low picogram-per-milliliter levels in healthy adults (Ichihara et al. 2009). Its precursor, prorenin, is specifically cleaved in lysosomes by proteolytic enzymes where the mature part (renin) can withstand the harsh environment (Xa et al. 2014). Renin is the key enzyme in the renin-angiotensin-aldosterone system (RAAS), which affects not only blood pressure but also glucose metabolism and electrolyte and fluid hemostasis. Consequently, renin plays an important role in diagnosis and pharmacotherapy (Valabhji et al. 2001; Paternostro et al. 2017).

Commonly in proteomic analysis, the one-factor-at-a-time (OFAT) approach, in which every factor impacting the procedure is analyzed separately, is widely applied. In the case of human renin, this approach would be inappropriate due to the large number of factors requiring assessment (Hecht et al. 2016), the large numbers of necessary experiments, and the fact that keeping one factor constant might not lead to the best conditions. Therefore, the statistical planning of experiments utilizing a quality-by-design approach called Design of Experiments (DOE) appears to be a more powerful tool for the evaluation of optimal assay conditions. The DOE combines all factors of relevance and facilitates the evaluation of optimal assay setting within a manageable amount of experiments. Its advantages were proven in optimizing absolute quantitation methods like AQUA (Shuford et al. 2012a; Loziuk et al. 2013) but showed also usefulness in analyzing instrumental settings to improve protein coverage or unique peptide discovery (Andrews et al. 2011).

This study aimed to develop a tailored procedure for the reliable measurement of endogenous human renin by an immunocapture LC-HRMS assay with a label-free determination. Key processes were comprehensively investigated by focusing on optimal yield while attempting to shorten the procedure duration.

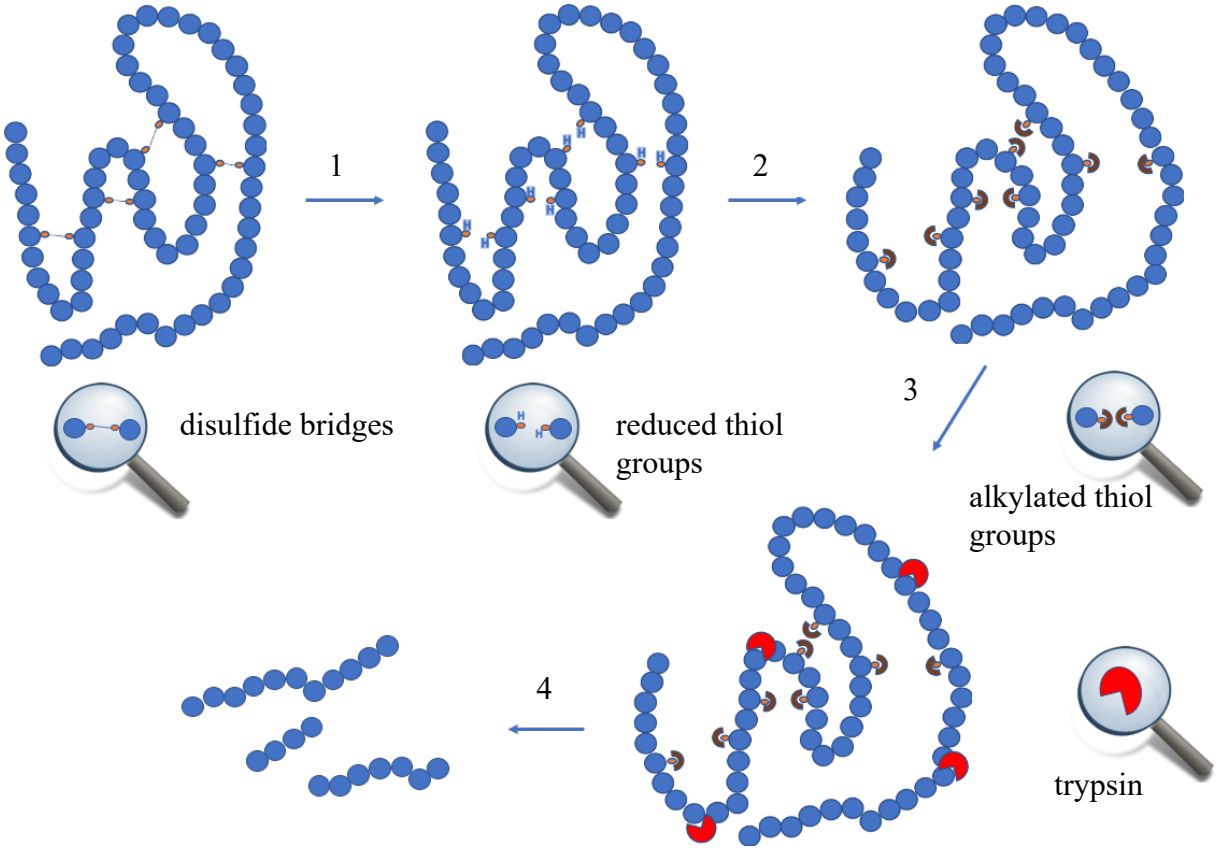

Figure 3-1 Bottom-up approach of protein characterization and surrogate peptide quantification. *1) First, the denaturation and reduction of the disulfide bridges; 2) the alkylation of the free cysteine thiol groups to avoid refolding; 3) proteolytical digestion by modified trypsin; 4) Unique surrogates*

3.2 Methods

3.2.1 Materials and methods

Human recombinant renin was obtained from Cayman Chemicals (Ann Arbor, USA). Two different lots (lot no. 0516032 and 050726) with a certified purity of > 85% and > 86%, respectively, were investigated. TCPK-threated modified trypsin and Dynabeads® Protein G kit was purchased from Thermo-Scientific (Rockford, USA). Tris-(2-carboxyethyl)-phosphine, bis(sulfosuccinimidyl)suberate (> 95%), dithiothreitol, sodium deoxycholate (> 99%), urea (> 99.5%), and ammonium bicarbonate (>99.5%) were supplied by Sigma-Aldrich (Taufkirchen, Germany).

Mixed-mode anion-exchange solid-phase extraction plates (Oasis® MAX µElution) and RapiGest® were purchased from Waters (Milford, USA). Anti-renin antibodies were obtained from DRG Instruments GmbH (Marburg, Germany). Methanol optima® (LC-MS grade) and

dimethyl sulfoxide (p.a.) were supplied by Fisher Chemicals (Geel, Belgium). Water (LC-MS grade) was provided by Riedel-de Haen (Seelze, Germany), while formic acid (98%, p.a.) and acetonitrile (UHPLC grade) were provided by Applichem (Darmstadt, Germany).
Finally, human blood plasma was collected from a healthy male volunteer in S-Monovette® K3 EDTA tubes (Sarstedt, Nuembrecht, Germany).

3.2.2 In-silico simulation of tryptic digestion

The online tool Prospector® (v 5.22.1, University of California) was used for the in-silico simulation aiming to imitate digestion and to identify unique fragments of renin for LC-MS determination. The simulation was conducted using the human renin amino acid sequence listed in the UniProt® database (entry number P00797). By utilizing Prospector®, the in-silico protein digestion was performed by "peptide/protein utility MS-Digest" selection. Moreover, the simulation was initiated by "custom protein sequences" with digest selection of trypsin set to zero missed cleavages. The peptide mass between 400 and 1500 Da was enclosed and multiple charges were reported for the generated peptide with a minimum of five amino acids. The uniqueness of the predicted amino acid sequences was verified using the BLAST® search at the UniProt® website. The surrogate was only considered for bioanalytical method development if an amino acid sequence was exclusive for a tryptic peptide of renin.

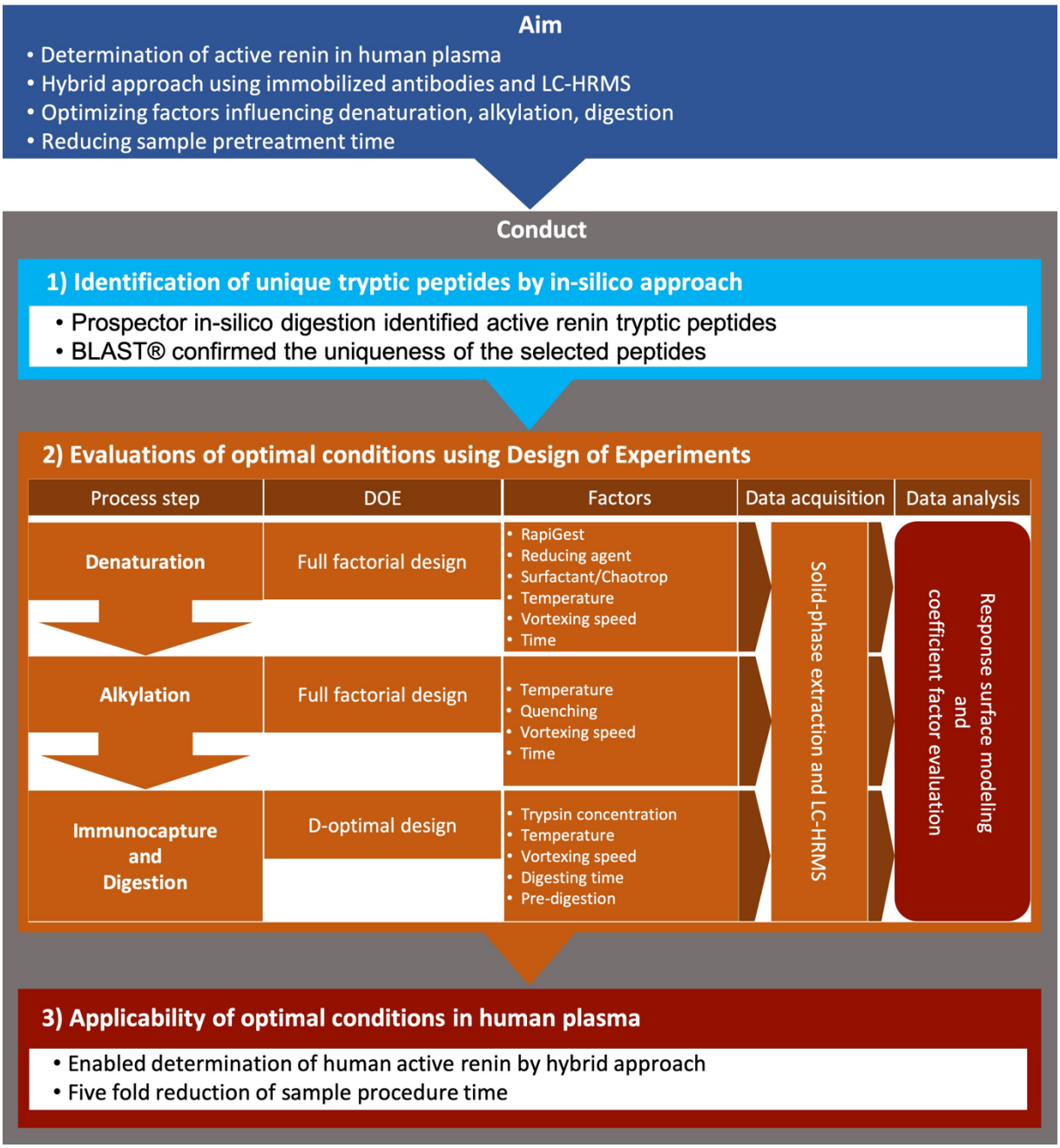

Figure 3-2 Flow diagram for sample pre-treatment and tryptic digestion. *This workflow shows the aims and the conduct which was performed in this work in subdivided steps: In-silico analysis, DOE design investigation the impact of each factor, data acquisition using LC-MS and data analysis.*

3.2.3 Design of Experiments

The MODDE pro© software program (MKS Instruments AB, Malmö, Sweden, version 12.0) was used to design and evaluate the experiments. The procedure was divided into three parts, each one separately addressing the denaturation, alkylation, and digestion processes (Fig.3-1).

Based on the factors that were selected for these three processes, different models were chosen (Fig.3-2).

3.2.3.1 Full factorial design of Denaturation and Alkylation experiments of active renin

A full factorial design was applied for evaluating the impact of parameters and settings within the denaturation and reduction steps. This two-level interaction model was planned by setting six factors, three center points, and two replicates each. A total of 201 runs of the experiment were required.

Denaturation of active renin's tertiary structure

Using the full factorial model, RapiGest® concentration (1% - 3%), sodium deoxycholate, urea, dithiothreitol (DTT), Tris(2-carboxyethyl)phosphine (TCEP), incubation temperature (20 °C - 80 °C), incubation time (20 minutes - 80 minutes), and vortexing speed (0 rpm - 1000 rpm) were all investigated in relation to denaturing efficiency. Sodium deoxycholate, urea and the reducing agents (TCEP and DTT) were set as qualitative factors at fixed concentrations.
For the experiments on denaturation efficiency, the alkylation and digestion were fixed to the following settings. Alkylation was performed by treating the samples with 300 mM of iodoacetamide for 25 minutes in the dark. Next, the samples were pre-digested for two hours with 100 ng trypsin followed by digestion with an additional 100 ng trypsin for 16 h before being quenched with 1 µL formic acid. The samples were subsequently analyzed by LC-HRMS as described in Sections 3.2.4.2 and 3.2.4.3.

Alkylation of renin's cysteine residues

The second step of sample pretreatment involved the alkylation of the cysteine thiol groups to avoid refolding of the protein's tertiary structure. 300 mM IAA was used as the alkylation agent. The evaluation of the most relevant factor influencing the alkylation performance resulted in 54 experiments, which consisted of three center-point points and analyzed each sample in triplicate. This design was also a full factorial two-level screening design. While the concentration of IAA was kept constant, other parameters were set as quantitative factors. The temperature was varied between 10 °C and 40 °C, time was altered between five minutes and

60 minutes, and the vortexing speed was analyzed between 0 rpm and 800 rpm. Moreover, the usefulness of a quenching step with 300 mM DTT was evaluated.
The digestion step was again fixed at two hours of pre-digestion with 100 ng trypsin, followed by digestion with an additional 100 ng trypsin for 16 h before being quenched with 1 µL formic acid. The samples were subsequently analyzed by LC-HRMS, as described in Sections 3.2.4.2 and 3.2.4.3.

3.2.3.2 D-optimal design of renin's digestion procedure

Based on the multiplicity of factors within the digestion procedure, a D-optimal model was applied in order to reduce both the number of experiments to 90 and the overall cost. To allow for sufficient comparison with the full factorial design, the G-efficiency was aimed to be ≥0.6. Subsequently, the model fit (R^2) and the Q^2 value, which estimates the predictive value of the design, had to be ≥0.5. Moreover, the appraisal of the overall model goodness-of-fit was defined by the difference between Q^2 and R^2, which had to be below 0.3 to estimate an appropriate design.
500 µL of human plasma was spiked with 20 ng of the human recombinant renin, followed by immunocapture using immobilized anti-renin antibodies (1 µg antibodies/sample). The immobilization of anti-renin antibodies was meant for solid support by applying magnetic Dynabeads® protein G. Incubation of the human plasma samples was done for 1.5 hours using tilting and rotating (Fig.3-3). Next, the samples were cleaned with PBST (0.01% Tween 20) three times and were incubated in the optimized denaturation buffer and continued by performing the alkylation. The immunocapture complex was digested by modified trypsin protease without the elution of the antigen. The cleavage was optimized using the following settings: the temperature varied between 15 °C and 70 °C, vortexing speed varied from 0 to 800 rpm, time ranged from six minutes to 30 hours, and pre-digestion (from zero to four hours) was conducted with half of the remaining trypsin added per run. The trypsin concentration altered between 50 ng and 1000 ng.
The samples were subsequently analyzed by LC-HRMS, as described in Sections 3.2.4.2 and 3.2.4.3.

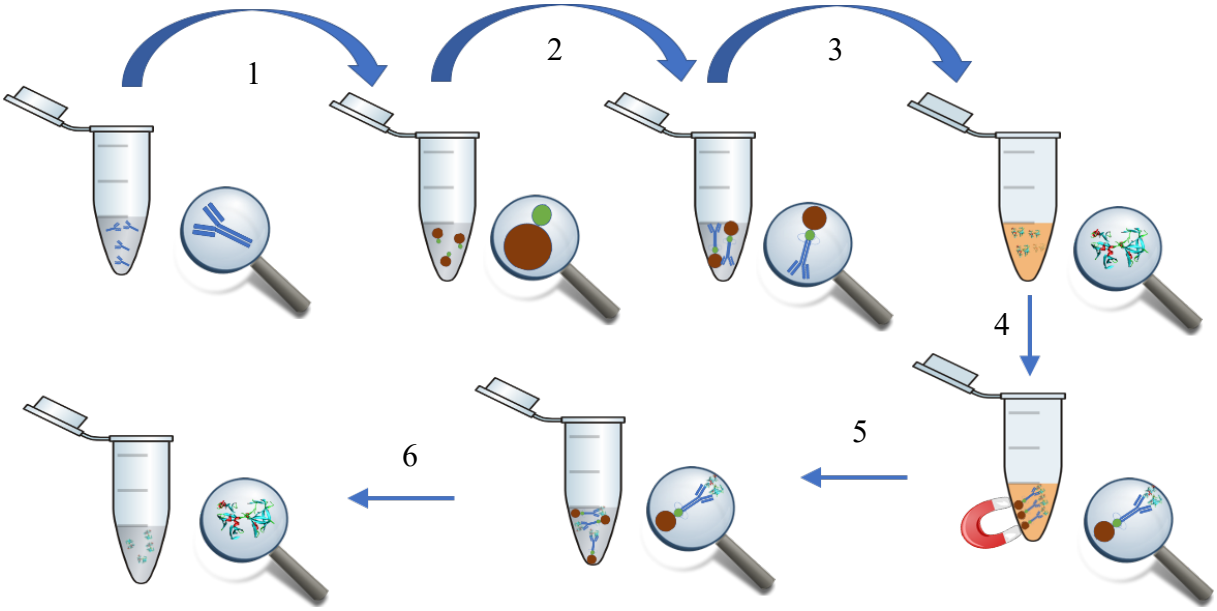

Figure 3-3 Immunocapture with magnetic beads immobilized antibodies as first purification step. *1) Dynabeads® Protein G bind anti human renin mouse IgG1 mAbs; 2) Crosslinking of Dynabeads Protein G and lgG1 mAbs; 3) 500µl of thawed human plasma was prepared and spiked with human recombinant renin; 4) The spiked plasma was incubated with the magnetic beads coupled antibodies; 5) After the incubation the tubes were placed on a magnet rack; 6) The plasma was discarded and the beads were washed with PBS-T buffer; 7) Elution of the antigen with a low pH buffer.*

3.2.4 Instrumentation and conditions

3.2.4.1 SPE clean-up of signature peptides

The clean-up of the digested samples was accomplished by using Oasis® MAX µElution SPE 96 well plates. The conditioning of the sorbent material was performed by using a mixture of acetonitrile, water, and formic acid (60/40/2, v/v/v). After the subsequent equilibration step with 5% ammonium hydroxide in water, the alkalized samples were pipetted onto the cartridges. The samples were then washed with 5% ammonium hydroxide in water, followed by a second washing step in 500 µL methanol. Elution was performed three times using 100 µL of a mixture of acetonitrile, water, and formic acid (60/38/2, v/v/v). The eluate was completely evaporated under a gentle flow of nitrogen. For reconstitution, a mixture of 50 µL containing 5% DMSO, 0.1% formic acid and 20% methanol in water [v/v/v] was applied.

3.2.4.2 Liquid chromatography and the conditions applied for signature peptides separation

Chromatographic separation was achieved using a Shimadzu Nexera UHPLC system (Shimadzu Europe, Duisburg, Germany). This liquid chromatography system consisted of a controller (CBM 20A), two separate pumps (LC-20ADxR), two separate degassers (DGU-20A5R and DGU-20A3 prominence), a switching valve unit (FCV-11AL), an autosampler (SIL-30AC), and a column oven (CTO-20AC). The separation process was performed on a Waters® XSelect CSH C18 column (130Å, 3.5 µm, 3.0 mm x 150 mm).
Mobile phase A consisted of 1% DMSO plus 0.1% formic acid in MS-grade water, while mobile phase B consisted of 1% DMSO plus 0.1% formic acid in MS-grade methanol [v/v/v]. The flow rate was set to 0.9 mL/min. The gradient started at 20% of mobile phase B and was increased between 1 and 1.2 minutes to 40%. This was followed by a further increase to 50% of mobile phase B after 2.25 minutes and was increased to 80% after 3 minutes. The gradient was kept at 80% until 4 minutes had elapsed, before being reduced to 20% of mobile phase B again. The injection volume was 10 µL, the oven temperature was set to 60 °C, and the autosampler conditions were controlled at 15 °C.

3.2.4.3 Mass spectrometry and conditions applied to the determination of signature peptides

Mass spectrometric detection was performed using a Sciex TripleTOF 6600 (Sciex, Concord, Canada) high-resolution mass spectrometer system with an IonDrive TurboV® electrospray ionization source. The ion spray voltage was set to 5500 eV, curtain gas remained at 35 psi and nebulizer gas (gas 1) and heater gas (gas 2) were adjusted to 80 psi and 60 psi, respectively, while interface heater temperature was adjusted to 300 °C.
For signature peptide I, the transitions of 854.9 *m/z* to 418.2296 *m/z* were chosen for quantification, while for signature peptide II, 417 *m/z* to 275.1550 *m/z* were chosen. Corresponding declustering potential was set to 54 V and the collision energy for the selected signature peptide I (VVFDTGSSNVWVPSSK) was adjusted to 54 eV. Regarding signature peptide II (LMEALGAK), declustering potential was set to 68 V and collision energy was set to 36 eV, respectively.
The system was controlled by Analyst TF 1.7.1, while data analysis was performed using PeakView 2.2 and MultiQuant 3.0.2 (Sciex, Concord, Canada).

3.2.5 Applicability of the hybrid approach in human plasma

As the optimizations of mass spectrometric response by the first and second DOE (denaturation and alkylation) were conducted in a neat solution, the applicability of the entire process in human matrix was additionally investigated. A comparison between conventional conditions and the aforementioned modified hybrid approach was conducted. In both settings, human blood samples spiked with 20 ng renin were analyzed. The conventional protocol consisted of denaturation at 60 °C for 60 min with DTT and RapiGest® (2%), 25 minutes IAA alkylation at room temperature, pre-digestion for two hours with 100 ng trypsin, and overnight digestion with additional 100 ng trypsin. For the performance evaluation of the hybrid approach, the optimal settings described above were applied: denaturation at 20 °C for 80 min, 1000 rpm with 1% RapiGest®, 2M urea and 150 mM DTT; alkylation at 10 °C for five minutes and 800 rpm; digestion at 15 °C for 2.16 hours using 800 rpm vortexing speed and 1000 ng trypsin. The investigation of the applicability of the modified approach was meant to address three aspects. First, verification of whether the hybrid mass spectrometric assay is in general capable to determine endogenous levels of renin; second, optimization of the required process duration to facilitate a more efficient and less labor-intensive method; and third, to access the repeatability of the developed hybrid approach in human matrix by three independent sample preparations and to evaluate the between-sample variability. In compliance with international bioanalytical guidelines, a maximum variability of 20% in signal response was regarded as acceptable. The evaluation was conducted using blood samples donated by a healthy male volunteer. Each approach was measured in triplicate and analyzed together on the same day by LC-HRMS as described in section 3.2.4.2 and 3.2.4.3

3.3 Results and discussion

3.3.1 Renin structure and Prospector® results

The complete in-silico digestion of renin resulted in 11 completely cleaved peptides that fulfilled the criteria entered into the Prospector® tool. Two signature peptides were chosen due to their high intensity in mass spectrometric screening. The peptide VVFDTGSSNVWVPSSK (signature peptide I), covering the positions from 101 to 116, determines a part of the active center of renin. The second signature peptide, LMEALGAK (signature peptide II) covers amino acids in positions 242 to 249, which is part of a beta-sheet structure.
The BLAST® experiment showed that both of the peptides selected are unique tryptic peptides enabling the reliable quantification of renin.

3.3.2 Denaturation of renin's tertiary structure

The denaturation was an essential part of the proteolytic resistant protein renin to make it better accessible for proteolytic cleavage. Therefore, the analysis of the coefficient effects represents the main impacting individual effects as well as the interaction effects (Fig.3-4; 3-5). After estimating the optimal denaturing conditions, the smaller surrogate peptide signature peptide II was excluded from further evaluation as it could not be as effectively generated as the larger signature peptide I. All below mentioned results focus subsequently on surrogate peptide I only.
The screening results of different RapiGest® concentrations on the signal intensity identified the concentration of 1% RapiGest® as most promising. By incubating at 20 °C, the intensity of signature peptide I was 1.57e6 counts per second (cps) for 1% concentration, with no substantial change in intensity by using more RapiGest® (-4.1% for 2 % and -8.2% of predicted cps for 3%). Using 1% of the acid-cleavable surfactant, it was indicated that the lowest analyzed temperature resulted in a 1.6-fold enhancement (1.0e6 vs. 1.57e6 cps for 1 % RapiGest® at 80 °C and 20 °C) of the cleaved signature peptide I, if compared to the highest incubation temperature.
In this screening study, two additional denaturing agents were added in fixed concentration. Sodium deoxycholate (SDC) was added at a final concentration of 4%, and urea was added at a 2 M concentration. Each denaturant had either solubilizing or destroying capabilities to the tertiary structure of the protein and allowed trypsin to cleave the surrogate peptide more efficient. With increasing temperature (20 °C to 80 °C), the intensity of surrogate peptide I

decreased. One possible reason for this could be the carbamylation of the signature peptide I lysine residue by elevated temperatures in urea containing the denaturation buffer (Sun Shisheng, Zhou Jian-Ying, Yang Weiming 2015). Signature peptide I showed only minor changes in intensity by using urea as additional denaturant (11% enhancement of intensity for SDC compared to urea) and due to urea's lower costs and easier removing by solid-phase extraction, it was eventually chosen as the denaturing buffer. Please also refer to Figure 3-4.

The impact of the two reducing agents, TCEP and DTT, on their denaturation power were investigated along with their signal intensity of surrogate peptide I. At a temperature of 20 °C, the most potent reducing agent was DTT, which was represented by much higher intensities for both peptides when compared to TCEP (signature peptide I had 27% higher intensity). At higher temperatures (80 °C), both reducing agents exhibited a reduction in their power (signature peptide I: 53% higher intensity by using DTT and 22.9 % higher intensity by using TCEP at 20 °C vs. 80 °C). However, DTT showed a significant reduction in its capabilities to reduce disulfide bridges (1.7e6 at 20 °C vs. 8.9e5 at 80 °C) due to thermal degradation. Please refer to Figure 3-5.

In conclusion, the average intensity was 1.5 times higher for the lowest analyzed temperature but had the longest incubation time (1.81e6 cps at 80 minutes vs. 1.18e6 cps at 20 minutes). The higher mixing of the samples also improved the intensities of both peptides 1.32-fold (1.4e6 cps for 1000 rpm vs. 1.1e6 cps for 300 rpm) and the prolonged incubation time was highly effective in facilitating denaturation. Based on the interactive effects, best performing conditions for denaturation were established at 20 °C, 80 minutes, and at 1000 rpm in a buffer solution that contained RapiGest® 1%, urea 2 M, and 150 mM DTT (Fig.3-8).

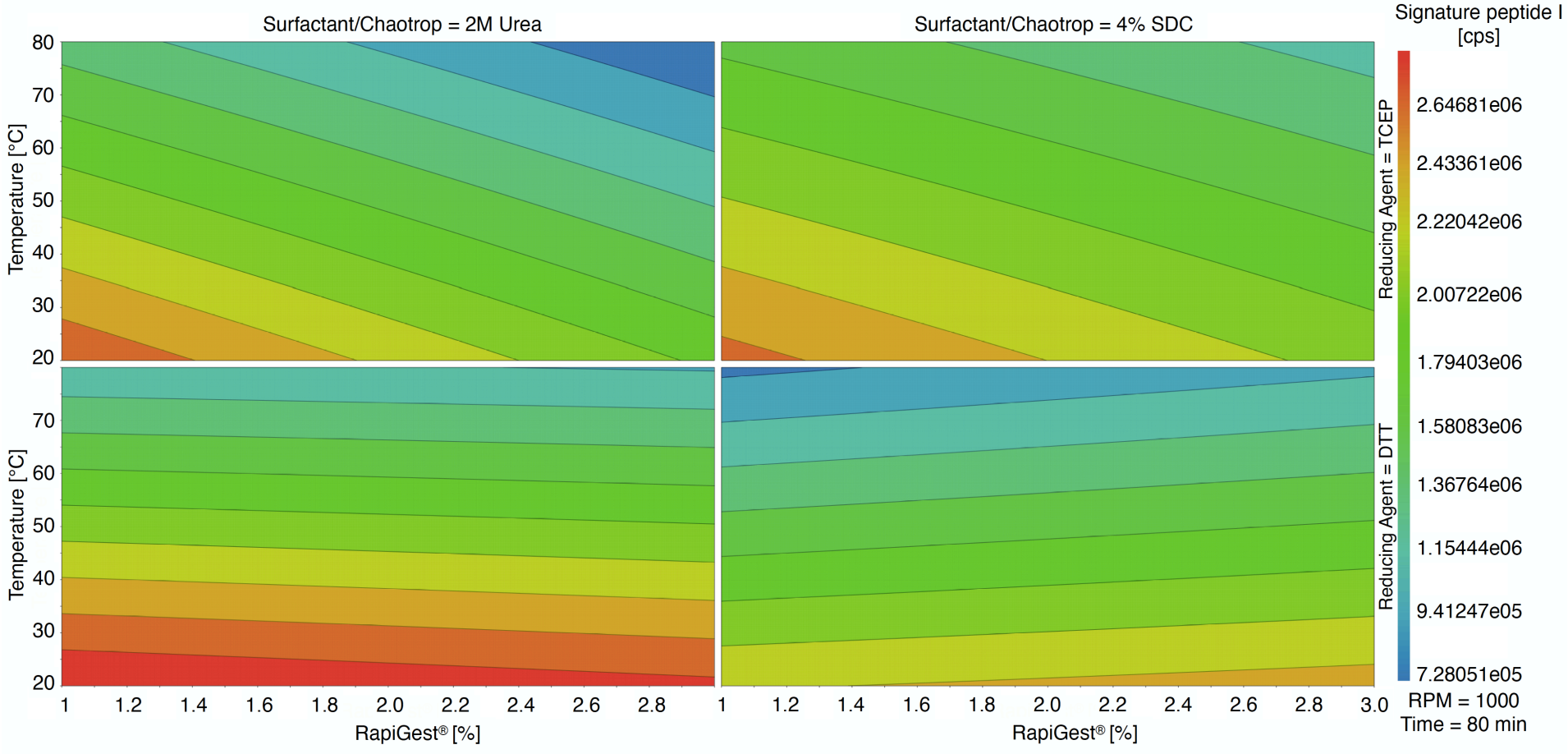

Figure 3-4 Interaction contour plot showing the impact of the chosen denaturation parameters *(surfactant, temperatures in °C, RapiGest® in %, and reduction agents) on the intensity of signature peptide I. The most desired region is illustrated in red and the undesired region is indicated by blue area.*

3.3.3 Alkylation of renin's cysteine residues

The incubation temperature was assumed to be an essential parameter in alkylating the thiol groups of cysteine residues. However, the generation of the surrogate peptide was not substantially improved at any temperature, except for a minor increase of 12% in intensity at 10 °C compared to 40 °C (4.4e6 cps at 10 °C for five minutes of incubation time vs. 3.9e6 cps for the same incubation time at 40 °C).

Compared to low temperature (10 °C), the high vortexing speed of 800 rpm produced a 10% higher intensity compared to the median speed (300 rpm). The predicted intensity decreased further when vortexing was not performed (0 rpm) resulting in a decrease in intensity of approximately 11% if compared to 800 rpm (4.5e6 cps for 800 rpm at 10 °C vs 4.1e6 cps at 0 rpm at 10 °C). Extended time showed no significant enhancements in surrogate peptide generation at all, while vortexing speed at higher temperatures showed similar behavior in signature peptide generation.

The quenching step was meant to avoid overalkylation of the tryptic peptides. Altering the temperature, vortexing speed and time showed that additional quenching was not advantageous in generating the signature peptide I (4.17e6 cps for the quenched reaction vs. 4.19e6 cps for the non-quenched reaction).

In conclusion, the best conditions for alkylation were found to be at 10 °C and 800 rpm for five minutes with no quenching. Corresponding to the coefficient effect plot, the individual effect was only significant ($\alpha<0.05$) for low temperature. Interactive effects were shown to be highly significant for vortexing speed and temperature (Fig. 3-8).

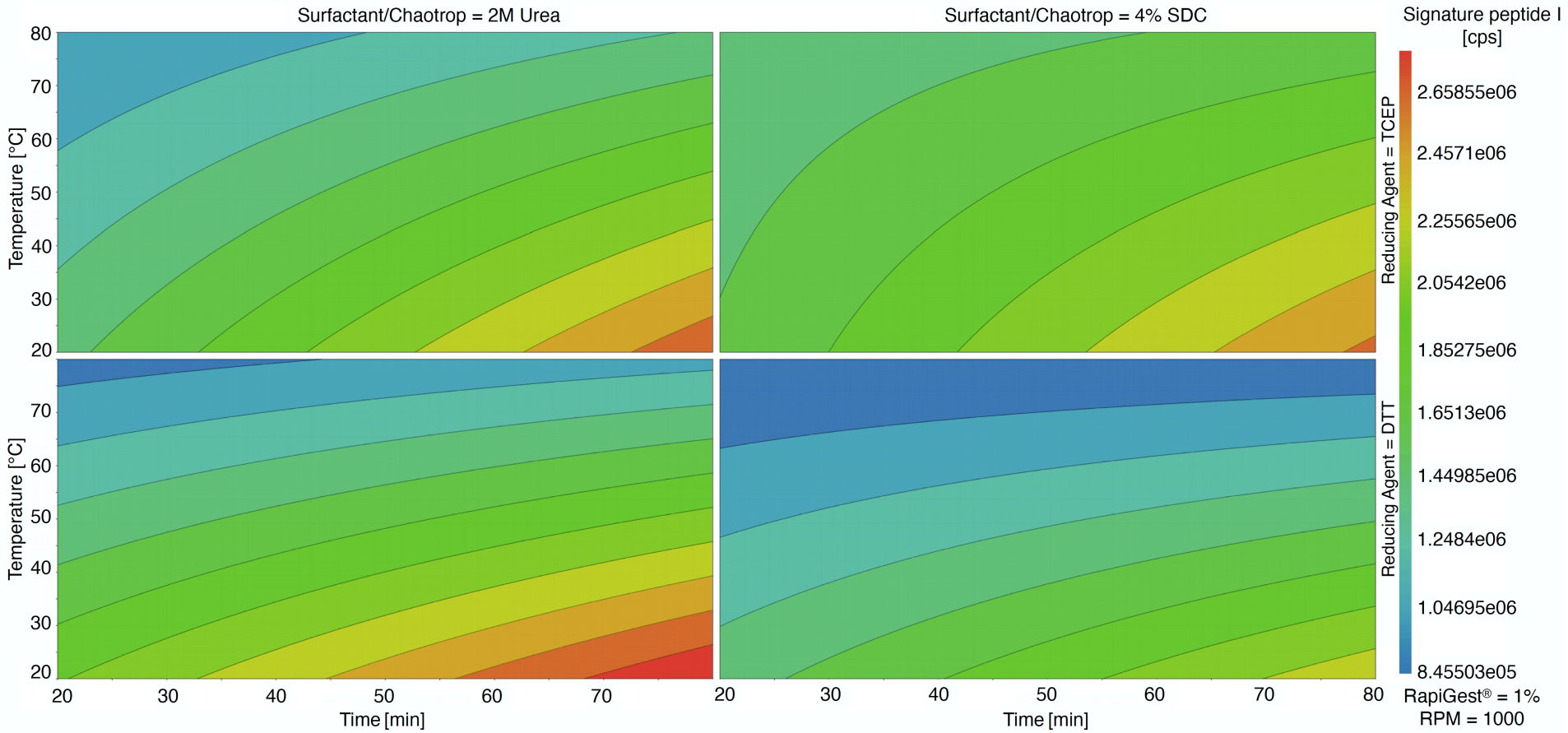

Figure 3-5 Interaction contour plot showing the impact of time and temperature on denaturation efficiency. *The surfactant/chaotropic agents and reducing agents were kept constant. The most desired region is illustrated in red and the undesired region is indicated by blue area (min: minutes; °C: degrees Celsius).*

3.3.4 Digestion procedure and immunocapture of active renin

In the case of renin, the direct digestion approach of the whole plasma matrix was not reasonable due to the low abundance. Consequently, assays like PC-IDMS, which were proven as a reliable method for protein quantification, were not suitable to develop a method for renin. A purification of either the whole renin protein or its surrogate was important to allow the detection and emphasized the need for an immunocapture procedure. The SISCAPA approach seemed an ideal opportunity to allow mass spectrometric measurement but the absence of the anti-renin surrogate specific antibody required high effort in the development of such an antibody. Moreover, immunogenicity was identified as an issue (Whiteaker et al. 2010). Therefore, the whole protein purification by commercially available antibodies was chosen in this work.

3.3.5 Response surface D-optimal model evaluation

Statistical analysis was performed using a multiple linear regression model. Due to the reduced numbers of experiments, the G-efficiency was estimated at 0.79, which fulfilled the criteria for a representative D-optimal design. The statistical values of the ANOVA results confirmed a good prediction of the model. Over the 90 performed experiments the Q^2 value was 0.916 and the R^2 value was 0.950. These results fulfilled the predefined requirements and proved a good fit as well as being a good predictive character of this model. The optimizer tool suggested a probability of failure of 0.1% by generating the optimal settings.

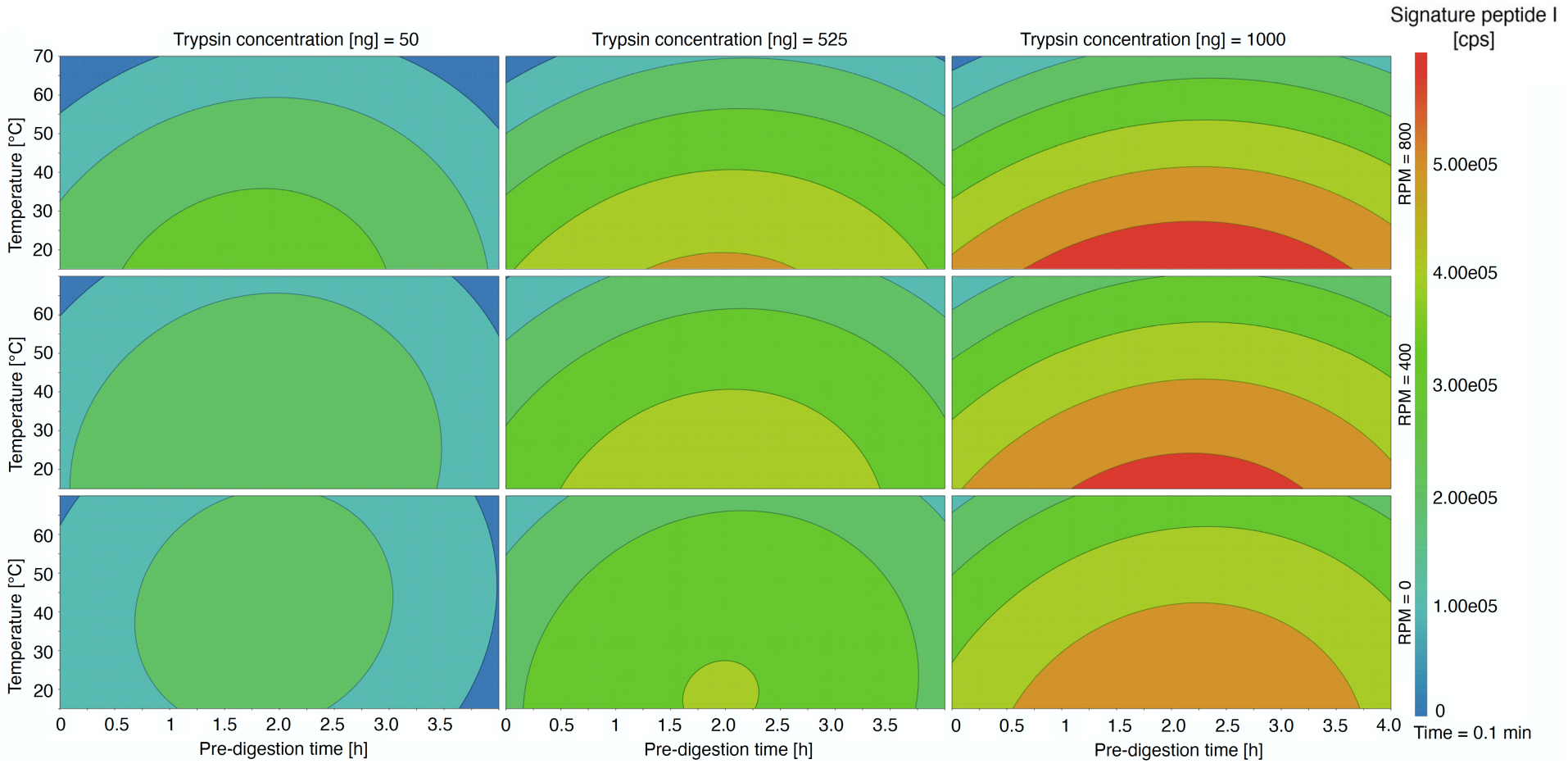

Figure 3-6 Interaction contour plot showing the impact of pre-digesting time, trypsin concentration and temperature on the digestion result. *The second digestion time was maintained at 0.1 h. The most desired region is illustrated in red and the undesired region is indicated by blue area (h: hour; ng: nanogram).*

3.3.5.1 Influence of trypsin concentration

The alteration of the trypsin concentration was identified as being the most effective component in optimizing digestion. The results for the RSM demonstrated that the best results in signal intensity and required processing time were achieved with trypsin concentrations of 1 µg. Trypsin concentrations greater than 1 µg were not investigated in order to avoid autolysis due to an imbalance between the available substrate (antibody concentration 1 µg) and trypsin. The smallest investigated amount of trypsin was 50 ng, which was not sufficient for reducing overall procedure time. By increasing the trypsin concentration, the generation of signature peptide I was substantially improved. The addition of 366 ng of trypsin into the sample increased signature peptide I's generation by 49.5%. This was further optimized by 525 ng, 683 ng and 1000 ng trypsin (73%, 97.5% and 138% signal improvement compared with 50 ng of trypsin). By adding larger amounts of trypsin, the time factor could be reduced. High trypsin concentrations (1µg) reduced the digestion time fivefold compared to a conventional overnight approach (16 hours). Low trypsin concentrations yielded almost identical levels of signature peptide generation but only after a longer period of time (30 hours digestion with 34% decrease of intensity for 50 ng trypsin vs. 1 µg trypsin; Fig. 3-6; 3-7; 3-8).

3.3.5.2 Influence of pre-digestion step, time, and instrumental conditions

The digestion process is highly influenced by time, but also by different kinds of energy—thermic (temperature) as well as kinetic (vortexing speed), which had a major impact on trypsin's performance and could not be evaluated alone. As shown by the DOE results, the generation of the signature peptide I was strongly correlated by these factors interacting with each other (Fig. 3-8).

Elevated temperatures (70 °C) could not enhance proteolytic cleavage. Based on the peptide's properties, signature peptide I was more prone to oxidation and deamidation due to containing tryptophan and asparagine residues. Moreover, trypsin might itself be denatured at higher temperatures. Lower temperatures (15 °C) seemed to preserve the integrity of the peptide, whereas trypsin's highest proteolytic performance was either achieved due to higher concentrations or a longer time. The effect of kinetic energy generated by vortexing had a higher relevance at a temperature of 15 °C (59 % increase of the signature peptide's intensity at 800 rpm vs. 0 rpm). At higher temperatures, this effect became negligible. During digestion, all individual effects were significant as seen in figure 3-8. Please also refer to figure 3-6 and 3-7.

The pre-digesting step combined with time revealed that optimal digestion was achieved after 2.16 hours of total digesting at a temperature of 15 °C and a vortexing speed of 800 rpm (Fig. 3-7). This means that the pre-digestion step is enough to generate the signature peptide I, as only a short additional digesting time (0.1 hours) was predicted for the second digestion step. The second digestion was subsequently skipped for the final setting.

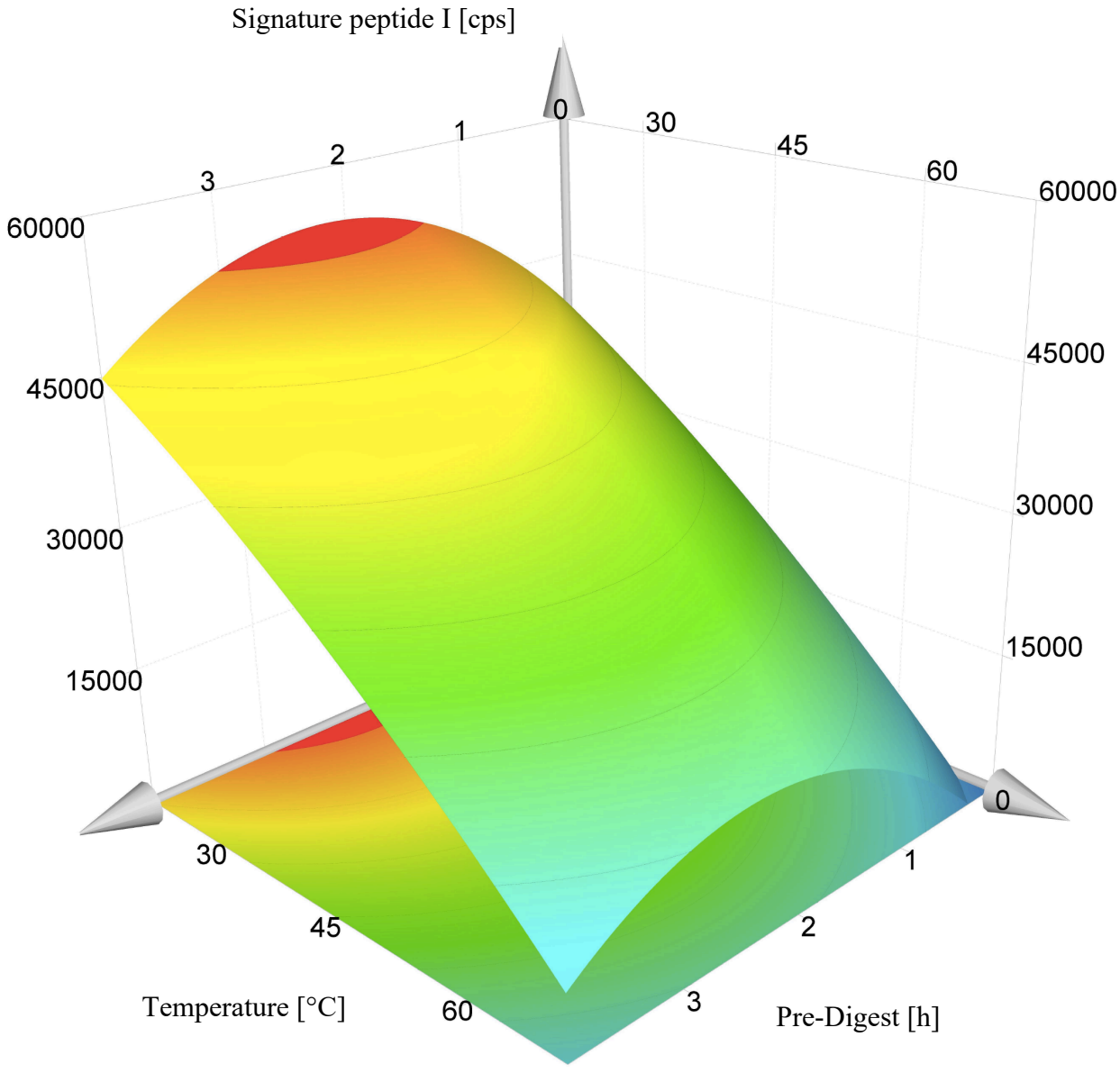

Figure 3-7 A response surface plot of pre-digestion time against temperature. *The red area is the optimal setting for the highest generation of signature peptide I.*

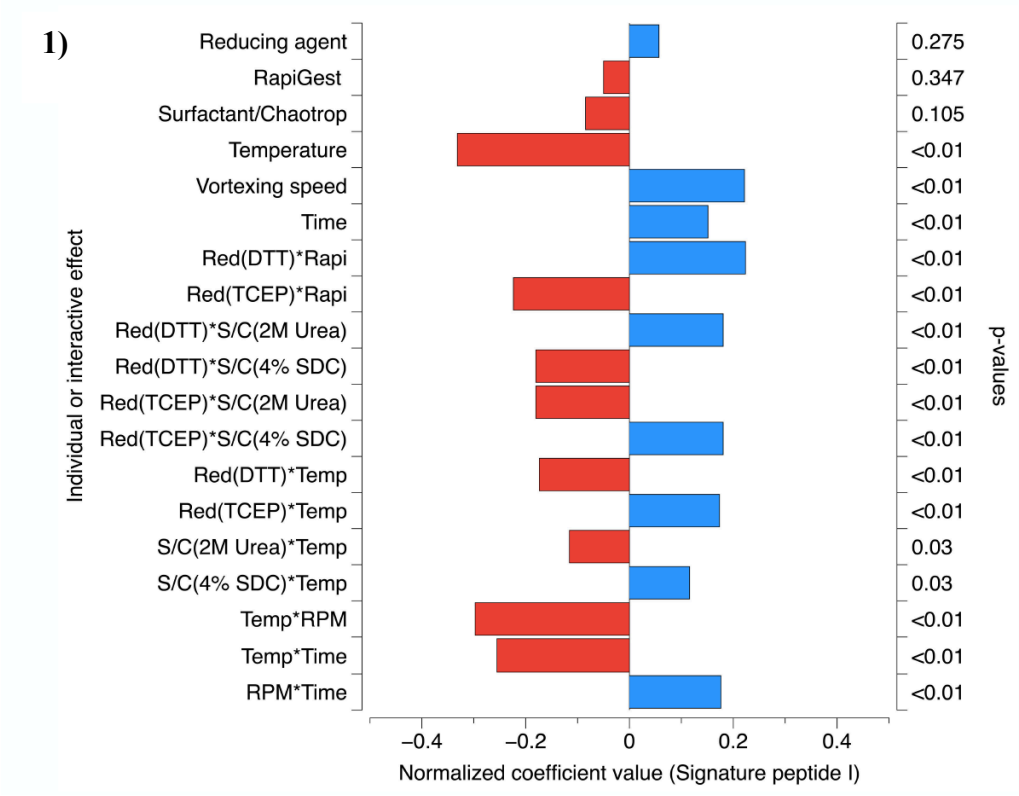
1)
Reducing agent
RapiGest
Surfactant/Chaotrop
Temperature
Vortexing speed
Time
Red(DTT)*Rapi
Red(TCEP)*Rapi
Red(DTT)*S/C(2M Urea)
Red(DTT)*S/C(4% SDC)
Red(TCEP)*S/C(2M Urea)
Red(TCEP)*S/C(4% SDC)
Red(DTT)*Temp
Red(TCEP)*Temp
S/C(2M Urea)*Temp
S/C(4% SDC)*Temp
Temp*RPM
Temp*Time
RPM*Time
0.275
0.347
0.105
<0.01
<0.01
<0.01
<0.01
<0.01
<0.01
<0.01
<0.01
<0.01
<0.01
<0.01
0.03
0.03
<0.01
<0.01
<0.01
Individual or interactive effect
p-values
−0.4
−0.2
0
0.2
0.4
Normalized coefficient value (Signature peptide I)

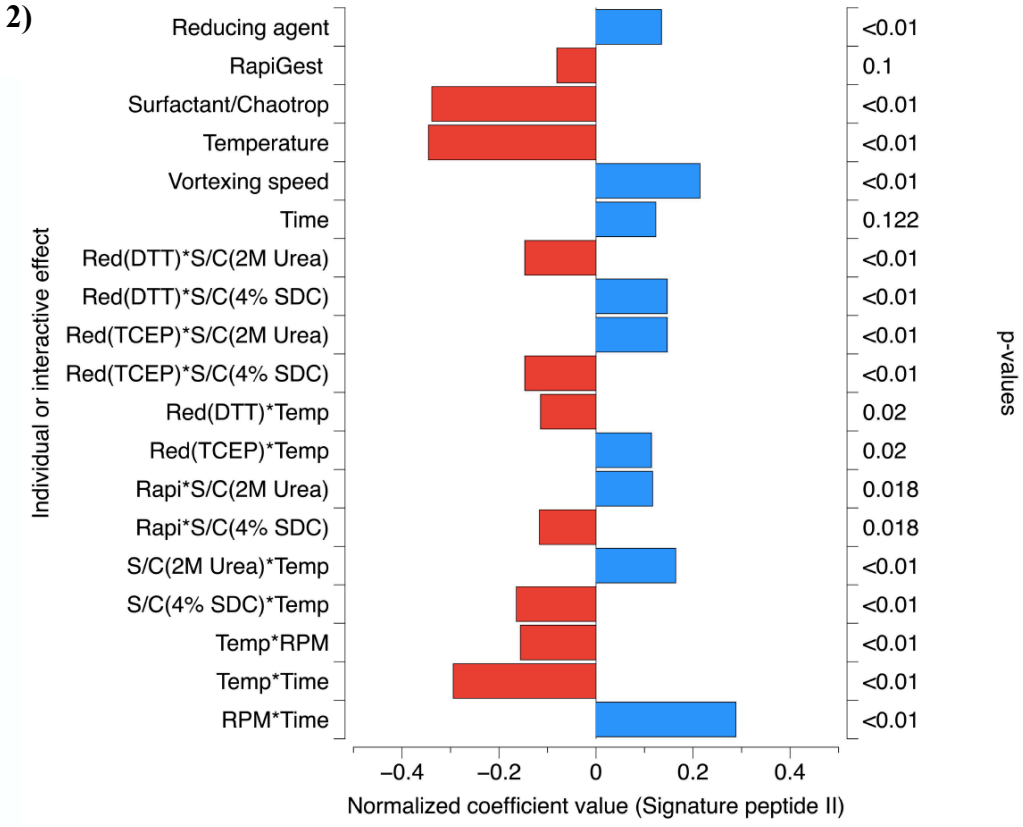
2)
Reducing agent
RapiGest
Surfactant/Chaotrop
Temperature
Vortexing speed
Time
Red(DTT)*S/C(2M Urea)
Red(DTT)*S/C(4% SDC)
Red(TCEP)*S/C(2M Urea)
Red(TCEP)*S/C(4% SDC)
Red(DTT)*Temp
Red(TCEP)*Temp
Rapi*S/C(2M Urea)
Rapi*S/C(4% SDC)
S/C(2M Urea)*Temp
S/C(4% SDC)*Temp
Temp*RPM
Temp*Time
RPM*Time
<0.01
0.1
<0.01
<0.01
<0.01
0.122
<0.01
<0.01
<0.01
<0.01
0.02
0.02
0.018
0.018
<0.01
<0.01
<0.01
<0.01
<0.01
Individual or interactive effect
p-values
−0.4
−0.2
0
0.2
0.4
Normalized coefficient value (Signature peptide II)

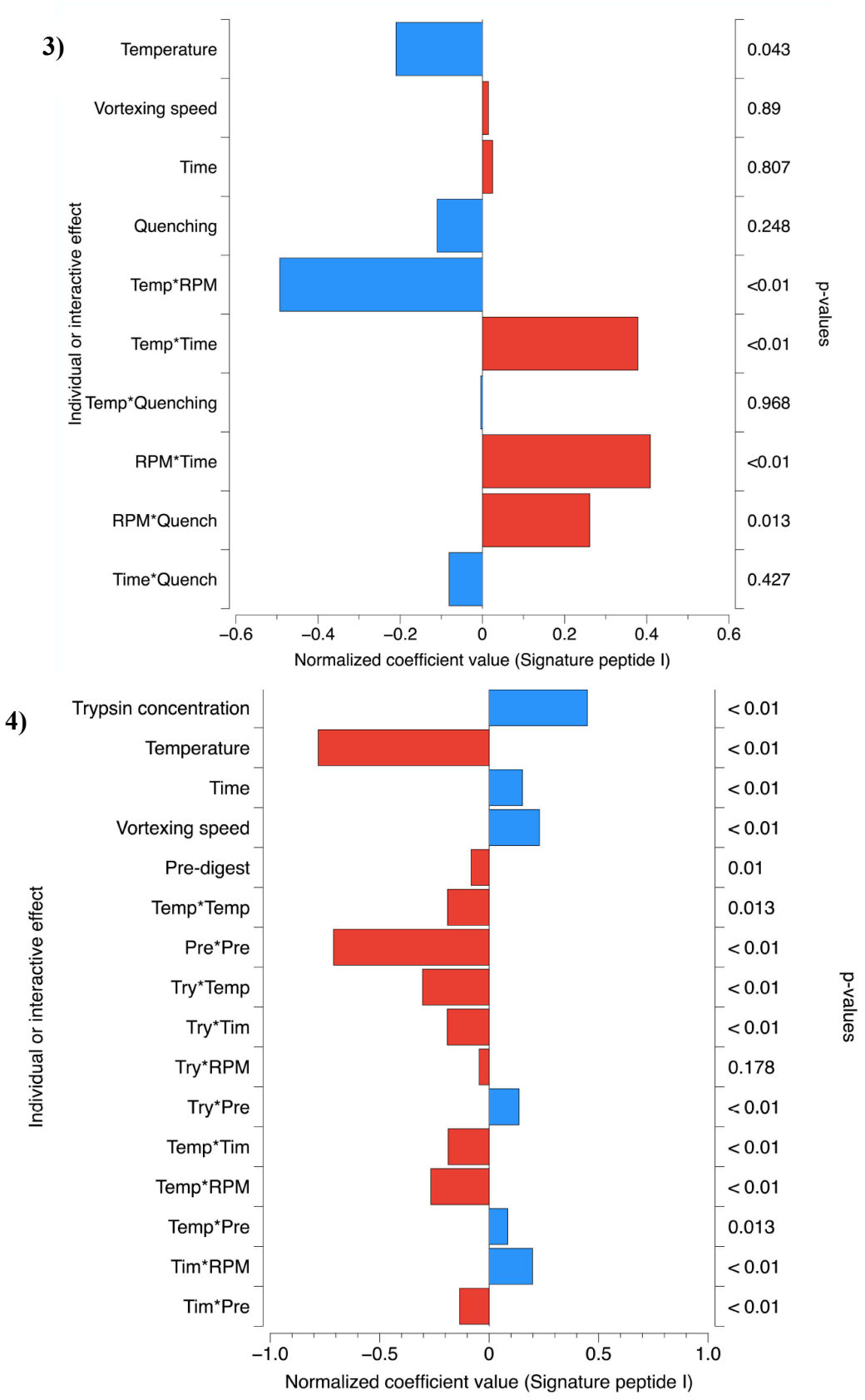

Figure 3-8 Normalized plots of the denaturation DOE for signature peptide I (1) and signature peptide II (2), alkylation DOE (3) and digestion DOE (4) *showing individual effects and interactive effects with normalized coefficient values.(Red: reducing agent; Rapi: RapiGest; S/C: surfactant/chaotrop; Temp: temperature; Quench: Quenching; RPM: vortexing speed; DTT: dithiothreitol; TCEP: tris(2-carboxyethyl)phosphine; Try: trypsin; Pre: pre-digestion).*

3.3.6 Solid-phase extraction, liquid chromatography, and mass spectrometry

Preliminary experiments had shown the superiority of mixed-mode strong-anion exchanger material (MAX; Fig. 3-9) if compared to a mixed-mode strong-cation exchanger (MCX; Fig. 3-10). Therefore, the customized SPE protocol development based on MAX material (Fig. 3-9) and included recommendations on peptide purification given by the vendor Waters (e.g. elution solvent acetonitrile instead of methanol). Based on the experimental procedure including the digestion of renin, the purification by SPE was customized for the digested tryptic peptides and not to whole renin protein. Tryptic peptides consist of a positively charged amino acid (lysine or arginine), therefore a strong-cation exchanger appeared reasonable. However, signature peptide I had a weak acidic character caused by the aspartic acid residue and the c-terminal end carboxy group. This character was used to improve enrichment, by performing the purification with mixed-mode strong-anion sorbent material leading to an increase of sixfold signal intensity.

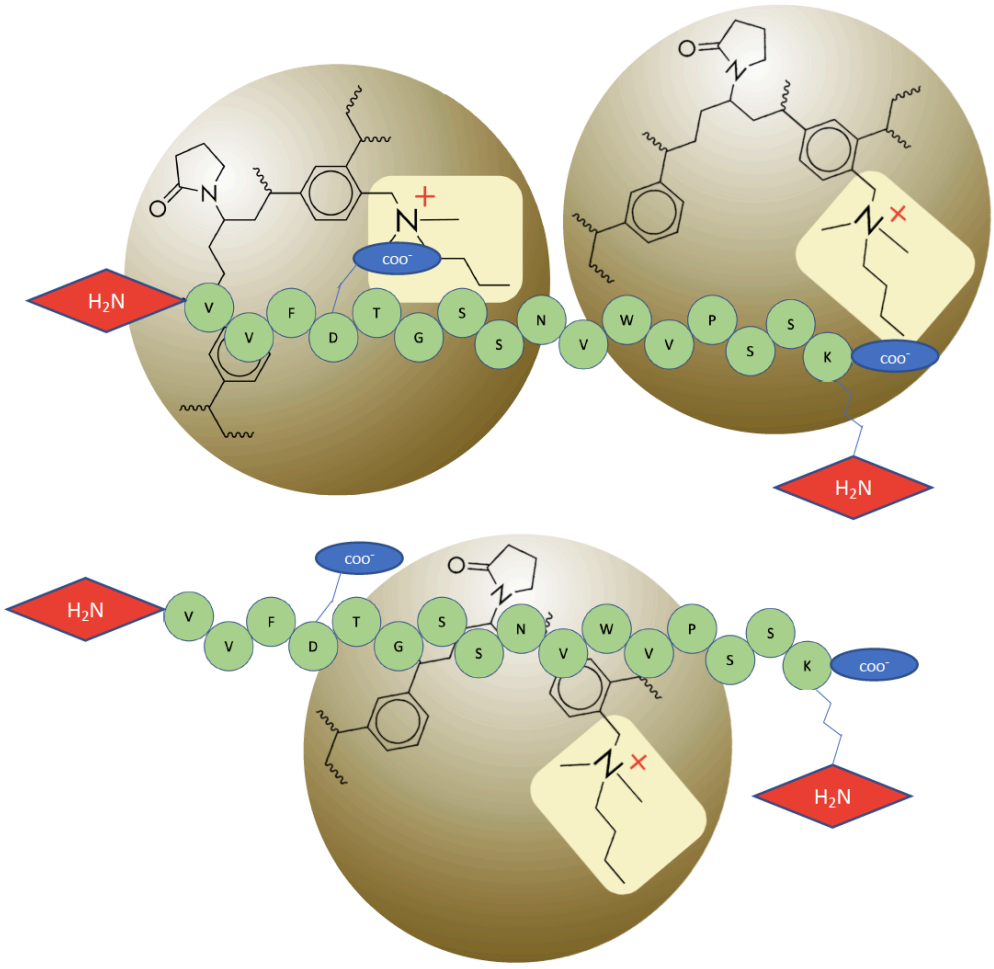

Figure 3-9 Interaction with OASIS strong anion mixed mode sorbent material and signature peptide I *(pH 12; Waters®)*

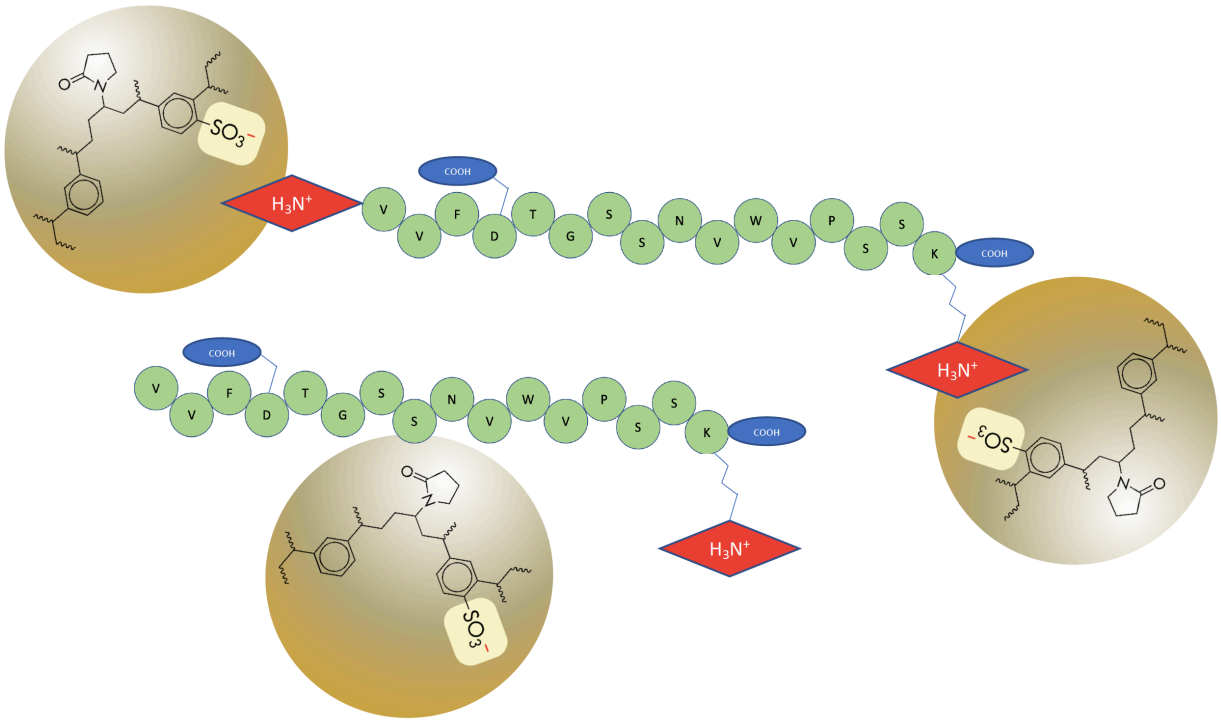

Figure 3-10 Interaction with OASIS strong cation mixed mode sorbent material and signature peptide I *(pH 2; Waters®)*

Based on the chromatographic separation results, the XSelect CSH C-18 column outperformed the XBridge BEH C-18 by its ability to enrich the signature peptide before mass spectrometric analysis. The optimized gradient allowed the best response and peak shape of the signature peptide leading to a high-throughput method with a runtime of four minutes. As a supercharging solvent, DMSO additionally improved the ionization of the peptides in the ESI source. This has also been confirmed by other research groups in proteomics (Hahne et al. 2013).

The peptide elucidation was conducted utilizing the TripleTOF, which confirmed the identity of the surrogate peptide by its typical y- and b-fragmentation scheme. Regarding the signature peptide I, the PSSK fragment (y4) showed the highest abundance in enhanced ion mode and was chosen for further determination. The mass to charge ratio for signature peptide I was 854.9 to 418.2296 *m/z*. Further details are depicted in Fig.3-11.

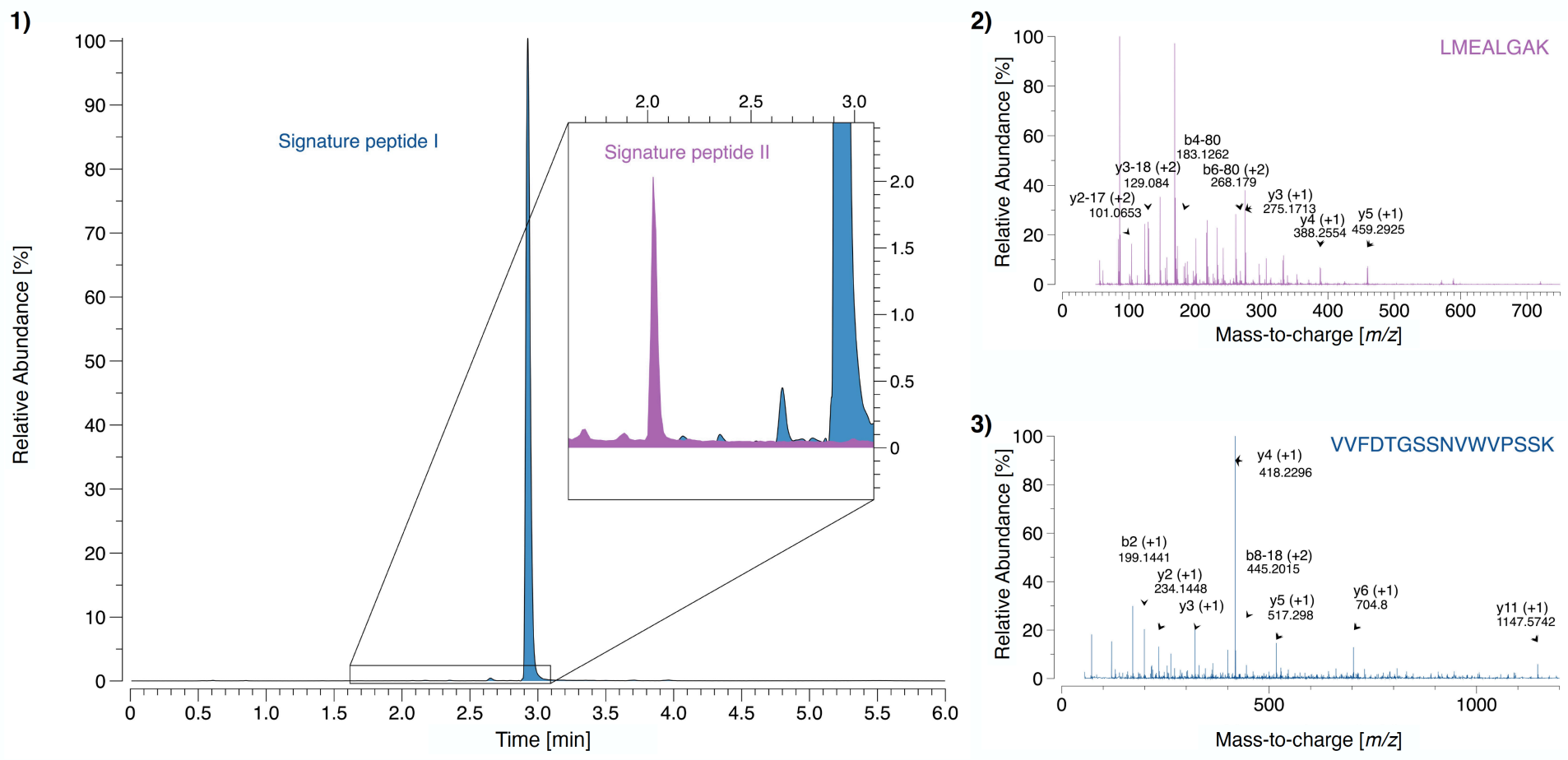

Figure 3-11 Chromatographic separation of signature peptide I and II. (1) MS/MS data for signature peptide II (2) and signature peptide I (3) *showing typical y and b-fragment of tryptic peptides*

3.3.7 Applicability of active renin hybrid approach in human plasma

This applicability investigation was meant to investigate three aspects of the here presented hybrid approach. First, it was verified that the hybrid mass spectrometric assay was capable of determining human renin levels. The transferability of the developed hybrid approach to human matrix was confirmed.

The second aim evaluating how much the required process duration can be shortened by the hybrid approach was also answered. The applicability of the hybrid approach with optimized sample pretreatment was assessed against a conventional approach in human plasma. While in the conventional approach an overall pretreatment time of 20.25 hours was required to obtained mass spectrometric responses of 4.5e4 cps, comparable results (4.4e4 cps) were achieved in 4.43 hours utilizing the here presented hybrid approach. By applying this optimized protocol, the prolonged digestion time could be reduced fivefold without any loss in final response of signature peptide I. It confirmed that the hybrid approach facilitated a more efficient and less labor-intensive method.

Third, a good repeatability of the hybrid approach in human plasma was achieved. Three human samples were independently prepared and measured separately. This triplicate resulted in a low variability of 2.24 % (CV). The finding indicated the robustness of assay and proved that this developed assay was capable of measuring reliable values of active renin.

3.4 Conclusion

Applying the multistep DOE approach to identify the optimal conditions for sample preparation successfully enabled the successful determination of human active renin in plasma by a hybrid approach of immunocapture and LC-HRMS. Moreover, the developed procedure reduced the time taken for the total assay procedure fivefold, without any loss in the sensitivity of the assay.

4. Human prorenin determination and differentiation to active renin by hybrid LC-MS

Parts of this chapter had been published in the peer-reviewed journal: 'Rapid Communications in Mass spectrometry' with the title 'Human prorenin determination by hybrid immunocapture liquid chromatography-mass spectrometry: A mixed-solvent-triggered digestion utilizing D-optimal design' (doi: 10.1002/rcm.8932).

4.1 Background and aim

Human prorenin, which seems to be an inactive precursor of mature renin, has gained attention since it was discovered that its concentration is correlated with different diseases. Some studies even suggest it as a potential biomarker, e.g. in diagnosing primary hyperaldosteronism or diabetes-induced nephropathy (Naruse et al. 1995; Berge et al. 2015). In addition to the pathological influence of prorenin, it also appears to have important functions, as evidenced by its secretion in reproductive tissues like ovaries (Sealey et al. 1986). Compared to active renin, which is usually analyzed for cardiovascular disease, prorenin is released continuously and is not influenced by acute stimuli such as a change in body position. Concerning the structural difference between prorenin and renin, a 43-amino-acid-long pro-segment that covers the catalytical center is the sole structural difference between their amino acid sequences (Hsueh and Baxter 1991; Suzuki et al. 2003). This pro-segment can change its conformation and uncover the proteolytical center, making the differentiation between active renin and prorenin difficult for many immunoassays (Menard et al. 2006). In most ligand-binding assays, reliable determination is only achieved by either proteolytical cleavage of the pro-segment after cryoactivation at 4 °C overnight, or by a renin inhibitor that promotes the unfolding of the pro-segment. These assays are time-consuming and require calculative levels that may lead to inconsistent and inaccurate results (Naruse et al. 1995; Derkx et al. 1996; Krop et al. 2011; Tu et al. 2012).

The current challenges in bioanalytical determination of low-abundance proteins using mass spectrometry are commonly addressed by combining immunocapture with a customized digestion procedure (Anderson et al. 2004). In the past, the common performed digestion procedure was often unsuitable due to their extensive preparation requirements and long procedure durations (Figeys 2013). Several approaches have been developed to accelerate these procedures, however, most of these approaches have their own benefits and limitations (Russell

et al. 2001; Son et al. 2007; Wang et al. 2008; Proc et al. 2010; Andrews Kingon et al. 2013; Serra et al. 2016). These approaches require additional chemicals or need special equipment to promote denaturation (Capelo et al. 2009; Kailasa and Wu 2014). The denaturing agents that are used in pure aqueous digestion procedures lead to difficulties with mass spectrometric detection as well as possible interference with reversed-phase chromatographic separation, resulting in unpredictable peptide retention and elution properties (Son et al. 2007). Moreover, unintentional reactivity of the used denaturing agents with the peptides of interest has been reported (Kollipara and Zahedi 2013). Other agents such as guanidinium hydrochloride require an extended cleanup and subsequent dilution before tryptic digestion, making them unsuitable for low-abundance proteins (Son et al. 2007).

Different types of organic solvents have shown their suitability for the denaturation of the protease-resistant proteins (Russell et al. 2001). These commonly applied organic solvents (e.g. acetonitrile and methanol) are characterized by a strong denaturation power. Moreover, these solvents have shown their compatibility with trypsin, particularly when modified (i.e. alkylated lysine-residues) (Batra and Gupta 1994; Östin et al. 2007; Sun et al. 2012). Several proteomic approaches have confirmed the usefulness of mixed aqueous-organic digestion for the acceleration and better production of surrogates for proteolytic-resistant proteins (Russell et al. 2001; Strader et al. 2006; Östin et al. 2007; Wall et al. 2011; Ranasinghe et al. 2018). However, it requires individual evaluation per analyte of interest and depends on structural particularities and amino acid sequence. For example, Shuford et al. found organic solvent as detriment to quantitative production of their peptides of interest (Shuford et al. 2012a).

To optimize digestion efficiency, the various factors that impact the generation of surrogates can be investigated either by analyzing one factor at a time or by using a statistical approach. By investigating each factor separately, the optimal set point might be missed. Additionally, the determination of two or more surrogates makes this approach inappropriate. Therefore, a statistically planned experimental design following the quality-by-design approach allows for the analysis of different factors interacting with each other within a manageable number of experiments, and is described as the Design of Experiments (DOE) (Loziuk et al. 2013; Feickert and Burckhardt 2019).

This study aims to investigate the suitability of a rapid mixed-solvent-digestion approach to prorenin determination using the DOE concept. The hybrid immunocapture LC-MS, which uses a label-free protein-level enrichment should facilitate the reliable determination of prorenin and differentiate it from structurally related compounds. Further optimization experiments had to

be performed to improve the method sensitivity and to avoid large variations by reducing non-specific adsorption and solubility issues by optimizing all of the preparative steps performed when conducting the hybrid immunocapture LC-MS assay. Lastly, its applicability in human plasma must be confirmed.

4.2 Methods

4.2.1 Experimental methods

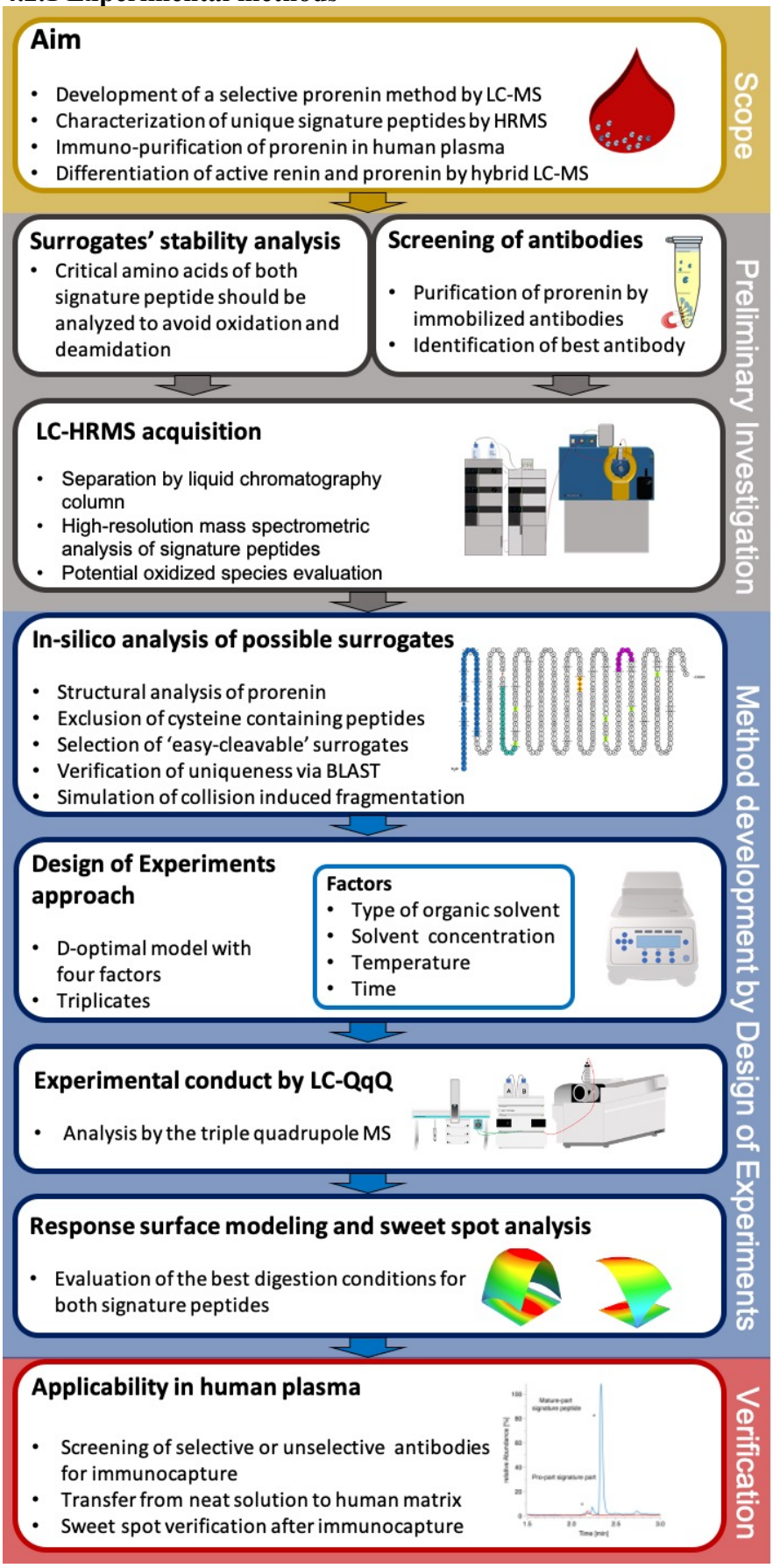

Figure 4-1 Illustration of developing and optimization processes for active renin and prorenin differentiation. *This flowchart shows the designed and performed experiments carrying out important steps of method development focusing on immunocapture, stability, organic digestion and applicability of the developed method.*

4.2.2 Materials and Chemicals

Human recombinant prorenin (≥85%) was supplied by Cayman Chemicals (Ann Arbor, USA). TCPK-treated modified trypsin and Dynabeads® Protein G kit was purchased from Thermo-Scientific (Rockford, USA). Anti-prorenin antibodies were purchased from three different vendors (Gentex, R&D systems, Molecular Innovations). Ammonium bicarbonate (>99.5%) was obtained from Sigma-Aldrich (Taufkirchen, Germany). Methanol optima® (LC-MS grade), tetrahydrofuran (HPLC-grade), 2-(4-(2-Hydroxyethyl)-1-piperazinyl)-ethansulfon acid (HEPES; >99%), acetone (HPLC-grade), and DMSO (p.a.) were supplied by Fisher Chemicals (Geel, Belgium). Water (LC-MS grade) and sodium phosphate dibasic (>99%) were provided by Riedel-de Haen (Seelze, Germany), and formic acid (98%, p.a.), potassium chloride (>99%) and acetonitrile (UHPLC grade) were supplied by Applichem (Darmstadt, Germany). Sodium chloride (>95%) and potassium dihydrogen phosphate (>99%) were obtained from Carl Roth (Karlsruhe, Germany). Tween 20 was supplied by Caelo (Hilden, Germany). Masterblock PP 96-well plates were obtained from Greiner Bio-One (Kremsmuenster, Austria). Anti-renin antibodies and polystyrene-coated plates were obtained from DRG Instruments GmbH (Marburg, Germany). Human blood plasma was collected from a healthy male volunteer in S-Monovette® K3 EDTA tubes (Sarstedt, Nuembrecht, Germany).

4.2.3 Selection of signature peptides for determination

The mature part (chain; entry number P00797) plus the pro-peptide (43 amino acids) forms the so called prorenin, which was extracted the UniProt® Database. The selection of the signature peptides was carried out by evaluation of the amino acid structure using protter®, and possible tryptic cleavage sites were found. Peptides that contained cysteines were excluded to accelerate the sample pretreatment by avoiding reduction and alkylation steps. As additional tool, Prospector® was used to prove the desired in-silico digested peptides and simulate their fragmentation scheme to identify possible transitions. The selected peptides were confirmed as suitable for tryptic digestion by in-silico proteolysis and appraised by their amino acid structures (Fig.4-1)

As shown by Shuford et al., the analysis of peptide characteristics is essential for the development of a reliable assay by using the surrogate peptide approach (Shuford et al. 2012b). By performing a combined in silico and experimental analysis of the surrogate peptide's properties [Peptide Analyzing Tool (ThermoFisher, Rockford, USA)], peptide characteristics of the digested prorenin were assessed. The quantitative profiling of prorenin was conducted

utilizing a sequential window acquisition of all theoretical fragment ion spectra mass spectrometry (SWATH).

4.2.4 Antibody screening for the hybrid approach

Human plasma is a highly complex matrix that makes the detection and determination of low-abundance proteins difficult. Therefore, immunocapture was chosen as a reliable and selective method for human prorenin purification. This study used antibodies against full-length prorenin. By using unselective as well as selective antibodies from different vendors, their capability to capture prorenin was examined. In total, seven different antibodies were screened for their suitability in a hybrid immunocapture LC-MS approach. Each antibody experiment was performed using an immobilization process on Dynabeads® Protein G magnetic beads.
For the performance evaluation, 20 ng human recombinant prorenin was spiked into the plasma matrix (300 µL). The Dynabeads® protein G beads combined with the antibodies were incubated for 1 hour while vortexing in spiked plasma. A three-step washing process was performed: the samples were washed twice with a phosphate-buffered saline buffer (PBS 0.01 % Tween 20) at the beginning, followed by a wash in a 25 mM ABC buffer to eliminate any interference by the Tween 20. All immunocapture complexes were digested completely in mixed solvents by adding 1 µg of modified trypsin and measured in triplicates using high-resolution TripleTOF mass spectrometry to confirm the identity of prorenin.

4.2.5 Analyzing the stability of signature peptide residues and the pro-segment

Human prorenin's pro-segment structure can change its conformation, which is influenced by temperature and pH. To analyze the effect of this unfolding and its influence on the digestion procedure, high (40 °C) and low (10 °C) incubation temperatures were used to investigate the effect on tryptic cleavage in the mixed solvent buffer following immunocapture.
The mature-part signature peptide and the pro-part signature peptide consist of a tryptophan residue that may be prone to different oxidized products. Kynurenine (+ 4 Da), hydroxytryptophan (+ 16 Da), and N-formylkynurenine/dihydroxytryptophan (+ 32 Da) represent different oxidative reaction products of tryptophan residue. Additionally, the methionine residue of the pro-part signature peptide was also considered for oxidation. Therefore, an investigation was performed on how potential oxidative agents such as acid and DMSO, which were used in the injection solvent mixture, influence these reactions (van de

Weert et al. 1998; Perdivara et al. 2010). Possible oxidative products of both the mature part or pro-part signature peptide were calculated using the Prospector® tool.

4.2.6 Design of experiments criteria for digestion

The design and evaluation of the experiments were accomplished using MODDE Pro© software (MKS Instruments AB Malmoe, Sweden, version 12.0). The D-optimal model was chosen as an experimental design due to the reduced costs and necessary number of experiments. In total, 114 experiments were required. To allow for a sufficient comparison to a full factorial design, we aimed for a G-efficiency of ≥ 0.6. Additionally, the model fit (R^2) and the Q^2 value, which estimate the predictive value of the design, were required to be ≥ 0.5. An appropriate design for overall model strength was defined as the difference between Q^2 and R^2 by values of below 0.3. Both signature peptides of human prorenin were incorporated into the model as a response, wherein the pro-part signature peptide was favored due to its uniqueness.

4.2.6.1 D-optimal design for mixed-solvent digestion

20 ng of human recombinant prorenin was added to the 20 mM ammonium bicarbonate buffer (ABC) followed by the addition of 1 µg modified trypsin and adjusted to 100 µL with an organic solvent. The aqueous–organic solvent ratio varied between the experiments based on the corresponding DOE. Different organic solvents (tetrahydrofuran, acetone, methanol, and acetonitrile) were used to analyze the influence of the organic solvent type and its concentration (60%–90%) on the digesting process. The incubation time ranged from 5 minutes to 2 hours. The temperature was varied from 10 °C to 40 °C to investigate its impact on signature peptide generation. The lower temperature limit was chosen because of instrumental limitation and the upper limit was set at maximum 40 °C to limit imprecision by irregular solvent evaporation. Following the tryptic proteolysis, the mixed solvents were evaporated under a nitrogen stream and reconstituted in a mixture of 5% DMSO, 20% methanol, and 0.1% formic acid in water [v/v/v/v].

4.2.6.2 Sweet-spot analysis of optimal digestion conditions

Due to the differences in the size as well as the amino acid composition and number of both investigated peptides, it was considered likely that distinct generation conditions for each signature peptide would be identified. Consequently, a sweet-spot analysis was performed in

order to determine optimal settings with given predeterminants for a reliable generation of both surrogates. These calculations were made with 50000 iterations at a resolution of 64 including all factors within the Monte Carlo simulation. For a robust and reliable result, the probability of failure, which estimates a false peak area prediction, was set to an acceptable limit of 0.5%.

4.2.7 Optimization of immunocapture by investigating optimal incubation and washing buffer

The impacts of using different buffers were examined on non-specific protein adsorption and solubility during the performance of the immunocapture procedure. The analysis of potentially suitable incubation and washing buffers was performed by spiking 5 ng of human active renin into each of three buffers (250 µL), 50 mM PBS, 50 mM HEPES, and 50 mM ABC, followed by incubation on the anti-active renin polypropylene-coated plates for 1.5 hours. After the incubation, the active renin and prorenin containing buffer was discarded and then the plate was washed three times with either the used buffer or pure water. A physiological environment is necessary for optimal binding between an antigen and an antibody, and these buffers were chosen because their optimal buffering capacities occur at pH 7.4. All buffers were sterile filtered by a 0.22 µm filter with a syringe to avoid any contamination. Along with evaluating the selected buffer systems, the addition of a non-ionic detergent (Tween 20) at non-denaturing concentrations (0.01% and 0.025%) was assessed for the two best-performing buffers.
The measured response for this investigation was the intensity of the mature-part signature peptide, which represented active renin, and prorenin, following the digestion procedure, using 38 µL 50 mM ammonium bicarbonate buffer (ABC), 1 µg of TCPK-treated modified trypsin, and 62 µL acetonitrile. After digestion, the solvent was evaporated under a nitrogen stream and reconstituted in the initially used injection solvent composition (93.9% water, 5% methanol, 1% DMSO, and 0.1% formic acid [v/v/v/v]).

4.2.8 Impact of container material and injection solvent composition on the analysis of signature peptides

To optimize the injection solvent composition, which is necessary to avoid non-specific adsorption after immunocapture tryptic digestion, the following analysis was accomplished. An organic-aqueous, mixed-solvent digestion was performed using 4 µL prorenin and active renin solution (10 ng), 32 µL 50 mM ABC, 1 µg of TCPK-treated modified trypsin, and 62 µL acetonitrile. After digestion, the mixture was completely evaporated and reconstituted in the DOE-generated mixture.

Therefore, various injection solvent compositions combined with five 96-well plates obtained from four vendors (Waters, Eppendorf, Greiner, and Brand) were analyzed. Different injection-solvent compositions, consisting of variable concentrations of water (10%–98%), methanol (0%–40%), DMSO (1%–40%), and formic acid (1%–10%) were evaluated for each plate separately. The D-optimal model facilitated the identification of the best performing injection solvent composition, which was characterized by the highest signal intensity and high precision. Precision was determined by performing repeated sample analysis in quadruplicate.

The optimal settings necessary for the reliable analysis of both surrogates were calculated using a set of predeterminants. These calculations were made using 50,000 iterations at a resolution of 64, which include all factors within the Monte Carlo simulation. For a robust and reliable result, the probability of failure, which estimates a false peak area prediction, was set to an acceptable limit of 0.5%.

To compare optimized compositions, either the initial injection solvent, which was the starting LC gradient, or the optimized DOE injection solvent were used.

4.2.9 Applicability of the hybrid approach in endogenous matrix

Two aspects of the method's applicability in plasma were verified: First, the identified sweet-spot conditions for the digestion were conformed following the immunocapture in neat solution as well as in plasma being donated by a healthy male volunteer. To this purpose, 20 ng human prorenin were spiked into either PBST buffer (neat solution) or 300 µL human plasma. The applied sweet-spot conditions concerning digestion using 84% acetonitrile, 16 °C digestion temperature, and 98-minute incubation time were measured in triplicate by LC-HRMS. Second, the selectivity of the developed method was determined in blood samples containing both prorenin and active renin. For this experiment, 20 ng of human prorenin plus 20 ng of human active renin were added to the plasma samples (300 µL). These spiked levels were chosen following the pathophysiological prorenin/renin levels reported by Stoicescu et. al (Stoicescu et al. 2011). The experimental conduct followed by a two-step approach in which prorenin was captured first, followed by the immunopurification of active renin (Burdman and Burckhardt 2019). The samples were digested using the sweet-spot conditions in triplicate and detected also by LC-HRMS.

Additionally, the limit of detection (LOD) in plasma was estimate according to criteria of International Conference on Technical Requirements for Registrations of Pharmaceuticals for Human Use (ICH) (European Medicines Agency 2006). LOD was calculated by using standard

error and slope of the regression line of specific calibration curve using following expressions:

$$\text{Limit of detection (LOD)} = 3.3 \times \sigma / s$$

Where σ is standard error of the y intercept, used as standard deviation and s is slope of regression line, respectively.

Equation 4-1 Limit of detection calculation according to ICH guideline

4.2.10 Instrumentation and conditions for LC-MS analysis of signature peptides

Two LC/MS systems were used for the analyses. The characterization and injection solvent optimization experiments were conducted on a Shimadzu Nexera UHPLC system (Shimadzu Europe, Duisburg, Germany) coupled to a Sciex TripleTOF 6600 (Sciex, Concord, Canada) high-resolution mass spectrometer with an IonDrive TurboV® electrospray ionization source (Sciex, Concord, Canada) operated in positive ion mode. The chromatographic separation was achieved using a Shimadzu Nexera UHPLC system (Shimadzu Europe, Duisburg, Germany) and a Phenomenex Kinetex® XB-C18 1.7 µm, 2.1 × 100 mm column. The aqueous mobile phase A consisted of 1% DMSO and 0.1% formic acid in water, whereas the organic phase B was 1% DMSO and 0.1% formic acid in methanol. The flow rate was set to 0.3 mL/min. The gradient started at 5% of mobile phase B and maintained at that level for 4.4 minutes, then increased between 4.5 and 4.7 minutes to 42%. This was followed by a further increase to 50% of mobile phase B after 5.7 minutes and was increased to 90% after 0.8 minutes. The gradient was maintained at 90% of mobile phase B until 8.5 minutes had elapsed before being reduced to 5% of mobile phase B. The injection volume was 50 µL, the oven temperature was set to 50°C, and the autosampler conditions were controlled at 15°C.

The settings applied for the TripleTOF mass spectrometer were as follows: curtain gas (N_2) pressure 35 psi, nebulizer gas (zero air) pressure 60 psi, heater gas (zero air) pressure 80 psi, ion spray voltage 5.5 kV, and interface heater temperature 300 °C. The declustering potential was set to 54 V for the mature signature part and 30 V for the pro- part signature peptide, while the collision energy was adjusted to 54 eV for the mature signature part and 30 eV for the pro-part signature peptide. The investigated transitions are listed in Table 4-1. The tryptic peptide abundance was analyzed by a SWATH acquisition with 33 variable windows

Table 4-1 Pro-part signature peptide and the mature-part signature peptide accompanied by their possible oxidized products *(Ox: oxidized; Diox: dioxidized; represented by one-letter amino acid code).*

Peptide amino acid sequence	Precursor Ion [*m/z*]	Product Ion [*m/z*]	Modification
Pro-part signature peptide			
LGPEWSQPMK	586.8 $[M+2H]^{2+}$	501.7484 $[M+2H]^{2+}$ (y8)	none
LGPEW(Ox)SQPMK	594.8 $[M+2H]^{2+}$	509.7368 $[M+2H]^{2+}$ (y8)	oxidized W (+8 m/z units)
LGPEW(Diox)SQPMK	602.8 $[M+2H]^{2+}$	517.7342 $[M+2H]^{2+}$ (y8)	dioxidized W (+16 m/z units)
LGPEWSQPM(Ox)K	594.8 $[M+2H]^{2+}$	509.7368 $[M+2H]^{2+}$ (y8)	oxidized M (+8 m/z units)
Mature-part signature peptide			
VVDFTGSSNVWVPSSK	854.9 $[M+2H]^{2+}$	418.2296 $[M+H]^{+}$ (y4)	none
VVDFTGSSNVW(Ox)VPSSK	862.9 $[M+2H]^{2+}$	418.2296 $[M+H]^{+}$ (y4)	oxidized W (+8 m/z units)
VVDFTGSSNVW(Diox)VPSSK	870.9 $[M+2H]^{2+}$	418.2296 $[M+H]^{+}$ (y4)	dioxidized W (+16 m/z units)

The Design of Experiment digestion measurements were performed on an Agilent 1200 SL LC system coupled to an AB Sciex® (Concord, Canada) 4000 triple quadrupole mass spectrometer operated in positive ion mode. The following multiple reaction monitoring (MRM) transitions were employed: m/z 855.1 to m/z 418 with 70 V declustering voltage and 36 eV collision energy for the mature-part signature peptide; and m/z 587.1 to m/z 501.7 with 30 V declustering voltage and 25 eV collision energy for the pro-peptide part. The source parameters were set to curtain gas (N2) pressure 30 psi, nebulizer gas (zero air) pressure 30 psi, heater gas (zero air) pressure 65 psi, ion spray voltage 5.5 kV, and interface heater temperature 450 °C. A Waters (Milford, MA, USA) XSelect CSH® C18 column (130Å, 3.5 µm, 3 mm x 150 mm) was used on both chromatographic systems to perform analyte enrichment and separation using a mixture of 1% DMSO, 0.1% formic acid in water [v/v/v] as mobile phase A and 1% DMSO, 0.1% formic acid in methanol [v/v/v] as mobile phase B.

4.2.11 Data Analysis

Data processing was done by using PeakView 2.2 and MultiQuant 3.0.2 (Sciex, Concord, Canada). The BiopharmaView 3.0.2 software was utilized for carrying out the in-silico tryptic digesting of human prorenin by downloading the FASTA file from UniProt (entry number P00797). The BiopharmaView 3.0.2 software was used for evaluation of the digest. The assay was constructed setting the digest agent as trypsin and zero missed cleavages were allowed. By adjusting the processing setting to a mass to charge tolerance of 5 ppm, XIC was set to 0.025 ppm and MS/MS matching tolerance was adjusted to 0.03 Da.

4.3 Results and discussion

4.3.1 Optimal signature peptides for prorenin determination and their properties

The better differentiation of mature renin and prorenin (chain + pro-peptide) was achieved by identifying possible surrogates from the pro-segment ('pro-part signature peptide') and the chain structure ('mature part signature peptide'). The in-silico digestion by Prospector® tool revealed thirteen signature peptides for prorenin, whereas two were unique for prorenin (confirmed by BLAST® analysis), and eleven for both, active renin and the mature part of prorenin (Table 4-2).

Table 4-2 Possible surrogates for active renin and prorenin. *The italic surrogate peptides represent unique part of prorenin pro-segment.*

m/z (average)	*m/z* (monoisotopic)	Amino acid sequence number		Amino Acid sequence code
512.2715^{+2}	512.5866^{+2}	1	9	LPTDTTTFK
586.7921^{+2}	587.1960^{+2}	33	42	LGPEWSQPMK
854.9307^{+2}	855.4577^{+2}	78	93	VVFDTGSSNVWVPSSK
549.2761^{+2}	549.6622^{+2}	97	105	LYTACVYHK
610.2775^{+2}	610.6466^{+2}	106	116	LFDASDSSSYK
520.7778^{+2}	521.0831^{+2}	117	125	HNGTELTLR
822.4720^{+2}	822.9856^{+2}	183	197	VTPIFDNIISQGVLK
670.3013^{+2}	670.7254^{+2}	198	207	EDVFSFYYNR
545.7893^{+2}	546.1664^{+2}	241	249	TGVWQIQMK
416.7335^{+2}	417.0256^{+2}	285	292	LMEALGAK
442.2498^{+2}	442.5384^{+2}	295	301	LFDYVVK
595.6260^{+3}	596.0145^{+3}	302	318	CNEGPTLPDISFHLGGK
489.2218^{+2}	489.5314^{+2}	366	372	FYTEFDR

Utilizing protter®, the beneficial position of three signature peptides were identified (Figure 4-2). The quantitative profiling of prorenin was conducted utilizing a sequential window acquisition of all theoretical fragment ion spectra mass spectrometry (SWATH). The plotting of hydrophobicity and determined amino acid sequence allowed for the identification of

suitable candidates for the mixed solvent approach. Both surrogates were chosen because of their beneficial amino acid structure for collision induced fragmentation in the mass spectrometric approach. The peptides that were more hydrophobic were either too large (33 amino acids) or cleaved only to a small extent. The SWATH spectra revealed the abundance of the generated peptides (Figure 4-3). Although SWATH first found other peptides to be more abundant than the two selected surrogates, final mass spectrometric optimization revealed that the pro-part signature peptide and the mature-part signature peptide were the most intensive.

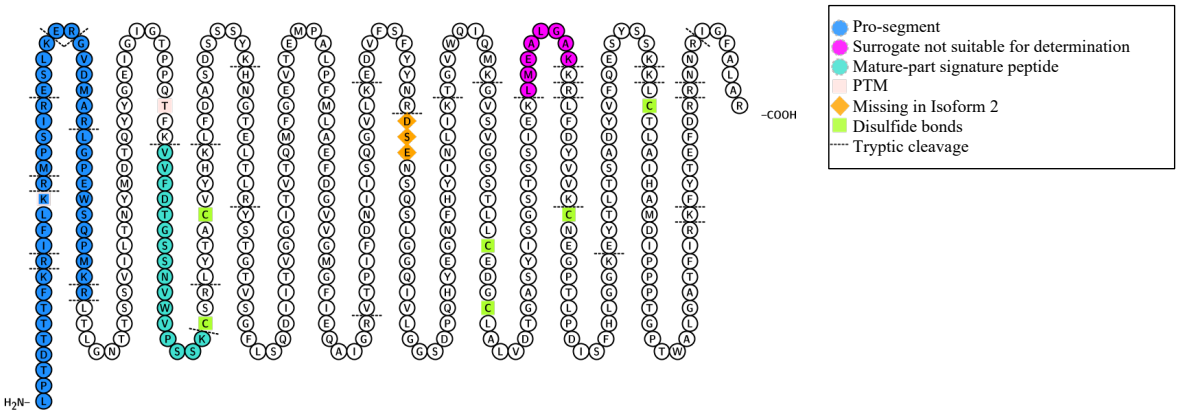

Figure 4-2 Protter illustration of prorenin and its possible tryptic cleavage sites

The most intensive surrogates that were named ‘pro-part signature peptide’ (LGPEWSQPMK, unique for prorenin) and ‘mature-part signature peptide’ (VVFDTGSSNVWVPSSK, unique for prorenin and active renin within the plasma proteome) were analyzed by the DOE.

Opposed to the SISCAPA approach, in which a labeled version of the proteotypic peptide is added as isotope-labeled internal standard, in the here presented setting the complete protein antigen is captured. This would have asked for a stable, labeled recombinant prorenin instead of a unique peptide sequence only as suitable internal standard. However, for prorenin as well as for renin a commercially available isotope-labeled full-length protein internal standards are lacking. The customized bioproduction would last for several months, be expensive, and the success would be uncertain. Therefore, a label-free approach was developed, which was already shown to be a promising approach (Al Shweiki et al. 2017).

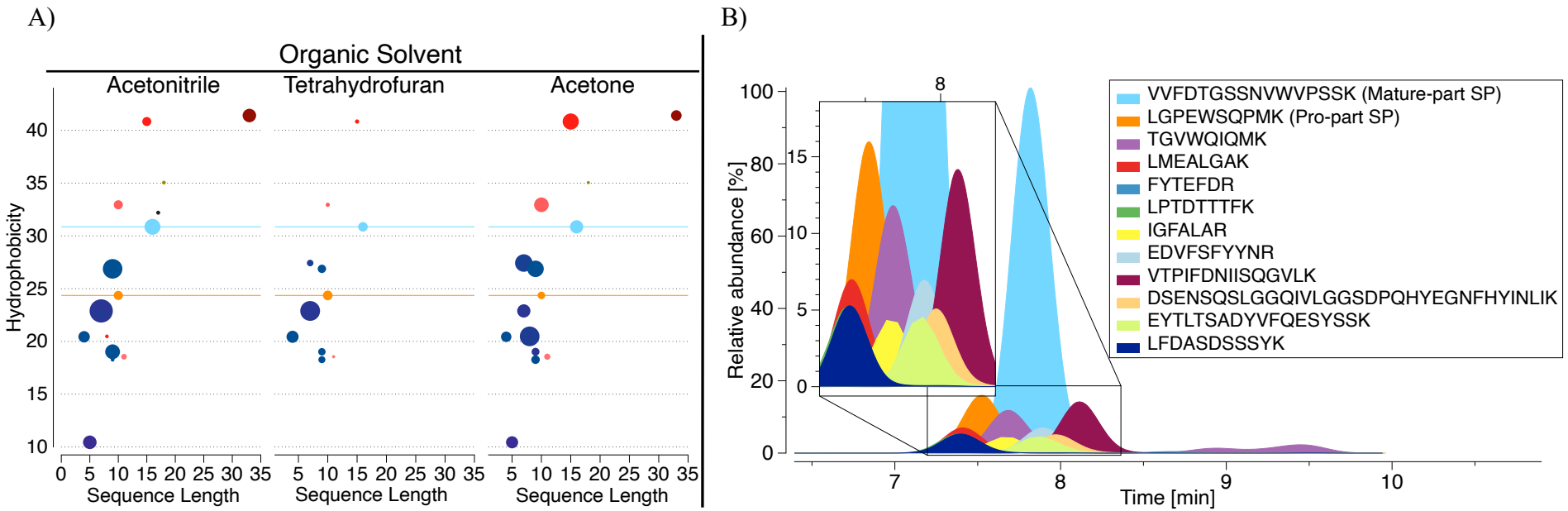

Figure 4-3 Obtained peptide characteristics of digested prorenin. *A) Quantitative profiling of different prorenin surrogates generated by mixed-solvent approach using SWATH acquisition. For each of the three investigated organic solvents (acetonitrile, tetrahydrofuran and acetone), the hydrophobicity, the corresponding amino acid sequence ("sequence length"), and its abundance (size of dots) is plotted. The color allows for identification of the different m/z fragments. The finally selected pro-part signature part is orange colored; mature-part signature peptide is light blue colored. B) Excerpt of a chromatogram representing the obtained peptides after organic solvent digestion using acetonitrile. The final optimization of mass spectrometric signal identified VVFDTGSSNVWVPSSK (mature-part signature peptide; light blue) and LGPEWSQPMK (pro-part signature peptide; orange) as the most intensive ones (SP: signature peptide).*

4.3.2 Immunocapture of prorenin

All seven screened antibodies of the three suppliers could capture human prorenin in a PBS buffer. However, only one antibody was effective enough to capture and differentiate between active renin and prorenin in human plasma. The elected antibody for the immunocapture in the hybrid approach also had inhibitory abilities that allowed it to avoid the conformational changes of the pro-segment of prorenin. This antibody was reported to bind selectively to the pro-segment (residues 32-39) (Krop et al. 2011). By applying immunocapture with the inhibitory antibody against full-length prorenin, the purification was effective enough to avoid any interaction with plasma components that could cause ion suppression of the low-abundance proteins. Moreover, this immunocapture complex was suitable for organic solvent digestion and LC-MS measurement.

4.3.3 Stability of signature peptides and pro-segment properties

The digestion temperature analysis revealed that the pro-part was more effectively cleaved at low temperatures (10 °C), which could be explained by the capability of its conformational change when it was exposed to cold environment (Pitarresi et al. 1992). Usually, this conformational change was reported at 0 °C and 4 °C; however, the addition of organic solvents may change the behavior of the pro-segment that promoted this structural conversion at higher temperatures (10 °C). This property of the conformational change commonly caused the existing immunosorbent and radiometric assays to be imprecise. Here, this character was used to enhance the response of the pro-part signature peptide (Campbell et al. 2009).

Neither oxidized nor dioxidized residues were observed in the pro-part signature peptide sequence. This may be a result of the amino acid sequence and cool digestion temperature, which protected this peptide from oxidative reactions. For the mature-part signature peptide, there was only one modification of the tryptophan amino acid observed, which was caused by high acidic content. A small amount of dioxidated species (50 cps) of tryptophan (dihydroxy species) was observed for the mass increase of 32 Da (y6-fragment; Fig. 4-4).

This investigation proved the stability of the surrogate peptide under the given conditions and therefore proved that it would facilitate human prorenin determination by hybrid LC-MS.

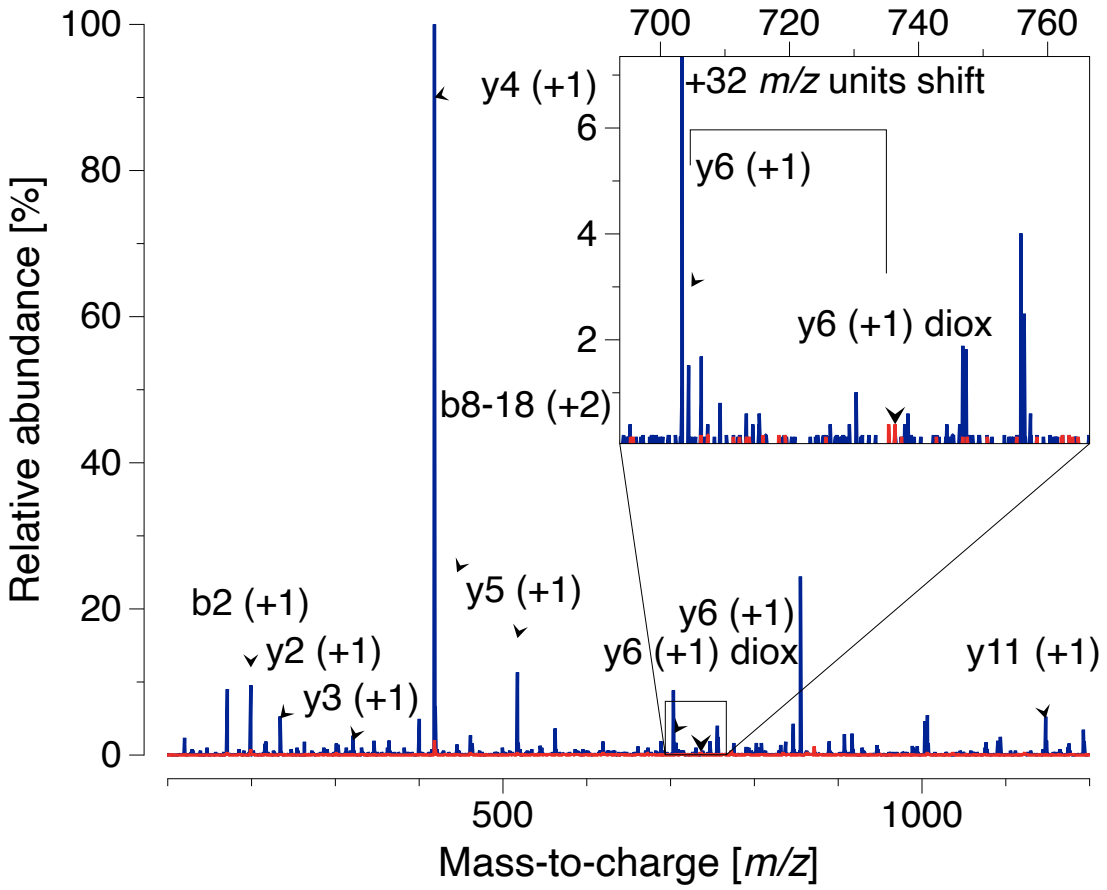

Figure 4-4 Product ion scan of the mature-part signature peptide in its native and dioxidized form. *Dioxidized species was detected at the y6 fragment of the mature-part signature peptide (overlaid red mass spectrum).*

4.3.4 Prorenin's organic digestion D-optimal evaluation

The calculated D-optimal design was analyzed by a multiple linear regression model. This model was chosen to ensure the robustness of the generated data and was described by the G-efficiency of 0.79, which met the predetermined criteria. The desired statistical values of the ANOVA results indicated a Q^2 value of 0.86 and an R^2 value of 0.90 which fulfilled the predefined requirements for a good model fit and a reliable prediction of the applied model. This model showed also a good reproducibility value of 0.95.

By using the D-optimal model, 114 experiments (4 outlier experiments were excluded) were evaluated, comprising 35 designed runs with 3 center-points measured all in triplicates (Table 4-3).

Table 4-3 D-optimal design summary

Design	D-Optimal	
Runs in design	35	
Center points	3	
Replicates	2	
N = actual runs	114	
Maximum runs	12000	
Constraints	No	
D-Optimal		
Potential terms		
Number of inclusions	0	
Constraints	No	
Selected design number	21	
Design statistics	G-efficiency	75,4671021
	log (Det. of X'X)	25,3628006
	Norm. log (Det. of X'X)	-0,415346
	Condition number	9,84998989

4.3.4.1 Effect of organic solvent type

The four organic solvents—THF, acetone, acetonitrile, and methanol—showed different results regarding the generation of both signature peptides. With the exception of acetone, each organic solvent had significantly beneficial influence on the production of the analyzed surrogates (Fig. 4-3). Each organic solvent allowed a proteolytical cleavage by modified trypsin that produced measurable levels of mature-part signature peptide and pro-part signature peptide. The best results for the generation of both peptides were obtained using acetonitrile or THF. Acetone had significant negative impact on the response of both surrogates. Methanol diminished the generation of the pro-part signature peptide.

4.3.4.2 Effect of organic solvent concentration

The aqueous-organic solvent ratio played a crucial role in whether the pro-part or the mature-part was more efficiently generated. The optimal composition for efficient digestion varied depending on the type of organic solvent used. The individual effect of increasing the organic solvent concentration had a significant positive impact on the pro-part signature peptide cleavage (Fig.4-5).

Concerning the individual effects regarding the mature-part signature peptide, the concentration did not have a significant influence on its generation; Nonetheless, a lower organic solvent ratio was slightly beneficial ($\alpha = 0.051$). However, the interactive effect of varying the concentration of the organic solvent type was the strongest effect on generation. The interaction of a low organic solvent concentration (60%) and acetonitrile resulted in the most potent production of the mature-part signature peptide (mean 1.00e5 cps). Two of the analyzed organic solvents (THF and acetone) interacted positively with high organic contents, however, only tetrahydrofuran had similar results to acetonitrile.

The pro-part signature peptide behaved differently by being generated at the highest concentration of almost all organic solvents; at 90 % concentration, the intensities had a mean value of 2.30e4 cps using acetone, 2.47e4 cps using acetonitrile, and 2.27e4 cps using THF. Overall, the optimal solvent concentration for the pro-part signature peptide was the highest concentration used (90%). However, if the concentration interacted with the different organic solvent types, only methanol had a significant decrease in pro-part signature peptide generation ($\alpha < 0.01$). For the mature-part, a high organic solvent concentration and a high temperature were unsuitable for cleavage (Fig. 4-5).

Therefore, the optimal settings for both peptides were determined using acetonitrile as the organic solvent, which showed a reliable generation at the lowest (60%) and highest (90%) analyzed organic solvent content. THF concentration displayed the opposite characteristic, with the best performance found at a high organic content (90%). In the end, acetonitrile outperformed the other organic solvents when interacting with other factors.

4.3.4.3 Effect of digestion temperature

The optimal digestion temperature, ranging from 10 °C to 40 °C, was strongly correlated with the type of organic solvent. The optimal temperature for the mature-part signature peptide was at 40 °C, whereas the pro-peptide part generation was favored by cooler temperatures (10 °C). This can be explained by the better unfolding of the pro-segment, which displayed an ability to change its conformation under the influence of cold temperature.

As an individual effect, elevated temperature was not favorable in generating the signature peptides. In the case of the interactive effects, increased temperature was only significantly advantageous for tetrahydrofuran and acetonitrile as the organic solvent for the mature-part signature peptide (Fig. 4-5). The mature-part signature peptide showed the best response at 10 °C incubation temperature (mean 9.04e4 cps) in methanol, followed by THF (mean 8.12e4 cps), while the lowest responses were observed in acetone and acetonitrile, with mean values of 7.20e4 cps and 7.12e4 cps, respectively. An additional increase of 10 °C was still beneficial for methanol (1.08e5 cps), while digestion intensity in THF and acetonitrile increased by 31% and 40%, respectively. An increase in incubation temperature up to 30 °C was shown to be advantageous for acetonitrile and THF, with respective mean values of 1.24e5 cps and 1.28e5 cps. A smaller effect was seen for methanol and acetone, with respective mean values of 1.22e5 cps and 1.04e5 cps. Forty degrees Celsius resulted in the highest intensity of mature-part peptide for all organic solvents, the highest being THF and acetonitrile with intensities of a mean 1.45e5 cps each.

The lower temperatures better promoted generation of the pro-part signature peptides (Fig. 4-5). With regard to acetone-water milieu for example, the generation of pro-part signature peptide was improved at the lower temperatures of 20 °C and 30 °C (with mean values of 1.66e4 cps and 1.65e4 cps, respectively) compared to temperatures of 40 °C.

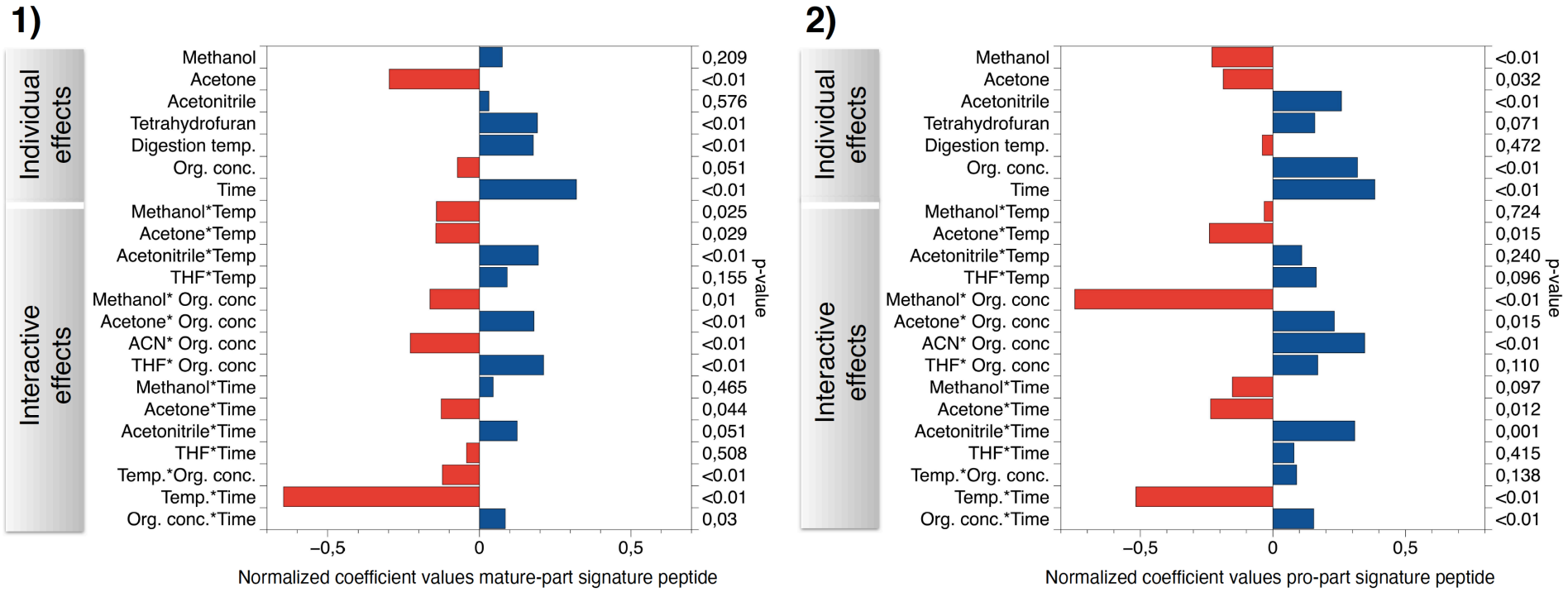

Figure 4-5 Normalized coefficient plots of the mixed solvent digestion D-optimal design *showing the impact of either individual or interactive effects with corresponding p-values (level of significance: $\alpha < 0.05$) for the generation of the 1) mature-part signature peptide and 2) pro-part (Temp.: temperature; THF: tetrahydrofuran; org. conc.: organic concentration; ACN: acetonitrile).*

4.3.4.4 Sweet spot analysis for mature-part and pro-part signature peptides

Prorenin uniqueness was defined by its pro-peptide, which is completely absent in the active renin. This property is beneficial for analyzing antibodies selectivity and ensuring the differentiation between both proteins. The optimal conditions for the generation of both surrogate peptides were a concentration of 84% acetonitrile, a digestion temperature of 16 °C, and an incubation time of 98 minutes. The Monte-Carlo-calculated optimal set point intensity was predicted as 1.2e5 cps for the mature-part signature peptide and 1.2e5 cps for the pro-part signature peptide, 3.7e4 cps. The robustness of the defined sweet-spot was calculated at 0.17 % probability of failure.

4.3.5 Optimized immunocapture procedure by improved incubation and washing buffer

The incubation buffer had a crucial effect on the polystyrene plates, which showed the high adsorption of prorenin and active renin in the absence of Tween 20. The investigation revealed that the best buffer was HEPES, with a mature-part signature peptide mean ± SD intensity of 1.00e4 ± 4.66e2 cps, followed by PBS, with a mean intensity of 5.32e3 ± 1.42e2 cps, and finally ABC buffer, with a mean intensity of 4.99e3 ± 7.98e2 cps. The effects of additional wash steps using only water instead of HEPES buffer on the antigen-antibody complex after incubation in the different buffers were found to be negligible for HEPES buffer (improvement for HEPES: 2%) but beneficial for PBS and ABC buffer (improvements of 33% PBS and 34% for ABC) when compared to performing the washes with the tested buffers. This improvement might be due to the removal of buffer components that affect the LC-MS analysis.

The addition of 0.01 % [v/v] Tween 20 was found to improve the intensity by ten-fold for PBS buffer, which made PBS containing Tween 20 the most appropriate incubation and washing buffer. Tween appears to maintain proteins in solution without affecting the immunocapture procedure.

4.3.6 Effect of container material and injection solvent composition on prorenin's assay sensitivity and robustness

This study used both regular materials and materials marketed as 'low-binding' to evaluate the impacts of the injection solvent composition.

The analysis of the container material that is distributed by Eppendorf® and classified as 'low binding' fulfilled the set DOE model criteria, which were 0.76 for the goodness of fit (R^2), 0.68 for the model's predictive power (Q^2), and a repeatability of 0.78 for the pro-part signature

peptide (Fig. 4-6). In contrast, these values for the mature-part signature peptide were 0.86 for the goodness of fit (R^2), 0.80 for the model's predictive power (Q^2), and a repeatability of 0.89 (Fig. 4-7). The coefficient plot used to analyze the individual and interactive results revealed the impacts of each factor. The factor water had significant impacts on the intensities of both the pro-part signature peptide and the mature-part signature peptide on the Eppendorf® plate. However, high concentrations of DMSO and methanol were not favorable for this plate, for either peptide. The manufacturer describes the low-binding modification of the material as the result of making the container less hydrophobic through additives such as glycerol stearate, glycerol palmitate, and *bis*-(3,3-dimethylbenzylidine sorbitol diacetal), which dissolve in organic solvents and contaminate samples while simultaneously reducing the analyte's intensity (Weikart et al. 2017). The acidic component (formic acid) showed a negative effect on the pro-part signature peptide while simultaneously improving the intensity of the mature-part signature peptide, although not significantly. The mean intensity of the setpoint using high water content (85%), low organic solvent content (13% methanol and 1% DMSO), and 1% formic acid (2.32e4 ± 2.20e3 cps, n = 4), compared with the mean intensity for the lowest analyzed water content (10%), with the highest organic solvent content (40% methanol and 40% DMSO) and 10% formic acid (4.52e3 ± 1.89e2 cps, n = 4) revealed the unsuitability using low-binding material with organic solvents. The best injection solvent composition was calculated using the Monte-Carlo analysis, which resulting in an optimal composition consisting of 82% water, 2% DMSO, 15% methanol, and 1% formic acid [v/v/v/v], with a failure probability of 0.19%.

Another distributor, Waters®, also classifies it's QuanRecovery plates as low-binding plate called. The performed analysis also fulfilled the DOE criteria, which were 0.77 for the goodness of fit (R^2), 0.74 for the model's predictive power (Q^2), and a repeatability of 0.72 for the pro-part signature peptide (Fig. 4-6), whereas the values for the mature-part signature peptide were 0.88 for the goodness of fit (R^2), 0.91 for the model's predictive power (Q^2), and a repeatability of 0.92 (Fig. 4-7). Similar to the previously described low-binding material, these plates showed a beneficial impact when using water and a negative impact when using a high percentage of organic solvent. The percentage of formic acid had the same negligible effect on both signature peptides. Comparing between the lowest water content (10%) conditions and the highest analyzed water content (85%) conditions, the gain in intensity was 188% for the mature-part signature peptide and 200% for the pro-part signature peptide (n = 4). Finally, the optimal injection solvent composition was 68% water, 9% DMSO, 17% methanol, and 6% formic acid [v/v/v/v] as calculated by the Monte-Carlo analysis (probability of failure: 0.2%).

Pro-part signature peptide	Eppendorf® Protein LowBind	Waters® regular	Waters® Quan Recovery	Brand®	Greiner®
R^2	0.76	0.51	0.77	0.94	0.93
Q^2	0.68	0.35	0.74	0.90	0.88
Repeatability	0.78	0.72	0.72	0.95	0.96

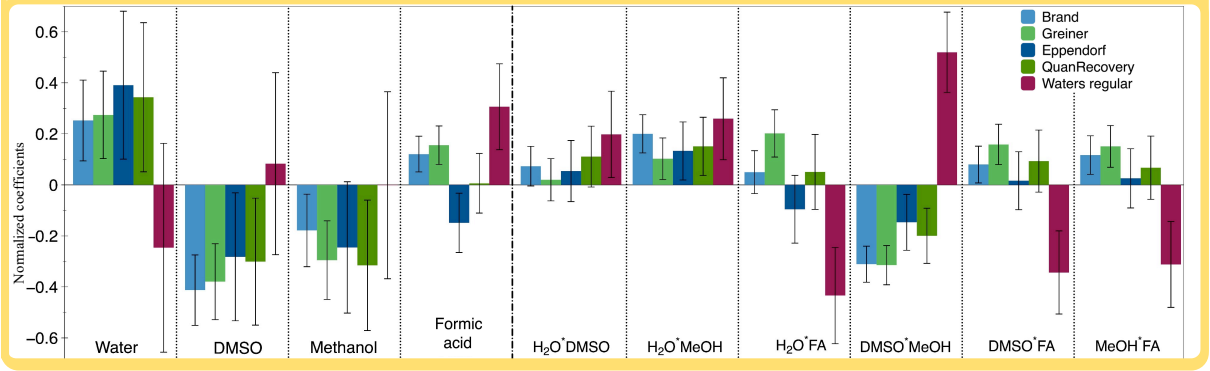

Figure 4-6 Goodness of fit and coefficient effects for the adsorption and solubility of the pro-part signature peptide, *as influenced by water (H_2O); dimethylsulfoxide (DMSO); methanol (MeOH); and formic acid (FA). All values are shown as the mean ± SD, and the significance is presented with the 95% confidence interval (Student's t-test). The section before the dashed line shows the individual effects of each parameter, whereas the section after the dashed line shows the interaction effects between each parameter. R^2 was calculated for the goodness of fit, and Q^2 represents the model's predictive power.*

The Waters® plates made with regular plastic showed a high degree of variation for the analysis of the pro-part signature, as represented by the DOE model evaluation, with values of 0.51 for the goodness of fit (R^2), 0.35 for the model's predictive power (Q^2), and a repeatability of 0.72 for the pro-part signature peptide (Fig. 4-6), which failed to fulfill the criteria for Q^2. For the mature-part signature peptide, these criteria were achieved, with 0.87 for the goodness of fit (R^2), 0.84 for the model's predictive power (Q^2), and a repeatability of 0.95 (Fig. 4-7). The evaluation for the pro-part signature peptide was difficult due to the non-significant coefficient effect of water, methanol, and DMSO, whereas formic acid appeared to improve the intensity. A better outcome was observed for the mature-part signature peptide, which was beneficially affected by low water content and high organic solvent amounts. The most important factor was for the mature-part was also formic acid, which significantly improved intensity. These plates were not favorable for obtaining reliable analyses. The optimal injection solvent composition was also calculated by Monte-Carlo analysis: 52% water, 12% DMSO, 29% methanol, and 7% formic acid [v/v/v/v] (probability of failure: 0.1%).

The Brand® plate chemometric driven investigation met the set DOE model criteria, with values of 0.94 for the goodness of fit (R^2), 0.90 for the model's predictive power (Q^2), and a repeatability of 0.95 for the pro-part signature peptide (Fig. 4-7). The values for the mature-part

signature peptide were 0.91 for the goodness of fit (R^2), 0.87 for the model's predictive power (Q^2), and a repeatability of 0.97 (Fig. 4-7). This plate also showed a beneficial intensity improvement when using water, but this effect had less impact than was observed for the low-binding containers. A moderate amount of organic solvents improved the intensities of both the pro-part and mature-part signature peptides. The interactions between water and methanol and between water and DMSO improved intensity, which was also supported by the addition of formic acid. When analyzing the setpoint for the highest water content (98%), only low intensities could be measured (mean ± SD of 8.20e3 ± 7.3e1 cps for the mature-part signature peptide and mean ± SD of 8.24e2 ± 4.92e2 cps for the pro-part signature peptide; n = 4). A moderate water content of 55% showed the best results: mean ± SD of 1.37e4 ± 7.17e2 cps for the mature-part signature peptide and mean ± SD of 2.56e3 ± 3.06e2 cps for the pro-part signature peptide. The optimal injection solvent composition was also calculated using a Monte-Carlo analysis, resulting in an optimal set point at 60% water, 2% DMSO, 28% methanol, and 10% formic acid [v/v/v/v] with a probability of failure ≤ 0.02%.

Mature-part signature peptide	Eppendorf® Protein LowBind	Waters® regular	Waters® Quan Recovery	Brand®	Greiner®
R^2	0.86	0.87	0.88	0.91	0,95
Q^2	0.80	0.84	0.91	0.87	0.94
Repeatability	0.89	0.95	0.92	0.97	0.97

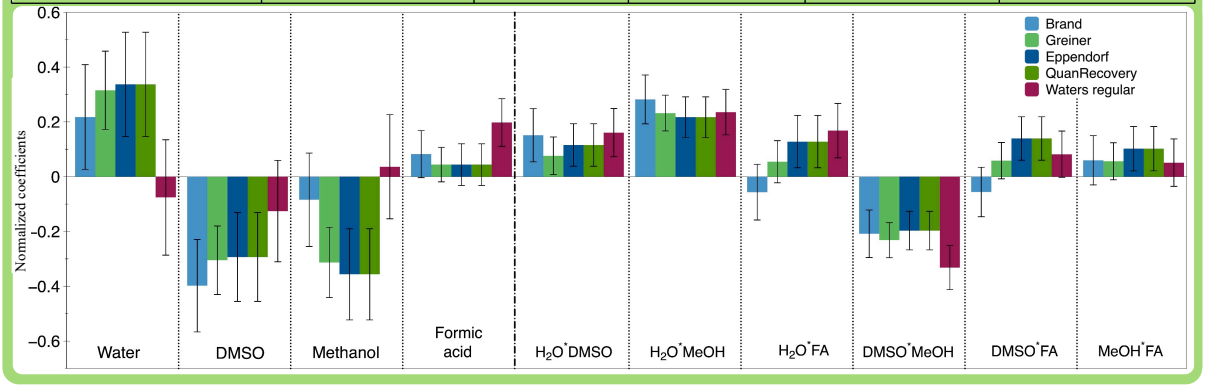

Figure 4-7 Goodness of fit and coefficient effects on adsorption and solubility of the mature-part signature peptide, *as influenced by water (H_2O); dimethylsulfoxide (DMSO); methanol (MeOH); and formic acid (FA). All values are shown as the mean ± SD, and significance is presented with a 95% confidence interval (Student's t-test). The section before the dashed line shows the individual effects of each parameter, whereas the section after the dashed line shows the interaction effects between each parameter. R^2 was calculated for the goodness of fit, and Q^2 represents the model's predictive power.*

Lastly, the Greiner® plate also met the DOE model criteria, with the following results: 0.93 for the goodness of fit (R^2), 0.88 for the model's predictive power (Q^2), and a repeatability of 0.96

for the pro-part signature peptide (Fig. 4-6). The matched criteria for the mature-part signature peptide was as follows: 0.95 for the goodness of fit (R^2), 0.94 for the model's predictive power (Q^2), and a repeatability of 0.97 (Fig. 4-7). This container material showed similar impacts on both the pro-part and mature-part signature peptide. All factors had the same impact as described for the Brand® plates, except for the intensity of the mature-part signature peptide, which was improved by higher water contents, leading to a slight different calculated optimal injection composition based on the Monte-Carlo analysis: 70% water, 4% DMSO, 20% methanol, and 6% formic acid [v/v/v/v] (probability of failure: 0.01%).

The direct comparison of the DOE optimized injection solvent compositions and the primary LC-gradient-depended injection solvent composition showed that the measured intensities of both the mature-part and pro-part signature peptides could be improved on the Eppendorf® plate by 42% and 10%, respectively, compared with the initial injection solvent composition (93.9% water, 5% methanol, 1% DMSO and 0.1% formic acid [v/v/v/v]). By comparing the same conditions (initial vs. DOE optimized) for the mature-part signature peptide, the intensities could be improved by 95% for the regular Waters® plate, 19% for the QuanRecovery plate, 30% for the Brand® plate, and 15% for the Greiner® plate. The intensities for the pro-part signature peptide improved by 16% for the regular Waters® plate, 2% for the QuanRecovery plate, 7% for the Brand® plate, and 2% for the Greiner® plate (Fig. 4-8).
In summary, by tailoring the composition of the injection solvent to the specific container material, no substantial differences in mature-part and pro-part signature peptide intensities was observed. By combining the specific injection solvent mixture with its consumable counterpart equal performances concerning the improvement signal intensity were achieved. Therefore, 96-well plates from Greiner® will be used for future approaches due to economic reasons.

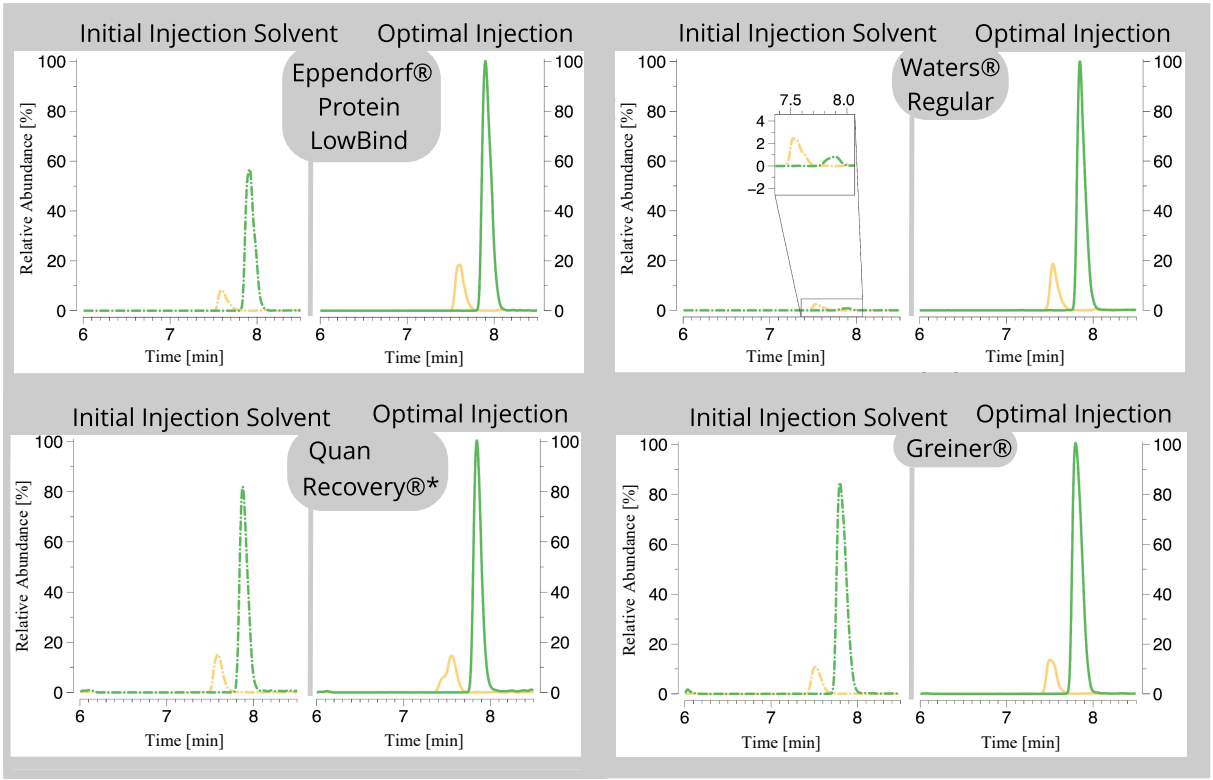

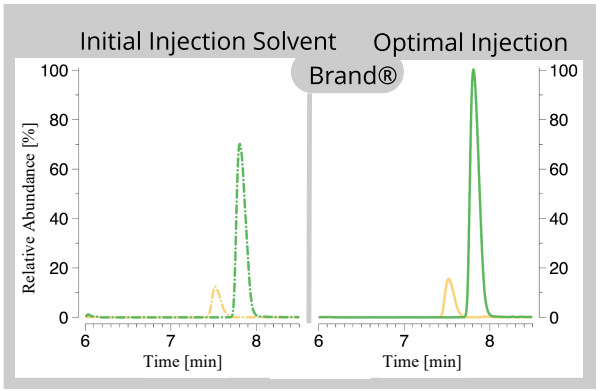

Figure 4-8 Comparison between initial injection solvent mixture (left side, dotted chromatogram) and Design of Experiments optimized injection solvent mixtures, *consisting of water, methanol, DMSO, and formic acid (right side) on Eppendorf protein low binding, Waters regular and QuanRecovery, Greiner and Brand 96-well plates. Yellow line: pro-part signature peptide; Green line: mature-part signature peptide (* Waters).*

4.3.7 Applicability in human plasma for active renin and prorenin determination

First, the evaluated sweet-spot conditions were confirmed following the immunocapture in neat solution as well as in human plasma. The condition resulted in detectable levels of pro-part and mature-part signature peptides in human plasma. Second, by applying the optimal conditions within the hybrid approach, a reliable determination of the spiked recombinant human prorenin was achieved. Prorenin as well as active renin were successfully captured by the selective antibodies and detected by LC-MS. The identities of both surrogates were confirmed by the typical fragmentation scheme of y- and b-fragments utilizing high-resolution MS. For the mature part signature peptide, the y4-fragment was the most intense, caused by the proline fragmentation side of the PSSK fragment. In the case of the pro-part signature peptide, the most intense fragments were the y8, representing the fragmentation on the proline side of the PEWSQPMK part, and the y3, with the other proline residue of the PMK part (Fig. 4-9). By improving the collision energy, the mature-part signature peptide was the most intense for the active renin and the pro-part signature peptide had the highest intensity for the pro-segment of prorenin (Figure 4-2). The absence of the pro-part signature peptide in the active renin digests underlines the selectivity of the hybrid immunocapture LC-MS method presented herein.

This assay optimization allowed for a LOD of 110 pg/mL for prorenin as well as a LOD of 26 pg/mL for active renin. These limits appear acceptable in the context of reported protein levels in human plasma (plasma prorenin mean±SD of 2,130±250 pg/mL for 38 weeks healthy old neonates (Terada et al. 2017); plasma active renin mean±SD of 226±58 pg/mL for 16h to one month old healthy neonates (Blazy et al. 1989). Plasma prorenin median of 552 pg/mL [interquartile range; IQR: 297 -1097 pg/mL] for cardiovascular diseased adults (Yoshida et al. 2015); Tomaschitz et al. plasma active renin median of 46.8 pg/mL [interquartile range; IQR:31.8–91.8 pg/mL] for cardiovascular diseased adults (Tomaschitz et al. 2011)).

Although a full validation was not yet conducted, the precision was determined in triplicate for both surrogates. A repeatability (CV) of 1% for the mature-part signature peptide and 7% for the pro-part signature peptide was obtained.

Beside the pure detection of prorenin, the developed LC-MS method is able to also differentiate between the open / unfolded form of prorenin and renin. This is a main advantage compared to available immunoassays. Even if the selective antibodies identified within the presented work would be used to develop better immunoassays, these assays still lack the ability to differentiate between the open form of prorenin and active renin. This is especially pronounced if samples of patients would be analyzed with highly elevated plasma levels of renin and prorenin. For

example, the pharmacotherapy with so called direct renin inhibitors like aliskiren in the treatment of hypertension promotes the unfolding of the pro-segment making this prorenin invisible for the prorenin ELISA and falsified visible for the active renin immunoassay. The author's developed assay can still differentiate this state of prorenin to active renin through the pro-part signature peptide which is absent in active renin. Overall, this development is a good illustration of symbiotic effects by applying the hybrid LC-MS approach. The immunocapture enables the required sensitivity current MS-approaches lack to determine endogenous levels in complex matrix, while the mass spectrometer ensures the necessary selectivity.

To the best of our knowledge, this is the first time a LC-MS for determination of endogenous levels of prorenin was described. Besides its benefits in overcoming the immunoassay's inability to properly differentiate between prorenin and related compounds like the active renin, the overall workflow is leaner than in most approaches available. First, the digestion part of the assay time was reduced by 98 minutes and an over-night digestion not necessary anymore. Second, a laboratory being equipped with an LC-MS system can easily implement this method into routine measurements without additional equipment. Since the sample purification of whole digest (e.g. by SPE) is not necessary in comparison to common purification methods, the approach is more cost-effective and time-effective (whole determination process lasts 3 hours). Third, the usefulness of the assay for clinical application of samples collected from vulnerable population (e.g. pediatrics) is ensured. Especially the advantage of re-use of blood plasma after immunocapture for other determination of parameters is beneficial to overcome ethical constraints concerning the limited blood volumes in those populations.

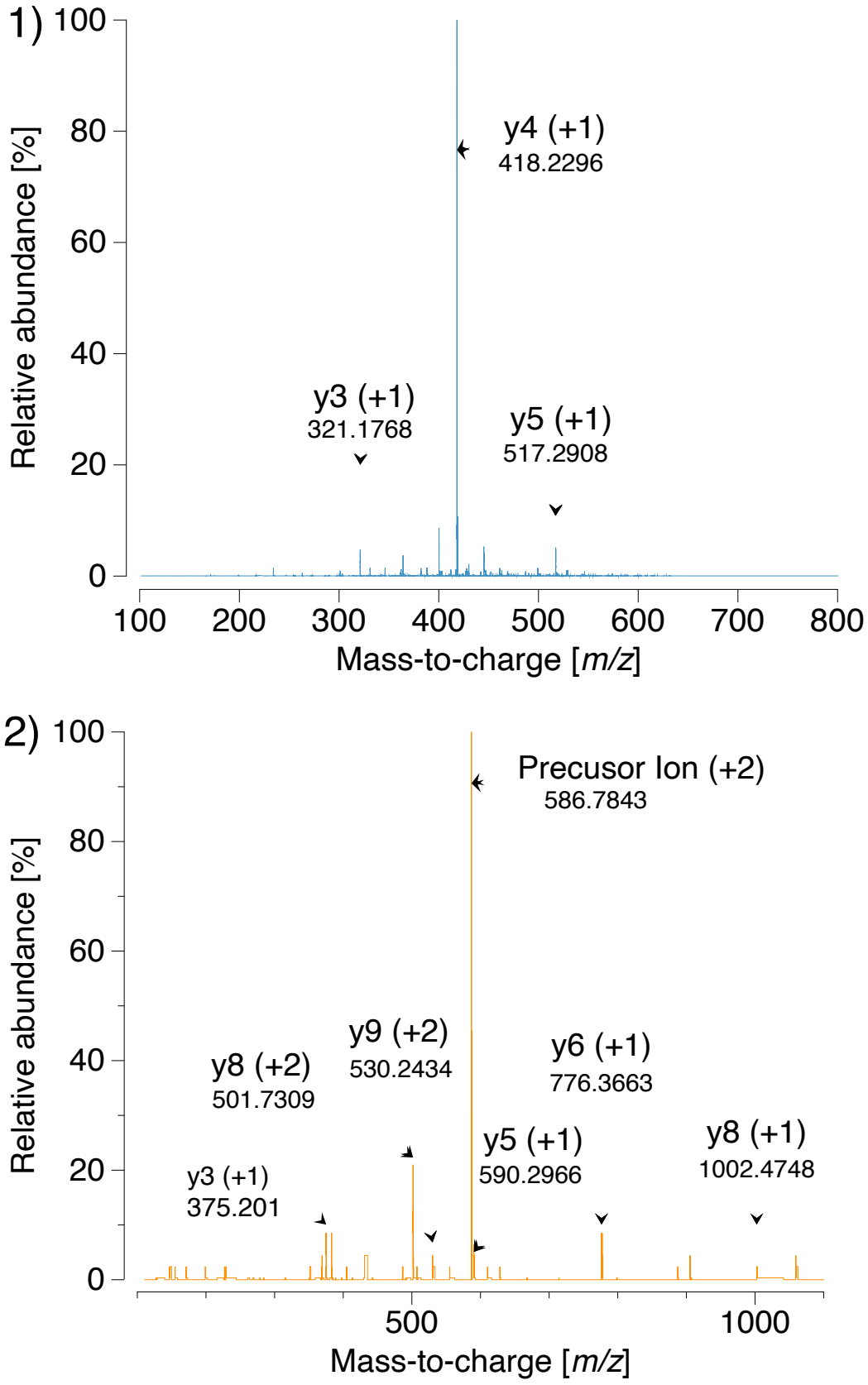

Figure 4-9 Product ion scan of 1) mature-part signature peptide and 2) pro-part signature part *representing the most abundant collision induced y- and b-fragments.*

4.4 Conclusion

This assay enabled the determination of human prorenin on triple quadrupole and QTOF systems by a simplified and fast hybrid protocol using immobilized, highly-specific antibodies for immunocapture and acetonitrile at high concentration as an organic denaturant. Due to the simultaneous determination of a signature peptide cleaved from the pro-segment and a signature peptide generated from the mature renin, two-level specificity was ensured. Further DOE optimizations enhanced the intensities of the mature-part and pro-part signature peptides by, first, improving the immunocapture procedure, using 50 mM PBS buffer and 0.01% [v/v] Tween 20 to avoid the adsorption of full-length prorenin and active renin, and second, by improving the injection solvent composition for the digested tryptic peptides. This optimization facilitated a sensitive and robust measurement of endogenous prorenin and active renin levels.

5. Verification of the developed hybrid immunocapture LC-HRMS approach of active renin

5.1 Introduction

The successful development of a hybrid assay has enabled the precise determination of prorenin and active renin concentrations. Additionally, the differentiation between these two proteins was achieved by the identification of a unique signature peptide from the pro-segment that only occurs in prorenin. In consequence, the developed method could be particularly useful if a diseased-related increase in prorenin and a concomitant decrease in active renin levels occurs like in patients with coronary artery disease and hyperaldosteronism, which delimits the use of immunoassays due to cross-reactivity, which is a main issue identified in the literature. Plasma prorenin levels typically occurred at high concentrations, as measured by Yoshida et al. (1,097 pg/mL), whereas active renin levels were generally low (12 pg/mL) in patients with coronary artery disease (Yoshida et al. 2015). Cross-reactivity reported by immunoassay manufacturers ranges from 0.4% to 0.7% (Bioassays 2016), indicating that as much as 7.7 pg/mL of the active renin concentration could instead be inactive prorenin due to cross-reactivity. Subsequently, compared with the estimated renin levels, more than half of the identified active renin could be measured inaccurately due to overestimation. In another example, pharmacological interventions into the RAAS, especially when using renin inhibitors, can crucially affect the ratio between the open-form and inactive prorenin (Krop et al. 2013), making it impossible to differentiate between open-form prorenin and active renin based on active renin immunoassays. In addition, the prorenin receptor (PRR) was identified as a prorenin activator (Ichihara et al. 2009), which can unfold the pro-segment of prorenin, which can also be recognized as active renin, leading further to inaccurate measurements and imprecise levels.

Regarding physiological levels in adults, cross-reactivity is negligible; however, in the case of elevated prorenin levels in diseased patients, the amount of open-form prorenin might be falsely quantified as active renin.

In contrast to the immunoassays, the developed hybrid assay is able to overcome these potential cross-reactivity problems by LC-MS detection providing a high selectivity of the analytes. However, variations associated with sample handling and instrumental variations may lead to imprecise results. These variations can be adjusted by implementing an internal standard into this procedure. Because isotopic full-length ^{13}C- and ^{15}N-labeled active and prorenin, which

represent the current state-of-the-art, are not yet commercially available, and the cost of biotechnological synthesis exceeds thousands of euros, the use of either a chemically modified (e.g. guanidated) or an ^{18}O labeled internal standard have been shown to be a suitable alternative (Jenkins et al. 2015).

Consequently, this study aimed to demonstrate the accuracy, precision and applicability of the developed method based on the previously performed optimizations. Moreover, this study introduced the generation of potential internal standards for the application to the accurate and precise measurement of active renin, to ensure that active renin can be correctly measured at endogenous levels while simultaneously differentiating between active renin and the open-form prorenin.

5.2 Methods

5.2.1 Materials

Human recombinant prorenin (>86% purity by SDS-PAGE) was obtained from Cayman Chemicals (Ann Arbor, USA). TCPK-treated modified trypsin was supplied by ThermoFisher (Rockford, USA). ^{18}O-labeled water (> 97% ^{18}O-atom), dimethyl sulfoxide (p.a.), trifluoracetic acid, and ammonium bicarbonate (>99.5%), nafamostat mesylate (>98%), hexadimethrine bromide (>94%) were supplied by Sigma-Aldrich (Taufkirchen, Germany), o-methylisourea hemi sulfate, acetonitrile (LC-MS grade) and methanol optima® (LC-MS grade) were purchased from Fisher Chemicals (Geel, Belgium). 3D-NHS 96-well plates were obtained from PolyAn (Berlin, Germany). Water (LC-MS grade) and sodium phosphate dibasic (>99%) were supplied by Riedel-de Haen (Seelze, Germany). Sodium chloride (>95%) and potassium dihydrogen phosphate (>99%) were obtained from Carl Roth (Karlsruhe, Germany). Tween 20 was supplied by Caelo (Hilden, Germany). Formic acid (98%, p.a.) and potassium chloride (>99%) were ordered from Applichem (Darmstadt, Germany). Aliskiren hemi fumarate (> 98 %) was supplied from MSN Laboratories (Hyderabad, India).

Blood plasma was collected from a healthy volunteer in S-Monovette® K3 EDTA tubes (Sarstedt, Nuembrecht, Germany). L-Glycine, ethanolamine, and citric acid were supplied by S3-chemicals (Bad Oeynhausen, Germany). Anti-renin antibodies were obtained from DRG Instruments GmbH (Marburg, Germany).

5.2.2 Coating of the PolyAn 3D-NHS plate with anti-renin antibodies

A Greiner® polypropylene 96-well plate was modified by PolyAn® (patent number: 20150353698) to allow for the covalent binding of antibodies. This modification resulted in the generation of 3D-N-Hydroxysuccinimide (NHS) groups, which covalently reacted with hydroxy, thiol, or amine groups found on amino acid residues. The anti-renin antibodies were diluted in the incubation buffer (0.1 M citrate-phosphate buffer, pH 3), and 100 µL of this mixture was added to each well, followed by an over-night (16 h) incubation at 4°C and shaking at 300 rpm. After coating, the free NHS-groups were blocked with a buffer consisting of 0.1 M citrate-phosphate, 400 mM ethanolamine, and 500 mM L-glycine for 2 h at 23°C. After blocking, the wells were washed three times with PBS-T buffer (0.01% Tween 20 [v/v]) and dried under a nitrogen stream.

5.2.3 Internal standard generation and synthesis for prorenin and active renin

Two approaches were analyzed to determine a suitable internal standard. The first approach was performed through the guanidation of the amino groups on the lysine residues at the C-terminal end. For this purpose, the O-methylisourea (OMI) reagent was prepared in an ammonium bicarbonate buffer (50 mM), at a concentration of 50 M. 20 µL prorenin was diluted 1:2 with Tris-buffer and treated with 10 µL 1 M sodium hydroxide (NaOH) solution. Finally, 10 µL of the freshly prepared 50 M OMI solution was added to the prorenin–NaOH mixture and incubated for 24 hours at room temperature.

The second approach was the enzymatic labeling of renin with ^{18}O-water to generate either ^{18}O-labeled mature-part or pro-part signature peptides. The insertion of the labeled water was performed by trypsin, according to the optimized, mixed-solvent-triggered digestion protocol developed for the mature-part signature peptide. Before digestion, the protein was immunopurified, and the wells were dried to avoid moisture interference due to unlabeled water. The digestion was performed with a mixture of 62% acetonitrile and 38% ^{18}O-water [v/v] at 37°C and 800 rpm for 57 minutes.

5.2.4 Preparation of plasma and calibration standards and quality controls

Human plasma was collected in S-Monovette® K3 EDTA tubes and centrifuged at 2,000 × g for 10 minutes at room temperature. 2 mL of the obtained plasma were spiked with 4 µL of the diluted active renin stock solution (5,000 pg/µL active renin) to obtain the highest standard at 10,000 pg/mL. Serial dilutions were conducted to generate the remaining calibration standards (5,000, 2,500, 1,250, 625, 312.5, 156.3 and 78.2 pg/mL). The calibration curve was always freshly prepared.

The calibration curve, which was prepared from eight non-zero calibration standards, covered a concentration range from 78 pg/mL to 10,000 pg/mL.

The other quality controls (QC) were generated by an independently prepared serial dilution from the 10,000 pg/mL standard (High-QC: 10,000 pg/mL; Mid-QC-1: 2,500 pg/mL; Mid-QC-2: 312.5 pg/mL; and Low-QC: 78.1 pg/mL).

5.2.5 Sample procedure of the hybrid approach to determine active renin

All standards were diluted at a ratio of 1:6 with PBS-T (0.125% [v/v] Tween 20), and 300 µL of this mixture was pipetted into each well of a 3D-NHS-PP plate with immobilized anti-renin antibodies immobilized on a 3D-NHS-PP plate. The incubations were performed for 1 ½ hours, followed by washing three times with PBS-T (0.01% [v/v] Tween 20) after the incubation period. After the last incubation, the wells were cleaned with pure water to remove any residual buffer. The digestion in cleaned wells was performed using a mixed-solvent approach containing 62% acetonitrile and 38% ABC-buffer [v/v] for 57 minutes at 37°C, followed by evaporation of the solvent and reconstitution in 70% water, 4% DMSO, 20% methanol, and 6% formic acid [v/v/v/v] and the addition of an ^{18}O-labeled internal standard (1 ng/mL) (Fig. 5-1).

5.2.6 In-house validation regarding accuracy and precision of the active renin hybrid assay

The analysis of within and between-run accuracy was performed using three separate runs on three separate days. Due to the absence of an international validation guideline for this specific research field, for the accuracy of the calibration standard, a deviation of ± 20% (± 25% LLOQ) was considered acceptable (Jenkins et al. 2015). If any single standard misses this maximum deviation, that particular standard was excluded, but 67% of the calibration standards or at least six calibration standards must fit the deviation from the nominal value, with linearity above 0.99.

The mean values of the quality controls were required to fall within a maximum mean deviation ± 30% from the calculated nominal concentration. At least three of the quintuplicates (n = 5) have to fulfill the set criteria. The one-way ANOVA was used to calculate inter-day precision. Additionally, the limit of detection (LOD) in plasma was estimate according to criteria of International Conference on Technical Requirements for Registrations of Pharmaceuticals for Human Use (ICH) (European Medicines Agency 2006). LOD was calculated by using standard error and slope of the regression line of specific calibration curve using following expressions:

$$\text{Limit of detection (LOD)} = 3.3\times\sigma/s$$

Where σ is standard error of the y intercept, used as standard deviation and s is slope of regression line, respectively.

Equation 5-1 Equation for calculating the Limit of detection *according to ICH guideline*

5.2.7 Applicability and proof-of-concept for active renin determination and cryoactivation

First, as a proof-of-concept, a native sample from a 28 years old healthy volunteer was sampled after a short rest in an upright position, which was collected in S-Monovette® K3 EDTA tubes and used to measure the active renin concentration. The blood sampling was done according to the principles of the Helsinki Declaration and the approvement by the ethical committee of the medicinal faculty (Heinrich Heine University, Dusseldorf; study number: 2019-800). A written informed consent was acquired from the volunteer.

Second, to ensure the ability to differentiate between active renin and open-form prorenin, the following experiments inducing cryoactivation of prorenin were conducted. The collected plasma was divided into five different experiments: the first sample only contained the spiked prorenin (5 ng/mL); the second sample contained spiked prorenin (5 ng/mL) and aliskiren (10 mmol/L); the third sample contained spiked prorenin (5 ng/mL), nafamostat mesylate (18 µM), and aliskiren (10 mmol/L). The fifth contained prorenin (5 ng/mL), nafamostat mesylate (18 µM), aliskiren (10 mmol/L) and hexadimethrine bromide (1g/mL) and the last sample contained only aliskiren (10 mmol/L). Each of these experiments was again divided into three setting described as follows: For the first setting, day 0, the samples from each approach were immediately frozen and stored at -20 °C. The second setting should induce the

cryoactivation by maintaining the left samples at 4°C for 24 hours which were frozen afterwards and stored at 20 °C. The last setting investigated the cryoactivation for 48h at 4 °C for a separate number of samples. All experiments were thawed and analyzed by the previously described hybrid approach.

5.2.8 Instrumentation and conditions

5.2.8.1 Liquid chromatography and the conditions applied to the determination of the signature peptides

A Shimadzu Nexera UHPLC system (Shimadzu Europe, Duisburg, Germany), which consisted of a controller (CBM 20A), two separate pumps (LC-20ADxR), two separate degassers (DGU-20A5R and DGU-20A3 prominence), a switching valve unit (FCV-11AL), an autosampler (SIL-30AC), and a column oven (CTO-20AC) was used. The separation process was performed on a Phenomenex Kinetex® XB-C18 column (100Å, 1.7 µm, 2.1 mm × 100 mm).
Mobile phase A consisted of 1% DMSO plus 0.1% formic acid in MS-grade water, whereas mobile phase B consisted of 1% DMSO plus 0.1% formic acid in MS-grade methanol [v/v/v]. The flow rate was set to 0.3 mL/min. The gradient started at 5% of mobile phase B and was increased between 4.5 and 4.7 minutes to 42% mobile phase B. This was followed by a further increase to 50% of mobile phase B after 5.7 minutes, which increased to 90% after 0.8 minutes. The gradient was maintained at 90% until 8.5 minutes had elapsed before being reduced to 5% of mobile phase B again. The injection volume was 50 µL, the oven temperature was set to 50°C, and the autosampler conditions were controlled at 15°C.

5.2.8.2 Targeted mass spectrometry and the conditions for signature peptides determination

Mass spectrometric detection was performed using a Sciex TripleTOF 6600 (Sciex, Concord, Canada) high-resolution mass spectrometer system with an IonDrive TurboV® electrospray ionization source. The ion spray voltage was set to 5500 V, curtain gas remained at 47 psi, and nebulizer gas (gas 1) and heater gas (gas 2) were adjusted to 47 psi and 69 psi, respectively, while the interface heater temperature was adjusted to 390°C.
Two signature peptides were applied to the method with the following transition: the transition was 854.9 *m/z* to 418.2296 *m/z,* with a 79 V declustering potential and a 30 eV collision energy, for the mature-part signature peptide (VVFDTGSSNVWVPSSK), and 586.7 *m/z* to 501.7356 *m/z,* with a 70 V declustering potential and a 30 eV collision energy, for the pro-part signature peptide (LGPEWSQPMK).

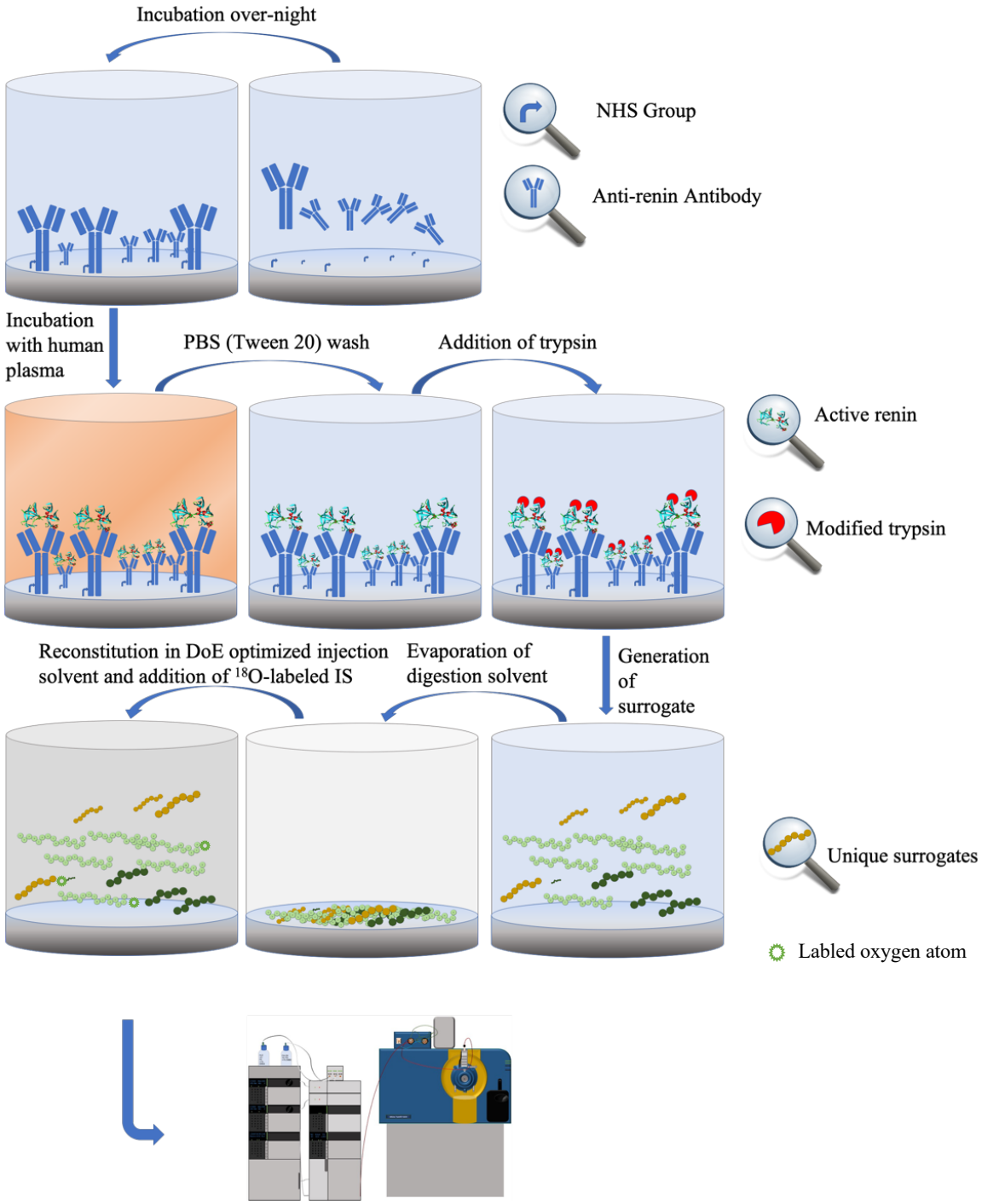

Figure 5-1 Final procedures for the optimized hybrid approach

The first step of the assay procedure is the over-night incubation of anti-human active renin mouse IgG antibodies on the PolyAn 3D-NHS activated plate at 4°C. Second, the unreacted 3D-NHS groups were blocked with a blocking buffer. Third, the coated wells were washed with PBS-T buffer and incubated with human plasma for 1.5 hours. Fourth, the immunocomplexes formed between antibodies and active renin were washed with PBS-T buffer and centrifuged to avoid any interference by the buffer, and the immunocomplexes were reconstituted in 38 µL ABC-buffer containing 1 µg trypsin. After the addition of 62 µL acetonitrile, the digestion solution was incubated at 37°C for 57 minutes. Fifth, the digested samples were evaporated under a gentle nitrogen stream at 60°C. The final step was the reconstitution with the optimized injection solvent composition, the addition of ^{18}O-labeled mature and pro-part signature peptides (peptides marked with a green star), and LC-HRMS measurement (NHS-N-Hydroxysuccinimid).

5.3 Results and discussion

5.3.1 Evaluation of internal standard generation

The evaluation of the guanidation reaction using O-methylisourea in alkaline solution showed the successful implementation of the homoarginine structure into the side-chain of lysine (Fig.5-2). The guanidated internal standard and the unlabeled mature-part signature peptide had the same retention time at 7.81 minutes. However, in immunocapture experiments, the guanidated internal standard could not be captured, likely due to possible changes in the tertiary structure. Despite adding this standard prior to the digestion, the variations, which ranged from -31% to 45% for the mean accuracy of the calibration curve, could not be adjusted, which may be due to better cleavage of the guanidated mature-part signature peptide by trypsin, as reported in the literature (Yang et al. 2014), or the better ionization by the mass spectrometer source due to the permanent charge in homoarginine; however, this guanidated internal standard was found to be unsuitable for improving the accuracy and precision for either the calibration standards or the quality controls.

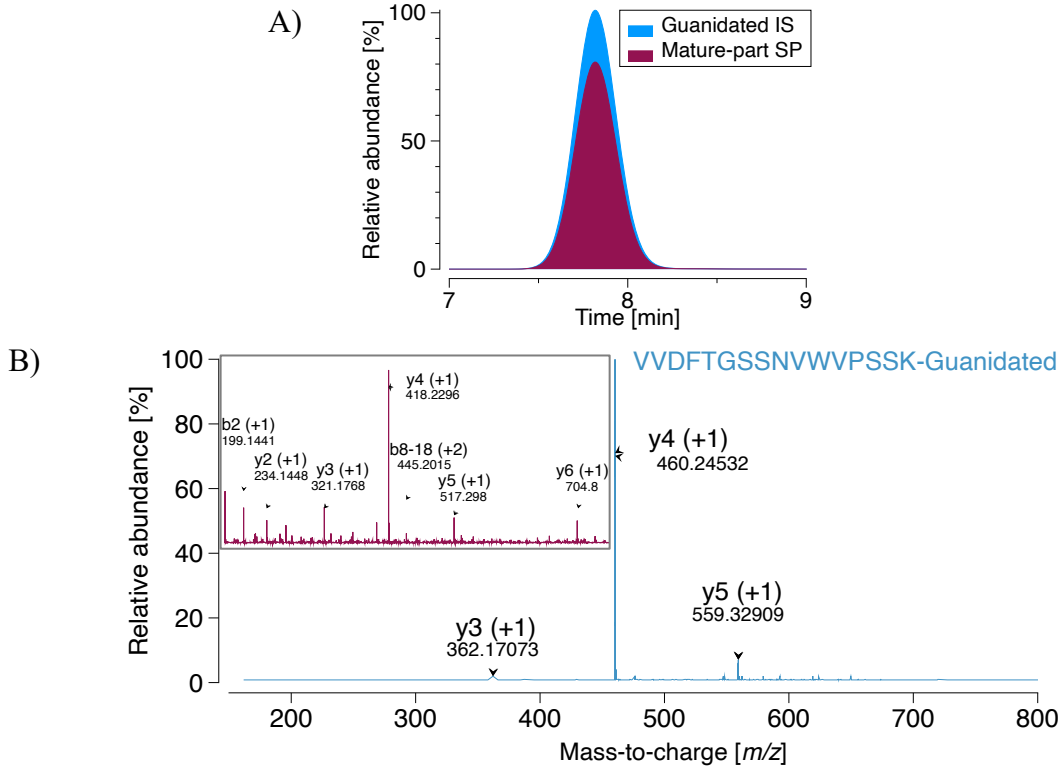

Figure 5-2 Guanidated mature-part signature peptide chromatogram and fragments. *A) Overlaid chromatograms of guanidated and native mature-part signature peptide. B) The one-letter amino acid code and the modification sides are shown on the upper right indication the guanidated lysine residue. The upper left side shows the mass spectrum of the native mature part-signature peptide. The mass spectrum of the guanidated signature peptide shows a mass shift of 42 m/z units for y-fragments with a charge of +1 show, whereas y-fragments with a charge state of +2 were found with a m/z increase of 21 units. The b-fragments remained the same mass (not shown; SP: signature peptide; IS: internal standard).*

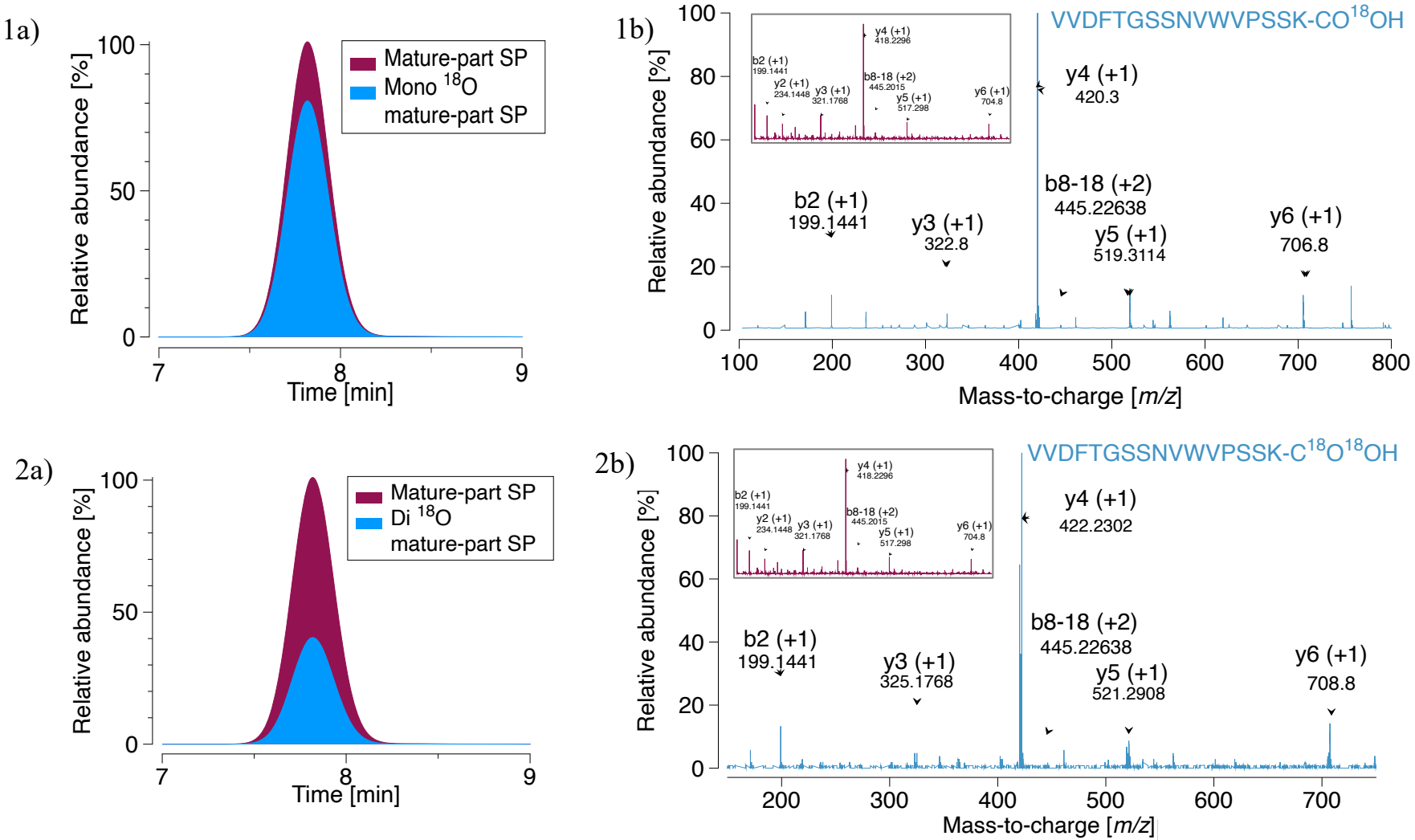

Figure 5-3 Mono and Di ^{18}O-labeled mature-part signature peptide chromatograms and fragments. *1a) Overlaid chromatograms of mono ^{18}O-labeled and native mature-part signature peptide. 1b) The one-letter amino acid code and the modification side are shown the upper left corner indication the will O-atom. On the upper left side, the is a mass spectrum of the native mature part-signature peptide. The main mass spectrum shows y-fragments a mass shift of 2 m/z units for +1 charged fragments, whereas y-fragments with a charge state of +2 are found with an m/z increase of 1 unit. 2a) Overlaid chromatograms of di ^{18}O-labeled and native mature-part signature peptide. 2b) The one-letter amino acid code and the modification side are shown the upper left corner indication the two labelled O-atoms. On the upper left side, the is a mass spectrum of the native mature part-signature peptide. The main mass spectrum shows y-fragments a mass shift of 4 m/z units for +1 charged fragments, whereas y-fragments with a charge state of +2 are found with a m/z increase of 2 units. The b-fragments remain the same mass (SP: signature peptide).*

The alternative method for internal standard generation is based on the use of ^{18}O water for labeling. The results indicated that trypsin was able to label the C-terminal end either once (one atom of the carboxy group of lysine) or two times (both atoms of the carboxy group of lysine). The di-labeled peptide was more beneficial due to the higher mass unit shift which should ensure the separation between the isotopic pattern of the mature-part signature peptide and its ^{18}O labeled internal standards (Haaf and Schlosser 2012). Despite the complete absence of visible moisture ($H_2{}^{16}O$-water), a complete conversion of the mature-part signature peptide into the di-labeled version of the peptide could not be achieved.

All species of either complete unlabeled, mono-labeled, and di-labeled peptides were found in the digest. A similar labeling pattern was also observed for the pro-part signature peptide, but the use of this species as an internal standard was not appropriate either. The isotopic pattern of the pro-part and mature-part signature peptide contained an overlay that might affect the internal standard correction. To ensure the integrity of the labeled peptides, the spiking of the internal standard into the digestion should not be performed to avoid the possible exchange of the ^{18}O-labeled carboxy-group because the digestion was performed in regular water ($H_2{}^{16}O$) (Angel and Orlando 2006).

However, the labeled peptides had the same retention time as their unlabeled signature peptides (Figure 5-3). Accordingly, this internal standard was only suitable for the monitoring of the post-digestion process, which included the reconstitution, the autosampler variabilities, and the LC-HRMS measurement. The immunocapture procedure could not be adjusted because a full-length capture antibody was chosen due to the unavailability of anti-mature-part signature peptide antibodies.

The missing adjustment of sample pretreatment steps, such as immunocapture and digestion, could not be adjusted by the generated ^{18}O internal standard.

These results demonstrated that the labeling procedure remains challenging and can be affected by laboratory particularities, including environmental humidity, as well as protein structures that may integrate water molecules, which can make the complete conversion to labeled surrogates impossible. The generation of a labeled, full-length protein is essential, especially when accompanied by tryptic digestion, to avoid the loss of the labeled atoms. Only the full-length internal standard may also adjust immunocapture and digestion steps that more prone to variations.

For controlling the variation during the LC-MS measurement, the ^{18}O internal standard showed a suitable adjustment regarding sample accuracy and precision. Therefore, it was implemented into the accuracy and precision runs.

5.3.2 Calibration range, the lower limit of quantification, and the limit of detection

The calibration range covered concentrations from 78 pg/mL (LLOQ) to 10,000 pg/mL (ULOQ), which fulfilled the in-house validation criteria by using eight non-zero calibration standards, fitted with a $1/x^2$ weighting and quadratic regression (Fig. 5-4). By using the mature-part signature peptide as the quantifier and the pro-part signature peptide as the qualifier, differentiation could be achieved between active renin and prorenin. All calibration curves showed acceptable linearity above 0.99 and normalized to the internal standard response. All calibration standards for three runs had an accuracy deviation from the nominal value between −19.8% and 19.65% (relative error). The variability associated with the calibration standard intensities was caused by the different charges of anti-active renin antibodies.

For the LLOQ, the coefficient of variation (CV) was 18% that fulfilled the set criteria.

The limit of detection (LOD) was 26 pg/mL for active renin, as calculated according to the ICH guideline (ICH 2018).

5.3.3 Accuracy and precision of the active renin's hybrid assay

The quality control standards were all within the set criteria during the in-house validation, showing a mean accuracy deviation from the nominal values that ranged from −26.6% to 4.4% (RE).

The mean within-day precision deviated from 9.65% to 17.1%, which fulfilled the pre-established precision criteria. The inter-day precision was estimated by performing three separate runs and was determined to be within 16.72% (CV). Additionally, the absence of the pro-part signature peptide demonstrated that the antibodies did not capture open-form prorenin.

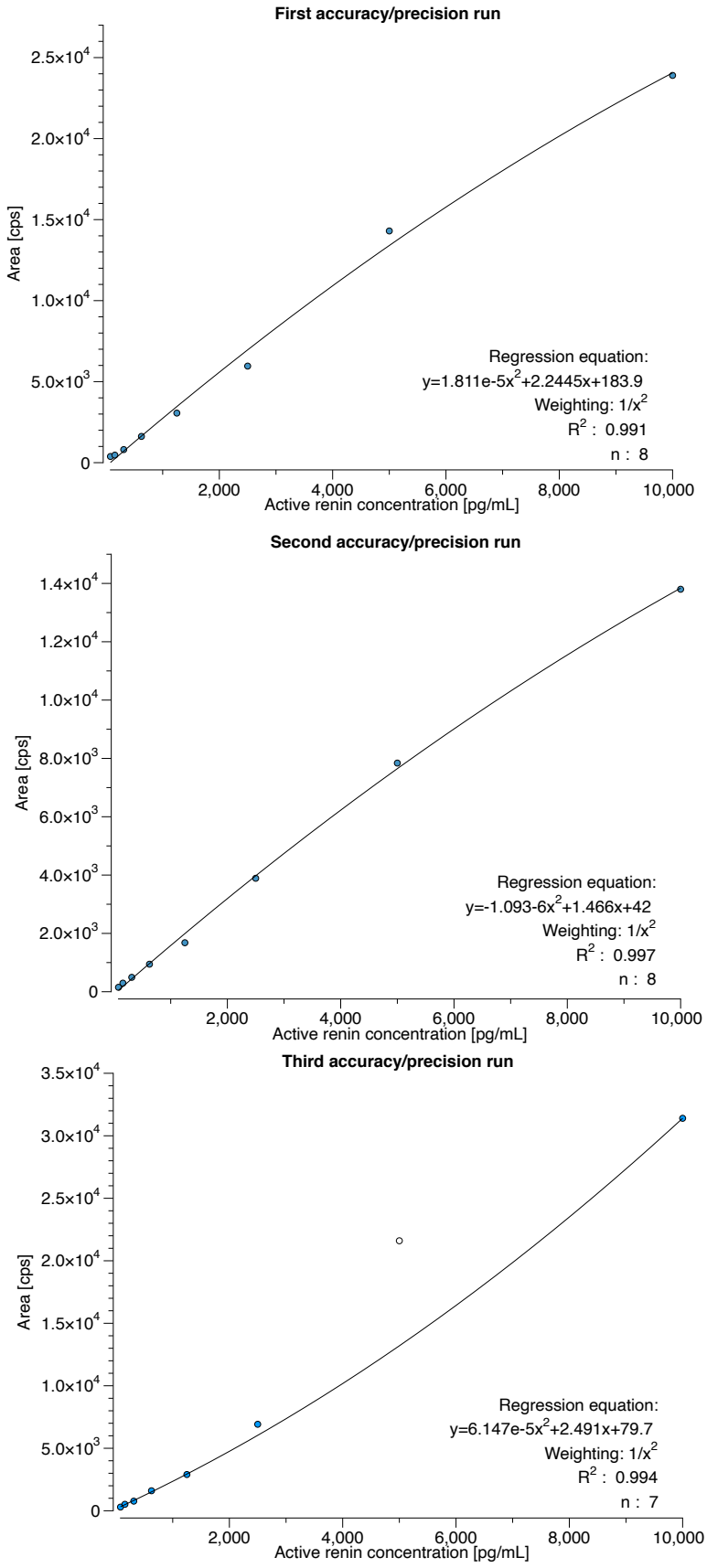

Figure 5-4 Calibration curves for active renin quantification. *The upper graph shows the first accuracy/precision run; the middle graph shows second accuracy/precision run; and the lower graph shows the third validation run. Outliers were excluded according to the 1.5σ test (white dot). A quadratic regression was used.*

5.4 Proof-of-concept results for active renin determination and cryoactivation of prorenin

As a proof-of-concept, this assay was used to determine endogenous renin levels from a healthy male volunteer. The volunteer was not on any RAAS-modifying medications and presented an active renin level of 52 pg/mL (extrapolated from the calibration range) (Fig. 5-5). The assay identified the mature-part signature peptide only, which ensured that no open-form prorenin was captured during the assay process which was done by avoiding the storage conditions at 4 °C that might induce cryoactivation.

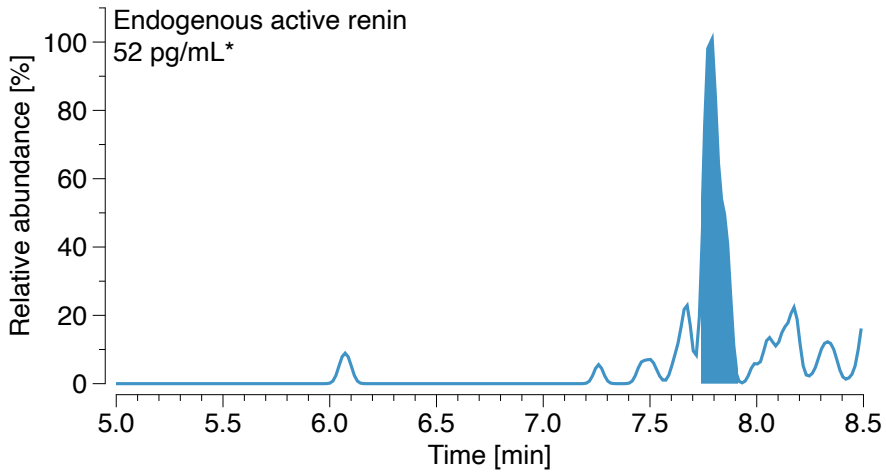

Figure 5-5 Endogenous human active renin measured by the hybrid approach *(*extrapolated level).*

The ability to differentiate between active renin and open-form prorenin has been successfully demonstrated by inducing the unfolding of prorenin's pro-segment, allowing the anti-active renin antibodies access to the catalytical center. A time-dependent activation could also be observed, as described in the literature (Krop et al. 2011). For the aliskiren-treated samples with spiked prorenin (5 ng/mL), an increase was detected, starting on day 0 (mean ± SD of 7.33e2 ± 1.01e2 cps) and increasing on day 1 (mean ± SD of 1.97e3 ± 6.20e1 cps) and day 2 (mean ± SD of 2.46e3 ± 2.51e2, Fig. 5-6). The serine-protease inhibitors showed an intensity-reducing effect which might be explained by possible interactions with the renin inhibitor limiting its ability to open the pro-segment of prorenin. This approach is unsuitable to avoid cryoactivation triggered by renin inhibitors. Additionally, after 48 hours of keeping the non-spiked samples at 4°C, the endogenous levels of activated prorenin also become detectable for the hybrid approach (LLOQ: 78 pg/mL).

The selectivity of this assay is likely to allow for precise measurements to be obtained, even if the sampled blood is taken from a patient on renin inhibitors.

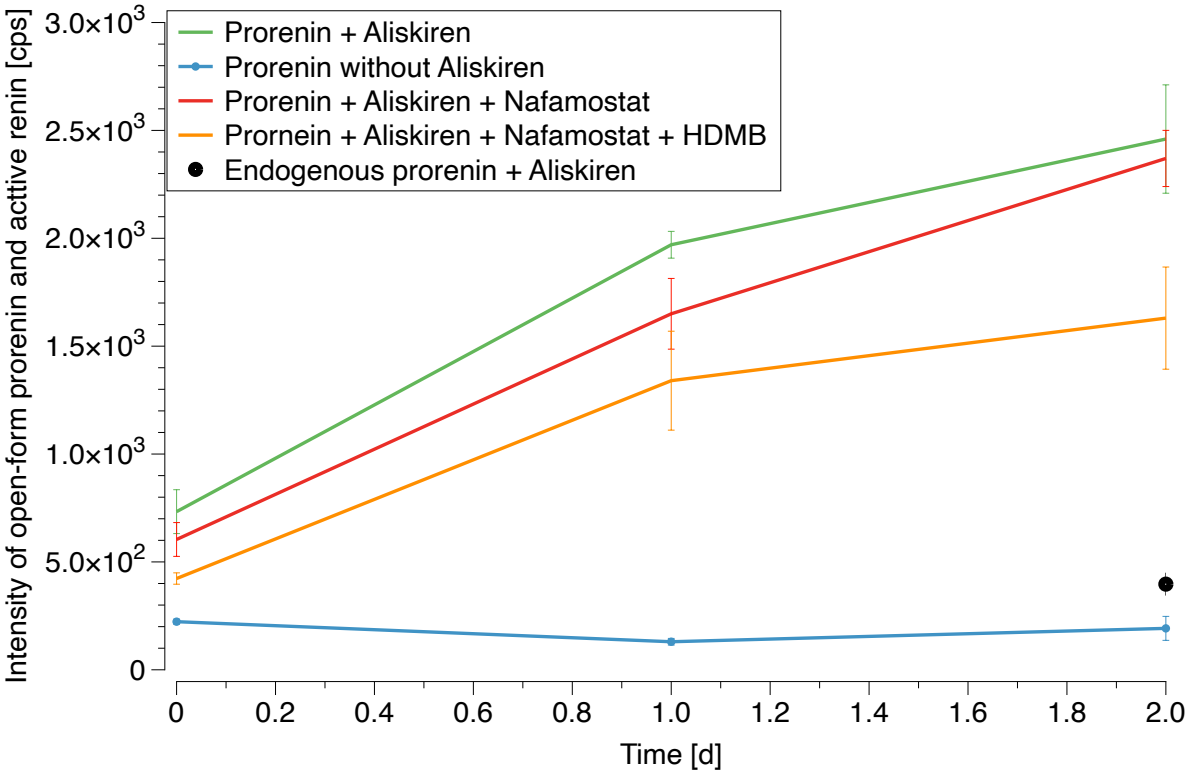

Figure 5-6 Aliskiren driven cryoactivation of prorenin with or without serine protease inhibitors. *The mature-part represents prorenin as well as active renin (all values represent the mean ± SD). Each graph shows the cold-induced activation of the 5 ng/mL spiked prorenin triggered by aliskiren; HDMB: hexadimethrine bromide).*

5.5 Conclusion

The hybrid approach allowed for the precise quantification of active renin within the calibration range, avoiding the false estimation associated with the cross-reactivity of current immunoassays with the open-form prorenin. The accuracy and precision of the established assay were successfully demonstrated within a calibration range between 78 pg/mL and 10,000 pg/mL, which is suitable for the determination of active renin levels in a pediatric population. Moreover, using the developed assay, the false detection of the open-form prorenin, which also occurs in human plasma (<2% of total prorenin) or might appear due to false sample storage and treatment, can be determined via the unique pro-part signature peptide.

6. Overall summary and future perspective

This thesis presents the current limited knowledge regarding prorenin and active renin levels in pediatrics, demonstrating an age-related decline in active renin levels and disease-related changes in these levels. The analysis of the currently available immunoassays demonstrated that the problem of cross-reactivity remains underestimated, which is particularly problematic if the ratio between prorenin and active renin is high, indicating the need for more sensitive and accurate assays to measure these protein levels. The use of both proteins for the diagnosis of diseased children could be improved by the development of more accurate assays to overcome the cross-reactivity problems. Furthermore, pharmacological interventions can affect the prorenin to active renin ratio resulting in the false determination of active renin levels.

An alternative technology, which provides more precise results is the application of LC-MS; however, LC-MS relies on extensive sample pretreatments for the measurement of proteins. The first time presented hybrid assay includes the benefits of an immunoassay's purification abilities, the generation of unique surrogate peptides through tryptic cleavage, the separation of the generated peptides by liquid chromatography, and the accurate and precise identification of these peptides by mass spectrometry. The successive and comprehensive implantation of the named steps resulted in the described hybrid active renin assay.

By utilizing this highly selective assay, the differentiation of active renin and prorenin was achieved through the investigation of unique surrogate peptides that were generated from the pro-segment which only occur in prorenin. Additionally, the time reduction of the digestion procedure led to a lean and fast assay that was able to measure prorenin and active renin levels and ensured that the open-form prorenin was not falsely identified as active renin.

Furthermore, the assays precision was optimized by avoiding non-specific binding during the immunocapture processes and the LC-MS application. Variations that have previously affected immunoassays were improved by using a Design of Experiments-driven optimization procedure. The final verification and application of the assay offers a method that can be implemented into a comprehensive analytical platform for the determination of whole biological systems, such as the RAAS. The possibility of reusing the analyzed blood plasma represents a huge advantage for further bioanalytical applications compared with other established low-volume assays.

Finally, the here-presented bioanalytical assay confirmed its capability to differentiate between prorenin and active renin. The problem of the immunoassay's cross-reactivity leading to an overestimation of active renin (up to 50%) had been overcome successfully. The established assay can now be used for the investigation and effect of 'true' renin in healthy and diseased populations without being affected by open-form prorenin. Additionally, the pediatric maturation processes regarding both proteins can also be monitored accurately in children.
Furthermore, ratios like prorenin-active-renin-ratio, the aldosterone-active-renin-ratio (ARR) and the aldosterone-prorenin-ratio (APR) which are used for diagnosing diabetes-related complications and primary hyperaldosteronism may be further evaluated for their diagnostic value.

7. Funding

Parts of this research leading to these results has received funding from the European Union Seventh Framework Programme (FP7/2007-2013) under grant agreement n°602295 (LENA).

Travel grants were received from the Heine Research Academy (HeRA) that supported the presentation of the here discussed research parts.

Printing sponsorship award was received from Cayman Chemical Company.

8. References

Abdel Ghafar MT (2019) Association of aldosterone synthase CYP11B2 (-344C/T) gene polymorphism with essential hypertension and left ventricular hypertrophy in the Egyptian population. Clin Exp Hypertens 41:779–786 . https://doi.org/10.1080/10641963.2018.1557679

Ackermann BL, Berna MJ (2007) Coupling immunoaffinity techniques with MS for quantitative analysis of low-abundance protein biomarkers. Expert Rev Proteomics 4:175–186 . https://doi.org/10.1586/14789450.4.2.175

Al Shweiki MHDR, Mönchgesang S, Majovsky P, Thieme D, Trutschel D, Hoehenwarter W (2017) Assessment of Label-Free Quantification in Discovery Proteomics and Impact of Technological Factors and Natural Variability of Protein Abundance. J Proteome Res 16:1410–1424 . https://doi.org/10.1021/acs.jproteome.6b00645

Allen TJ, Cooper ME, Gilbert RE, Winikoff J, Skinner SL, Jerums G (1996) Serum total renin is increased before microalbuminuria in diabetes. Kidney Int 50:902–907 . https://doi.org/10.1038/ki.1996.390

Anderson NL, Anderson NG, Haines LR, Hardie DB, Olafson RW, Pearson TW (2004) Mass Spectrometric Quantitation of Peptides and Proteins Using Stable Isotope Standards and Capture by Anti-Peptide Antibodies (SISCAPA). J Proteome Res 3:235–244 . https://doi.org/10.1021/pr034086h

Andrews GL, Dean RA, Hawkridge AM, Muddiman DC (2011) Improving proteome coverage on a LTQ-orbitrap using design of experiments. J Am Soc Mass Spectrom 22:773–783 . https://doi.org/10.1007/s13361-011-0075-2

Andrews Kingon GL, Petitte JN, Muddiman DC, Hawkridge AM (2013) Multi-peptide nLC-PC-IDMS-SRM-based Assay for the Quantification of Biomarkers in the Chicken Ovarian Cancer Model. Methods 61:323–330 . https://doi.org/10.1038/jid.2014.371

Angel PM, Orlando R (2006) Trypsin is the primary mechanism by which the 18O isotopic label is lost in quantitative proteomic studies. Anal Biochem 359:26–34 . https://doi.org/10.1016/j.ab.2006.08.036

Bajcetic M, de Wildt SN, Dalinghaus M, Breitkreutz J, Klingmann I, Lagler FB, Keatley-Clarke A, Breur JM, Male C, Jovanovic I, Szatmári A, Ablonczy L, Burckhardt BB, Cawello W, Kleine K, Obarcanin E, Spatenkova L, Swoboda V, van der Meulen M, Wagner P, Walsh J, Läer S (2019) Orodispersible minitablets of enalapril for use in children with heart failure (LENA): Rationale and protocol for a multicentre

pharmacokinetic bridging study and follow-up safety study. Contemp Clin Trials Commun 15:100393 . https://doi.org/10.1016/j.conctc.2019.100393

Batra R, Gupta MN (1994) Enhancement of enzyme activity in aqueous-organic solvent mixtures. Biotechnol Lett 16:1059–1064 . https://doi.org/10.1007/BF01022403

Berge C, Courand PY, Harbaoui B, Paget V, Khettab F, Bricca G, Fauvel JP, Lantelme P (2015) Decreased plasma prorenin levels in primary aldosteronism: Potential diagnostic implications. J Hypertens 33:118–125 . https://doi.org/10.1097/HJH.0000000000000367

Bhardwaj C, Hanley L (2014) Ion sources for mass spectrometric identification and imaging of molecular species. Nat Prod Rep 31:756–767 . https://doi.org/10.1039/c3np70094a

Bioassays C (2016) Human Renin ELISA Kit (Renin III Generation). https://www.cisbio.eu/media/asset/c/i/cisbio_ivd_pi_renine_mod020_eng.pdf. Accessed 1 Jul 2020

Blazy I, Guillot F, Laborde K, Dechaux M (1989) Comparison of plasma renin and prorenin in healthy infants and children as determined with an enzymatic method and a new direct immunoradiometric assay. Scand J Clin Lab Invest 49:413–8 . https://doi.org/10.1080/00365518909089115

Blumenfeld JD, Sealey JE, Mann SJ, Bragat A, Marion R, Pecker MS, Sotelo J, August P, Pickering TG, Laragh JH (1999) β-Adrenergic receptor blockade as a therapeutic approach for suppressing the renin-angiotensin-aldosterone system in normotensive and hypertensive subjects. Am J Hypertens 12:451–459 . https://doi.org/10.1016/S0895-7061(99)00005-9

Bringans SD, Ito J, Stoll T, Winfield K, Phillips M, Peters K, Davis WA, Davis TME, Lipscombe RJ (2017) Comprehensive mass spectrometry based biomarker discovery and validation platform as applied to diabetic kidney disease. EuPA Open Proteomics 14:1–10 . https://doi.org/10.1016/j.euprot.2016.12.001

Buchhorn R, Bartmus D, Siekmeyer W, Hulpke-Wette M, Schulz R, Bürsch J (1998) Beta-blocker therapy of severe congestive heart failure in infants with left to right shunts. Am J Cardiol 81:1366–8 . https://doi.org/10.1016/s0002-9149(98)00175-1

Buchhorn R, Hammersen A, Bartmus D, Bursch J (2001a) The pathogenesis of heart failure in infants with congenital heart disease. Cardiol Young 11:498–504

Buchhorn R, Hulpke-Wette M, Hilgers R, Bartmus D, Wessel A, Bursch J, Bürsch J (2001b) Propranolol treatment of congestive heart failure in infants with congenital heart disease: The CHF-PRO-INFANT Trial. Int J Cardiol 79:167–173 . https://doi.org/10.1016/S0167-5273(01)00413-2

Buchhorn R, Hulpke-Wette M, Ruschewski W, Ross RD, Fielitz J, Pregla R, Hetzer R, Regitz-Zagrosek V (2003) Effects of therapeutic beta blockade on myocardial function and cardiac remodelling in congenital cardiac disease. Cardiol Young 13:36–43 . https://doi.org/10.1017/S1047951103000076

Buchhorn R, Ross RD, Bartmus D, Wessel A, Hulpke-Wette M, Bürsch J (2001c) Activity of the renin-angiotensin-aldosterone and sympathetic nervous system and their relation to hemodynamic and clinical abnormalities in infants with left-to-right shunts. Int J Cardiol 78:225–30 . https://doi.org/10.1016/s0167-5273(01)00398-9

Burdman I, Burckhardt BB (2019) A concept to make low-abundance endogenous renin accessible to mass spectrometry: A multistep experimental design approach. J Chromatogr B 1134–1135:121856 . https://doi.org/10.1016/j.jchromb.2019.121856

Campbell DJ, Nussberger J, Stowasser M, Danser AHJJ, Morganti A, Frandsen E, Ménard J (2009) Activity Assays and Immunoassays for Plasma Renin and Prorenin: Information Provided and Precautions Necessary for Accurate Measurement. Clin Chem 55:867–877 . https://doi.org/10.1373/clinchem.2008.118000

Cantinotti M, Law Y, Vittorini S, Crocetti M, Marco M, Murzi B, Clerico A (2014) The potential and limitations of plasma BNP measurement in the diagnosis, prognosis, and management of children with heart failure due to congenital cardiac disease: an update. Heart Fail Rev 19:727–742 . https://doi.org/10.1007/s10741-014-9422-2

Capelo JL, Carreira R, Diniz M, Fernandes L, Galesio M, Lodeiro C, Santos HM, Vale G (2009) Overview on modern approaches to speed up protein identification workflows relying on enzymatic cleavage and mass spectrometry-based techniques. Anal Chim Acta 650:151–159 . https://doi.org/10.1016/j.aca.2009.07.034

Chiarelli F, Pomilio M, De Luca FA, Vecchiet J, Verrotti A (2001) Plasma prorenin levels may predict persistent microalbuminuria in children with diabetes. Pediatr Nephrol 16:116–20 . https://doi.org/10.1007/s004670000514

Chiaruttini G, Felisi M, Bonifazi D (2018) Challenges in Paediatric Clinical Trials: How to Make It Feasible. In: The Management of Clinical Trials. InTech, pp 12–33 (Book)

Daneman D, Crompton CH, Balfe JW, Sochett EB, Chatzilias A, Cotter BR, Osmond DH (1994) Plasma prorenin as an early marker of nephropathy in diabetic (IDDM) adolescents. Kidney Int 46:1154–1159 . https://doi.org/10.1038/ki.1994.379

Derkx FH, de Bruin RJ, van Gool JM, van den Hoek MJ, Beerendonk CC, Rosmalen F, Haima P, Schalekamp MA (1996) Clinical validation of renin monoclonal antibody-based sandwich assays of renin and prorenin, and use of renin inhibitor to enhance

prorenin immunoreactivity. Clin Chem 42:1051–63

Derkx FHM, Alberda AT, De Jong FH, Zeilmaker FH, Makovitz JW, Schalekamp MADH (1987a) Source of plasma prorenin in early and late pregnancy: Observations in a patient with primary ovarian failure. J Clin Endocrinol Metab 65:349–354 . https://doi.org/10.1210/jcem-65-2-349

Derkx FHM, Schalekamp PA, Schalekamp MADH (1987b) Two-step Prorenin-Renin Conversion. J Biol Chem 262–2:2472–2477

Douglass K (2014) Fundamental Studies of Protein Ionization for Improved Analysis by Electrospray Ionization Mass Spectrometry and Related Methods, PhD thesis. Western Michigan University

Eriksson L, Johansson E, Kettaneh-Wold N, WikstrÄom C, Wold S (2008) Design of Experiments: Principles and Applications (Book)

European Commission Expert group on clinical trials (2017) Ethical considerations for clinical trials on medicinal products conducted with minors. Recommendations of the expert group on clinical trials for the implementation of Regulation (EU) No 536/2014 on clinical trials on medicinal products for human use. https://ec.europa.eu/health/sites/health/files/files/eudralex/vol-10/2017_09_18_ethical_consid_ct_with_minors.pdf. Accessed 29 Aug 2020

European Medicines Agency (2009) Committee for Medicinal Producs for Human Use (Chmp) and Paediatric Committee (Pdco). Guideline on the Investigation of Medicinal Products in the Term and Preterm Neonate. ema.europa.eu/en/documents/scientific-guideline/guideline-investigation-medicinal-products-term-preterm-neonate-first-version_en.pdf. Accessed 29 Aug 2020

European Medicines Agency (2006) ICH Topic Q 2 (R1) Validation of Analytical Procedures: Text and Methodology. https://www.ema.europa.eu/en/documents/scientific-guideline/ich-q-2-r1-validation-analytical-procedures-text-methodology-step-5_en.pdf. Accessed 27 Jul 2020

Feickert M, Burckhardt BB (2019) A design of experiments concept for the minimization of nonspecific peptide adsorption in the mass spectrometric determination of substance P and related hemokinin-1. J Sep Sci 1–11 . https://doi.org/10.1002/jssc.201901038

Feickert M, Burdman I, Makowski N, Ali M, Bartel A, Burckhardt BB (2020) A continued method performance monitoring approach for the determination of pediatric renin samples – application within a European clinical trial. Clin Chem Lab Med 1–9 . https://doi.org/10.1515/cclm-2019-1162

Figeys D (2013) Integrative Proteomics. Proteomics 13:1231–1232 . https://doi.org/10.1002/pmic.201370074

Franken AAM, Derkx FHM, In't Veld AJM, Hop WCJ, Rens GHV, Peperkamp E, Jong PTVMD, Schalekamp MADH (1990) High plasma prorenin in diabetes mellitus and its correlation with some complications. J Clin Endocrinol Metab 71:994–1002 . https://doi.org/10.1210/jcem-71-4-1008

Funder JW, Carey RM, Mantero F, Murad MH, Reincke M, Shibata H, Stowasser M, Young WF (2016) The management of primary aldosteronism: Case detection, diagnosis, and treatment: An endocrine society clinical practice guideline. J Clin Endocrinol Metab 101:1889–1916 . https://doi.org/10.1210/jc.2015-4061

Gangnus T, Burckhardt BB (2019) Potential and Limitations of Atrial Natriuretic Peptide as Biomarker in Pediatric Heart Failure—A Comparative Review. Front Pediatr 6:420 . https://doi.org/10.3389/fped.2018.00420

Ganorkar SB, Shirkhedkar AA (2017) Design of experiments in liquid chromatography (HPLC) analysis of pharmaceuticals: Analytics, applications, implications and future prospects. Rev Anal Chem 36: 3 . https://doi.org/10.1515/revac-2016-0025

Glinicki P, Jeske W, Gietka-Czernel M, Bednarek-Papierska L, Kruszyńska A, Słowińska-Srzednicka J, Zgliczyński W (2015) The effect of blood collection procedure on plasma renin activity (PRA) and concentrations of direct renin (DRC) and aldosterone. JRAAS - J Renin-Angiotensin-Aldosterone Syst 16:339–343 . https://doi.org/10.1177/1470320313494434

Gomez RA, Lynch KR, Sturgill BC, Elwood JP, Chevalier RL, Carey RM, Peach MJ (1989) Distribution of renin mRNA and its protein in the developing kidney. Am J Physiol Physiol 257:F850–F858 . https://doi.org/10.1152/ajprenal.1989.257.5.F850

Gomez RA, Sequeira Lopez MLS, Fernandez L, Chernotavvsky DR, Norwood VF (1999) The Maturing Kidney: Development and Susceptibility. Ren Fail 21:283–291 . https://doi.org/10.3109/08860229909085090

Haaf E, Schlosser A (2012) Peptide and Protein Quantitation by Acid-Catalyzed 18 O-Labeling of Carboxyl Groups. Anal Chem 84:304–311 . https://doi.org/10.1021/ac202561m

Hahne H, Pachl F, Ruprecht B, Maier SK, Klaeger S, Helm D, Médard G, Wilm M, Lemeer S, Kuster B (2013) DMSO enhances electrospray response, boosting sensitivity of proteomic experiments. Nat Methods 10:989–991 . https://doi.org/10.1038/nmeth.2610

Harris TH, Gossett JG (2016) Diagnosis and Diagnostic Modalities in Pediatric Patients with

Elevated Troponin. Pediatr Cardiol 37:1469–1474 . https://doi.org/10.1007/s00246-016-1459-7

Havliš J, Shevchenko A (2004) Absolute quantification of proteins in solutions and in polyacrylamide gels by mass spectrometry. Anal Chem 76:3029–3036 . https://doi.org/10.1021/ac035286f

Hecht ES, Oberg AL, Muddiman DC (2016) Optimizing Mass Spectrometry Analyses: A Tailored Review on the Utility of Design of Experiments. J Am Soc Mass Spectrom 27:767–785 . https://doi.org/10.1007/s13361-016-1344-x

Hjortdal VE, Stenbøg E V, Ravn HB, Emmertsen K, Jensen KT, Pedersen EB, Olsen KH, Hansen OK, Sørensen KE (2000) Neurohormonal activation late after cavopulmonary connection. Heart 83:439–43 . https://doi.org/10.1136/heart.83.4.439

Hsueh W, Baxter JD (1991) Human prorenin. Hypertension 17:469–477 . https://doi.org/10.1161/01.HYP.17.4.469

ICH (2018) Q14: Analytical Procedure Development and Revision of Q2(R1) Analytical Validation. http://academy.gmp-compliance.org/guidemgr/files/Q2R2Q14EWG_ConceptPaper_2018_1115%20(1).pdf. Accessed 06 Aug 2020

Ichihara A, Sakoda M, Kurauchi-Mito A, Kaneshiro Y, Itoh H (2009) Renin, prorenin and the kidney: A new chapter in an old saga. J Nephrol 22:306–311

Iwamoto N, Shimada T, Terakado H, Hamada A (2016) Validated LC-MS/MS analysis of immune checkpoint inhibitor Nivolumab in human plasma using a Fab peptide-selective quantitation method: Nano-surface and molecular-orientation limited (nSMOL) proteolysis. J Chromatogr B Anal Technol Biomed Life Sci 1023–1024:9–16 . https://doi.org/10.1016/j.jchromb.2016.04.038

Jenkins R, Duggan JX, Aubry A-F, Zeng J, Lee JW, Cojocaru L, Dufield D, Garofolo F, Kaur S, Schultz GA, Xu K, Yang Z, Yu J, Zhang YJ, Vazvaei F (2015) Recommendations for validation of LC-MS/MS bioanalytical methods for protein biotherapeutics. AAPS J 17:1–16 . https://doi.org/10.1208/s12248-014-9685-5

Jia G, Aroor AR, Hill MA, Sowers JR (2018) Role of Renin-Angiotensin-Aldosterone System Activation in Promoting Cardiovascular Fibrosis and Stiffness. Hypertension 72:537–548 . https://doi.org/10.1161/HYPERTENSIONAHA.118.11065

Kailasa S, Wu H-F (2014) Advances in Nanomaterial-Based Microwaves and Infrared Wave-Assisted Tryptic Digestion for Ultrafast Proteolysis and Rapid Detection by MALDI-MS. Comb Chem High Throughput Screen 17:68–79 .

https://doi.org/10.2174/138620731666613111021135 3

Kearns GL, Abdel-Rahman SM, Alander SW, Blowey DL, Leeder JS, Kauffman RE (2003) Developmental Pharmacology — Drug Disposition, Action, and Therapy in Infants and Children. N Engl J Med 349:1157–1167 . https://doi.org/10.1056/NEJMra035092

Keith Williams D, Muddiman DC (2009) Absolute quantification of C-reactive protein in human plasma derived from patients with epithelial ovarian cancer utilizing protein cleavage isotope dilution mass spectrometry. J Proteome Res 8:1085–1090 . https://doi.org/10.1021/pr800922p

Kilpatrick EL, Bunk DM (2009) Reference Measurement Procedure Development for C-Reactive Protein in Human Serum. Anal Chem 81:8610–8616 . https://doi.org/10.1021/ac901597h

Kim S, Hiruma M, Ikemoto F, Yamamoto K (1988) Importance of glycosylation for hepatic clearance of renal renin. Am J Physiol Metab 255:E642–E651 . https://doi.org/10.1152/ajpendo.1988.255.5.E642

Kollipara L, Zahedi RP (2013) Protein carbamylation: In vivo modification or in vitro artefact? Proteomics 13:941–944 . https://doi.org/10.1002/pmic.201200452

Krop M, Danser AHJ (2008) Circulating versus tissue renin-angiotensin system: On the origin of (Pro)renin. Curr Hypertens Rep 10:112–118 . https://doi.org/10.1007/s11906-008-0022-1

Krop M, Lu X, Verdonk K, Schalekamp MADH, Van Gool JMG, McKeever BM, Gregg R, Danser AHJ (2013) New renin inhibitor VTP-27999 alters renin immunoreactivity and does not unfold prorenin. Hypertension 61:1075–1082 . https://doi.org/10.1161/HYPERTENSIONAHA.111.00967

Krop M, Van Gool JMG, Day D, Hollenberg NK, Danser AHJ (2011) Evaluation of a direct prorenin assay making use of a monoclonal antibody directed against residues 32-39 of the prosegment. J Hypertens 29:2138–2146 . https://doi.org/10.1097/HJH.0b013e32834b1978

Kruger C, Hoper K, Weissortel R, Hensen J, Dorr HG (1996) Value of direct measurement of active renin concentrations in congenital adrenal hyperplasia due to 21-hydroxylase deficiency. Eur J Pediatr 155:858–861

Kruger C, Rauh M, Dorr HG (1998) Immunoreactive renin concentrations in healthy children from birth to adolescence. Clin Chim Acta 274:15–27

Lamarre-Cliche M, De Champlain J, Lacourcière Y, Poirier L, Karas M, Larochelle P (2005) Effects of circadian rhythms, posture, and medication on renin-aldosterone interrelations

in essential hypertensives. Am J Hypertens 18:56–64 . https://doi.org/10.1016/j.amjhyper.2004.08.025

Lequin RM (2005) Enzyme immunoassay (EIA)/enzyme-linked immunosorbent assay (ELISA). Clin Chem 51:2415–2418 . https://doi.org/10.1373/clinchem.2005.051532

Lipshultz SE, Law YM, Asante-Korang A, Austin ED, Dipchand AI, Everitt MD, Hsu DT, Lin KY, Price JF, Wilkinson JD, Colan SD (2019) Cardiomyopathy in Children: Classification and Diagnosis: A Scientific Statement From the American Heart Association. Circulation 140:E9–E68 . https://doi.org/10.1161/CIR.0000000000000682

Loziuk PL, Wang J, Li Q, Sederoff RR, Chiang VL, Muddiman DC (2013) Understanding the role of proteolytic digestion on discovery and targeted proteomic measurements using liquid chromatography tandem mass spectrometry and design of experiments. J Proteome Res 12:5820–5829 . https://doi.org/10.1021/pr4008442

Ludwig C, Gillet L, Rosenberger G, Amon S, Collins BC, Aebersold R (2018) Data-independent acquisition-based SWATH - MS for quantitative proteomics: a tutorial . Mol Syst Biol 14:1–23 . https://doi.org/10.15252/msb.20178126

Maas MH, Cransberg K, van Grotel M, Pieters R, van den Heuvel-Eibrink MM (2007) Renin-induced hypertension in Wilms tumor patients. Pediatr Blood Cancer 48:500–503 . https://doi.org/10.1002/pbc.20938

Mahler B, Kamperis K, Schroeder M, Frøkiær J, Djurhuus JC, Rittig S (2012) Sleep deprivation induces excess diuresis and natriuresis in healthy children. Am J Physiol - Ren Physiol 302:236–243 . https://doi.org/10.1152/ajprenal.00283.2011

Makowski N, Ciplea AM, Ali M, Burdman I, Bartel A, Burckhardt BB (2020) A comprehensive quality control system suitable for academic research: application in a pediatric study. Bioanalysis 12:319–333 . https://doi.org/10.4155/bio-2019-0242

Martinerie L, Pussard E, Foix-L'Hélias L, Petit F, Cosson C, Boileau P, Lombès M, Laetitia M, Eric P, Laurence FLH, Francois P, Claudine C, Pascal B, Lombès M (2009) Physiological partial aldosterone resistance in human newborns. Pediatr Res 66:323–8 . https://doi.org/10.1203/PDR.0b013e3181b1bbec

Menard J, Guyene T-T, Peyrard S, Azizi M (2006) Conformational changes in prorenin during renin inhibition in vitro and in vivo. J Hypertens 24:529–534 . https://doi.org/10.1097/01.hjh.0000209989.59230.2e

Mladek AC, Kromidas S (2014) HPLC für Neueinsteiger. https://www.kromidas.de/Uploads/Dokumente/HPLCfuerNeueinsteiger.pdf. Accessed 26 Aug 2020

Momma K (2006) ACE Inhibitors in Pediatric Patients with Heart Failure. Pediatr Drugs 8:55–69 . https://doi.org/10.2165/00148581-200608010-00005

Naruse M, Wasada T, Naruse K, Yoshimoto T, Omori Y, Demura H (1995) Pathophysiological significance of plasma total renin and prorenin in patients with diabetes mellitus. Endocr J 42:225–233 . https://doi.org/10.1507/endocrj.42.225

Nelson RW, Nedelkov D, Tubbs KA, Kiernan UA (2004) Quantitative Mass Spectrometric Immunoassay of Insulin Like Growth Factor 1 research articles. J Proteome Res 3:851–855 . https://doi.org/10.1021/pr0499388

Neves FAR, Duncan KG, Baxter JD (1996) Cathepsin B Is a Prorenin Processing Enzyme. Hypertens 27:514–517 . https://doi.org/10.1161/01.HYP.27.3.514

Nguyen G (2011) Renin, (pro)renin and receptor: an update. Clin Sci 120:169–178 . https://doi.org/10.1042/CS20100432

Nguyen G, Blanchard A, Curis E, Bergerot D, Chambon Y, Hirose T, Caumont-Prim A, Tabard SB, Baron S, Frank M, Totsune K, Azizi M (2014) Plasma Soluble (Pro)Renin Receptor Is Independent of Plasma Renin, Prorenin, and Aldosterone Concentrations But Is Affected by Ethnicity. Hypertension 63:297–302 . https://doi.org/10.1161/hypertensionaha.113.02217

Nguyen G, Delarue F, Burcklé C, Bouzhir L, Giller T, Sraer J (2002) Pivotal role of the renin / prorenin receptor in angiotensin II production and cellular responses to renin. J Clin Invest 109:1417–1427 . https://doi.org/10.1172/JCI200214276.Introduction

Nicol GR, Han M, Kim J, Birse CE, Brand E, Nguyen A, Mesri M, FitzHugh W, Kaminker P, Moore PA, Ruben SM, He T (2008) Use of an Immunoaffinity-Mass Spectrometry-based Approach for the Quantification of Protein Biomarkers from Serum Samples of Lung Cancer Patients. Mol Cell Proteomics 7:1974–1982 . https://doi.org/10.1074/mcp.M700476-MCP200

Nicolaidou P, Georgouli H, Matsinos Y, Psychou F, Messaritaki A, Gourgiotis D, Zeis P (2003) Endothelin-1 in children with acute poststreptococcal glomerulonephritis and hypertension. Pediatr Int 45:35–8 . https://doi.org/10.1046/j.1442-200x.2003.01661.x

Niedz RP, Evens TJ (2016) Design of experiments (DOE)—history, concepts, and relevance to in vitro culture. Vitr Cell Dev Biol - Plant 52:547–562 . https://doi.org/10.1007/s11627-016-9786-1

Ohyama K, Ohta M, Fujimoto M, Nakagomi Y, Yamori T, Kato K (1989) Plasma Active Renin Concentration in Children. Endocrinol Jpn 36:605–610 . https://doi.org/10.1507/endocrj1954.36.605

Östin A, Bergström T, Fredriksson S-Å, Nilsson C (2007) Solvent-Assisted Trypsin Digestion of Ricin for Forensic Identification by LC-ESI MS/MS. Anal Chem 79:6271–6278 . https://doi.org/10.1021/ac0701740

Pan S, Aebersold R, Chen R, Rush J, Goodlett DR, Martin W, Zhang J, Brentnall TA (2010) Mass spectrometry based targeted protein quantification: methods and applications. J Proteome Res 8:787–797 . https://doi.org/10.1021/pr800538n.Mass

Paternostro R, Reiberger T, Mandorfer M, Schwarzer R, Schwabl P, Bota S, Ferlitsch M, Trauner M, Peck-Radosavljevic M, Ferlitsch A (2017) Plasma renin concentration represents an independent risk factor for mortality and is associated with liver dysfunction in patients with cirrhosis. J Gastroenterol Hepatol 32:184–190 . https://doi.org/10.1111/jgh.13439

Peng X, Liu B, Li Y, Wang H, Chen X, Guo H, Guo Q, Xu J, Wang H, Zhang D, Dai J, Hou S, Guo Y (2015) Development and Validation of LC–MS/MS Method for the Quantitation of Infliximab in Human Serum. Chromatographia 78:521–531 . https://doi.org/10.1007/s10337-015-2866-2

Perdivara I, Deterding LJ, Przybylski M, Tomer KB (2010) Mass spectrometric identification of oxidative modifications of tryptophan residues in proteins: Chemical artifact or post-translational modification? J Am Soc Mass Spectrom 21:1114–1117 . https://doi.org/10.1016/j.jasms.2010.02.016

Picotti P, Aebersold R, Domon B (2007) The Implications of Proteolytic Background for Shotgun Proteomics. Mol Cell Proteomics 6:1589–1598 . https://doi.org/10.1074/mcp.M700029-MCP200

Pitarresi TM, Rubattu S, Heinrikson R, Sealey JE (1992) Reversible cryoactivation of recombinant human prorenin. J Biol Chem 267:11753–11759

Proc JL, Kuzyk MA, Hardie DB, Yang J, Smith DS, Jackson AM, Parker CE, Borchers CH (2010) A quantitative study of the effects of chaotropic agents, surfactants, and solvents on the digestion efficiency of human plasma proteins by trypsin. J Proteome Res 9:5422–5437 . https://doi.org/10.1021/pr100656u

Ranasinghe A, Mehl J, D'Arienzo C, Nabbie F, Chiu C, Thevanayagam L, Srinivasan M, Hogan J, Ponath P, Olah T (2018) Fucosyl monosialoganglioside: Quantitative analysis of specific potential biomarkers of lung cancer in biological matrices using immunocapture extraction/tandem mass spectrometry. Rapid Commun Mass Spectrom 32:1481–1490 . https://doi.org/10.1002/rcm.8194

Rickers C, Laeer S, Diller GP, Janousek J, Hoppe U, Mir TS, Weil J Leitlinie Pädiatrische

Kardiologie: Chronische Herzinsuffizienz. https://www.awmf.org/uploads/tx_szleitlinien/023-006l_S2k_Chronische_Herzinsuffizienz_Kinder_Jugendliche_2015-10.pdf. Accessed 27 Aug 2020

Roepstorff P, Fohlman J (1984) Proposal for a Common Nomenclaturefor Sequence Ions in Mass Spectra of Peptides. Biol Mass Spectrom 11:601–601 . https://doi.org/10.1002/bms.1200111109

Rossano JW, Cabrera AG, Jefferies JL, Naim MPHMY, Humlicek T (2016) Pediatric Cardiac Intensive Care Society 2014 Consensus Statement: Pharmacotherapies in Cardiac Critical Care Chronic Heart Failure. Pediatr Crit Care Med 17:S20-34 . https://doi.org/10.1097/PCC.0000000000000624

Russell WK, Park Z-Y, Russell DH (2001) Proteolysis in Mixed Organic−Aqueous Solvent Systems: Applications for Peptide Mass Mapping Using Mass Spectrometry. Anal Chem 73:2682–2685 . https://doi.org/10.1021/ac001332p

Schroten NF, Gaillard CAJM, Van Veldhuisen DJ, Szymanski MK, Hillege HL, De Boer RA (2012) New roles for renin and prorenin in heart failure and cardiorenal crosstalk. Heart Fail Rev 17:191–201 . https://doi.org/10.1007/s10741-011-9262-2

Schütz S, Le Moullec JM, Corvol P, Gasc JM (1996) Early expression of all the components of the renin-angiotensin-system in human development. Am J Pathol 149:2067–79

Schweda F, Friis U, Wagner C, Skott O, Kurtz A (2007) Renin Release. Physiology 22:310–319 . https://doi.org/10.1152/physiol.00024.2007

Sealey JE, Glorioso N, Itskovitz J, Laragh JH (1986) Prorenin as a reproductive hormone. New form of the renin system. Am J Med 81:1041–1046 . https://doi.org/10.1016/0002-9343(86)90402-X

Serra A, Zhu H, Gallart-Palau X, Park JE, Ho HH, Tam JP, Sze SK (2016) Plasma proteome coverage is increased by unique peptide recovery from sodium deoxycholate precipitate. Anal Bioanal Chem 408:1963–1973 . https://doi.org/10.1007/s00216-016-9312-7

Shamsuzzaman A, Szczesniak RD, Fenchel MC, Amin RS (2015) Plasma renin levels and renin-blood pressure relationship in normal-weight and overweight children with obstructive sleep apnea and matched controls. Sleep Med 16:101–106 . https://doi.org/10.1016/j.sleep.2014.05.022

Shuford CM, Li Q, Sun YH, Chen HC, Wang J, Shi R, Sederoff RR, Chiang VL, Muddiman DC (2012a) Comprehensive quantification of monolignol-pathway enzymes in populus trichocarpa by protein cleavage isotope dilution mass spectrometry. J Proteome Res

11:3390–3404 . https://doi.org/10.1021/pr300205a

Shuford CM, Sederoff RR, Chiang VL, Muddiman DC (2012b) Peptide production and decay rates affect the quantitative accuracy of protein cleavage isotope dilution mass spectrometry (PC-IDMS). Mol Cell Proteomics 11:814–823 . https://doi.org/10.1074/mcp.O112.017145

Sielecki A, Hayakawa K, Fujinaga M, Murphy M, Fraser M, Muir A, Carilli C, Lewicki J, Baxter J, James M (1989) Structure of recombinant human renin, a target for cardiovascular-active drugs, at 2.5 A resolution. Science (80-) 243:1346–1351 . https://doi.org/10.1126/science.2493678

Sigirci A, Hallac T, Akyncy A, Temel I, Gulcan H, Aslan M, Kocer M, Kahraman B, Alkan A, Kutlu R (2006) Renal interlobar artery parameters with duplex Doppler sonography and correlations with age, plasma renin, and aldosterone levels in healthy children. AJR Am J Roentgenol 186:828–832 . https://doi.org/10.2214/AJR.04.1445

Son D, Le NT, Pannacciulli N, Chen K, Salbe AD, Hill JO, Rena R, Reiman EM, Krakoff J (2007) A Quantitative Study of the Effects of Chaotropic Agents, Surfactants, and Solvents on the Digestion Efficiency of Human Plasma Proteins by Trypsin. J Proteome Res 86:573–579 . https://doi.org/10.1109/TMI.2012.2196707.Separate

Stoicescu M, Csepento C, Muţiu G, Bungău S (2011) The role of increased plasmatic renin level in the pathogenesis of arterial hypertension in young adults. Rom J Morphol Embryol 52:419–23

Strader MB, Tabb DL, Hervey WJ, Pan C, Hurst GB (2006) Efficient and specific trypsin digestion of microgram to nanogram quantities of proteins in organic-aqueous solvent systems. Anal Chem 78:125–134 . https://doi.org/10.1021/ac051348l

Sun L, Zhu G, Li Y, Yang P, Dovichi NJ (2012) Coupling Methanol Denaturation, Immobilized Trypsin Digestion, and Accurate Mass and Time Tagging for Liquid-Chromatography- Based Shotgun Proteomics of Low Nanogram Amounts of RAW 264.7 Cell Lysate. Anal Chem 84:8715–8721 . https://doi.org/10.1021/ac3019608

Sun Shisheng, Zhou Jian-Ying, Yang Weiming ZH (2015) Inhibition of Protein Carbamylation in Urea Solution Using Ammonium Containing Buffers. Anal Biochem 6:790–795 . https://doi.org/10.1016/j.ab.2013.10.024

Suzuki F, Hayakawa M, Nakagawa T, Nasir UM, Ebihara A, Iwasawa A, Ishida Y, Nakamura Y, Murakami K (2003) Human prorenin has “gate and handle” regions for its non-proteolytic activation. J Biol Chem 278:22217–22222 . https://doi.org/10.1074/jbc.M302579200

Switzar L, Giera M, Lingeman H, Irth H, Niessen WMA (2011) Protein digestion optimization for characterization of drug-protein adducts using response surface modeling. J Chromatogr A 1218:1715–1723 . https://doi.org/10.1016/j.chroma.2010.12.043

Tang X-J, Boyd RK, Bertrand MJ (1992) An investigation of fragmentation mechanisms of doubly protonated tryptic peptides. Rapid Commun Mass Spectrom 6:651–657 . https://doi.org/10.1002/rcm.1290061105

Tassinari MS, Benson K, Elayan I, Espandiari P, Davis-Bruno K (2011) Juvenile animal studies and pediatric drug development retrospective review: use in regulatory decisions and labeling. Birth Defects Res Part B Dev Reprod Toxicol 92:261–265 . https://doi.org/10.1002/bdrb.20304

Terada T, Urushihara M, Saijo T, Nakagawa R, Kagami S (2017) (Pro)renin and (pro)renin receptor expression during kidney development in neonates. Eur J Pediatr 176:183–189 . https://doi.org/10.1007/s00431-016-2820-9

Tigerstedt R, Bergman PQ (1898) Niere und Kreislauf 1. Skand Arch Physiol 8:223–271 . https://doi.org/10.1111/j.1748-1716.1898.tb00272.x

Tomaschitz A, Pilz S, Ritz E, Morganti A, Grammer T, Amrein K, Boehm BO, Marz W, Mrz W, Marz W (2011) Associations of plasma renin with 10-year cardiovascular mortality, sudden cardiac death, and death due to heart failure. Eur Heart J 32:2642–2649 . https://doi.org/10.1093/eurheartj/ehr150

Torsetnes SB, Løvbak SG, Claus C, Lund H, Nordlund MS, Paus E, Halvorsen TG, Reubsaet L (2013) Immunocapture and LC-MS/MS for selective quantification and differentiation of the isozymes of the biomarker neuron-specific enolase in serum. J Chromatogr B Anal Technol Biomed Life Sci 929:125–132 . https://doi.org/10.1016/j.jchromb.2013.04.010

Triefenbach F (2008) Design of Experiments: The D-Optimal Approach and Its Implementation As a Computer Algorithm, Bachelor Thesis. Umea University

Trudu M, Janas S, Lanzani C, Debaix H, Schaeffer C, Ikehata M, Citterio L, Demaretz S, Trevisani F, Ristagno G, Glaudemans B, Laghmani K, Dell'Antonio G, Loffing J, Rastaldi MP, Manunta P, Devuyst O, Rampoldi L (2013) Common noncoding UMOD gene variants induce salt-sensitive hypertension and kidney damage by increasing uromodulin expression. Nat Med 19:1655–1660 . https://doi.org/10.1038/nm.3384

Tu W, Eckert GJ, Pratt JH, Jan Danser AH (2012) Plasma levels of prorenin and renin in blacks and whites: Their relative abundance and associations with plasma aldosterone concentration. Am J Hypertens 25:1030–1034 . https://doi.org/10.1038/ajh.2012.83

Valabhji J, Donovan J, Kyd P a, Schachter M, Elkeles RS (2001) The relationship between active renin concentration and plasma renin activity in Type 1 diabetes. Diabet Med 18:451–8

van de Weert M, Lagerwerf FM, Haverkamp J, Heerma W (1998) Mass spectrometric analysis of oxidized tryptophan. J Mass Spectrom 33:884–891 . https://doi.org/10.1002/(SICI)1096-9888(199809)33:9<884::AID-JMS698>3.0.CO;2-S

Wall MJ, Crowell AMJ, Simms GA, Liu F, Doucette AA (2011) Implications of partial tryptic digestion in organic-aqueous solvent systems for bottom-up proteome analysis. Anal Chim Acta 703:194–203 . https://doi.org/10.1016/j.aca.2011.07.025

Wang S, Zhang L, Yang P, Chen G (2008) Infrared-assisted tryptic proteolysis for peptide mapping. Proteomics 8:2579–2582 . https://doi.org/10.1002/pmic.200800086

Weikart CM, Klibanov AM, Breeland AP, Taha AH, Maurer BR, Martin SP (2017) Plasma-Treated Microplates with Enhanced Protein Recoveries and Minimized Extractables. SLAS Technol Transl Life Sci Innov 22:98–105 . https://doi.org/10.1177/2211068216666258

Whiteaker JR, Zhao L, Anderson L, Paulovich AG (2010) An automated and multiplexed method for high throughput peptide immunoaffinity enrichment and multiple reaction monitoring mass spectrometry-based quantification of protein biomarkers. Mol Cell Proteomics 9:184–196 . https://doi.org/10.1074/mcp.M900254-MCP200

Xa LK, Lacombe M-J, Mercure C, Lazure C, Reudelhuber TL (2014) General lysosomal hydrolysis can process prorenin accurately. Am J Physiol Integr Comp Physiol 307:R505–R513 . https://doi.org/10.1152/ajpregu.00467.2013

Yalow RS, Berson SA (1959) Assay of plasma insulin in human subjects by immunological methods. Nature 184:1648–1649 . https://doi.org/10.1038/1841648b0

Yang W, Kernstock R, Simmons N, Alak A (2014) Guanidinated protein internal standard for immunoaffinity-liquid chromatography/tandem mass spectrometry quantitation of protein therapeutics. Rapid Commun Mass Spectrom 28:1489–1500 . https://doi.org/10.1002/rcm.6924

Yoshida G, Kawasaki M, Murata I, Hayakawa Y, Aoyama T, Miyazaki N, Yamada Y, Nishigaki K, Arai Y, Suzuki F, Minatoguchi S (2015) Higher plasma prorenin concentration plays a role in the development of coronary artery disease. Biomark Res 3:1–7 . https://doi.org/10.1186/s40364-015-0044-1

Zhang H, Gu H, Shipkova P, Ciccimaro E, Sun H, Zhao Q, Olah T V. (2017) Immunoaffinity LC-MS/MS for quantitative determination of a free and total protein target as a target engagement biomarker. Bioanalysis 9:1573–1588 . https://doi.org/10.4155/bio-2017-0152

9. Appendix

Appendix Table 1 Design of denaturation experiments

Worksheet of the D-optimal modeled experimental design and the results of the performed experiments. (Exp.: experiment; TCEP: tris-(2-carboxyethyl)-phosphine; DTT: dithiothreitol; SDC: sodium deoxycholate; rpm: rounds per minute; min: minutes; cps: counts per minute)

Exp Name	Run Order	Reducing Agent	RapiGest [%]	Surfactant/ Chaotrop	Temp. [°C]	Vortexing speed [rpm]	Time [min]	Signature peptide II [cps]	Signature peptide I [cps]
N1	20	TCEP	1	2M Urea	20	300	20	1.22E+04	8.56E+05
N2	191	DTT	1	2M Urea	20	300	20	4.05E+04	1.44E+06
N3	58	TCEP	3	2M Urea	20	300	20	5.85E+01	1.13E+04
N4	144	DTT	3	2M Urea	20	300	20	5.73E+03	1.60E+06
N5	45	TCEP	1	4% SDC	20	300	20	2.96E+04	1.11E+06
N6	150	DTT	1	4% SDC	20	300	20	1.80E+04	1.21E+05
N7	99	TCEP	3	4% SDC	20	300	20	3.66E+04	2.26E+06
N8	184	DTT	3	4% SDC	20	300	20	6.66E+04	2.21E+06
N9	120	TCEP	1	2M Urea	80	300	20	2.41E+04	1.56E+06
N10	89	DTT	1	2M Urea	80	300	20	2.42E+04	1.42E+06
N11	59	TCEP	3	2M Urea	80	300	20	5.84E+03	1.00E+06
N12	66	DTT	3	2M Urea	80	300	20	1.06E+04	1.08E+06

Exp Name	Run Order	Reducing Agent	RapiGest [%]	Surfactant/ Chaotrop	Temp. [°C]	Vortexing speed [rpm]	Time [min]	Signature peptide II [cps]	Signature peptide I [cps]
N13	88	TCEP	1	4% SDC	80	300	20	1.93E+04	3.88E+05
N14	195	DTT	1	4% SDC	80	300	20	2.71E+04	3.78E+05
N15	172	TCEP	3	4% SDC	80	300	20	7.07E+04	2.29E+06
N16	9	DTT	3	4% SDC	80	300	20	2.94E+04	9.87E+05
N17	95	TCEP	1	2M Urea	20	1000	20	1.39E+04	1.08E+06
N18	34	DTT	1	2M Urea	20	1000	20	9.62E+03	7.89E+05
N19	126	TCEP	3	2M Urea	20	1000	20	4.41E+03	1.05E+06
N20	8	DTT	3	2M Urea	20	1000	20	3.24E+03	8.60E+05
N21	29	TCEP	1	4% SDC	20	1000	20	2.24E+04	8.68E+05
N22	181	DTT	1	4% SDC	20	1000	20	4.25E+04	1.36E+06
N23	14	TCEP	3	4% SDC	20	1000	20	2.74E+04	1.51E+06
N24	71	DTT	3	4% SDC	20	1000	20	4.36E+04	1.73E+06
N25	7	TCEP	1	2M Urea	80	1000	20	2.43E+04	1.41E+06
N26	79	DTT	1	2M Urea	80	1000	20	3.39E+04	1.80E+06
N27	149	TCEP	3	2M Urea	80	1000	20	2.57E+03	3.50E+05
N28	94	DTT	3	2M Urea	80	1000	20	1.60E+04	1.38E+06
N29	164	TCEP	1	4% SDC	80	1000	20	1.46E+04	4.79E+05
N30	180	DTT	1	4% SDC	80	1000	20	3.54E+04	8.46E+05

Exp Name	Run Order	Reducing Agent	RapiGest [%]	Surfactant/ Chaotrop	Temp. [°C]	Vortexing speed [rpm]	Time [min]	Signature peptide II [cps]	Signature peptide I [cps]
N31	124	TCEP	3	4% SDC	80	1000	20	3.13E+04	1.06E+06
N32	65	DTT	3	4% SDC	80	1000	20	3.67E+04	1.29E+06
N33	129	TCEP	1	2M Urea	20	300	80	4.48E+03	2.61E+05
N34	186	DTT	1	2M Urea	20	300	80	2.76E+04	1.63E+06
N35	1	TCEP	3	2M Urea	20	300	80	5.76E+03	1.67E+06
N36	123	DTT	3	2M Urea	20	300	80	1.29E+04	1.61E+06
N37	176	TCEP	1	4% SDC	20	300	80	1.89E+04	7.39E+05
N38	2	DTT	1	4% SDC	20	300	80	4.92E+04	1.16E+06
N39	56	TCEP	3	4% SDC	20	300	80	4.16E+04	5.76E+05
N40	16	DTT	3	4% SDC	20	300	80	4.65E+04	9.31E+05
N41	38	TCEP	1	2M Urea	80	300	80	6.70E+02	5.43E+05
N42	63	DTT	1	2M Urea	80	300	80	1.05E+03	5.12E+05
N43	49	TCEP	3	2M Urea	80	300	80	4.64E+02	6.09E+05
N44	83	DTT	3	2M Urea	80	300	80	6.88E+02	4.41E+05
N45	101	TCEP	1	4% SDC	80	300	80	1.77E+03	1.10E+06
N46	32	DTT	1	4% SDC	80	300	80	2.19E+03	5.67E+05
N47	41	TCEP	3	4% SDC	80	300	80	3.40E+03	1.39E+06
N48	51	DTT	3	4% SDC	80	300	80	3.12E+03	1.11E+06

Exp Name	Run Order	Reducing Agent	RapiGest [%]	Surfactant/ Chaotrop	Temp. [°C]	Vortexing speed [rpm]	Time [min]	Signature peptide II [cps]	Signature peptide I [cps]
N49	74	TCEP	1	2M Urea	20	1000	80	1.68E+04	1.97E+06
N50	64	DTT	1	2M Urea	20	1000	80	5.51E+04	3.22E+06
N51	43	TCEP	3	2M Urea	20	1000	80	4.31E+04	3.38E+06
N52	158	DTT	3	2M Urea	20	1000	80	4.27E+04	3.55E+06
N53	13	TCEP	1	4% SDC	20	1000	80	8.21E+04	1.23E+06
N54	11	DTT	1	4% SDC	20	1000	80	1.39E+05	2.05E+06
N55	114	TCEP	3	4% SDC	20	1000	80	1.45E+05	3.15E+06
N56	52	DTT	3	4% SDC	20	1000	80	1.77E+05	2.87E+06
N57	121	TCEP	1	2M Urea	80	1000	80	6.93E+02	7.30E+05
N58	98	DTT	1	2M Urea	80	1000	80	1.69E+04	7.36E+05
N59	197	TCEP	3	2M Urea	80	1000	80	3.51E+03	5.48E+05
N60	110	DTT	3	2M Urea	80	1000	80	6.94E+02	4.15E+05
N61	157	TCEP	1	4% SDC	80	1000	80	2.10E+04	6.35E+05
N62	178	DTT	1	4% SDC	80	1000	80	2.50E+04	6.00E+05
N63	161	TCEP	3	4% SDC	80	1000	80	6.74E+04	1.70E+06
N64	18	DTT	3	4% SDC	80	1000	80	2.07E+04	5.98E+05
N65	36	DTT	2	2M Urea	50	650	50	1.03E+04	1.06E+06
N66	82	DTT	2	2M Urea	50	650	50	2.93E+04	1.14E+06

Exp Name	Run Order	Reducing Agent	RapiGest [%]	Surfactant/ Chaotrop	Temp. [°C]	Vortexing speed [rpm]	Time [min]	Signature peptide II [cps]	Signature peptide I [cps]
N67	199	DTT	2	2M Urea	50	650	50	1.68E+04	1.48E+06
N68	162	TCEP	1	2M Urea	20	300	20	1.60E+04	1.21E+06
N69	175	DTT	1	2M Urea	20	300	20	5.18E+04	1.50E+06
N70	27	TCEP	3	2M Urea	20	300	20	7.13E+01	6.32E+03
N71	105	DTT	3	2M Urea	20	300	20	2.61E+03	1.21E+06
N72	73	TCEP	1	4% SDC	20	300	20	7.65E+03	9.79E+04
N73	136	DTT	1	4% SDC	20	300	20	1.85E+04	1.12E+05
N74	78	TCEP	3	4% SDC	20	300	20	4.08E+04	2.29E+06
N75	70	DTT	3	4% SDC	20	300	20	6.34E+04	2.18E+06
N76	134	TCEP	1	2M Urea	80	300	20	1.91E+04	9.02E+05
N77	125	DTT	1	2M Urea	80	300	20	3.06E+04	1.25E+06
N78	167	TCEP	3	2M Urea	80	300	20	6.29E+03	7.46E+05
N79	106	DTT	3	2M Urea	80	300	20	1.52E+04	1.13E+06
N80	122	TCEP	1	4% SDC	80	300	20	2.34E+04	5.61E+05
N81	179	DTT	1	4% SDC	80	300	20	2.50E+04	4.15E+05
N82	160	TCEP	3	4% SDC	80	300	20	5.44E+04	1.87E+06
N83	97	DTT	3	4% SDC	80	300	20	2.74E+04	7.03E+05
N84	28	TCEP	1	2M Urea	20	1000	20	7.15E+03	9.98E+05

Exp Name	Run Order	Reducing Agent	RapiGest [%]	Surfactant/ Chaotrop	Temp. [°C]	Vortexing speed [rpm]	Time [min]	Signature peptide II [cps]	Signature peptide I [cps]
N85	3	DTT	1	2M Urea	20	1000	20	1.22E+04	8.96E+05
N86	190	TCEP	3	2M Urea	20	1000	20	7.87E+03	1.25E+06
N87	10	DTT	3	2M Urea	20	1000	20	1.62E+04	1.08E+06
N88	112	TCEP	1	4% SDC	20	1000	20	1.92E+04	9.21E+05
N89	44	DTT	1	4% SDC	20	1000	20	4.44E+04	1.25E+06
N90	37	TCEP	3	4% SDC	20	1000	20	2.56E+04	1.27E+06
N91	148	DTT	3	4% SDC	20	1000	20	3.54E+04	1.36E+06
N92	138	TCEP	1	2M Urea	80	1000	20	1.51E+04	1.31E+06
N93	128	DTT	1	2M Urea	80	1000	20	1.87E+04	1.70E+06
N94	141	TCEP	3	2M Urea	80	1000	20	4.66E+03	1.46E+06
N95	177	DTT	3	2M Urea	80	1000	20	8.97E+03	8.88E+05
N96	113	TCEP	1	4% SDC	80	1000	20	1.45E+04	5.06E+05
N97	170	DTT	1	4% SDC	80	1000	20	3.88E+04	8.34E+05
N98	168	TCEP	3	4% SDC	80	1000	20	2.24E+04	9.75E+05
N99	6	DTT	3	4% SDC	80	1000	20	2.58E+04	9.24E+05
N100	40	TCEP	1	2M Urea	20	300	80	7.56E+03	1.80E+06
N101	107	DTT	1	2M Urea	20	300	80	1.56E+04	6.77E+05
N102	4	TCEP	3	2M Urea	20	300	80	1.05E+04	1.95E+06

Exp Name	Run Order	Reducing Agent	RapiGest [%]	Surfactant/ Chaotrop	Temp. [°C]	Vortexing speed [rpm]	Time [min]	Signature peptide II [cps]	Signature peptide I [cps]
N103	153	DTT	3	2M Urea	20	300	80	8.22E+03	1.64E+06
N104	100	TCEP	1	4% SDC	20	300	80	1.57E+04	4.58E+05
N105	33	DTT	1	4% SDC	20	300	80	7.03E+04	1.49E+06
N106	47	TCEP	3	4% SDC	20	300	80	4.25E+04	6.51E+05
N107	188	DTT	3	4% SDC	20	300	80	5.09E+04	8.58E+05
N108	174	TCEP	1	2M Urea	80	300	80	1.20E+03	6.10E+05
N109	118	DTT	1	2M Urea	80	300	80	1.00E+03	5.70E+05
N110	21	TCEP	3	2M Urea	80	300	80	1.90E+02	4.55E+05
N111	57	DTT	3	2M Urea	80	300	80	2.92E+02	5.65E+05
N112	84	TCEP	1	4% SDC	80	300	80	1.96E+03	9.68E+05
N113	194	DTT	1	4% SDC	80	300	80	2.23E+03	7.40E+05
N114	183	TCEP	3	4% SDC	80	300	80	4.68E+03	1.67E+06
N115	5	DTT	3	4% SDC	80	300	80	2.92E+03	1.55E+06
N116	30	TCEP	1	2M Urea	20	1000	80	4.25E+04	2.42E+06
N117	140	DTT	1	2M Urea	20	1000	80	2.51E+04	2.70E+06
N118	15	TCEP	3	2M Urea	20	1000	80	1.47E+04	3.27E+06
N119	77	DTT	3	2M Urea	20	1000	80	1.73E+04	3.51E+06
N120	12	TCEP	1	4% SDC	20	1000	80	9.67E+04	1.92E+06

Exp Name	Run Order	Reducing Agent	RapiGest [%]	Surfactant/ Chaotrop	Temp. [°C]	Vortexing speed [rpm]	Time [min]	Signature peptide II [cps]	Signature peptide I [cps]
N121	25	DTT	1	4% SDC	20	1000	80	1.45E+05	2.24E+06
N122	146	TCEP	3	4% SDC	20	1000	80	1.47E+05	3.28E+06
N123	130	DTT	3	4% SDC	20	1000	80	1.56E+05	2.70E+06
N124	145	TCEP	1	2M Urea	80	1000	80	1.87E+04	8.21E+05
N125	169	DTT	1	2M Urea	80	1000	80	1.29E+03	5.31E+05
N126	187	TCEP	3	2M Urea	80	1000	80	4.45E+03	5.40E+05
N127	103	DTT	3	2M Urea	80	1000	80	7.05E+03	3.42E+05
N128	46	TCEP	1	4% SDC	80	1000	80	3.93E+04	8.30E+05
N129	156	DTT	1	4% SDC	80	1000	80	1.69E+04	4.94E+05
N130	201	TCEP	3	4% SDC	80	1000	80	8.27E+03	1.19E+06
N131	17	DTT	3	4% SDC	80	1000	80	2.32E+04	6.52E+05
N132	91	DTT	2	2M Urea	50	650	50	8.05E+03	1.50E+06
N133	26	DTT	2	2M Urea	50	650	50	2.08E+04	1.39E+06
N134	23	DTT	2	2M Urea	50	650	50	5.09E+03	1.58E+06
N135	24	TCEP	1	2M Urea	20	300	20	1.24E+04	1.17E+06
N136	189	DTT	1	2M Urea	20	300	20	3.97E+04	1.54E+06
N137	192	TCEP	3	2M Urea	20	300	20	7.43E+01	6.76E+03
N138	90	DTT	3	2M Urea	20	300	20	7.64E+03	1.66E+06

Exp Name	Run Order	Reducing Agent	RapiGest [%]	Surfactant/ Chaotrop	Temp. [°C]	Vortexing speed [rpm]	Time [min]	Signature peptide II [cps]	Signature peptide I [cps]
N139	127	TCEP	1	4% SDC	20	300	20	7.12E+03	8.60E+04
N140	72	DTT	1	4% SDC	20	300	20	2.38E+04	1.47E+05
N141	185	TCEP	3	4% SDC	20	300	20	7.62E+04	4.44E+06
N142	135	DTT	3	4% SDC	20	300	20	7.59E+04	2.55E+06
N143	159	TCEP	1	2M Urea	80	300	20	2.08E+04	1.15E+06
N144	151	DTT	1	2M Urea	80	300	20	2.91E+04	1.31E+06
N145	96	TCEP	3	2M Urea	80	300	20	1.08E+04	1.09E+06
N146	80	DTT	3	2M Urea	80	300	20	1.07E+04	1.18E+06
N147	137	TCEP	1	4% SDC	80	300	20	2.36E+04	5.74E+05
N148	22	DTT	1	4% SDC	80	300	20	2.79E+04	4.74E+05
N149	182	TCEP	3	4% SDC	80	300	20	5.60E+04	2.01E+06
N150	68	DTT	3	4% SDC	80	300	20	4.41E+04	1.37E+06
N151	19	TCEP	1	2M Urea	20	1000	20	1.07E+04	1.43E+06
N152	60	DTT	1	2M Urea	20	1000	20	1.68E+04	1.01E+06
N153	48	TCEP	3	2M Urea	20	1000	20	1.16E+04	1.38E+06
N154	133	DTT	3	2M Urea	20	1000	20	1.97E+04	1.65E+06
N155	61	TCEP	1	4% SDC	20	1000	20	1.91E+04	7.91E+05
N156	200	DTT	1	4% SDC	20	1000	20	4.17E+04	1.25E+06

Exp Name	Run Order	Reducing Agent	RapiGest [%]	Surfactant/ Chaotrop	Temp. [°C]	Vortexing speed [rpm]	Time [min]	Signature peptide II [cps]	Signature peptide I [cps]
N157	86	TCEP	3	4% SDC	20	1000	20	2.67E+04	1.73E+06
N158	198	DTT	3	4% SDC	20	1000	20	5.47E+04	2.11E+06
N159	108	TCEP	1	2M Urea	80	1000	20	2.25E+04	1.45E+06
N160	87	DTT	1	2M Urea	80	1000	20	2.78E+04	1.89E+06
N161	139	TCEP	3	2M Urea	80	1000	20	8.16E+03	1.48E+06
N162	131	DTT	3	2M Urea	80	1000	20	1.21E+04	1.95E+06
N163	109	TCEP	1	4% SDC	80	1000	20	1.26E+04	3.73E+05
N164	31	DTT	1	4% SDC	80	1000	20	3.45E+04	7.57E+05
N165	92	TCEP	3	4% SDC	80	1000	20	1.68E+04	6.02E+05
N166	75	DTT	3	4% SDC	80	1000	20	4.09E+04	1.18E+06
N167	76	TCEP	1	2M Urea	20	300	80	4.54E+03	7.81E+05
N168	142	DTT	1	2M Urea	20	300	80	4.06E+04	2.31E+06
N169	165	TCEP	3	2M Urea	20	300	80	2.01E+04	2.30E+06
N170	104	DTT	3	2M Urea	20	300	80	7.25E+03	1.05E+06
N171	117	TCEP	1	4% SDC	20	300	80	1.69E+04	4.24E+05
N172	42	DTT	1	4% SDC	20	300	80	5.02E+04	8.93E+05
N173	171	TCEP	3	4% SDC	20	300	80	3.98E+04	5.00E+05
N174	85	DTT	3	4% SDC	20	300	80	4.82E+04	7.92E+05

Exp Name	Run Order	Reducing Agent	RapiGest [%]	Surfactant/ Chaotrop	Temp. [°C]	Vortexing speed [rpm]	Time [min]	Signature peptide II [cps]	Signature peptide I [cps]
N175	196	TCEP	1	2M Urea	80	300	80	1.50E+03	6.31E+05
N176	35	DTT	1	2M Urea	80	300	80	1.65E+03	6.45E+05
N177	55	TCEP	3	2M Urea	80	300	80	3.12E+02	4.07E+05
N178	163	DTT	3	2M Urea	80	300	80	2.53E+02	4.96E+05
N179	54	TCEP	1	4% SDC	80	300	80	1.96E+03	9.84E+05
N180	193	DTT	1	4% SDC	80	300	80	3.37E+03	9.43E+05
N181	111	TCEP	3	4% SDC	80	300	80	4.27E+03	1.47E+06
N182	119	DTT	3	4% SDC	80	300	80	3.23E+03	1.24E+06
N183	39	TCEP	1	2M Urea	20	1000	80	2.64E+03	1.69E+06
N184	102	DTT	1	2M Urea	20	1000	80	3.23E+04	2.66E+06
N185	173	TCEP	3	2M Urea	20	1000	80	2.65E+04	3.21E+06
N186	62	DTT	3	2M Urea	20	1000	80	5.19E+03	3.22E+06
N187	147	TCEP	1	4% SDC	20	1000	80	1.08E+05	2.34E+06
N188	132	DTT	1	4% SDC	20	1000	80	1.51E+05	2.19E+06
N189	53	TCEP	3	4% SDC	20	1000	80	1.22E+05	2.97E+06
N190	115	DTT	3	4% SDC	20	1000	80	1.92E+05	3.35E+06
N191	67	TCEP	1	2M Urea	80	1000	80	8.38E+03	7.21E+05
N192	116	DTT	1	2M Urea	80	1000	80	4.45E+03	5.78E+05

Exp Name	Run Order	Reducing Agent	RapiGest [%]	Surfactant/ Chaotrop	Temp. [°C]	Vortexing speed [rpm]	Time [min]	Signature peptide II [cps]	Signature peptide I [cps]
N193	152	TCEP	3	2M Urea	80	1000	80	2.99E+03	5.33E+05
N194	143	DTT	3	2M Urea	80	1000	80	1.67E+02	4.60E+04
N195	50	TCEP	1	4% SDC	80	1000	80	2.01E+04	5.84E+05
N196	154	DTT	1	4% SDC	80	1000	80	3.90E+04	9.33E+05
N197	155	TCEP	3	4% SDC	80	1000	80	4.48E+04	1.68E+06
N198	69	DTT	3	4% SDC	80	1000	80	2.44E+04	7.35E+05
N199	93	DTT	2	2M Urea	50	650	50	1.11E+04	1.56E+06
N200	81	DTT	2	2M Urea	50	650	50	1.62E+04	9.85E+05
N201	166	DTT	2	2M Urea	50	650	50	2.11E+04	1.46E+06

Appendix Table 2 Design and acquisition of tryptic digestion

Worksheet of the D-optimal modeled experimental design and the results of the performed experiments (exp: experiment; ng. nanogram; µL: microliter; °C: degrees Celsius; rpm: round per minutes; h: hours; cps: counts per minute)

Exp Name	Run Order	Trypsin Concentration [ng/µL]	Temperature [°C]	Time [h]	Vortexing speed [rpm]	Pre-Digest [h]	Signature peptide I [cps]
N1	24	50	15	0.1	0	0	7.49E+02
N2	56	1000	15	30	0	0	3.52E+04
N3	51	50	70	30	0	0	4.39E+04
N4	18	1000	15	0.1	800	0	4.01E+04
N5	11	50	15	30	800	0	4.73E+04
N6	40	1000	70	30	800	0	0.00E+00
N7	3	50	70	0.1	0	4	2.27E+02
N8	52	50	15	30	0	4	2.27E+02
N9	73	1000	70	30	0	4	4.19E+04
N10	70	50	15	0.1	800	4	6.90E+03
N11	29	1000	15	30	800	4	5.03E+04
N12	36	50	70	30	800	4	0.00E+00
N13	26	50	70	0.1	800	1.33333	4.86E+01
N14	28	50	70	20.0333	800	0	9.16E+01
N15	48	50	51.6667	0.1	800	0	1.55E+03
N16	86	1000	15	0.1	0	2.66667	5.30E+04
N17	13	1000	70	0.1	533.333	0	8.35E+03
N18	33	1000	70	0.1	266.667	4	2.80E+03
N19	85	1000	70	10.0667	0	0	8.54E+02
N20	69	1000	51.6667	0.1	0	0	1.52E+04
N21	87	1000	33.3333	0.1	800	4	4.16E+04
N22	53	683.333	15	0.1	0	4	2.07E+04
N23	77	366.667	70	0.1	0	0	4.04E+03
N24	8	683.333	70	0.1	800	4	3.12E+03

Exp Name	Run Order	Trypsin Concentration [ng/µL]	Temperature [°C]	Time [h]	Vortexing speed [rpm]	Pre-Digest [h]	Signature peptide I [cps]
N25	76	525	42.5	30	400	2	3.01E+04
N26	38	525	42.5	15.05	800	2	2.94E+04
N27	4	525	42.5	15.05	400	4	2.30E+04
N28	63	525	42.5	15.05	400	2	2.94E+04
N29	57	525	42.5	15.05	400	2	3.09E+04
N30	41	525	42.5	15.05	400	2	3.28E+04
N31	9	50	15	0.1	0	0	6.54E+02
N32	27	1000	15	30	0	0	3.50E+04
N33	15	50	70	30	0	0	4.40E+04
N34	35	1000	15	0.1	800	0	3.70E+04
N35	84	50	15	30	800	0	5.41E+04
N36	19	1000	70	30	800	0	0.00E+00
N37	6	50	70	0.1	0	4	1.81E+02
N38	58	50	15	30	0	4	1.81E+02
N39	7	1000	70	30	0	4	4.41E+04
N40	61	50	15	0.1	800	4	8.15E+03
N41	67	1000	15	30	800	4	4.81E+04
N42	66	50	70	30	800	4	0.00E+00
N43	65	50	70	0.1	800	1.33333	3.22E+01
N44	72	50	70	20.0333	800	0	4.39E+04
N45	37	50	51.6667	0.1	800	0	1.68E+03
N46	44	1000	15	0.1	0	2.66667	5.39E+04
N47	88	1000	70	0.1	533.333	0	8.57E+03
N48	62	1000	70	0.1	266.667	4	3.57E+03
N49	46	1000	70	10.0667	0	0	1.83E+02
N50	90	1000	51.6667	0.1	0	0	1.20E+04
N51	2	1000	33.3333	0.1	800	4	4.49E+04
N52	78	683.333	15	0.1	0	4	1.87E+04
N53	43	366.667	70	0.1	0	0	5.49E+03
N54	59	683.333	70	0.1	800	4	2.91E+03
N55	21	525	42.5	30	400	2	3.16E+04

Exp Name	Run Order	Trypsin Concentration [ng/µL]	Temperature [°C]	Time [h]	Vortexing speed [rpm]	Pre-Digest [h]	Signature peptide I [cps]
N56	89	525	42.5	15.05	800	2	3.09E+04
N57	49	525	42.5	15.05	400	4	1.55E+04
N58	32	525	42.5	15.05	400	2	3.18E+04
N59	64	525	42.5	15.05	400	2	3.21E+04
N60	74	525	42.5	15.05	400	2	3.46E+04
N61	25	50	15	0.1	0	0	8.86E+02
N62	81	1000	15	30	0	0	4.04E+04
N63	10	50	70	30	0	0	4.41E+04
N64	50	1000	15	0.1	800	0	3.62E+04
N65	79	50	15	30	800	0	5.26E+04
N66	34	1000	70	30	800	0	2.15E+02
N67	23	50	70	0.1	0	4	1.82E+02
N68	1	50	15	30	0	4	1.82E+02
N69	55	1000	70	30	0	4	4.55E+04
N70	75	50	15	0.1	800	4	8.53E+03
N71	5	1000	15	30	800	4	5.65E+04
N72	17	50	70	30	800	4	0.00E+00
N73	30	50	70	0.1	800	1.33333	4.41E+04
N74	68	50	70	20.0333	800	0	4.70E+01
N75	31	50	51.6667	0.1	800	0	1.10E+03
N76	60	1000	15	0.1	0	2.66667	5.54E+04
N77	82	1000	70	0.1	533.333	0	8.81E+03
N78	20	1000	70	0.1	266.667	4	2.35E+03
N79	71	1000	70	10.0667	0	0	0.00E+00
N80	12	1000	51.6667	0.1	0	0	1.65E+04
N81	45	1000	33.3333	0.1	800	4	3.71E+04
N82	39	683.333	15	0.1	0	4	2.00E+04
N83	80	366.667	70	0.1	0	0	3.83E+03
N84	83	683.333	70	0.1	800	4	2.51E+03
N85	14	525	42.5	30	400	2	3.18E+04
N86	22	525	42.5	15.05	800	2	3.28E+04

Exp Name	Run Order	Trypsin Concentration [ng/µL]	Temperature [°C]	Time [h]	Vortexing speed [rpm]	Pre-Digest [h]	Signature peptide I [cps]
N87	47	525	42.5	15.05	400	4	1.98E+04
N88	42	525	42.5	15.05	400	2	3.07E+04
N89	54	525	42.5	15.05	400	2	2.99E+04
N90	16	525	42.5	15.05	400	2	3.21E+04

Appendix Table 3 Experimental design and result for mixed solvent digestion

Worksheet of the D-optimal modeled experimental design and the results of the performed experiments. (Gray: experiments are excluded because they were qualified as outliers; Exp.: experiment; THF: tetrahydrofuran; cps: counts per minute; outliers were excluded by the software according to the 4-standard deviation rule; min: minutes)

Exp Name	Run Order	Organic Solvent	Digestion Temperature [°C]	Organic solvent concentration [%]	Time [min]	Mature-part signature peptide [cps]	Pro-part signature peptide [cps]
N1	32	Methanol	10	60	5	2.88E+04	6.14E+03
N2	36	Acetone	10	60	5	7.88E+03	3.20E+03
N3	10	Acetonitrile	10	60	5	1.15E+04	3.44E+03
N4	77	THF	10	60	5	7.33E+03	2.62E+03
N5	50	Acetonitrile	30	60	5	5.51E+04	8.37E+03
N6	120	Methanol	40	60	5	1.46E+05	2.81E+04
N7	119	Acetone	40	60	5	9.66E+04	1.44E+04
N8	13	THF	40	60	5	1.14E+05	1.11E+04
N9	63	Acetonitrile	10	80	5	1.20E+04	4.53E+03
N10	102	THF	40	80	5	1.53E+05	1.96E+04
N11	14	Methanol	10	90	5	1.54E+04	1.73E+03
N12	104	Acetone	10	90	5	1.37E+04	7.27E+03
N13	22	Acetone	30	90	5	7.28E+04	2.45E+04
N14	53	Methanol	40	90	5	6.09E+04	8.46E+03
N15	62	Acetonitrile	40	90	5	7.32E+04	1.67E+04
N16	61	Acetonitrile	40	60	60	1.90E+05	1.58E+04
N17	39	Methanol	20	70	60	1.03E+05	1.95E+04
N18	21	Acetone	40	70	60	8.05E+04	1.17E+04
N19	56	Acetonitrile	20	90	60	1.05E+05	4.45E+04
N20	92	THF	40	90	60	1.38E+05	5.74E+04
N21	25	Methanol	10	60	120	1.29E+05	3.72E+04
N22	34	Acetone	10	60	120	7.56E+04	1.84E+04
N23	55	Acetonitrile	10	60	120	1.12E+05	2.60E+04

Exp Name	Run Order	Organic Solvent	Digestion Temperature [°C]	Organic solvent concentration [%]	Time [min]	Mature-part signature peptide [cps]	Pro-part signature peptide [cps]
N24	20	THF	10	60	120	9.21E+04	1.99E+04
N25	58	Acetone	30	60	120	5.30E+04	4.31E+03
N26	44	Methanol	40	60	120	7.00E+04	7.99E+03
N27	91	Acetonitrile	40	60	120	8.04E+04	8.01E+03
N28	75	THF	40	60	120	5.66E+04	7.13E+03
N29	101	THF	10	80	120	1.25E+05	4.39E+04
N30	109	Acetonitrile	40	80	120	8.94E+04	4.13E+04
N31	41	Methanol	10	90	120	1.30E+05	1.53E+04
N32	19	Acetone	10	90	120	1.07E+05	3.09E+04
N33	51	Acetonitrile	10	90	120	8.68E+04	3.59E+04
N34	107	THF	30	90	120	9.40E+04	2.50E+04
N35	17	Methanol	40	90	120	4.36E+04	6.17E+03
N36	94	Acetone	40	90	120	4.98E+04	1.35E+04
N37	64	THF	30	80	60	1.80E+05	2.01E+04
N38	4	THF	30	80	60	1.69E+05	2.41E+04
N39	117	THF	30	80	60	1.69E+05	1.71E+04
N40	24	Methanol	10	60	5	1.68E+04	7.25E+03
N41	11	Acetone	10	60	5	2.80E+04	4.65E+03
N42	65	Acetonitrile	10	60	5	6.23E+03	2.15E+03
N43	118	THF	10	60	5	1.05E+04	3.06E+03
N44	1	Acetonitrile	30	60	5	6.87E+04	2.85E+03
N45	67	Methanol	40	60	5	9.75E+04	2.82E+04
N46	23	Acetone	40	60	5	7.89E+04	1.09E+04
N47	66	THF	40	60	5	7.87E+04	1.06E+04
N48	79	Acetonitrile	10	80	5	1.67E+04	5.57E+03
N49	9	THF	40	80	5	1.09E+05	2.31E+04
N50	43	Methanol	10	90	5	2.02E+04	2.14E+03
N51	18	Acetone	10	90	5	1.29E+04	6.31E+03
N52	3	THF	10	90	5	1.67E+04	7.03E+03
N53	81	Acetone	30	90	5	6.23E+04	2.66E+04

Exp Name	Run Order	Organic Solvent	Digestion Temperature [°C]	Organic solvent concentration [%]	Time [min]	Mature-part signature peptide [cps]	Pro-part signature peptide [cps]
N54	82	Methanol	40	90	5	5.24E+04	7.63E+03
N55	115	Acetonitrile	40	90	5	5.33E+04	1.58E+04
N56	16	Acetonitrile	40	60	60	1.88E+05	1.37E+04
N57	42	Methanol	20	70	60	1.04E+05	1.79E+04
N58	6	Acetone	40	70	60	8.74E+04	9.49E+03
N59	70	Acetonitrile	20	90	60	1.16E+05	4.39E+04
N60	83	THF	40	90	60	1.38E+05	4.88E+04
N61	74	Methanol	10	60	120	1.31E+05	3.95E+04
N62	35	Acetone	10	60	120	6.74E+04	1.66E+04
N63	100	Acetonitrile	10	60	120	9.89E+04	1.99E+04
N64	26	THF	10	60	120	9.09E+04	4.39E+04
N65	99	Acetone	30	60	120	5.98E+04	4.45E+03
N66	59	Methanol	40	60	120	6.83E+04	7.35E+03
N67	71	Acetonitrile	40	60	120	8.85E+04	7.11E+03
N68	85	THF	40	60	120	7.18E+04	1.68E+04
N69	38	THF	10	80	120	1.26E+05	3.59E+04
N70	52	Acetonitrile	40	80	120	7.68E+04	3.73E+04
N71	86	Methanol	10	90	120	1.27E+05	1.56E+04
N72	88	Acetone	10	90	120	8.73E+04	4.55E+04
N73	98	Acetonitrile	10	90	120	9.19E+04	3.37E+04
N74	105	THF	30	90	120	9.98E+04	2.52E+04
N75	96	Methanol	40	90	120	4.69E+04	7.39E+03
N76	68	Acetone	40	90	120	4.31E+04	1.01E+04
N77	12	THF	30	80	60	1.47E+05	2.97E+04
N78	113	THF	30	80	60	1.83E+05	1.67E+04
N79	76	THF	30	80	60	1.55E+05	3.21E+04
N80	116	Methanol	10	60	5	2.35E+04	4.14E+03
N81	45	Acetone	10	60	5	7.01E+03	2.19E+03
N82	110	Acetonitrile	10	60	5	1.13E+04	2.75E+03
N83	112	THF	10	60	5	5.35E+03	2.06E+03

Exp Name	Run Order	Organic Solvent	Digestion Temperature [°C]	Organic solvent concentration [%]	Time [min]	Mature-part signature peptide [cps]	Pro-part signature peptide [cps]
N84	103	Acetonitrile	30	60	5	7.12E+04	1.01E+04
N85	15	Methanol	40	60	5	1.29E+05	2.46E+04
N86	5	Acetone	40	60	5	7.29E+04	1.37E+04
N87	40	Acetonitrile	10	80	5	1.46E+04	5.07E+03
N88	80	THF	40	80	5	1.00E+05	2.26E+04
N89	57	Methanol	10	90	5	1.25E+04	1.78E+03
N90	7	Acetone	10	90	5	1.23E+04	6.87E+03
N91	95	THF	10	90	5	1.13E+04	5.95E+03
N92	28	Acetone	30	90	5	5.36E+04	2.00E+04
N93	90	Methanol	40	90	5	6.16E+04	7.61E+03
N94	31	Acetonitrile	40	90	5	6.67E+04	1.96E+04
N95	97	Acetonitrile	40	60	60	1.89E+05	1.37E+04
N96	46	Methanol	20	70	60	7.92E+04	1.75E+04
N97	48	Acetone	40	70	60	9.77E+04	9.11E+03
N98	60	Acetonitrile	20	90	60	1.17E+05	3.75E+04
N99	84	THF	40	90	60	1.28E+05	3.91E+04
N100	54	Methanol	10	60	120	1.15E+05	3.05E+04
N101	69	Acetone	10	60	120	7.18E+04	1.53E+04
N102	8	Acetonitrile	10	60	120	1.08E+05	1.84E+04
N103	29	THF	10	60	120	8.74E+04	1.82E+04
N104	72	Acetone	30	60	120	6.24E+04	4.66E+03
N105	89	Methanol	40	60	120	6.36E+04	7.85E+03
N106	47	Acetonitrile	40	60	120	7.91E+04	6.89E+03
N107	49	THF	40	60	120	5.57E+04	1.27E+04
N108	30	THF	10	80	120	1.19E+05	2.60E+04
N109	33	Acetonitrile	40	80	120	7.37E+04	3.39E+04
N110	87	Methanol	10	90	120	1.14E+05	1.42E+04
N111	37	Acetone	10	90	120	9.51E+04	4.00E+04
N112	106	Acetonitrile	10	90	120	9.08E+04	3.51E+04
N113	27	THF	30	90	120	6.18E+04	2.34E+04

Exp Name	Run Order	Organic Solvent	Digestion Temperature [°C]	Organic solvent concentration [%]	Time [min]	Mature-part signature peptide [cps]	Pro-part signature peptide [cps]
N114	73	Methanol	40	90	120	4.00E+04	7.47E+03
N115	2	Acetone	40	90	120	6.29E+04	1.13E+04
N116	108	THF	30	80	60	1.54E+05	4.22E+04
N117	114	THF	30	80	60	1.43E+05	3.21E+04
N118	93	THF	30	80	60	1.44E+05	2.02E+04

Appendix Table 4 Injection solvent optimization for Eppendorf® plates

Worksheet of the D-optimal modeled experimental design and the results of the performed experiments (Injection solvent analysis for Eppendorf® protein low binding plate; exp: experiment; DMSO: dimethylsulfoxid; cps: counts per minute)

Exp Name	Run Order	Water [fraction]	DMSO [fraction]	Methanol [fraction]	Formic Acid [fraction]	Mature-part signature peptide [cps]	Pro-part signature peptide [cps]
N1	80	0.980	0.010	0.000	0.010	1.45E+04	2.05E+03
N2	41	0.100	0.400	0.400	0.100	5.22E+03	1.09E+03
N3	27	0.590	0.400	0.000	0.010	1.74E+04	3.06E+03
N4	45	0.580	0.010	0.400	0.010	2.49E+04	4.57E+03
N5	23	0.190	0.400	0.400	0.010	5.43E+03	1.05E+03
N6	30	0.890	0.010	0.000	0.100	1.55E+04	3.38E+03
N7	35	0.500	0.400	0.000	0.100	1.27E+04	2.77E+03
N8	70	0.490	0.010	0.400	0.100	1.76E+04	2.94E+03
N9	39	0.920	0.010	0.000	0.070	1.54E+03	3.80E+02
N10	21	0.560	0.400	0.000	0.040	1.40E+04	3.21E+03
N11	79	0.850	0.140	0.000	0.010	1.52E+04	2.57E+03
N12	24	0.760	0.140	0.000	0.100	1.40E+04	2.50E+03
N13	75	0.550	0.010	0.400	0.040	1.16E+04	2.09E+03
N14	5	0.847	0.010	0.133	0.010	2.39E+04	4.14E+03
N15	40	0.623	0.010	0.267	0.100	1.44E+04	3.04E+03
N16	20	0.130	0.400	0.400	0.070	4.70E+03	8.06E+02
N17	59	0.323	0.400	0.267	0.010	1.29E+04	1.63E+03
N18	71	0.367	0.400	0.133	0.100	1.37E+04	1.37E+03
N19	1	0.320	0.270	0.400	0.010	1.03E+04	1.59E+03
N20	72	0.230	0.270	0.400	0.100	8.08E+03	1.47E+03
N21	89	0.540	0.205	0.200	0.055	1.40E+04	2.37E+03
N22	93	0.540	0.205	0.200	0.055	1.33E+04	2.72E+03
N23	56	0.540	0.205	0.200	0.055	1.48E+04	2.63E+03
N24	62	0.540	0.205	0.200	0.055	1.41E+04	2.84E+03
N25	77	0.980	0.010	0.000	0.010	2.22E+04	4.34E+03

Exp Name	Run Order	Water [fraction]	DMSO [fraction]	Methanol [fraction]	Formic Acid [fraction]	Mature-part signature peptide [cps]	Pro-part signature peptide [cps]
N26	17	0.100	0.400	0.400	0.100	4.87E+03	1.00E+03
N27	9	0.590	0.400	0.000	0.010	1.90E+04	3.82E+03
N28	33	0.580	0.010	0.400	0.010	2.29E+04	4.55E+03
N29	12	0.190	0.400	0.400	0.010	5.39E+03	1.02E+03
N30	31	0.890	0.010	0.000	0.100	1.59E+04	3.12E+03
N31	3	0.500	0.400	0.000	0.100	1.27E+04	2.43E+03
N32	26	0.490	0.010	0.400	0.100	1.30E+04	2.57E+03
N33	94	0.920	0.010	0.000	0.070	1.27E+04	1.99E+03
N34	78	0.560	0.400	0.000	0.040	1.33E+04	2.61E+03
N35	42	0.850	0.140	0.000	0.010	2.36E+04	3.98E+03
N36	14	0.760	0.140	0.000	0.100	1.47E+04	3.08E+03
N37	28	0.550	0.010	0.400	0.040	1.38E+04	2.75E+03
N38	54	0.847	0.010	0.133	0.010	2.50E+04	4.68E+03
N39	95	0.623	0.010	0.267	0.100	1.33E+04	2.81E+03
N40	53	0.130	0.400	0.400	0.070	4.52E+03	8.23E+02
N41	61	0.323	0.400	0.267	0.010	1.42E+04	1.67E+03
N42	90	0.367	0.400	0.133	0.100	1.39E+04	1.74E+03
N43	11	0.320	0.270	0.400	0.010	6.98E+03	1.15E+03
N44	50	0.230	0.270	0.400	0.100	7.16E+03	1.27E+03
N45	52	0.540	0.205	0.200	0.055	1.46E+04	3.16E+03
N46	16	0.540	0.205	0.200	0.055	1.32E+04	2.80E+03
N47	67	0.540	0.205	0.200	0.055	1.43E+04	3.05E+03
N48	32	0.540	0.205	0.200	0.055	1.44E+04	3.38E+03
N49	51	0.980	0.010	0.000	0.010	5.54E+03	2.83E+03
N50	13	0.100	0.400	0.400	0.100	5.19E+03	9.64E+02
N51	73	0.590	0.400	0.000	0.010	2.06E+04	3.57E+03
N52	96	0.580	0.010	0.400	0.010	1.89E+04	3.27E+03
N53	25	0.190	0.400	0.400	0.010	5.35E+03	1.10E+03
N54	88	0.890	0.010	0.000	0.100	1.31E+04	2.80E+03
N55	19	0.500	0.400	0.000	0.100	1.13E+04	2.48E+03

Exp Name	Run Order	Water [fraction]	DMSO [fraction]	Methanol [fraction]	Formic Acid [fraction]	Mature-part signature peptide [cps]	Pro-part signature peptide [cps]
N56	4	0.490	0.010	0.400	0.100	1.21E+04	1.75E+03
N57	15	0.920	0.010	0.000	0.070	1.51E+04	2.81E+03
N58	82	0.560	0.400	0.000	0.040	1.45E+04	2.77E+03
N59	68	0.850	0.140	0.000	0.010	2.29E+04	3.80E+03
N60	60	0.760	0.140	0.000	0.100	1.51E+04	2.85E+03
N61	63	0.550	0.010	0.400	0.040	1.47E+04	2.52E+03
N62	64	0.847	0.010	0.133	0.010	2.08E+04	3.50E+03
N63	2	0.623	0.010	0.267	0.100	1.43E+04	3.22E+03
N64	36	0.130	0.400	0.400	0.070	4.33E+03	8.47E+02
N65	43	0.323	0.400	0.267	0.010	1.43E+04	2.03E+03
N66	69	0.367	0.400	0.133	0.100	1.38E+04	1.79E+03
N67	46	0.320	0.270	0.400	0.010	6.91E+03	1.08E+03
N68	6	0.230	0.270	0.400	0.100	5.83E+03	1.10E+03
N69	76	0.540	0.205	0.200	0.055	1.24E+04	2.75E+03
N70	87	0.540	0.205	0.200	0.055	1.23E+04	2.49E+03
N71	84	0.540	0.205	0.200	0.055	1.43E+04	3.22E+03
N72	29	0.540	0.205	0.200	0.055	1.49E+04	3.03E+03
N73	34	0.980	0.010	0.000	0.010	2.11E+04	5.90E+03
N74	44	0.100	0.400	0.400	0.100	4.01E+03	9.25E+02
N75	58	0.590	0.400	0.000	0.010	2.17E+04	3.85E+03
N76	65	0.580	0.010	0.400	0.010	1.96E+04	3.55E+03
N77	7	0.190	0.400	0.400	0.010	5.10E+03	1.10E+03
N78	48	0.890	0.010	0.000	0.100	1.43E+04	3.42E+03
N79	66	0.500	0.400	0.000	0.100	1.24E+04	2.77E+03
N80	86	0.490	0.010	0.400	0.100	1.57E+04	3.13E+03
N81	37	0.920	0.010	0.000	0.070	1.42E+04	3.02E+03
N82	81	0.560	0.400	0.000	0.040	1.46E+04	2.58E+03
N83	18	0.850	0.140	0.000	0.010	1.97E+04	3.80E+03
N84	22	0.760	0.140	0.000	0.100	1.41E+04	2.96E+03
N85	10	0.550	0.010	0.400	0.040	1.49E+04	3.08E+03

Exp Name	Run Order	Water [fraction]	DMSO [fraction]	Methanol [fraction]	Formic Acid [fraction]	Mature-part signature peptide [cps]	Pro-part signature peptide [cps]
N86	55	0.847	0.010	0.133	0.010	1.92E+04	3.92E+03
N87	38	0.623	0.010	0.267	0.100	1.54E+04	3.16E+03
N88	57	0.130	0.400	0.400	0.070	5.04E+03	9.03E+01
N89	85	0.323	0.400	0.267	0.010	1.38E+04	1.89E+03
N90	47	0.367	0.400	0.133	0.100	1.44E+04	1.94E+03
N91	92	0.320	0.270	0.400	0.010	7.19E+03	1.22E+03
N92	74	0.230	0.270	0.400	0.100	8.00E+03	1.31E+03
N93	91	0.540	0.205	0.200	0.055	1.38E+04	2.45E+03
N94	8	0.540	0.205	0.200	0.055	1.34E+04	3.12E+03
N95	83	0.540	0.205	0.200	0.055	1.47E+04	2.68E+03
N96	49	0.540	0.205	0.200	0.055	1.36E+04	3.16E+03

Appendix Table 5 Injection solvent optimization for Waters® plates

Worksheet of the D-optimal modeled experimental design and the results of the performed experiments (Injection solvent analysis for waters® plate; exp: experiment DMSO: dimethylsulfoxid; cps: counts per minute)

Exp Name	Run Order	Water [fraction]	DMSO [fraction]	Methanol [fraction]	Formic Acid [fraction]	Mature-part signature peptide [cps]	Pro-part signature peptide [cps]
N1	80	0.980	0.010	0.000	0.010	6.37E+01	4.10E+02
N2	41	0.100	0.400	0.400	0.100	5.16E+03	1.23E+03
N3	27	0.590	0.400	0.000	0.010	1.43E+04	3.07E+03
N4	45	0.580	0.010	0.400	0.010	1.49E+04	3.82E+03
N5	23	0.190	0.400	0.400	0.010	5.63E+03	1.13E+03
N6	30	0.890	0.010	0.000	0.100	2.27E+03	2.99E+03
N7	35	0.500	0.400	0.000	0.100	1.34E+04	3.26E+03
N8	70	0.490	0.010	0.400	0.100	1.64E+04	4.01E+03
N9	39	0.920	0.010	0.000	0.070	1.30E+04	3.21E+03
N10	21	0.560	0.400	0.000	0.040	1.47E+04	3.27E+03
N11	79	0.850	0.140	0.000	0.010	3.58E+03	2.45E+03
N12	24	0.760	0.140	0.000	0.100	1.34E+04	2.94E+03
N13	75	0.550	0.010	0.400	0.040	1.78E+04	3.33E+03
N14	5	0.847	0.010	0.133	0.010	4.00E+03	2.70E+03
N15	40	0.623	0.010	0.267	0.100	1.70E+04	3.58E+03
N16	20	0.130	0.400	0.400	0.070	4.84E+03	1.08E+03
N17	59	0.323	0.400	0.267	0.010	9.08E+03	1.45E+03
N18	71	0.367	0.400	0.133	0.100	1.42E+04	3.07E+03
N19	1	0.320	0.270	0.400	0.010	6.61E+03	1.25E+03
N20	72	0.230	0.270	0.400	0.100	1.01E+04	1.66E+03
N21	89	0.540	0.205	0.200	0.055	1.48E+04	3.58E+03
N22	93	0.540	0.205	0.200	0.055	1.48E+04	3.31E+03
N23	56	0.540	0.205	0.200	0.055	1.56E+04	3.71E+03
N24	62	0.540	0.205	0.200	0.055	1.52E+04	3.31E+03

Exp Name	Run Order	Water [fraction]	DMSO [fraction]	Methanol [fraction]	Formic Acid [fraction]	Mature-part signature peptide [cps]	Pro-part signature peptide [cps]
N25	77	0.980	0.010	0.000	0.010	8.14E+01	4.32E+02
N26	17	0.100	0.400	0.400	0.100	4.52E+03	1.03E+03
N27	9	0.590	0.400	0.000	0.010	1.27E+04	3.92E+03
N28	33	0.580	0.010	0.400	0.010	1.58E+04	3.50E+03
N29	12	0.190	0.400	0.400	0.010	5.58E+03	1.09E+03
N30	31	0.890	0.010	0.000	0.100	3.33E+03	3.41E+03
N31	3	0.500	0.400	0.000	0.100	1.43E+04	3.42E+03
N32	26	0.490	0.010	0.400	0.100	1.78E+04	3.44E+03
N33	94	0.920	0.010	0.000	0.070	1.01E+04	3.03E+03
N34	78	0.560	0.400	0.000	0.040	1.24E+04	3.49E+03
N35	42	0.850	0.140	0.000	0.010	4.48E+03	3.28E+03
N36	14	0.760	0.140	0.000	0.100	1.45E+04	3.39E+03
N37	28	0.550	0.010	0.400	0.040	1.71E+04	3.81E+03
N38	54	0.847	0.010	0.133	0.010	5.23E+03	3.14E+03
N39	95	0.623	0.010	0.267	0.100	1.49E+04	3.40E+03
N40	53	0.130	0.400	0.400	0.070	5.24E+03	1.25E+03
N41	61	0.323	0.400	0.267	0.010	8.24E+03	1.23E+03
N42	90	0.367	0.400	0.133	0.100	1.46E+04	3.11E+03
N43	11	0.320	0.270	0.400	0.010	7.01E+03	1.69E+03
N44	50	0.230	0.270	0.400	0.100	8.98E+03	1.54E+03
N45	52	0.540	0.205	0.200	0.055	1.33E+04	3.85E+03
N46	16	0.540	0.205	0.200	0.055	1.40E+04	3.04E+03
N47	67	0.540	0.205	0.200	0.055	1.56E+04	3.55E+03
N48	32	0.540	0.205	0.200	0.055	1.52E+04	3.15E+03
N49	51	0.980	0.010	0.000	0.010	2.60E+01	1.36E+02
N50	13	0.100	0.400	0.400	0.100	4.34E+03	1.02E+03
N51	73	0.590	0.400	0.000	0.010	1.31E+04	2.91E+03
N52	96	0.580	0.010	0.400	0.010	1.63E+04	3.61E+03
N53	25	0.190	0.400	0.400	0.010	5.35E+03	1.13E+03
N54	88	0.890	0.010	0.000	0.100	3.77E+03	2.70E+03

Exp Name	Run Order	Water [fraction]	DMSO [fraction]	Methanol [fraction]	Formic Acid [fraction]	Mature-part signature peptide [cps]	Pro-part signature peptide [cps]
N55	19	0.500	0.400	0.000	0.100	1.28E+04	3.11E+03
N56	4	0.490	0.010	0.400	0.100	1.43E+04	3.82E+03
N57	15	0.920	0.010	0.000	0.070	1.70E+04	3.93E+03
N58	82	0.560	0.400	0.000	0.040	1.26E+04	3.19E+03
N59	68	0.850	0.140	0.000	0.010	6.76E+03	2.82E+03
N60	60	0.760	0.140	0.000	0.100	1.27E+04	2.72E+03
N61	63	0.550	0.010	0.400	0.040	1.60E+04	3.16E+03
N62	64	0.847	0.010	0.133	0.010	5.60E+03	2.94E+03
N63	2	0.623	0.010	0.267	0.100	1.43E+04	3.35E+03
N64	36	0.130	0.400	0.400	0.070	4.63E+03	1.21E+03
N65	43	0.323	0.400	0.267	0.010	7.73E+03	1.23E+03
N66	69	0.367	0.400	0.133	0.100	1.21E+04	3.37E+03
N67	46	0.320	0.270	0.400	0.010	8.82E+03	1.57E+03
N68	6	0.230	0.270	0.400	0.100	5.88E+03	1.52E+03
N69	76	0.540	0.205	0.200	0.055	1.47E+04	3.60E+03
N70	87	0.540	0.205	0.200	0.055	1.28E+04	3.77E+03
N71	84	0.540	0.205	0.200	0.055	1.41E+04	3.30E+03
N72	29	0.540	0.205	0.200	0.055	1.45E+04	3.17E+03
N73	34	0.980	0.010	0.000	0.010	1.94E+02	5.08E+02
N74	44	0.100	0.400	0.400	0.100	5.61E+03	1.21E+03
N75	58	0.590	0.400	0.000	0.010	1.23E+04	2.99E+03
N76	65	0.580	0.010	0.400	0.010	1.66E+04	3.45E+03
N77	7	0.190	0.400	0.400	0.010	4.98E+03	1.14E+03
N78	48	0.890	0.010	0.000	0.100	2.31E+03	3.12E+03
N79	66	0.500	0.400	0.000	0.100	1.20E+04	3.19E+03
N80	86	0.490	0.010	0.400	0.100	1.51E+04	3.42E+03
N81	37	0.920	0.010	0.000	0.070	1.17E+04	3.54E+03
N82	81	0.560	0.400	0.000	0.040	1.35E+04	2.62E+03
N83	18	0.850	0.140	0.000	0.010	1.68E+03	2.07E+03
N84	22	0.760	0.140	0.000	0.100	1.32E+04	3.26E+03

Exp Name	Run Order	Water [fraction]	DMSO [fraction]	Methanol [fraction]	Formic Acid [fraction]	Mature-part signature peptide [cps]	Pro-part signature peptide [cps]
N85	10	0.550	0.010	0.400	0.040	1.46E+04	3.81E+03
N86	55	0.847	0.010	0.133	0.010	5.66E+03	3.15E+03
N87	38	0.623	0.010	0.267	0.100	1.44E+04	3.63E+03
N88	57	0.130	0.400	0.400	0.070	5.51E+03	9.60E+02
N89	85	0.323	0.400	0.267	0.010	9.90E+03	1.46E+03
N90	47	0.367	0.400	0.133	0.100	1.46E+04	2.94E+03
N91	92	0.320	0.270	0.400	0.010	1.01E+04	1.61E+03
N92	74	0.230	0.270	0.400	0.100	9.13E+03	1.81E+03
N93	91	0.540	0.205	0.200	0.055	1.41E+04	3.20E+03
N94	8	0.540	0.205	0.200	0.055	1.41E+04	3.14E+03
N95	83	0.540	0.205	0.200	0.055	1.54E+04	3.48E+03
N96	49	0.540	0.205	0.200	0.055	1.53E+04	3.66E+03

Appendix Table 6 Injection solvent optimization for Waters QuanRecovery® plates

Worksheet of the D-optimal modeled experimental design and the results of the performed experiments (Injection solvent analysis for Waters QuanRecovery® plate; exp: experiment DMSO: dimethylsulfoxid; cps: counts per minute)

Exp Name	Run Order	Water [fraction]	DMSO [fraction]	Methanol [fraction]	Formic Acid [fraction]	Mature-part signature peptide [cps]	Pro-part signature peptide [cps]
N1	80	0.980	0.010	0.000	0.010	1.65E+04	3.32E+03
N2	41	0.100	0.400	0.400	0.100	6.75E+03	1.33E+03
N3	27	0.590	0.400	0.000	0.010	1.72E+04	3.58E+03
N4	45	0.580	0.010	0.400	0.010	1.72E+04	3.67E+03
N5	23	0.190	0.400	0.400	0.010	7.79E+03	1.55E+03
N6	30	0.890	0.010	0.000	0.100	1.72E+04	3.63E+03
N7	35	0.500	0.400	0.000	0.100	1.68E+04	3.04E+03
N8	70	0.490	0.010	0.400	0.100	1.83E+04	3.20E+03
N9	39	0.920	0.010	0.000	0.070	1.86E+04	3.92E+03
N10	21	0.560	0.400	0.000	0.040	1.85E+04	4.15E+03
N11	79	0.850	0.140	0.000	0.010	1.73E+04	3.75E+03
N12	24	0.760	0.140	0.000	0.100	1.88E+04	4.50E+03
N13	75	0.550	0.010	0.400	0.040	1.74E+04	2.97E+03
N14	5	0.847	0.010	0.133	0.010	1.60E+04	3.65E+03
N15	40	0.623	0.010	0.267	0.100	1.80E+04	3.73E+03
N16	20	0.130	0.400	0.400	0.070	6.38E+03	1.21E+03
N17	59	0.323	0.400	0.267	0.010	1.25E+04	1.88E+03
N18	71	0.367	0.400	0.133	0.100	1.58E+04	3.18E+03
N19	1	0.320	0.270	0.400	0.010	1.18E+04	2.13E+03
N20	72	0.230	0.270	0.400	0.100	1.20E+04	1.57E+03
N21	89	0.540	0.205	0.200	0.055	1.67E+04	3.05E+03
N22	93	0.540	0.205	0.200	0.055	1.89E+04	3.50E+03
N23	56	0.540	0.205	0.200	0.055	1.98E+04	4.17E+03
N24	62	0.540	0.205	0.200	0.055	1.86E+04	3.85E+03
N25	77	0.980	0.010	0.000	0.010	1.68E+04	3.21E+03

Exp Name	Run Order	Water [fraction]	DMSO [fraction]	Methanol [fraction]	Formic Acid [fraction]	Mature-part signature peptide [cps]	Pro-part signature peptide [cps]
N26	17	0.100	0.400	0.400	0.100	5.85E+03	1.16E+03
N27	9	0.590	0.400	0.000	0.010	1.74E+04	3.89E+03
N28	33	0.580	0.010	0.400	0.010	1.87E+04	3.48E+03
N29	12	0.190	0.400	0.400	0.010	7.15E+03	1.16E+03
N30	31	0.890	0.010	0.000	0.100	1.80E+04	3.93E+03
N31	3	0.500	0.400	0.000	0.100	1.80E+04	3.97E+03
N32	26	0.490	0.010	0.400	0.100	1.71E+04	3.61E+03
N33	94	0.920	0.010	0.000	0.070	1.73E+04	3.10E+03
N34	78	0.560	0.400	0.000	0.040	1.90E+04	4.25E+03
N35	42	0.850	0.140	0.000	0.010	1.75E+04	3.77E+03
N36	14	0.760	0.140	0.000	0.100	1.54E+04	3.48E+03
N37	28	0.550	0.010	0.400	0.040	1.75E+04	3.80E+03
N38	54	0.847	0.010	0.133	0.010	1.76E+04	3.51E+03
N39	95	0.623	0.010	0.267	0.100	1.77E+04	3.01E+03
N40	53	0.130	0.400	0.400	0.070	6.24E+03	9.08E+02
N41	61	0.323	0.400	0.267	0.010	1.35E+04	1.74E+03
N42	90	0.367	0.400	0.133	0.100	1.49E+04	1.48E+03
N43	11	0.320	0.270	0.400	0.010	1.06E+04	1.85E+03
N44	50	0.230	0.270	0.400	0.100	8.73E+03	1.23E+03
N45	52	0.540	0.205	0.200	0.055	1.91E+04	3.73E+03
N46	16	0.540	0.205	0.200	0.055	1.92E+04	2.03E+03
N47	67	0.540	0.205	0.200	0.055	1.75E+04	3.57E+03
N48	32	0.540	0.205	0.200	0.055	1.93E+04	3.78E+03
N49	51	0.980	0.010	0.000	0.010	1.65E+04	3.45E+03
N50	13	0.100	0.400	0.400	0.100	5.33E+03	9.25E+02
N51	73	0.590	0.400	0.000	0.010	1.49E+04	2.66E+03
N52	96	0.580	0.010	0.400	0.010	1.91E+04	3.80E+03
N53	25	0.190	0.400	0.400	0.010	7.30E+03	1.33E+03
N54	88	0.890	0.010	0.000	0.100	1.52E+04	2.64E+03
N55	19	0.500	0.400	0.000	0.100	1.74E+04	3.70E+03

Exp Name	Run Order	Water [fraction]	DMSO [fraction]	Methanol [fraction]	Formic Acid [fraction]	Mature-part signature peptide [cps]	Pro-part signature peptide [cps]
N56	4	0.490	0.010	0.400	0.100	1.57E+04	3.47E+03
N57	15	0.920	0.010	0.000	0.070	1.71E+04	3.38E+03
N58	82	0.560	0.400	0.000	0.040	1.87E+04	3.77E+03
N59	68	0.850	0.140	0.000	0.010	1.79E+04	3.36E+03
N60	60	0.760	0.140	0.000	0.100	1.66E+04	3.65E+03
N61	63	0.550	0.010	0.400	0.040	1.84E+04	3.55E+03
N62	64	0.847	0.010	0.133	0.010	1.73E+04	3.65E+03
N63	2	0.623	0.010	0.267	0.100	1.81E+04	4.11E+03
N64	36	0.130	0.400	0.400	0.070	6.83E+03	1.29E+03
N65	43	0.323	0.400	0.267	0.010	1.12E+04	1.48E+03
N66	69	0.367	0.400	0.133	0.100	1.70E+04	1.97E+03
N67	46	0.320	0.270	0.400	0.010	1.06E+04	1.60E+03
N68	6	0.230	0.270	0.400	0.100	7.45E+03	1.46E+03
N69	76	0.540	0.205	0.200	0.055	1.83E+04	3.85E+03
N70	87	0.540	0.205	0.200	0.055	1.55E+04	2.71E+03
N71	84	0.540	0.205	0.200	0.055	1.54E+04	3.57E+03
N72	29	0.540	0.205	0.200	0.055	1.88E+04	1.77E+03
N73	34	0.980	0.010	0.000	0.010	1.84E+04	3.23E+03
N74	44	0.100	0.400	0.400	0.100	5.83E+03	9.72E+02
N75	58	0.590	0.400	0.000	0.010	1.59E+04	3.03E+03
N76	65	0.580	0.010	0.400	0.010	1.98E+04	3.75E+03
N77	7	0.190	0.400	0.400	0.010	6.99E+03	1.31E+03
N78	48	0.890	0.010	0.000	0.100	1.54E+04	2.89E+03
N79	66	0.500	0.400	0.000	0.100	1.59E+04	3.62E+03
N80	86	0.490	0.010	0.400	0.100	1.88E+04	3.37E+03
N81	37	0.920	0.010	0.000	0.070	1.67E+04	3.22E+03
N82	81	0.560	0.400	0.000	0.040	1.80E+04	3.61E+03
N83	18	0.850	0.140	0.000	0.010	1.77E+04	3.62E+03
N84	22	0.760	0.140	0.000	0.100	1.77E+04	4.13E+03
N85	10	0.550	0.010	0.400	0.040	1.80E+04	4.07E+03

Exp Name	Run Order	Water [fraction]	DMSO [fraction]	Methanol [fraction]	Formic Acid [fraction]	Mature-part signature peptide [cps]	Pro-part signature peptide [cps]
N86	55	0.847	0.010	0.133	0.010	1.83E+04	3.69E+03
N87	38	0.623	0.010	0.267	0.100	1.81E+04	3.45E+03
N88	57	0.130	0.400	0.400	0.070	6.57E+03	9.70E+02
N89	85	0.323	0.400	0.267	0.010	1.33E+04	1.56E+03
N90	47	0.367	0.400	0.133	0.100	1.69E+04	1.54E+03
N91	92	0.320	0.270	0.400	0.010	1.33E+04	1.86E+03
N92	74	0.230	0.270	0.400	0.100	1.30E+04	1.84E+03
N93	91	0.540	0.205	0.200	0.055	1.82E+04	3.70E+03
N94	8	0.540	0.205	0.200	0.055	1.71E+04	1.81E+03
N95	83	0.540	0.205	0.200	0.055	1.81E+04	3.29E+03
N96	49	0.540	0.205	0.200	0.055	1.84E+04	3.35E+03

Appendix Table 7 Injection solvent optimization for Brand® plates

Worksheet of the D-optimal modeled experimental design and the results of the performed experiments (Injection solvent analysis for Brand® plate; exp: experiment DMSO: dimethylsulfoxid; cps: counts per minute)

Exp Name	Run Order	Water [fraction]	DMSO [fraction]	Methanol [fraction]	Formic Acid [fraction]	Mature-part signature peptide [cps]	Pro-part signature peptide [cps]
N1	80	0.980	0.010	0.000	0.010	5.20E+04	8.97E+03
N2	41	0.100	0.400	0.400	0.100	2.88E+04	4.13E+03
N3	27	0.590	0.400	0.000	0.010	5.08E+04	8.96E+03
N4	45	0.580	0.010	0.400	0.010	5.83E+04	9.78E+03
N5	23	0.190	0.400	0.400	0.010	2.66E+04	2.98E+03
N6	30	0.890	0.010	0.000	0.100	5.10E+04	7.82E+03
N7	35	0.500	0.400	0.000	0.100	5.05E+04	8.68E+03
N8	70	0.490	0.010	0.400	0.100	7.30E+04	1.15E+04
N9	39	0.920	0.010	0.000	0.070	5.57E+04	9.43E+03
N10	21	0.560	0.400	0.000	0.040	5.43E+04	9.33E+03
N11	79	0.850	0.140	0.000	0.010	5.19E+04	8.51E+03
N12	24	0.760	0.140	0.000	0.100	5.31E+04	9.73E+03
N13	75	0.550	0.010	0.400	0.040	5.83E+04	9.58E+03
N14	5	0.847	0.010	0.133	0.010	5.41E+04	9.88E+03
N15	40	0.623	0.010	0.267	0.100	6.02E+04	1.08E+04
N16	20	0.130	0.400	0.400	0.070	2.67E+04	3.59E+03
N17	59	0.323	0.400	0.267	0.010	5.87E+04	5.87E+03
N18	71	0.367	0.400	0.133	0.100	5.32E+04	8.39E+03
N19	1	0.320	0.270	0.400	0.010	1.07E+04	1.45E+03
N20	72	0.230	0.270	0.400	0.100	6.59E+04	6.01E+03
N21	89	0.540	0.205	0.200	0.055	5.81E+04	9.99E+03
N22	93	0.540	0.205	0.200	0.055	5.28E+04	9.52E+03
N23	56	0.540	0.205	0.200	0.055	5.47E+04	9.47E+03
N24	62	0.540	0.205	0.200	0.055	5.35E+04	9.09E+03
N25	77	0.980	0.010	0.000	0.010	4.91E+04	8.77E+03

Exp Name	Run Order	Water [fraction]	DMSO [fraction]	Methanol [fraction]	Formic Acid [fraction]	Mature-part signature peptide [cps]	Pro-part signature peptide [cps]
N26	17	0.100	0.400	0.400	0.100	2.49E+04	2.92E+03
N27	9	0.590	0.400	0.000	0.010	5.36E+04	9.17E+03
N28	33	0.580	0.010	0.400	0.010	5.82E+04	1.06E+04
N29	12	0.190	0.400	0.400	0.010	2.56E+04	3.09E+03
N30	31	0.890	0.010	0.000	0.100	4.95E+04	7.97E+03
N31	3	0.500	0.400	0.000	0.100	5.08E+04	1.01E+04
N32	26	0.490	0.010	0.400	0.100	6.13E+04	9.95E+03
N33	94	0.920	0.010	0.000	0.070	5.72E+04	9.78E+03
N34	78	0.560	0.400	0.000	0.040	5.30E+04	8.71E+03
N35	42	0.850	0.140	0.000	0.010	5.06E+04	8.24E+03
N36	14	0.760	0.140	0.000	0.100	4.82E+04	7.89E+03
N37	28	0.550	0.010	0.400	0.040	5.74E+04	1.02E+04
N38	54	0.847	0.010	0.133	0.010	5.26E+04	9.09E+03
N39	95	0.623	0.010	0.267	0.100	6.09E+04	9.68E+03
N40	53	0.130	0.400	0.400	0.070	2.79E+04	3.30E+03
N41	61	0.323	0.400	0.267	0.010	4.96E+04	5.05E+03
N42	90	0.367	0.400	0.133	0.100	5.49E+04	8.66E+03
N43	11	0.320	0.270	0.400	0.010	4.04E+04	5.05E+03
N44	50	0.230	0.270	0.400	0.100	5.14E+04	5.06E+03
N45	52	0.540	0.205	0.200	0.055	5.67E+04	1.06E+04
N46	16	0.540	0.205	0.200	0.055	5.34E+04	9.66E+03
N47	67	0.540	0.205	0.200	0.055	5.72E+04	8.77E+03
N48	32	0.540	0.205	0.200	0.055	5.44E+04	8.72E+03
N49	51	0.980	0.010	0.000	0.010	5.18E+04	8.98E+03
N50	13	0.100	0.400	0.400	0.100	2.66E+04	3.59E+03
N51	73	0.590	0.400	0.000	0.010	5.38E+04	8.96E+03
N52	96	0.580	0.010	0.400	0.010	5.87E+04	9.85E+03
N53	25	0.190	0.400	0.400	0.010	2.76E+04	3.60E+03
N54	88	0.890	0.010	0.000	0.100	5.12E+04	8.30E+03
N55	19	0.500	0.400	0.000	0.100	4.95E+04	8.26E+03

Exp Name	Run Order	Water [fraction]	DMSO [fraction]	Methanol [fraction]	Formic Acid [fraction]	Mature-part signature peptide [cps]	Pro-part signature peptide [cps]
N56	4	0.490	0.010	0.400	0.100	6.57E+04	1.18E+04
N57	15	0.920	0.010	0.000	0.070	5.12E+04	8.95E+03
N58	82	0.560	0.400	0.000	0.040	4.93E+04	8.49E+03
N59	68	0.850	0.140	0.000	0.010	5.13E+04	8.06E+03
N60	60	0.760	0.140	0.000	0.100	5.06E+04	9.16E+03
N61	63	0.550	0.010	0.400	0.040	5.74E+04	1.02E+04
N62	64	0.847	0.010	0.133	0.010	5.69E+04	8.85E+03
N63	2	0.623	0.010	0.267	0.100	6.13E+04	1.01E+04
N64	36	0.130	0.400	0.400	0.070	2.69E+04	3.37E+03
N65	43	0.323	0.400	0.267	0.010	4.87E+04	4.74E+03
N66	69	0.367	0.400	0.133	0.100	5.40E+04	4.08E+03
N67	46	0.320	0.270	0.400	0.010	4.46E+04	4.80E+03
N68	6	0.230	0.270	0.400	0.100	4.58E+04	5.46E+03
N69	76	0.540	0.205	0.200	0.055	5.49E+04	9.49E+03

Appendix Table 8 Injection solvent optimization for Greiner® plates

Worksheet of the D-optimal modeled experimental design and the results of the performed experiments (Injection solvent analysis for Greiner® plate; DMSO: dimethylsulfoxid; cps: counts per minute)

Exp Name	Run Order	Water [fraction]	DMSO [fraction]	Methanol [fraction]	Formic Acid [fraction]	Mature-part signature peptide [cps]	Pro-part signature peptide [cps]
N1	80	0.980	0.010	0.000	0.010	5.28E+04	6.97E+03
N2	41	0.100	0.400	0.400	0.100	1.91E+04	2.07E+03
N3	27	0.590	0.400	0.000	0.010	5.65E+04	6.62E+03
N4	45	0.580	0.010	0.400	0.010	5.69E+04	7.26E+03
N5	23	0.190	0.400	0.400	0.010	2.29E+04	2.37E+03
N6	30	0.890	0.010	0.000	0.100	5.20E+04	7.31E+03
N7	35	0.500	0.400	0.000	0.100	5.55E+04	6.80E+03
N8	70	0.490	0.010	0.400	0.100	6.32E+04	8.93E+03
N9	39	0.920	0.010	0.000	0.070	5.75E+04	7.48E+03
N10	21	0.560	0.400	0.000	0.040	5.43E+04	7.43E+03
N11	79	0.850	0.140	0.000	0.010	5.48E+04	6.45E+03
N12	24	0.760	0.140	0.000	0.100	5.86E+04	7.10E+03
N13	75	0.550	0.010	0.400	0.040	5.72E+04	8.07E+03
N14	5	0.847	0.010	0.133	0.010	5.57E+04	5.98E+03
N15	40	0.623	0.010	0.267	0.100	5.78E+04	7.44E+03
N16	20	0.130	0.400	0.400	0.070	2.27E+04	2.63E+03
N17	59	0.323	0.400	0.267	0.010	3.66E+04	2.87E+03
N18	71	0.367	0.400	0.133	0.100	5.33E+04	5.52E+03
N19	1	0.320	0.270	0.400	0.010	2.99E+04	3.10E+03
N20	72	0.230	0.270	0.400	0.100	3.33E+04	3.36E+03
N21	89	0.540	0.205	0.200	0.055	5.81E+04	7.83E+03
N22	93	0.540	0.205	0.200	0.055	5.43E+04	8.01E+03
N23	56	0.540	0.205	0.200	0.055	5.52E+04	7.82E+03
N24	62	0.540	0.205	0.200	0.055	5.42E+04	6.89E+03
N25	77	0.980	0.010	0.000	0.010	5.05E+04	6.48E+03

Exp Name	Run Order	Water [fraction]	DMSO [fraction]	Methanol [fraction]	Formic Acid [fraction]	Mature-part signature peptide [cps]	Pro-part signature peptide [cps]
N26	17	0.100	0.400	0.400	0.100	2.00E+04	2.29E+03
N27	9	0.590	0.400	0.000	0.010	5.53E+04	7.15E+03
N28	33	0.580	0.010	0.400	0.010	5.61E+04	6.89E+03
N29	12	0.190	0.400	0.400	0.010	2.28E+04	2.30E+03
N30	31	0.890	0.010	0.000	0.100	5.60E+04	7.64E+03
N31	3	0.500	0.400	0.000	0.100	5.38E+04	7.25E+03
N32	26	0.490	0.010	0.400	0.100	5.88E+04	7.58E+03
N33	94	0.920	0.010	0.000	0.070	5.52E+04	7.90E+03
N34	78	0.560	0.400	0.000	0.040	5.74E+04	7.07E+03
N35	42	0.850	0.140	0.000	0.010	5.12E+04	6.22E+03
N36	14	0.760	0.140	0.000	0.100	5.21E+04	6.82E+03
N37	28	0.550	0.010	0.400	0.040	5.60E+04	7.44E+03
N38	54	0.847	0.010	0.133	0.010	5.54E+04	6.66E+03
N39	95	0.623	0.010	0.267	0.100	6.19E+04	8.07E+03
N40	53	0.130	0.400	0.400	0.070	2.22E+04	2.47E+03
N41	61	0.323	0.400	0.267	0.010	3.54E+04	2.96E+03
N42	90	0.367	0.400	0.133	0.100	5.65E+04	3.54E+03
N43	11	0.320	0.270	0.400	0.010	2.92E+04	2.73E+03
N44	50	0.230	0.270	0.400	0.100	2.79E+04	3.06E+03
N45	52	0.540	0.205	0.200	0.055	5.81E+04	7.80E+03
N46	16	0.540	0.205	0.200	0.055	0	0
N47	67	0.540	0.205	0.200	0.055	5.72E+04	7.96E+03
N48	32	0.540	0.205	0.200	0.055	5.57E+04	7.08E+03
N49	51	0.980	0.010	0.000	0.010	4.89E+04	7.58E+03
N50	13	0.100	0.400	0.400	0.100	2.08E+04	2.34E+03
N51	73	0.590	0.400	0.000	0.010	5.67E+04	7.23E+03
N52	96	0.580	0.010	0.400	0.010	5.63E+04	7.83E+03
N53	25	0.190	0.400	0.400	0.010	2.32E+04	2.21E+03
N54	88	0.890	0.010	0.000	0.100	5.50E+04	7.46E+03
N55	19	0.500	0.400	0.000	0.100	5.61E+04	8.24E+03

Exp Name	Run Order	Water [fraction]	DMSO [fraction]	Methanol [fraction]	Formic Acid [fraction]	Mature-part signature peptide [cps]	Pro-part signature peptide [cps]
N56	4	0.490	0.010	0.400	0.100	5.42E+04	6.87E+03
N57	15	0.920	0.010	0.000	0.070	5.54E+04	7.21E+03
N58	82	0.560	0.400	0.000	0.040	5.23E+04	6.76E+03
N59	68	0.850	0.140	0.000	0.010	5.25E+04	6.80E+03
N60	60	0.760	0.140	0.000	0.100	5.39E+04	6.66E+03
N61	63	0.550	0.010	0.400	0.040	5.81E+04	7.73E+03
N62	64	0.847	0.010	0.133	0.010	5.44E+04	7.16E+03
N63	2	0.623	0.010	0.267	0.100	5.26E+04	6.78E+03
N64	36	0.130	0.400	0.400	0.070	2.22E+04	2.01E+03
N65	43	0.323	0.400	0.267	0.010	3.24E+04	2.75E+03
N66	69	0.367	0.400	0.133	0.100	5.61E+04	5.79E+03
N67	46	0.320	0.270	0.400	0.010	3.02E+04	3.38E+03
N68	6	0.230	0.270	0.400	0.100	2.62E+04	3.08E+03
N69	76	0.540	0.205	0.200	0.055	5.75E+04	7.21E+03

Appendix Table 9 Experimental design and results of gradient optimization

Worksheet of the D-optimal modeled experimental design and the results of the performed experiments (Chromatography gradient with Phenomenex Kinetex XB-18; temp: temperature; °C: degrees Celsius; cps: counts per minute, min: minutes; H2O: water; SP: signature peptide)

Exp Name	Run Order	Oven temp. [°C]	Elution Organic [%]	Gradient H20 [min]	Gradient Step1 [min]	Gradient Step2 [min]	Mature-part SP Area [cps]	Mature-part SP Retention time [min]	Mature-part SP Asymmetry	Pro-part SP Area [cps]	Pro-part SP Retention time [min]	Pro-part SP Asymmetry
N1	24	70	50	0.1	0.1	1	2.88E+04	2.84	1.37	1.14E+04	2.7	0.9
N2	43	50	90	0.1	0.1	1	4.12E+04	2.75	1.29	8.43E+03	2.66	1.08
N3	72	50	50	0.1	3	1	6.25E+04	6.07	1.22	1.47E+04	5.85	1.03
N4	2	70	90	0.1	3	1	5.95E+04	5.46	1.51	1.40E+04	5.31	0.97
N5	7	70	50	3	3	1	6.63E+04	8.81	1.11	1.59E+04	8.53	1.21
N6	44	50	90	3	3	1	8.27E+04	8.65	0.93	1.66E+04	8.51	1.08
N7	54	50	50	0.1	0.1	6	5.62E+04	6.16	1.21	1.02E+04	4.76	1.39
N8	34	50	90	3	0.1	6	9.08E+04	7.82	1.2	1.85E+04	6.83	0.86
N9	39	70	50	0.1	3	6	6.70E+04	8.33	1.29	1.27E+04	6.45	0.97
N10	22	50	90	0.1	3	6	8.45E+04	7.4	1.08	1.97E+04	6.57	0.98
N11	86	50	50	3	3	6	8.61E+04	11.84	0.9	1.87E+04	10.26	1.07
N12	84	70	90	3	3	6	7.50E+04	9.72	1.25	1.58E+04	8.87	0.98
N13	12	50	50	3	0.1	2.66667	7.13E+04	7.53	0.99	1.72E+04	6.6	1.38

Exp Name	Run Order	Oven temp [°C]	Elution Organic [%]	Gradient H20 [min]	Gradient Step1 [min]	Gradient Step2 [min]	Mature-part SP Area [cps]	Mature-part SP Retention time [min]	Mature-part SP Asymmetry	Pro-part SP Area [cps]	Pro-part SP Retention time [min]	Pro-part SP Asymmetry
N14	61	50	50	3	2.03333	1	7.30E+04	8.12	0.96	1.82E+04	7.89	1.16
N15	33	50	50	2.03333	0.1	1	7.24E+04	5.2	1.02	1.52E+04	4.98	1.5
N16	77	70	50	1.06667	0.1	6	7.64E+04	6.45	0.95	1.33E+04	4.69	0.98
N17	36	70	90	0.1	0.1	4.33333	2.80E+04	3.57	0.94	5.17E+03	3.08	1.1
N18	40	70	90	3	1.06667	1	5.65E+04	5.68	1.5	1.34E+04	5.57	1.48
N19	30	70	90	2.03333	0.1	1	5.93E+04	4.61	0.94	1.58E+04	4.5	0.98
N20	81	70	63.3333	3	0.1	1	6.79E+04	5.77	0.9	1.60E+04	5.61	1.21
N21	21	70	76.6667	3	0.1	6	6.48E+04	7.16	1.38	1.39E+04	6.17	0.94
N22	80	63.3333	50	3	0.1	6	1.03E+04	8.72	1.12	1.66E+03	6.94	1.01
N23	52	63.3333	90	0.1	0.1	6	6.33E+04	4.13	1.06	1.15E+04	3.28	1.48
N24	8	56.6667	90	3	0.1	1	6.06E+04	5.67	1.18	1.40E+04	5.55	1.14
N25	20	60	50	1.55	1.55	3.5	6.66E+04	7.64	1.07	1.39E+04	6.5	1.09
N26	16	60	70	1.55	3	3.5	6.97E+04	8.25	0.92	1.55E+04	7.54	1.23

Exp Name	Run Order	Oven temp [°C]	Elution Organic [%]	Gradient H20 [min]	Gradient Step1 [min]	Gradient Step2 [min]	Mature-part SP Area [cps]	Mature-part SP Retention time [min]	Mature-part SP Asymmetry	Pro-part SP Area [cps]	Pro-part SP Retention time [min]	Pro-part SP Asymmetry
N27	13	60	70	1.55	1.55	6	6.55E+04	7.67	0.94	1.61E+04	6.5	1.15
N28	31	60	70	1.55	1.55	3.5	6.79E+04	6.81	0.93	1.61E+04	6.12	0.9
N29	89	60	70	1.55	1.55	3.5	7.90E+04	6.82	1.01	1.58E+04	6.13	1
N30	46	60	70	1.55	1.55	3.5	6.98E+04	6.81	0.98	1.44E+04	6.11	1.38
N31	35	70	50	0.1	0.1	1	3.14E+04	2.84	1.37	1.04E+04	2.7	0.9
N32	59	50	90	0.1	0.1	1	0	0	0	0	0	0
N33	29	50	50	0.1	3	1	6.66E+04	6.09	0.92	1.48E+04	5.85	1.1
N34	23	70	90	0.1	3	1	5.66E+04	5.45	1.47	1.51E+04	5.31	0.94
N35	9	70	50	3	3	1	6.78E+04	8.81	1.09	1.69E+04	8.52	1.06
N36	85	50	90	3	3	1	7.60E+04	8.66	1.08	1.75E+04	8.54	1.35
N37	18	50	50	0.1	0.1	6	7.43E+04	6.17	1.3	1.40E+04	4.74	1.07
N38	78	50	90	3	0.1	6	8.03E+04	7.81	1.07	1.82E+04	6.81	1.11
N39	19	70	50	0.1	3	6	6.24E+04	8.33	1.24	1.34E+04	6.44	0.73
N40	14	50	90	0.1	3	6	7.83E+04	7.41	1.13	1.76E+04	6.56	0.89
N41	76	50	50	3	3	6	4.59E+04	11.85	0.95	8.45E+03	10.28	1.22
N42	3	70	90	3	3	6	6.95E+04	9.73	1.46	1.69E+04	8.87	1

Exp Name	Run Order	Oven temp [°C]	Elution Organic [%]	Gradient H20 [min]	Gradient Step1 [min]	Gradient Step2 [min]	Mature-part SP Area [cps]	Mature-part SP Retention time [min]	Mature-part SP Asymmetry	Pro-part SP Area [cps]	Pro-part SP Retention time [min]	Pro-part SP Asymmetry
N43	49	50	50	3	0.1	2.66667	7.77E+04	7.54	1.02	1.77E+04	6.61	0.98
N44	47	50	50	3	2.03333	1	7.29E+04	8.1	1.2	1.79E+04	7.88	1.04
N45	15	50	50	2.03333	0.1	1	6.57E+04	5.2	1	1.42E+04	4.97	1.23
N46	50	70	50	1.06667	0.1	6	6.73E+04	6.45	0.87	1.22E+04	4.7	1.04
N47	45	70	90	0.1	0.1	4.33333	6.05E+04	3.54	1.05	1.25E+04	3	1.37
N48	1	70	90	3	1.06667	1	5.03E+04	5.68	1.35	1.40E+04	5.57	1.44
N49	79	70	90	2.03333	0.1	1	5.88E+04	4.61	0.96	1.45E+04	4.51	1.01
N50	90	70	63.3333	3	0.1	1	6.82E+04	5.77	0.92	1.67E+04	5.61	1.25
N51	66	70	76.6667	3	0.1	6	7.06E+04	7.17	0.88	1.51E+04	6.17	0.94
N52	10	63.3333	50	3	0.1	6	6.58E+04	8.73	1.26	1.31E+04	6.93	0.99
N53	53	63.3333	90	0.1	0.1	6	6.26E+04	4.12	1.02	1.10E+04	3.28	0.86
N54	71	56.6667	90	3	0.1	1	3.08E+04	5.67	1.32	6.74E+03	5.57	1.53
N55	55	60	50	1.55	1.55	3.5	6.91E+04	7.63	1	1.55E+04	6.5	1.05

Exp Name	Run Order	Oven temp [°C]	Elution Organic [%]	Gradient H20 [min]	Gradient Step1 [min]	Gradient Step2 [min]	Mature-part SP Area [cps]	Mature-part SP Retention time [min]	Mature-part SP Asymmetry	Pro-part SP Area [cps]	Pro-part SP Retention time [min]	Pro-part SP Asymmetry
N56	56	60	70	1.55	3	3.5	7.19E+04	8.25	0.98	1.62E+04	7.55	0.87
N57	57	60	70	1.55	1.55	6	7.14E+04	7.67	0.98	1.51E+04	6.51	1.35
N58	42	60	70	1.55	1.55	3.5	2.44E+04	6.82	1.04	4.10E+03	6.15	1.28
N59	88	60	70	1.55	1.55	3.5	7.53E+04	6.81	0.9	1.49E+04	6.11	0.88
N60	64	60	70	1.55	1.55	3.5	7.32E+04	6.82	1.02	1.53E+04	6.12	0.97
N61	6	70	50	0.1	0.1	1	2.87E+04	2.84	1.42	1.30E+04	2.7	0.86
N62	28	50	90	0.1	0.1	1	2.33E+04	2.77	0.99	5.18E+03	2.68	1.46
N63	65	50	50	0.1	3	1	6.21E+04	6.09	0.94	1.31E+04	5.86	1.06
N64	68	70	90	0.1	3	1	6.08E+04	5.46	0.9	1.53E+04	5.31	0.98
N65	25	70	50	3	3	1	6.71E+04	8.81	1.1	1.53E+04	8.52	1.09
N66	82	50	90	3	3	1	7.29E+04	8.65	1.4	1.84E+04	8.5	1.02
N67	67	50	50	0.1	0.1	6	7.00E+04	6.14	1.05	1.40E+04	4.71	1.25
N68	69	50	90	3	0.1	6	8.84E+04	7.83	1.33	1.81E+04	6.8	1.03
N69	63	70	50	0.1	3	6	7.05E+04	8.33	1.26	1.25E+04	6.43	0.74
N70	83	50	90	0.1	3	6	8.00E+04	7.41	1.13	1.90E+04	6.56	0.89
N71	75	50	50	3	3	6	8.43E+04	11.87	1.2	1.77E+04	10.28	1.23

Exp Name	Run Order	Oven temp [°C]	Elution Organic [%]	Gradient H20 [min]	Gradient Step1 [min]	Gradient Step2 [min]	Mature-part SP Area [cps]	Mature-part SP Retention time [min]	Mature-part SP Asymmetry	Pro-part SP Area [cps]	Pro-part SP Retention time [min]	Pro-part SP Asymmetry
N72	70	70	90	3	3	6	7.69E+04	9.72	1.31	1.62E+04	8.86	0.95
N73	62	50	50	3	0.1	2.66667	7.82E+04	7.54	1.03	1.77E+04	6.61	0.97
N74	26	50	50	3	2.03333	1	7.17E+04	8.11	1.46	1.61E+04	7.89	1.14
N75	5	50	50	2.03333	0.1	1	6.16E+04	5.2	0.99	1.53E+04	4.98	1.38
N76	17	70	50	1.06667	0.1	6	1.67E+04	6.45	0.92	2.48E+03	4.67	1.4
N77	51	70	90	0.1	0.1	4.33333	5.80E+04	3.55	1.15	1.40E+04	3.01	1.39
N78	48	70	90	3	1.06667	1	5.63E+04	5.68	1.43	1.19E+04	5.57	1.53
N79	11	70	90	2.03333	0.1	1	5.76E+04	4.61	0.98	1.45E+04	4.51	0.98
N80	38	70	63.3333	3	0.1	1	6.05E+04	5.76	1.29	1.49E+04	5.59	1.02
N81	58	70	76.6667	3	0.1	6	2.85E+04	7.17	0.91	5.26E+03	6.2	1.39
N82	74	63.3333	50	3	0.1	6	8.01E+04	8.7	0.96	1.57E+04	6.92	1.42
N83	41	63.3333	90	0.1	0.1	6	5.83E+04	4.12	0.97	1.16E+04	3.28	1.49
N84	32	56.6667	90	3	0.1	1	5.97E+04	5.67	1.25	1.29E+04	5.57	1.4

Exp Name	Run Order	Oven temp [°C]	Elution Organic [%]	Gradient H20 [min]	Gradient Step1 [min]	Gradient Step2 [min]	Mature-part SP Area [cps]	Mature-part SP Retention time [min]	Mature-part SP Asymmetry	Pro-part SP Area [cps]	Pro-part SP Retention time [min]	Pro-part SP Asymmetry
N85	37	60	50	1.55	1.55	3.5	6.70E+04	7.64	1.16	1.51E+04	6.51	1.17
N86	4	60	70	1.55	3	3.5	7.48E+04	8.26	1.04	1.62E+04	7.55	0.89
N87	60	60	70	1.55	1.55	6	7.87E+04	7.66	0.93	1.62E+04	6.5	1.16
N88	87	60	70	1.55	1.55	3.5	3.39E+04	6.82	0.98	5.43E+03	6.13	1.04
N89	27	60	70	1.55	1.55	3.5	6.89E+04	6.82	1.02	1.50E+04	6.12	0.91
N90	73	60	70	1.55	1.55	3.5	6.98E+04	6.82	0.99	1.53E+04	6.12	0.98

10. List of Publications

Peer-reviewed publications

Burdman I, Burckhardt BB (2020) Human prorenin determination by hybrid immunocapture LC-MS: A mixed-solvent-triggered digestion utilizing D-optimal design. *Rapid Communications in Mass Spectrometry* 34:e8932.
DOI: 10.1002/rcm.8932

Burdman I, Burckhardt BB (2020) Prorenin and active renin levels in paediatrics: a bioanalytical review. *Clinical Chemistry and Laboratory Medicine* Published online 19 August 2020, ahead of print.
DOI:10.1515/cclm-2020-0857

Makowski N, Ciplea A, Ali M, **Burdman I**, Bartel A, Burckhardt BB, on behalf of the LENA consortium (2020). A comprehensive quality control system suitable for academic research-Application in a paediatric clinical study. *Bioanalysis* 12:319-333.
DOI:10.4155/bio-2019-0242

Feickert M, **Burdman I**, Makowski N, Ali M, Bartel A, Burckhardt BB, on behalf of the LENA consortium (2020) A continued method performance monitoring approach for the determination of pediatric renin samples – application within a European clinical trial. *Clinical Chemistry and Laboratory Medicine* 58, 11:1847-1855.
DOI:10.1515/cclm-2019-1162

Burdman I, Burckhardt BB (2019) A concept to make low-abundance endogenous renin accessible to mass spectrometry: A multistep experimental design approach. *Journal of Chromatography B* 2019:1134-1135(August):121856.
DOI:10.1016/j.jchromb.2019.121856

Poster Presentations

Burdman I, Burckhardt BB Appraisal of immunocapture by different antibodies prior to a surrogate peptide approach utilizing LC-HRMS analysis for quantification of the low abundant protein renin in human plasma. DPhG Jahrestagung 2018. Hamburg. Tagungsband (2018) POS. 100. p. 134.

Gangnus T, Süßenbach FK, Makowski N, **Burdman I**. Läer S, Burckhardt BB: Reference ranges of blood NT-proBNP in paediatric heart failure and healthy controls: compilation of literature data. ESDPPP Basel. Switzerland. P37 *Archives of Disease in Childhood* (2019);104**:**e32.

Feickert M, **Burdman I**, Makowski N, Ali M, Farahani S, Majid H, Ciplea AM, Bartel A, Burckhardt BB: Reliable results in continuous bioanalysis of paediatric renin samples – comprehensive quality assessment within clinical studies in children. ESDPPP Congress Basel. Switzerland. P34 *Archives of Disease in Childhood* (2019);104**:**e31.

Burdman I, Burckhardt BB: Towards determination of endogenous prorenin in paediatric samples using a hybrid approach – impact of antibody selection for immunocapture. ESDPPP Congress Basel. Switzerland. P16 *Archives of Disease in Childhood* (2019);104**:**e23.

Süßenbach FK, Gangnus T, **Burdman I**, Makowski N, Läer S, Burckhardt BB: Compilation of available plasma renin activity levels in the healthy and cardiac diseased paediatric population. ESDPPP Congress Basel. Switzerland. P37 *Archives of Disease in Childhood* (2019);104**:**e56-e57.

Makowski N, **Burdman I**, Ali M, Majid H, Farahani S, Ciplea AM, Bartel A, Burckhardt BB: Quality assessment for the continuous bioanalysis of aldosterone: application in an European paediatric study. ESDPPP Congress Basel. Switzerland (2019). P64 *Archives of Disease in Childhood* (2019);104**:**e43-e44.

Burdman I, Burckhardt BB: Investigation of the optimal conditions for a surrogate peptide approach by analyzing human active renin captured by immobilized antibodies: A D-optimal response surface model approach. Euroanalysis XX 2019. Istanbul. Turkey (2019) PP 2-021. 275.

Burdman I, Burckhardt BB: The determination of human active renin and prorenin by LC-MS: the impact of injection solvent composition and material on precision and signal intensity. MSACL Connect Palm Springs. USA (2020). https://www.msacl.org/presenter_posters/2020_US_64a_ilja.burdman_67858_poster.pdf. Accessed: 17 August 2020